In-Situ Passive Sampling for the Evaluation and Management of Hydrophobic Organic Compounds Contaminated Sediment

by

Alex V. Smith, B.S., M.S.

A Dissertation

In

Civil Engineering

Submitted to the Graduate Faculty
of Texas Tech University in
Partial Fulfillment of
the Requirements for
the Degree of

DOCTOR OF PHILOSOPHY

Danny Reible, Ph.D.
Chair of the Committee

W. Andrew Jackson, Ph.D.

Todd Anderson, Ph.D.

Jennifer Guelfo, Ph.D.

Mark Sheridan, Ph.D.
Dean of the Graduate School

August 2022

ACKNOWLEDGEMENTS

I have been quite fortunate in my early career to work, learn, and collaborate on legacy environmental pollutants and their presence in our society. I am beyond grateful to my advisor, Danny Reible, for his continued encouragement and willingness to mentor me over the years. I can humbly say I would not be where I am today without his guidance. I hope to pay it forward in others I meet as the way I conduct myself and view the world critically and analytically will always be a tribute to him.

I write this with my parents in mind. When I told them I wanted to pursue my doctorate I was met with overwhelming praise and compassion. Over the years of failures and accomplishments I continually look back and recognize their support system is why I believed in myself. Mom and Dad this is for you.

Furthermore, I would like to give my appreciation to Mihna Lewis. I know she did not expect to go on this journey with me initially, and as much as I wanted to apologize for the late nights and the cancelled plans she encouraged me to keep going. She recognized my passion, fueled my determination and I am elated to call you my partner. I look forward to the rest of our lives together.

Certainly, I cannot forget to acknowledge my colleagues, some of the most determined people I will ever get the chance to meet. Uriel Garza-Rubalcava and Hasti Ziaei, I hope you both never change. You have a genuine personality and I feel honored to call you my friends. Thank you, Magdalena Rakowska, for guiding me when I was a research assistant and taking a chance on me to help grow your startup, Envirostatus, LLC. I would also like to thank Ilektra Drygiannaki for staying with me at those

Wednesday happy hours, and always willing to network with me at the many conferences we attended together. Those will be memories I will never forget. I would like to thank Dimitrios Athanasiou, Tea Vrtlar, Songjing Yan, and Xiaolong Shen for being role models when I first joined. I continue to look up to each of you.

This work is the culmination of research performed at Texas Tech University and field studies performed across the United States of America.

TABLE OF CONTENTS

ABSTRACT

Environmental pollution from legacy contaminants poses difficult challenges to assess and manage. An increasingly utilized approach to assessment is passive sampling that measures contaminants in the sediment without disturbing or changing the surrounding environment or remedial design. For hydrophobic organics this is typically through the use of polymeric materials that concentrate interstitial water contaminants *in-situ.* By measuring contaminants in the interstitial water, the mobility and availability of the contaminants are more directly measured than by bulk solid concentrations. Passive sampling has been shown to provide a more environmentally relevant measure of contamination and the resulting exposure and effects to the ecology.

However, passive sampling techniques have not received full regulatory acceptance and most decision making for Superfund and other contaminated sediment sites is based on traditional bulk solid methods that can be misleading. Passive sampling tools are typically used as a supporting approach during site assessment and have been largely developed and applied by research teams at universities. They will never see widespread use until standardized approaches are implemented and sufficient experience has been gained by use of the approaches at a wide range of sites. It is toward the improvement, standardization, and demonstration of passive sampling of HOCs that this dissertation is directed. Performance reference compounds (PRCs) are often preloaded on the polymeric passive samplers to assess equilibration but there are a variety of issues that may limit their accuracy. A chapter is dedicated to the challenges of loading performance reference compounds and the effects of non-uniform loading on the interpretation of equilibration of target compounds. The use of passive samplers is then

demonstrated at four different contaminated sites illustrating their use to address different assessment objectives. In two of the four projects, passive sampling was used to assess the long-term (5-10 year) performance of *in-situ* capping as a remedial approach for sediments contaminated with polycyclic aromatic hydrocarbons (PAHs). In one, a conventional sand and gravel cap was placed over PAH contaminated sediments subject to groundwater upwelling and significant tidal fluctuations. In the other, substantial subsurface contamination was capped with a cap containing both sand and an organophilic clay.

Polychlorinated biphenyls were the primary contaminant of concern in the two remaining demonstration sites. In one, passive sampling was used in an effort to identify source areas through the placement of 163 low density polyethylene (LDPE) samplers at the sediment-water interface. In the final demonstration, passive sampling was employed to evaluate the performance of two commercial materials for placement of activated carbon in a sediment environment in a pilot study.

The results indicate that passive sampling is a viable and promising tool for identifying source areas, evaluating exposure and risk of hydrophobic organic contaminated sediments, and the effectiveness of remediation via *in-situ* treatment or engineered caps. It was also shown that under most conditions, non-uniform loading of PRCs does not compromise the ability to determine equilibration with respect to target compounds as long as the actual initial loading of the PRC on the polymeric material is measured.

LIST OF TABLES

LIST OF FIGURES

CHAPTER 1

INTRODUCTION

1.1. BACKGROUND AND PROBLEM STATEMENT

Contaminated sediment site management starts with understanding how hydrophobic organic compounds (HOCs) partition between different environmental compartments and quantifying the risk that is associated with each. These environmental compartments each have their own unique characteristics and the exposure to aquatic organisms, wildlife, and humans differs between them. Defining each compartment involves examining the physical size and chemical characteristics of the materials that make up that phase (e.g., sorption capacity in the compartment). Many of the contaminants of concern will typically be associated with the organic fraction of the particulate phase which is not readily available to be taken up by aquatic organisms. A smaller portion is associated with the colloidal and dissolved organic carbon (DOC) phase and may also be partially unavailable to organisms. Finally, a smaller fraction of the contaminant will often be found in the truly dissolved phase where the compounds are most readily available for uptake by organisms. The dissolved phase concentration provides insight into the fraction of the contaminants that are available to biological organisms, or bioavailability (National Academies, 2003; United States Environmental Protection Agency, 2012). The dissolved phase may not be the direct route of uptake to organisms (e.g., deposit feeding organisms), but has come to be viewed as an indicator of what can be easily assimilated by organisms rather by water uptake routes or deposit uptake routes and should be evaluated when planning remedial efforts (U.S. Environmental Protection Agency, 2005; Wilson et al., 2018).

With in-situ remedies such as capping (active or conventional) bulk solid concentrations are typically unchanged, and the freely dissolved concentration migrating into the cap should be considered as the main line of evidence when assessing remedial performance. Capping of contaminated sediments typically tries to contain the sediments and reduce the migration of contaminants in the porewater. This separation reduces the contaminant flux and limits the exchange to the capping material in the hyporheic zone (D. D. Reible, 2014). A sediment cap can be composed of an inert sand material, or, for greater retardation of organics, contain sorbents such as activated carbon (AC). A vertical profile of porewater concentration can thus be a sensitive indicator of the degree of containment and the effectiveness of the cap that are needed to address exposure and risk.

Passive samplers began to emerge as a viable option for contaminated sediment monitoring due to the ability to measure the freely dissolved concentration directly (Burgess et al., 2012; Mayer et al., 2014). Passive sampling methods provide a line of evidence for contaminant availability and mobility through native and capped sediment that can be far more indicative of risks than bulk chemistry at contaminated sediment sites (Greenberg et al., 2014). By evaluating the dissolved phase, or freely available, concentration the human health and environmental risk can be defined more directly to evaluate contaminant risks and remedial effectiveness. Recent work has focused on the development of passive samplers with organic polymers such as low-density polyethylene (LDPE) (Apell & Gschwend, 2016; Cornelissen et al., 2008), polyoxymethylene (POM) (Hawthorne et al., 2011; Jonker & Koelmans, 2001), or solid phase microextraction (SPME) using polydimethylsiloxane (PDMS) (Maruya et al., 2009; Thomas et al., 2014) to which the freely dissolved HOC can partition and thus

indicate the freely dissolved concentration of HOCs in porewater. These polymers are similar but differ in their commonly available geometry which can affect their application in the field. Most commonly, PE and POM are used in thin sheets in various shapes and thicknesses while PDMS is used as an adsorbent onto a solid support, for example PDMS can be spin coated onto a glass fiber. The latter geometry is especially convenient for vertical profiling of contaminants in-situ in that the fiber can be easily inserted into soils or sediments using a small diameter pointed rod as shielding and as a support. The sheet-like polymers typically require a frame which can be more difficult to insert. The purpose of this document is to identify uncertainties and in the use of in-situ passive samplers at contaminated sediment sites and incorporate studies to resolve those uncertainties.

The attention of this document is on hydrophobic organic compounds including polychlorinated biphenyls (PCBs) and polycyclic aromatic hydrocarbons (PAHs) since these persistent HOCs have been shown to bioaccumulate in aquatic organisms and drive the risk making decisions at many contaminated sediment sites. By examining the motivation and need for in-situ passive samplers and present four case studies that are designed to develop and demonstrate the use of in-situ passive samplers to identify source areas and to evaluate the effectiveness of capping for in-situ remedy performance at contaminated sediment sites.

1.2. RESEARCH OBJECTIVES

The above citations indicate that there has been use of passive sampling to assess the performance of in-situ treatment and capping remedies for contaminated sediments. The studies have typically been limited to single assessments or in specific easy to access environments. Often the passive sampling has been used only to assess current conditions

and have not been applied to post-remedy performance monitoring. In the proposed work, this gap will be addressed by expanding the range of environments where passive sampling has been used to assess post-remedy performance and to explore novel uses and interpretations of the passive sampling at particular sites. We also have the opportunity to examine long-term (5 – 8 years) performance of these remedies. There has also been limited use of passive sampling to infer contaminant processes that are operative at a site and further work is needed to develop and demonstrate this capability of passive sampling.

1.3. DISSERTATION STRUCTURE

The dissertation is divided into the following chapters:

i. a literature review that will focus on organic legacy pollutants typically found in sediments, partitioning of HOCs between various environmental compartments with a focus on sediment porewater, contaminant transport modelling in caps, passive sampling strategies for monitoring remedial effectiveness, and finishes with the use of performance reference compounds in determining equilibrium between the passive sampler and adjacent sediment

ii. the development of a mathematical modeling approach to evaluate the effect of non-equilibrium loading of performance reference compounds on the estimated equilibrium of target compounds in passive samplers

iii. the novel application of a high density of LDPE passive samplers placed at the sediment-water interface as a mapping tool to identify likely source areas at historical disposal locations for contaminated sediments

iv. the application of PDMS using SPME sampling devices to estimate groundwater upwelling from the release of performance reference compounds to infer long-term remedial effectiveness of a sediment cap at a tidally influenced shoreline

v. the application of PDMS using SPME a field study within the West Branch of the Grand Calumet River (Hammond, Indiana) with a focus on the statistical significance of long-term contaminant profile changes from the sampled years and modelled remedy performance of the organophilic clay cap liner

vi. the application of in-situ passive samplers for evaluating a pilot test on the use of varying activated carbon amendments for long-term remedy performance

vii. a summary of research objectives, conclusions of previous chapters, and recommendations for future research work in this field of study.

1.4. REFERENCES

Apell, J. N., & Gschwend, P. M. (2016). In situ passive sampling of sediments in the Lower Duwamish Waterway Superfund site: Replicability, comparison with ex situ measurements, and use of data. *Environmental Pollution*. https://doi.org/10.1016/j.envpol.2016.08.023

Burgess, R. M., Environmental Protection Agency, U., of Research, O., Human, N., Health Research Laboratory, E., Ecology Division, A., & Island, R. (2012). *Guidelines for Using Passive Samplers to Monitor Organic Contaminants at Superfund Sediment Sites*.

Cornelissen, G., Pettersen, A., Broman, D., Mayer, P., & Breedveld, G. D. (2008). Field testing of equilibrium passive samplers to determine freely dissolved native polycyclic aromatic hydrocarbon concentrations. *Environmental Toxicology and Chemistry*, *27*(3), 499–508. https://doi.org/10.1897/07-253.1

Greenberg, M. S., Chapman, P. M., Allan, I. J., Anderson, K. A., Apitz, S. E., Beegan, C., Bridges, T. S., Brown, S. S., Cargill, J. G., McCulloch, M. C., Menzie, C. A., Shine, J. P., & Parkerton, T. F. (2014). Passive sampling methods for contaminated sediments: risk assessment and management. In *Integrated environmental assessment and management*. https://doi.org/10.1002/ieam.1511

Hawthorne, S. B., Jonker, M. T. O., Van Der Heijden, S. A., Grabanski, C. B., Azzolina, N. A., & Miller, D. J. (2011). Measuring picogram per liter concentrations of freely dissolved parent and alkyl PAHs (PAH-34), using passive sampling with polyoxymethylene. *Analytical Chemistry*, *83*(17), 6754–6761. https://doi.org/10.1021/ac201411v

Jonker, M. T. O., & Koelmans, A. A. (2001). Polyoxymethylene solid phase extraction as a partitioning method for hydrophobic organic chemicals in sediment and soot. *Environmental Science and Technology*, *35*(18), 3742–3748. https://doi.org/10.1021/es0100470

Maruya, K. A., Zeng, E. Y., Tsukada, D., & Bay, S. M. (2009). A passive sampler based on solid-phase microextraction for quantifying hydrophobic organic contaminants in sediment pore water. *Environmental Toxicology and Chemistry*, *28*(4), 733–740. https://doi.org/10.1897/08-322R.1

Mayer, P., Parkerton, T. F., Adams, R. G., Cargill, J. G., Gan, J., Gouin, T., Gschwend, P. M., Hawthorne, S. B., Helm, P., Witt, G., You, J., & Escher, B. I. (2014). Passive sampling methods for contaminated sediments: scientific rationale supporting use of freely dissolved concentrations. In *Integrated environmental assessment and management*. https://doi.org/10.1002/ieam.1508

National Academies. (2003). Bioavailability of contaminants in soils and sediments: Processes, tools, and applications. In *The National Academies Press, Washington*. https://doi.org/10.17226/661

Reible, D. D. (2014). Contaminant Processes in Sediments. In *Processes, Assessment and Remediation of Contaminated Sediments*. https://doi.org/10.1007/978-1-4614-6726-7

Thomas, C., Lampert, D., & Reible, D. (2014). Remedy performance monitoring at contaminated sediment sites using profiling solid phase microextraction (SPME) polydimethylsiloxane (PDMS) fibers. *Environmental Sciences: Processes and Impacts*. https://doi.org/10.1039/c3em00695f

U.S. Environmental Protection Agency. (2005). Contaminated sediment remediation guidance for hazardous waste sites. In *Office of Solid Waste and Emergency Response*.

United States Environmental Protection Agency. (2012). *Equilibrium partitioning sediment benchmarks (ESBs) for the protection of benthic organisms: procedures for the determination of the freely dissolved interstitial water concentrations of nonionic organics. EPA-600-R-02-012*. *December*, 65. http://www.epa.gov/nheerl/download_files/publications/RB ESB 2012final_2.pdf

Wilson, D. J., Clarke, J. H., Reible, D. D., & Mutch, R. D. (2018). Contaminant Transport and Behavior in the Subsurface. In *Hazardous Waste Site Soil Remediation* (pp. 1–49). CRC Press. https://doi.org/10.1201/9780203752258-1

CHAPTER 2

LITERATURE REVIEW

2.1. HYDROPHOBIC ORGANIC COMPOUND CONTAMINATION IN SEDIMENTS

The dissolved phase concentrations provide insight into the fraction of the contaminants that are available to biological organisms, or bioavailability. Bioavailable contaminants can be defined as those that directly relate to observed organism effects (National Academies, 2003). Varying bioavailability can be associated with physical or chemical sequestrating processes occurring within the sediment or colloidal organic matter and the freely dissolved concentration provides an indication of HOCs not associated with these sequestering phases. Assessment of what is bioavailable can lead to better measures of what is truly protective (United States Environmental Protection Agency, 2012). An early approach to estimate the availability of HOCs in contaminated sediments used contaminant concentrations normalized to organic carbon content and organic carbon porewater partitioning coefficients (Di Toro et al., 1991). This did not fully account for differences in availability (United States Environmental Protection Agency, 2012). Although HOCs typically partition to organic carbon, there is great variability in the characteristics of that carbon. Among these different forms are organic carbon in its more condense crystalline forms (e.g., black carbon, soot, char) as well as amorphous natural organic matter and understanding that variability in carbon has assisted in understanding bioavailability (Ghosh et al., 2003). To address the separate forms of organic carbon in sediments a two-carbon model was introduced to incorporate black carbon along with natural organic carbon for making equilibrium partitioning estimations (United States Environmental Protection Agency, 2012).

An alternative approach to assessing partitioning to the various carbon phases is simply measuring the concentration in the interstitial water. Interstitial water (porewater) is the water occupying the spaces between sediment or soil particles. Traditional methods for the measurement of contaminants in porewater involve the sample collection and extraction of large volumes of porewater to meet the detection limits for HOCs (ASTM, 2008). It is rarely possible to extract that much porewater without disturbing the soil or sediment which can alter the porewater concentration and the distribution of natural organic matter between the solid phase and the interstitial water. In addition natural organic matter binding with the contaminant can lead to the overestimation of the freely dissolved porewater concentration which has been found to be most directly related to partitioning from the solids and availability (Berry et al., 2003).

2.2. PASSIVE SAMPLING METHODS

Passive samplers began to emerge as a viable option for contaminated sediment monitoring due to the ability to measure the freely dissolved concentration directly. The three most common polymers used for passive sampling can be found in Figure 2-1.

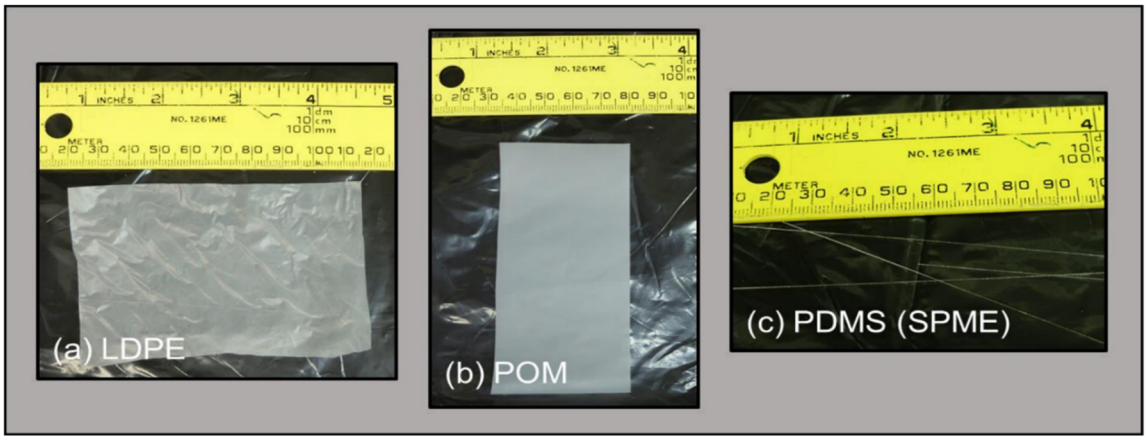

Figure 2-1 Images of passive samplers discussed in this document: (a) LDPE at 25 µm thickness, (b) POM at 76 µm thickness, and (c) PDMS which is shown in a SPME configuration at 30 µm coating thickness around a 500 µm inner diamter

Passive samplers have the versatility to assess the bioavailability of contaminants in the lab (ex-situ) and in the field (in-situ) by simply exposing the polymer to the sediments and allowing the contaminant to absorb and concentrate the contaminants. Although there are benefits of simplicity and control in an ex-situ analysis (Ghosh et al., 2014; Gschwend et al., 2011; Hawthorne et al., 2009), it cannot capture field conditions such as vertical profiles of contamination or effects of upwelling or isolated source areas. In addition, concentrations in the interstitial water are often so low that they cannot be determined with concentration. After retrieval from either an in-situ or ex-situ exposure a solvent is used to extract the absorbed contaminant off the sampler. The mass of contaminate on the polymer (C_p) is quantified by extraction into a solvent and analyzed. Typical analytical methods are performed on a gas chromatograph coupled with mass spectrometry (GC/MS) or a high-performance liquid chromatography (HPLC) for HOCs. The analytical detection limits can be manipulated by controlling the mass or volume of polymer to be analyzed and the final volume of solvent extract.

The mass on the polymer is calculated based on the mass of contaminant accumulated from the sediment which is dependent upon the pore water concentration and the mass of sorbent as well as the volume of solvent used to extract the contaminants (2.1).

$$C_p = \frac{A * RSF_{HOC} * V_s}{L_f * V_f} \quad (2.1)$$

Where A represents the integration area from the analytical instrument (e.g., GC/MS), RSF_{HOC} is the response factor from a standard calibration curve unique to each chemical class of HOCs, V_s is the volume of solvent used, and V_f is the volume of fiber per L_f, or length of fiber. Once the concentration on the fiber is determined the polymer-water partitioning coefficient (K_{pw}) can relate that to the concentration in the porewater. The K_{pw} relationship for PAHs and PCBs on PDMS is shown in (2.2) and (2.3), respectively. Ghosh et al., (2014) also offers polymer-water partitioning coefficients for POM and LDPE targeting PCBs and PAHs.

$$PAH\text{: } \log(K_{pw}) = 0.725 * \log(\mathrm{K_{ow}}) + 0.479 \quad (2.2)$$

$$PCB\text{: } \log(K_{pw}) = 0.947 * \log(K_{ow}) - 0.017 \quad (2.3)$$

To capture the freely available concentration the methodology needs to account for the extent of equilibrium of the target compounds achieved during the period of exposure. Performance reference compounds (PRCs) are typically incorporated in passive samplers to indicate the degree of non-equilibrium. PRCs are typically non-native compounds chemically similar to the target HOCs preloaded to the polymer before deployment (e.g., C^{13} labeled PCBs or deuterated PAHs). Uptake of the target

compounds to the polymer is inversely related to the transport of PRCs off of the polymer (Ghosh et al., 2014) if the process of PRC release and target compound loading are assumed reversible. The ratio of PRCs remaining after retrieval of the sampler compared to the concentration before deployment determines the fractional approach to steady state (f_{ss}) of the target HOCs. It is this extent of equilibrium needed to account for the inherent variability witnessed in contaminated sediments to measure the freely dissolved porewater concentration (C_{pw}), shown in (2.4).

$$C_{pw} = \frac{C_p}{K_{pw} * f_{ss}} \tag{2.4}$$

With in-situ remedies such as capping (active or conventional) bulk solid concentrations are typically unchanged, and the freely dissolved concentration should be considered as the main line of evidence when assessing remedial performance. Rakowska et al., (2012) provides useful information on the use of activated carbon as an in-situ sediment treatment or cap amendment. Rakowska (2014) also performed research to explore ex-situ extraction of hydrophobic organic contaminants in sediment by granular activated carbon compared to in-situ applications. The efficiency assessed by the granular activated carbon was quantified by the use of PDMS using SPME inserted into the sediment layer.

Passive samplers, specifically SPME using PDMS, have been used to measure contaminate migration through inert sandy caps (Lampert et al., 2011; Thomas et al., 2014). Although sediment cores can be evaluated to interpret HOC migration within a cap, and the physical thickness of each layer of the cap can be identified, laboratory

evaluations may not adequately characterize migration through groundwater upwelling or hyporheic exchange (Ghosh et al., 2014; D. D. Reible, 2014).

Reible et al., (2006) demonstrated the usefulness of inspecting sediment cores from an active capping demonstration at the Anacostia River in Washington D.C., but the bulk sediment concentration analyzed after 6, 18, and 30 months was abandoned in favor of direct passive sampling of porewater for PAHs performed by Lampert et al., (2013). The porewater data analyzed years later was able to show some migration through the caps. Forty-four months after the initial cap placement of sand, coke breeze (a carbon sorbent), and AquaBlok™ (a low permeability clay cap material), SPME PDMS porewater samplers indicated non-zero concentrations throughout the cap (Lampert et al., 2013). Because of the non-sorbing nature (sand) of the bulk of the cap layers, solid concentrations were not able to indicate migration.

A different approach was conducted by Beckingham & Ghosh (2013), where coupons of POM were exposed to the sediment-water interface and into the water column to monitor changes in bioavailability of PCBs after AC placement. Passive sampling was conducted in 2006, immediately after AC placement, and at yearly monitoring events in 2007, 2008, and 2009. The study showed concentrations in the water column to be similar each year indicating a well-mixed system, but the samplers exposed at the interface indicated a response to the AC amendment. When compared to pre-amendment conditions, the freely dissolved concentration at the interface were reduced by 96%, 91%, and 82% in the 2007, 2008, and 2009 sampling events, respectively. It was assumed the decrease in remedial effectiveness was from AC mixing into the deeper sediment

(potentially via bioturbation) and newly deposited sediment place on top. POM was also used in other efforts to measure diffusive transport of HOCs in sediments to the overlying water column (Fernandez et al., 2014).

Thomas et al. (2014) evaluated the remedy performance of clean sediment material using SPME PDMS passive samplers at the Eagle Harbor Superfund site (Bainbridge Island, WA) as well as an AquaBlok™ clay cap at Chattanooga Creek (Chattanooga, TN). The interpretation of the SPME depth profiles at Chattanooga showed good separation of the contaminant in the cap layer versus the contaminated layer below. Thomas et al. (2014) showed similar profiles both soon after capping and 12-months later showing continued isolation by the cap.

Ongoing costs of contaminant monitoring at Superfund sites can be better managed when targeting areas that would results in the greatest environmental improvement (Greenberg et al., 2014). Apell & Gschwend (2016), with the help of the U.S. Environmental Protection Agency (EPA) Dive Team, deployed 10 cm x 50 cm polyethylene sheets housed in an aluminum frame to infer transport of PCBs into the overlying water. A relative standard deviation (RSD) was determined for each sample duplicate and each PCB congener pair (n = 225 and 522, respectively). The RSD precision ranged from 22% to 43% for the individual congeners. Where only 9% of duplicate pairs (n = 47/522) showed differences of greater than a factor of two. Indicating the reproducibility of passive sampler data can build greater confidence in its use for evaluating remedial performance. Researchers have explored the use of various polymeric passive samplers to monitor in-situ remedial performance within the upper

sediment layers (Amstaetter et al., 2012; Cornelissen et al., 2011, 2016; Eek et al., 2008). These vertical pore water profiles have shown good agreement among the measurement and calculated methods (Abel & Akkanen, 2018; Patmont et al., 2015; Thompson et al., 2015) providing a driving force for continued remedial monitoring from porewater measurements derived from polymeric passive samplers. Despite these early efforts, however, there have been limited demonstrations of passive sampling to assess the long-term performance of in-situ sediment remedies at contaminated sediment sites. Yan et al. (2020) evaluated the performance after 14-months of an activated carbon treatment layer at Hunter's Point Naval Shipyard using profiling PDMS passive sampling. They showed excellent performance of the activated carbon in both a Sedimite™ and Aquagate™ form. Sedimite™ and Aquagate™ are commercial formulations of activated carbon designed to allow the placement of powdered activated carbon by binding with a carrier phase of clays and biopolymers. Schaanning et al. (2021) examined the remedy performance of a sediment cap with clay and activated carbon over 9 years (2009-2018). Caps of clay mixed with AC reduced dioxin uptake by 69-88% during the first two years, decreasing to 54-61% nine years after cap placement. These efficiencies compared well with efficiencies reported from other field and mesocosm studies performance over much shorter periods of time (Adams et al., 2007; Khairy & Lohmann, 2020).

2.2.1 Standardized Practices

Contaminant bioavailability is a central issue in sediment risk assessment and management, and potential exposure to sediment-associated contaminants is best characterized and estimated by focusing on the freely dissolved porewater concentration measured by passive samplers. These samplers afford a unique opportunity for improving

the current state of the science used in assessment and management of contaminated sediments and practical guidance is routinely needed for further acceptance (Ghosh et al., 2014; Greenberg et al., 2014; Lydy et al., 2014; Mayer et al., 2014; Parkerton & Maruya, 2014). According to regulatory investigations passive samplers are best suited for legacy, nonpolar organic contaminants (National Academies, 2003; USEPA, 2012a; USEPA, 2012b). However, some limitations for the intercomparison of passive sampler data from these studies may exist, in part, from the absence of a standard approach for evaluating data. For HOCs the United States Environmental Protection Agency (USEPA) has provided guidance documents on the use of passive samplers (Burgess et al., 2017; USEPA, 2012) for the protection of the benthic community and higher trophic level organisms, yet research still yields comparisons to bioconcentration factors (S. Wang et al., 2020), whereas others report lipid normalized body residues (Khairy & Lohmann, 2020). These methods are expected to produce consistent predictive relationships, however, standardization and comparative studies would lead to improved confidence in the method for management applications (Greenberg et al., 2014).

The use of commercially available polymers (Figure 2-1) is helpful for standardization as it consolidates efforts, reduces uncertainty, and the fact they are commercially available can aide in the feasibility of interlaboratory standardization practices (Ghosh et al., 2014). One of the largest, to date, was performed by Jonker et al. (2018) where eleven research laboratories from four different countries (U.S.A., The Netherlands, Norway, and the Czech Republic) participated in a interlaboratory standardization practice for monitoring HOCs in sheet polymers (e.g., LDPE and POM) and PDMS using SPME fibers. Each laboratory had a proven history in passive sampling

in sediments and contributed to the study by applying its own passive sampling procedures from previously published peer-reviewed literature in hopes to further the acceptance of the design of sediment management approaches despite largely being used in a scientific laboratory setting. Relative standard deviations (RSDs) of the 5-fold measurements for sheet polymers (e.g., POM and LDPE) were <5% while for PDMS using SPME RSDs were somewhat higher with values increasing with decreasing coating thickness (i.e., RSDs 10 μm > 30 μm > 100 μm > sheets). Overall, the authors felt the study concluded that passive sampling is ready for implementation in actual risk assessment and management practices of contaminated sediments. More recently Michalsen et al., (2021) continued these efforts to standardize polymer sampler procedures for quantifying the freely dissolved concentration in contaminated sediment porewater by multiple participating public- and private-sector analytical laboratories, Texas Tech University being one, thereby increasing commercial availability, promoting wider acceptance, and increased use. By documenting method accuracy, the reliability of passive samplers can be demonstrated in hopes to dramatically improve regulatory acceptance. For these significant contributions Michalsen et al., (2021) received the 2021 ESTCP Project of the Year Award for Environmental Restoration.

Although passive samplers have progressed to the point where practical application is clearly feasible practical applications still lack when visualizing environmental drivers responsible for contaminant mobility and availability (e.g., porewater upwelling and bioturbation). Additional guidance on the use of performance reference compounds would aid in the above-mentioned standardization practices.

2.3. PERFORMANCE REFERENCE COMPOUNDS

The use of PRCs suggest that PRC desorption and target contaminant uptake is linear and reversible. If it is assumed that desorption of PRCs and sorption of target compounds is controlled by external mass transfer resistances and the polymer geometry is in the form of flat sheets (e.g. LDPE), the fractional approach to steady state for the uptake of target compounds ($f_{ss-target}$) is governed by (2.5) derived from Lampert et al. (2015).

$$f_{ss-target}(t) = 1 - \exp\left(\frac{RDt}{L^2 K_{pw}^2}\right) erfc\left(\frac{\sqrt{RDt}}{LK_{pw}}\right) \tag{2.5}$$

This model shows that fractional approach to steady state relies on the volume-to-surface-area ratio of the sorbent, L, the polymer-water partitioning coefficient (K_{pw}) to account for contaminant specific hydrophobicity, and is dependent on time, t. Lastly, RD is an effective transport parameter containing the retardation factor (ratio of total concentration in the media to concentration in the water phase), R, and the effective diffusivity, D, for the surrounding media. The retardation factor characteristically scales linearly with the octanol-water partitioning coefficient, while D is, at most, only weakly dependent on the target compound. Thus RD should be linearly related to K_{ow} (D. D. Reible, 2014) and can be fit to the PRC data to develop a model capable of predicting f_{ss}.

Models are typically used to interpret the PRC release to estimate equilibration of homologous compounds (Fernandez, Harvey, et al., 2009; Lampert et al., 2015; Shen & Reible, 2019). Fernandez et al. (2009) offers a one-dimensional sorption-diffusion model in an infinite sediment bed to predict the fate and transport of PRCs and target compounds. Tcaciuc et al. (2015) modeled the transfer of chemicals from a well-mixed

infinitely large water body through a water boundary layer, where internal diffusion would dominate, while Lampert et al. (2015) explored the internal and external resistance to the one-dimensional model to develop site specific partitioning coefficients, assuming external resistances dominate. These models are limited to rectangular sheets of LDPE, PDMS and POM. Although PDMS fibers have a thin coating around a cylindrical geometry, the geometry if effectively flat as long as the concentration boundary layer outside of the fiber is small compared to the diameter of the fiber (D. J. Lampert et al., 2015). If the radius of influence of the sampler extends to distances similar to the radius of the fiber the curvature of the PDMS becomes important. Shen & Reible (2019) have addressed this concern by providing the fractional approach to steady state for short-time approximations both by a numerically inverted Laplace domain solution and an asymptotic analytical solution by a modified Bessel function. The solution in the Laplace domain can be inverted numerically to generate estimates of PRC release and target compound uptake (2.6) and (2.7), respectively.

$$f_{ss-target} = 1 - \frac{1}{2}\left(\left(\frac{1}{\omega}+1\right)e^{(1+\omega)^2\frac{\tau}{\xi^2}}erfc\left((1+\omega)\frac{\sqrt{\tau}}{\xi}\right)\right. \\ \left. -\left(\frac{1}{\omega}-1\right)e^{(1-\omega)^2}\frac{\tau}{\xi^2}erfc\left((1-\omega)\frac{\sqrt{\tau}}{\xi}\right)\right) \tag{2.6}$$

Where;

$$\xi = \frac{K_{pw}}{R}(1-\delta^2), \qquad \omega^2 = 1-\xi, \qquad \tau = \frac{Dt}{RL_0^2} \tag{2.7}$$

Equilibrium mass loading in the thin polymer layer relative to the displaced sediment is represented by ξ, while τ defines the effective diffusion rate in the surrounding media. Both parameters involve the retardation by sorption in the surrounding media. By characterizing the molecular fate and transport within the system over time, the freely dissolved porewater concentration can be evaluated over a specific depth interval (2.4).

2.4. CONTAMINANT TRANSPORT MODELING IN CAPS

Contaminant transport processes provide evidence of dominant environmental drivers by which the magnitude and spatial extent can be observed, but also the extent of future contaminant exposures for the site and remedial design can be considered. Contaminant fate and transport pose many challenges in the assessment of remedial options, some of which include understanding the geological make-up of the environmental media, determining the specific location(s) that are sources of concern, and remediating those areas to reduce contaminant exposures. Overall, these transport processes play a large role in determining the pattern and magnitude of future exposures which is why a comprehensive conceptual site model is needed (Greenberg et al., 2014; National Academies, 2003; Reible, 2014).

To combat this historical release of contaminants into the environment, and shelter the increasing expenses of dredging operations, a proposed barrier which had to include a sufficiently thick layer of sediment, i.e., cap, could isolate the contaminant from the aquatic ecosystem (U.S. Army Corps of Engineers, 1979). To appropriately assess the remedial effectiveness of caps, numerical models are needed that are able to predict the relationship of design parameters and remedial objectives (Go et al., 2009; Murphy et al.,

2006). Predicting chemical migration through porous media is normally accomplished using transient advection-diffusion models (Eek et al., 2008), as it is generally appropriate to assume a cap is composed of multiple homogenous layers that can be modeled with a series of equations like those found in (2.8) (Reible, 2014).

$$R_i \frac{\partial C_i}{\partial t} - U \frac{\partial C_i}{\partial z} = D_i \frac{\partial^2 C_i}{\partial z^2} - \varepsilon_i \lambda_i C_i \tag{2.8}$$

The subscript refers to the layer number and the variables represent.

C_i = porewater concentration in Layer i

z = depth downward from the cap-water interface

t = time

R_i = retardation factor in Layer i

U = effective advective velocity (assumed upward, though can be negative)

D_i = effective diffusion coefficient in Layer i

ε_i = porosity in Layer i

λ_i = decay rate constant in Layer i (assumed only in the porewater)

However, in many instances it is not possible to find exact solutions to the transport equation of the form shown in (2.8). Numerical simulation allows for non-linear sorption and multiple cap layers of varying geochemistry in addition to environmental transport processes such as porewater upwelling , hyporheic exchange, bioturbation including particle mixing, etc. Such a model has been made publicly available for the purpose of cap design, CapSim®, and although a brief description is provided below a more thorough description of the software can be found in Shen et al. (2018).

The user begins by selecting a compounds or class of chemicals desired to model within a particular system made up of multiple geologic layers. Once the user has defined each layer of the simulation (e.g., sand, activated carbon, native sediment), sorption in each layer can be characterized by specifying the sediment partition coefficient, K_d, through the estimation of K_{oc} and f_{oc} (organic carbon partitioning coefficient and fraction of organic carbon, respectively), experimental data, or using nonlinear Langmuir or Freundlich isotherm to estimate K_d for sorptive layers. For the following examples of environmental processes equilibrium kinetics will be assumed, however, should the user want to determine the contaminant transport in a cap before the contamination reaches the bioturbation layer a transient model can be employed (Go et al., 2009; Lampert et al., 2015). By assuming the cap is infinitely thick and the concentration in the underlying sediment is constant at the bottom boundary layer the concentration profile can be modelled by Van Genuchten (1981). Note that the assumption of a constant concentration at the bottom boundary layer results in a non-depletive mass from the underlying sediment.

The layers are then assembling beginning with the layer closest to the sediment-water interface. The dispersion coefficient is often expressed as the product of the Darcy Velocity, V, and hydrodynamic dispersivity, α, that is expressive of the heterogeneity in the medium ((2.9)).

$$D_{disp} = \alpha V \tag{2.9}$$

Since the dispersion is thought to describe the large-scale motion of microscopic difference in the media, α is claimed to be dependent on the length scale of the

movement (Wilson et al., 2018). For example, the movement of a non-aqueous phase liquid (NAPL) through one foot of sediment will not disperse in the same manner when moving through ten feet of the same material. In the absence of site specific information, a conservative estimate would be to scale the dispersivity with the cap thickness at roughly 10% of the cap thickness (Clarke, 1993).

Typically, in porous media containing spheres (e.g., sand) within an unsaturated media the Millington-Quirk diffusion model is appropriate (Millington & Quirk, 1961), while materials that are well consolidated (e.g., silt/clay) particle movement through the cap can be projected by Fick's First Law to estimate solute fluxes through fine-grained unlithified sediments (Boudreau, 1996). Researchers have demonstrated the efficacy of sand caps to mitigate environmental risks associated with sediments provided the depth exceeds that of bioturbation by benthic organisms and substantial groundwater upwelling does not occur (Fernandez et al., 2014; Lampert et al., 2011; Reible et al., 2006; Steevens et al., 2020). Conversely, in environments with substantial upwelling, amended caps or in-situ treatment with sorptive materials such as organoclay (Cornelissen et al., 2011; Ghosh et al., 2003; Schaanning et al., 2021; Steevens et al., 2020), or activated carbon (Kupryianchyk et al., 2013; Lin et al., 2014) have been employed to improve the efficacy of the remedy. Sometimes the activated carbon may be placed within a capping material such as sand to aid retention of the relatively light material (Gidley et al., 2022).

The following section will provide four CapSim® simulations to observe what effect various environmental processes have on the porewater concentration. Porewater

concentration depth profiles of phenanthrene and benzo(a)pyrene, spanning a range of hydrophobicity, are considered in each scenario.

2.4.1 DIFFUSION WITH BIOTURBATION IN AN INERT LAYER

A common approach to modeling the effect of the benthic community through bioturbation is to assume the mixing is random and can be modelled by Fick's First Law of diffusion with a compound-independent bio-diffusion coefficient, D_{bio}. Bioturbation is commonly characterized as an expected depth and mixing intensity (Boudreau, 1996; Boudreau & Jørgensen, 2001). Note that unlike hyporheic exchange, which involves the movement of only porewater, bioturbation often involves the movement of solid mass (particles) and porewater at the interface due to organism burrowing and ingestion and defecation of sediment deposits. Which can be written in terms of porewater concentration, C_{pw}, in (2.10).

$$F_{bio} = -D_{bio} R \frac{\partial C_{pw}}{\partial x} \tag{2.10}$$

Where;

F_{bio} = flux of a solute with a total concentration in the "x" direction

D_{bio} = bio-diffusion coefficient

R = Retardation factor relating the bulk density and porosity to C_{pw}

In lieu of experimental data, Thoms et al. (1995) provides a summary of measured bio-diffusion coefficients and the depth of bioturbation at a number of sites throughout the United States.

In Figure 2-2 and Figure 2-3 a depth dependent bioturbation model is examined to understand the behavior of phenanthrene and benzo(a)pyrene in an inert sand layer. Due to the sediment and sand-gravel layers, relative to the depth microorganisms can disturb, we examine the change in porewater concentration over time of a thin sand/gravel cap being placed at the surface ($C_{pw-cap} = 0$ at $t = 0$).

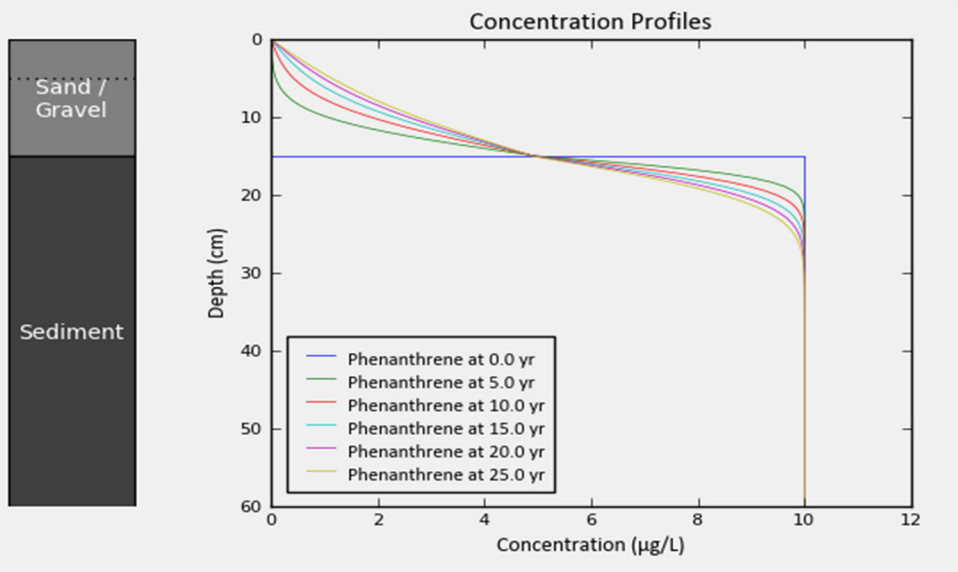

Figure 2-2 CapSim simulation of bioturbation effects on Phenanthrene with a 10 µg/L flux-matching porewater concentration beneath a 15-cm thick inert sand / gravel cap

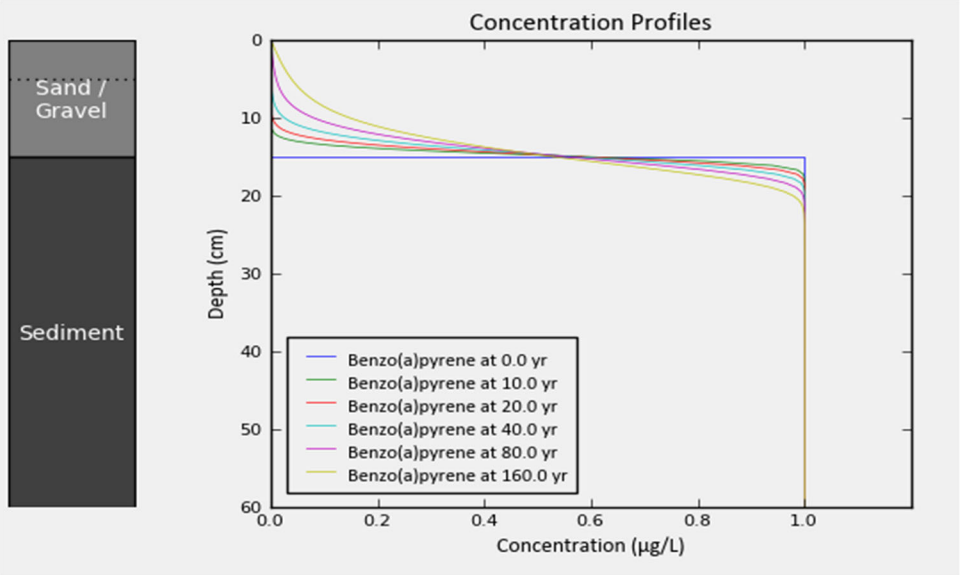

Figure 2-3 CapSim simulation of bioturbation effects on Benzo(a)pyrene with a 1 µg/L flux-matching porewater concentration beneath a 15-cm thick sand / gravel cap

The Gaussian model coefficients for bioturbation assumes a normal distribution, that 68% of the bioturbation depth will occur within one standard deviation of the intensity distribution provided. Considering particle size impact for the layer material. The above simulation mimics a stagnant freshwater system based on the geometric mean of found in Thoms et al. (1995).

Reworking of the surficial sediments causes the inert cap layer to show varying behaviors between phenanthrene ($\log(K_{ow}) = 4.57$) and benzo(a)pyrene ($\log(K_{ow}) = 6.04$) over varying timescales. For strongly hydrophobic contaminants the dominant mechanism of contaminant transport is due to particle transport and the flux is insensitive to porewater pumping. Notice the difference in pumping within the sand/gravel cap layer (15-cm thickness) for benzo(a)pyrene, likely due to the increase sorption capacity compared to diffusional transport dominated phenanthrene.

2.4.2 GROUNDWATER UPWELLING IN AN INERT LAYER

In a stable sediment bed, the transport processes within the mobile phase of the porewater in sediments becomes dominated by particle diffusion, dispersion and advective processes (2.8). Unlike diffusion and dispersion, advection can be a far more rapid mechanism of contaminant transport. These discharges typically display significant spatial and temporal variability making assessments difficult (Burnett et al., 2006). The flow of water in sediments may be upward or downward depending upon local groundwater gradients or both in the case of tidal systems.

The nearshore portions of rivers are common groundwater discharge areas giving rise to upwelling in the sediment. Upwelling can be detrimental to the life span of an engineered cap and an armoring layer may be justified. The advective flux is related to the upwelling velocity, U, times the porewater concentration, C (2.11).

$$F_{adv} = UC \tag{2.11}$$

Should these methods not be available the flow may be modeled using Darcy's Law. This relates the flow per unit area through a porous media subject to a hydraulic gradient, i, multiplied by the hydraulic conductivity, k_h (2.12).

$$U = k_h i \tag{2.12}$$

This calculation of the Darcy Velocity should be carefully considered based on the site-specific geology and cap material. As some commercially available cap materials (e.g., Aquagate+PAC™) are engineered to displace upwelling of groundwater and avoid this process. Groundwater fluxes can be directly measured by using seepage meters or mini-piezometers (Lee & Cherry, 1979), alternatively, Cook et al. (2003) was able to estimate fluxes through the injection of a tracer.

Greenberg et al. (2002) evaluated the role, following the work of (Lee & Cherry, 1979) through the use of mini-piezometers, of upwelling and downwelling on sediment toxicology and bioaccumulation to more accurately measure contaminant exposure. They found these hydrologic measurements were useful, but noted continuous monitoring may be warranted due to the inherent change in the system due to groundwater recharge (Li et al., 1999) or tidally influenced zones on a shoreline could result in changes in chemical bioavailability (Burnett et al., 2006; Nielsen, 1990). These processes do not necessarily imply failure of a cap, however, where dissolved chemical migration has the potential to pose unacceptable exposures to benthic and surface water biota, modeling chemical transport may be necessary to predict cap performance and to optimize performance by specifying the addition of cap amendments (Cornelissen et al., 2016; Gidley et al., 2012; Danny Reible et al., 2004).

Figure 2-4 and Figure 2-5 show simulations for phenanthrene and benzo(a)pyrene, with a moderate upwelling velocity (100 cm/yr). The cap thickness is doubled (30-cm thickness compared to 15-cm thickness in Figure 2-2 and Figure 2-3) to show the magnitude of upwelling on HOCs.

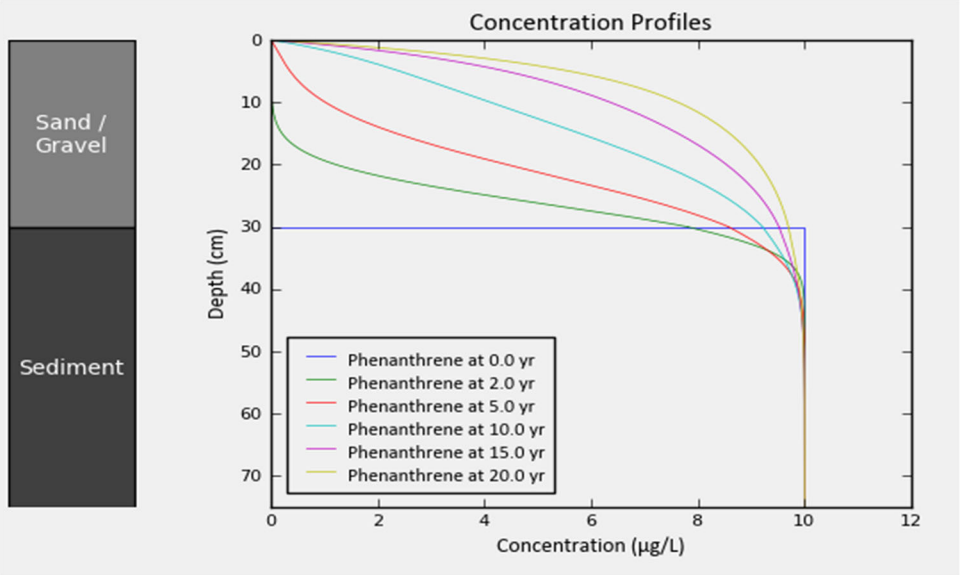

Figure 2-4 CapSim simulated contaminant transport of 10 µg/L phenanthrene in a 30-cm thick sand / gravel cap with a constant upwelling velocity of 100 cm/yr

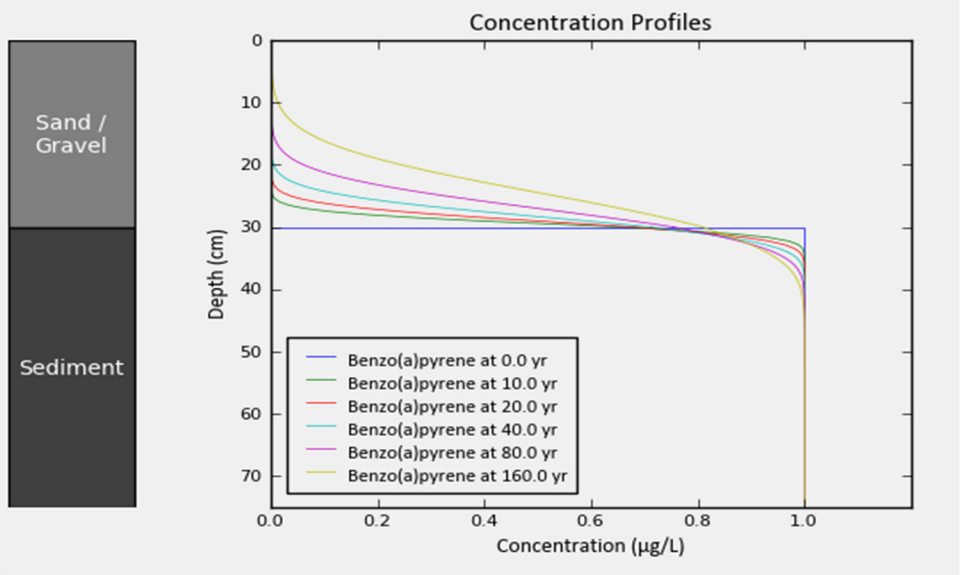

Figure 2-5 CapSim simulated contaminant transport of 1 µg/L benzo(a)pyrene in a 30-cm thick sand / gravel cap with a constant upwelling velocity of 100 cm/yr

The sorption characteristics of inert cap are irrelevant since the cap is designed to contain the underlying sediments. Although in situations where significant groundwater upwelling through a cap is expected we can observe that a 30-cm sand / gravel cap may not suffice for more mobile compounds such as phenanthrene. The course-grained gravel

and permeability of the materials could pose such a problem. At some field sites, regular sand caps may work better than these models would suggest. Certain situations could experience lower discharge rates, more organic carbon in the cap, dilution of porewater near the surface with overlying water, and the presence of biological activity, especially near the sediment-water interface. These simulations show that in the absence of organic carbon in the sand/gravel cap, and in the presence of significant groundwater advection, there can be breakthrough of dissolved PAHs in a relatively brief period of time. Reinforcing the idea that cap efficacy is better monitored by measuring the porewater concentration than by measuring solid core samples that have low sorption capacity (Gidley et al., 2012; Greenberg et al., 2002).

2.4.3 Sorptive Layer with a Thin Organophilic Clay as a Cap Layer

The first term in (2.8) accounts for the accumulation in a control volume and incorporates sorption of the contaminant onto media. When contaminant partitioning is linear, as is the case in clay cap layers, the derivative term in (2.8) has a constant value of K_d. Organophilic clays is a modified bentonite containing such substitutions that has been evaluated for control of non-aqueous phase liquids (NAPLs) and other organic contaminants (D. D. Reible, 2014). The effect of sorption is primarily due to slow porewater processes such as diffusion and advection. The effective partitioning coefficient for phenanthrene and benzo(a)pyrene vary by three log units (Endo et al., 2011). The retardation factor is determined by the rate that HOCs are sorbed to the solid and can be defined by (2.13), where ρ_b refers to the dry bulk density.

$$R = \rho_b K_d \tag{2.13}$$

Where the retardation factor, R, compares the ratio of contaminant in the mobile phase (porewater) to the total mass in the system. The effective advection velocity and diffusivity of the contaminant through sediment or cap material can be much slower for more strongly sorbing compounds. This relationship can be viewed below.

$$U_{eff} = \frac{U}{R} \tag{2.14}$$

$$D_{eff} = \frac{D_s}{R} \tag{2.15}$$

Since R for strongly sorbing compounds can be of the order of 10^3 – 10^6 (Schwarzenbach et al., 2002), this can dramatically slow the migration of contaminants through an organophilic clay (OC) cap layer. Pernyeszi et al., (2006) found that 2,4-dichlorophenol ($\log K_{ow} = 3.06$) was adsorbed effectively onto organoclay in laboratory isotherm experiments and were able to model transport of the solute through an organoclay column using the convection-dispersion equation. The increased adsorbent capacity of these clays is due to their large specific surface areas, and the ability to sequester and retain HOCs at their surfaces has made these materials subject to study in both laboratory and field experiments (Cornelissen et al., 2011; Phillips et al., 1995; Schaanning et al., 2021) as modeled for phenanthrene and benzo(a)pyrene in Figure 2-6 and Figure 2-7, respectively.

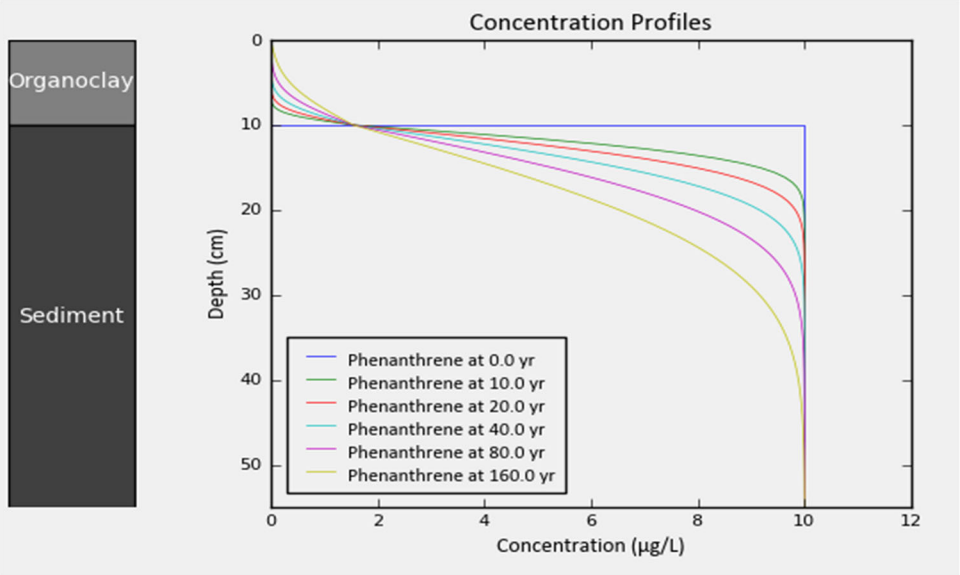

Figure 2-6 CapSim simulation of phenanthrene transport within a 10-cm thick organophilic clay cap layer

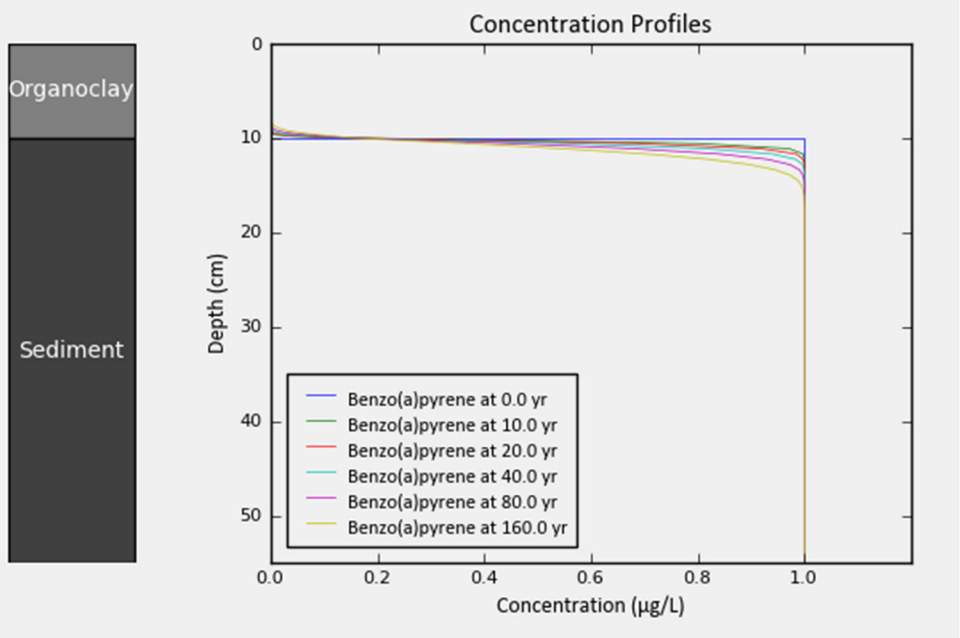

Figure 2-7 CapSim simulation of benzo(a)pyrene transport within a 10-cm thick organophilic clay cap layer

The modeled results did not contain phenanthrene at these concentrations, only after ~100 years. However, mixtures of sand and organoclay would more closely approach batch absorption capacities due to the more effective utilization of the organoclay

(Reible, 2005, 2014). Armoring, however, can occur regardless of whether the bed consists predominantly of cohesive, non-cohesive, or a mixture of the two (i.e., sand and organoclays) (McDonough et al., 2007). The sorptive capacity of organoclays is less than that of activated carbon, although the potential for fouling with natural organic matter is also less (Van Der Heijden & Jonker, 2009). In general, however, activated carbons are more effective sorbents of dissolved HOCs and organoclays are more effective sorbents for NAPLs (Alther, 2002; Hawthorne et al., 2011; Reible, 2014).

2.4.4 Sorptive Layer with a Thin Activated Carbon Layer

The use of capping materials that exhibit greater containment effectiveness than sand is often referred to as active capping. Active capping provides an increased sorption capacity of the cap layer to increase sorption-related retardation of HOCs. Organic contaminants exhibit a wide range of sorption behavior depending on the contaminant type, molecular weight, and corresponding hydrophobicity, as well as the sediment mixing. Activated carbon has been shown to be useful for reducing bioavailability of polychlorinated biphenyls (PCBs) and polycyclic aromatic hydrocarbons (PAHs) (Amstaetter et al., 2012; Cornelissen et al., 2016; Sharma et al., 2009; Thomas et al., 2014; Yan et al., 2020). Researchers have performed scientific analyses on the sorption capacity of activated carbon (Grossman & Ghosh, 2009; Luthy et al., 1997; Murphy et al., 2006; Walters & Luthy, 1984) and experiences where activated carbon has been used as a remedial design alternative (Abel & Akkanen, 2018; Cornelissen et al., 2011; M. I. Rakowska et al., 2012) where these experiments have characterized the effects of competition with other HOCs within the environment.

Sorption to activated carbon is very strong for HOCs and is often subject to non-linear as K_d is a function of concentration (Reible, 2014). This non-linearity for activated carbon amendments is typically described using Langmuir (2.16) or Freundlich sorption isotherms (2.17). This contrasts with what is experienced in organophilic clays, which exhibit linear sorption and minimal competition effects.

$$q = \frac{q_{max} b C}{(1 + bC)} \tag{2.16}$$

$$q = K_f C^{\frac{1}{n}} \tag{2.17}$$

For sorption onto a limited number of specific sites the Langmuir model (2.16) is often used to predict sorption of contaminants. Where q_{max} is the maximum sorption capacity and b is the relative intensity of sorption. Unlike the linear partitioning of HOCs, expected for OC, the value of K_d is a function of concentration and the Freundlich model (2.17) is frequently used to predict q from concentration, C, for activated carbon. Where K_f is the adsorption capacity at a unit concentration and $1/n$ is the adsorption intensity. Typically, for a given carbon, batch experiments are conducted over a desired range of equilibrium concentration to determine the Freundlich or other model parameters (Hawthorne et al., 2009). To better address these concerns of non-linear sorption and other limitations and more realistically describe surficial sediment processes was a driving force in the creation of the software tool for these model, CapSim (Shen et al., 2018).

Below is an example that pulls several of the previously discussed environmental factors into a thin activated carbon cap liner to demonstrate the superior sorption and

containment effectiveness to inert materials, and the usefulness of CapSim in remedial design (Figure 2-8). A cap consisting of 5-cm of activated carbon beneath 25-cm of sand is being considered for a 50-cm layer of sediment contaminated with phenanthrene at a fixed porewater concentration of 10 µg/L. The bioturbation depth is assumed to be 20-cm deep with D_{bio} = 20 cm^2/yr and the upwelling velocity equal to 100 cm/yr. The Freundlich parameters for the activated carbon are K_f = 1.03e+5 µg/kg/(µg/L)^N with N = 0.8, K_d in the sand is 10 L/kg, the f_{oc} of the underlying sediment is 0.01 and the cap materials are expected to be clean ($C_{pw} = 0$ at $t = 0$).

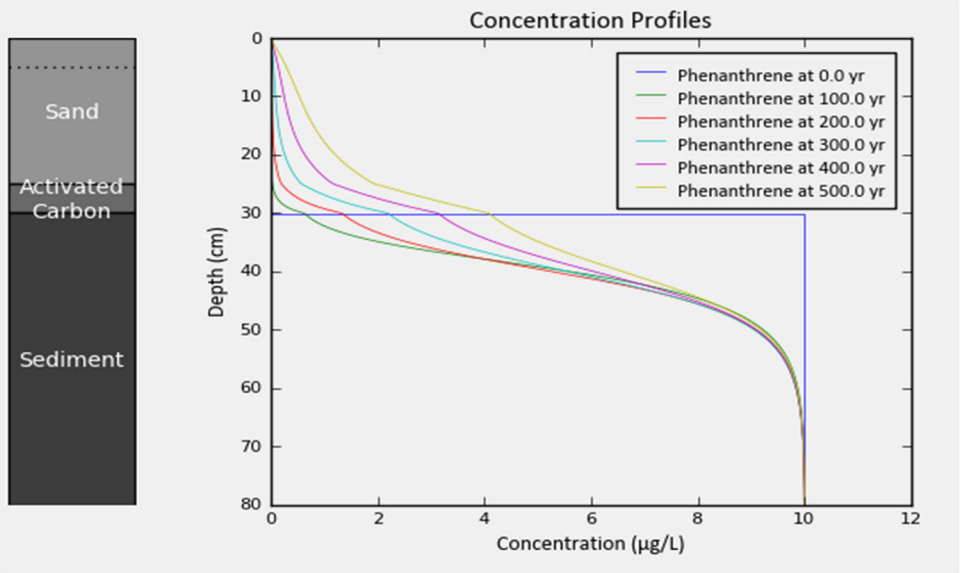

Figure 2-8 Five-hundred-year simulation results for phenanthrene transport within a thin activated carbon layer beneath a sand layer

The concentration in the sediment is depleted in the bottom of the cap. The 5-cm activated carbon layer prevents significant migration for the first ~100 years, after which the contaminant moves through the sand fairly quickly. Notice the change in slope once the compound reaches the bioturbation layer. The use of numerical models allows for the

interpretation of many complexities found at contaminated sediments sites and can be sufficient for theoretical case studies.

2.5. SUMMARY

The use of passive samplers has been developed and studied as a monitoring tool for contaminated sediment management. The ability to measure the truly dissolved, porewater concentration directly aids in investigation and contaminant migration, especially when engineered caps are the remedial design of choice. Taking various inputs, whether derived experimentally or theoretically, can aide in the development of a robust site model capable of modeling the fate and transport of HOCs even before sampling is to be conducted. Sorell & Mcevoy (2013), although mostly point to the work done by the National Research Council (National Academies, 2003), aid in this discussion by promoting bioavailability considerations into multiple stages of site characterization and remedy selection.

Specifically, the work described herein will use passive sampling to assess remedy performance and contaminant transport processes with hopes to aid in the understanding of HOC transport within capped contaminated sediments and further promote best practices of the use of polymeric passive samplers in contaminated sediment management.

The use of performance reference compounds provides valuable insight to the state of equilibration and mobility of target compounds but have also resulted in a state of confusion when loading is incomplete or leads to variable responses. The effort of these studies adds to the literature supporting the use of PRCs for in-situ passive sampling of

sediments by developing and demonstrating an improved approach to monitoring in-situ treatment. Most importantly, these projects, along with the other studies reported in the literature has shown that in-situ passive sampling in sediment beds can provide precise and more accurate estimates of porewater concentrations compared to traditional approaches. The utilization of software program CapSim® can also provide site specific transport models to verify the use of passive sampling and will be explored further in the following chapters.

In the following chapters several applications of passive sampling technologies are utilized to further the current understanding on equilibrium loading in the passive sampler, the extent of equilibration of target compounds when polymeric passive samplers are not at equilibrium, the vertical transport of contaminants within a cap, and the remedial effectiveness of various capping materials by evaluating the passive sampler depth porewater concentration profiles.

2.6. REFERENCES

Abel, S., & Akkanen, J. (2018). A Combined Field and Laboratory Study on Activated Carbon-Based Thin Layer Capping in a PCB-Contaminated Boreal Lake. *Environmental Science and Technology*. https://doi.org/10.1021/acs.est.7b05114

Adams, R. G., Lohmann, R., Fernandez, L. A., Macfarlane, J. K., & Gschwend, P. M. (2007). Polyethylene Devices: Passive Samplers for Measuring Dissolved Hydrophobic Organic Compounds in Aquatic Environments. *Environmental Science & Technology*, 1317–1323. https://doi.org/10.1021/es0621593

Alther, G. R. (2002). Removing oils from water with organoclays. *American Water Works Association*, *94*(7), 115–123. https://www.proquest.com/docview/221608868?accountid=7098&parentSessionId=lj8ISan1sFEPW3%2FpChgnEfHTtS2easrLtayKkZ5idgY%3D&pq-origsite=primo

Amstaetter, K., Eek, E., & Cornelissen, G. (2012). Sorption of PAHs and PCBs to activated carbon: Coal versus biomass-based quality. *Chemosphere*. https://doi.org/10.1016/j.chemosphere.2012.01.007

Apell, J. N., & Gschwend, P. M. (2016). In situ passive sampling of sediments in the Lower Duwamish Waterway Superfund site: Replicability, comparison with ex situ measurements, and use of data. *Environmental Pollution*. https://doi.org/10.1016/j.envpol.2016.08.023

ASTM. (2008). E1367-03 (redline) - Standard test method for measuring the toxicity of sediment-associated contaminants with estuarine and marine invertebrates. *Annual Book of ASTM Standards: Waters and Environmental Technology*. https://doi.org/10.1520/E1367-03R08

Beckingham, B., & Ghosh, U. (2013). Polyoxymethylene passive samplers to monitor changes in bioavailability and flux of PCBs after activated carbon amendment to sediment in the field. *Chemosphere*, *91*(10), 1401–1407. https://doi.org/10.1016/j.chemosphere.2012.12.074

Berry, W. J., Burgess, R. M., & Hansen, D. J. (2003). Procedures for the Derivation of Equilibrium Partitioning Sediment Benchmarks (ESBs) for the Protection of Benthic Organisms: PAH Mixtures. *Environmental Protection Agency*.

Boudreau, B. P. (1996). The diffusive tortuosity of fine-grained unlithified sediments. In *Geochimica et Cosmochimica Acta* (Vol. 60, Issue 16, pp. 3139–3142). Elsevier Ltd. https://doi.org/10.1016/0016-7037(96)00158-5

Boudreau, B. P., & Jørgensen, B. B. (2001). The Benthic Boundary Layer: Transport Processes and Biogeochemistry - Google Books. In B. P. Boudreau & B. B. Jørgensen (Eds.), *The Benthic Boundary Layer: Transport Processes and Biogeochemistry*. Oxford University Press. https://books.google.com/books?hl=en&lr=&id=Z8sw1jriW6YC&oi=fnd&pg=PR11&ots=a23lhqWHzX&sig=wigav5K9imwT8tSDohVvkb9o08U#v=onepage&q&f=false

Burgess, R. M., Environmental Protection Agency, U., of Research, O., Human, N., Health Research Laboratory, E., Ecology Division, A., & Island, R. (n.d.). *Guidelines for Using Passive Samplers to Monitor Organic Contaminants at Superfund Sediment Sites*.

Burnett, W. C., Aggarwal, P. K., Aureli, A., Bokuniewicz, H., Cable, J. E., Charette, M. A., Kontar, E., Krupa, S., Kulkarni, K. M., Loveless, A., Moore, W. S., Oberdorfer, J. A., Oliveira, J., Ozyurt, N., Povinec, P., Privitera, A. M. G., Rajar, R., Ramessur, R. T., Scholten, J., … Turner, J. V. (2006). Quantifying submarine groundwater discharge in the coastal zone via multiple methods. *Science of The Total Environment*, *367*(2–3), 498–543. https://doi.org/10.1016/J.SCITOTENV.2006.05.009

Clarke, K. R. (1993). Non-parametric multivariate analyses of changes in community structure. *Australian Journal of Ecology*. https://doi.org/10.1111/j.1442-9993.1993.tb00438.x

Cook, P. G., Favreau, G., Dighton, J. C., & Tickell, S. (2003). Determining natural groundwater influx to a tropical river using radon, chlorofluorocarbons and ionic environmental tracers. *Journal of Hydrology*. https://doi.org/10.1016/S0022-1694(03)00087-8

Cornelissen, G., Elmquist Kruså, M., Breedveld, G. D., Eek, E., Oen, A. M. P., Arp, H. P. H., Raymond, C., Samuelsson, G., Hedman, J. E., Stokland, Ø., & Gunnarsson, J. S. (2011). Remediation of contaminated marine sediment using thin-layer capping with activated carbon-A field experiment in Trondheim harbor, Norway. *Environmental Science and Technology*. https://doi.org/10.1021/es2011397

Cornelissen, G., Schaanning, M., Gunnarsson, J. S., & Eek, E. (2016). A large-scale field trial of thin-layer capping of PCDD/F-contaminated sediments: Sediment-to-water fluxes up to 5 years post-amendment. *Integrated Environmental Assessment and Management*, *12*(2), 216–221. https://doi.org/10.1002/IEAM.1665

Di Toro, D. M., Zarba, C. S., Hansen, D. J., Berry, W. J., Swartz, R. C., Cowan, C. E., Pavlou, S. P., Allen, H. E., Thomas, N. A., & Paquin, P. R. (1991). Technical basis for establishing sediment quality criteria for nonionic organic chemicals using equilibrium partitioning. In *Environmental Toxicology and Chemistry*. https://doi.org/10.1002/etc.5620101203

Eek, E., Cornelissen, G., Kibsgaard, A., & Breedveld, G. D. (2008). Diffusion of PAH and PCB from contaminated sediments with and without mineral capping; measurement and modelling. *Chemosphere*. https://doi.org/10.1016/j.chemosphere.2008.01.051

Endo, S., Hale, S. E., Goss, K. U., & Arp, H. P. H. (2011). Equilibrium partition coefficients of diverse polar and nonpolar organic compounds to polyoxymethylene (POM) passive sampling devices. *Environmental Science and Technology*, *45*(23), 10124–10132. https://doi.org/10.1021/es202894k

Fernandez, L. A., Harvey, C. F., & Gschwend, P. M. (2009). Using performance reference compounds in polyethylene passive samplers to deduce sediment porewater concentrations for numerous target chemicals. *Environmental Science and Technology*. https://doi.org/10.1021/es901877a

Fernandez, L. A., Lao, W., Maruya, K. A., & Burgess, R. M. (2014). Calculating the diffusive flux of persistent organic pollutants between sediments and the water column on the palos verdes shelf superfund site using polymeric passive samplers. *Environmental Science and Technology*. https://doi.org/10.1021/es404475c

Ghosh, U., Kane Driscoll, S., Burgess, R. M., Jonker, M. T. O., Reible, D., Gobas, F., Choi, Y., Apitz, S. E., Maruya, K. A., Gala, W. R., Mortimer, M., & Beegan, C. (2014). Passive sampling methods for contaminated sediments: practical guidance for selection, calibration, and implementation. *Integrated Environmental Assessment and Management*, *10*(2), 210–223. https://doi.org/10.1002/ieam.1507

Ghosh, U., Zimmerman, J. R., & Luthy, R. G. (2003). PCB and PAH speciation among particle types in contaminated harbor sediments and effects on PAH bioavailability. *Environmental Science and Technology*. https://doi.org/10.1021/es020833k

Gidley, P. T., Kwon, S., Yakirevich, A., Magar, V. S., & Ghosh, U. (2012). Advection dominated transport of polycyclic aromatic hydrocarbons in amended sediment caps. *Environmental Science and Technology*, *46*(9), 5032–5039. https://doi.org/10.1021/ES202910C/SUPPL_FILE/ES202910C_SI_001.PDF

Gidley, P. T., Lotufo, G. R., Kennedy, A. J., Melby, N. L., Wooley, A. H., Laber, C. H., Burgess, R. M., Ruiz, C. E., & Bridges, T. S. (2022). Effect of Activated Carbon in Thin Sand Caps Challenged with Ongoing PCB Inputs from Sediment Deposition: PCB Uptake in Clams (Mercenaria mercenaria) and Passive Samplers. *Archives of Environmental Contamination and Toxicology*, *82*(1), 95–104. https://doi.org/10.1007/S00244-021-00894-4/FIGURES/4

Go, J., Lampert, D. J., Stegemann, J. A., & Reible, D. D. (2009). Predicting contaminant fate and transport in sediment caps: Mathematical modelling approaches. *Applied Geochemistry*, *24*(7), 1347–1353. https://doi.org/10.1016/j.apgeochem.2009.04.025

Greenberg, M. S., Burton, G. A., & Rowland, C. D. (2002). Optimizing interpretation of in situ effects of riverine pollutants: Impact of upwelling and downwelling. *Environmental Toxicology and Chemistry*, *21*(2), 289–297. https://doi.org/10.1002/ETC.5620210210

Greenberg, M. S., Chapman, P. M., Allan, I. J., Anderson, K. A., Apitz, S. E., Beegan, C., Bridges, T. S., Brown, S. S., Cargill, J. G., McCulloch, M. C., Menzie, C. A., Shine, J. P., & Parkerton, T. F. (2014). Passive sampling methods for contaminated sediments: risk assessment and management. In *Integrated environmental assessment and management*. https://doi.org/10.1002/ieam.1511

Grossman, A., & Ghosh, U. (2009). Measurement of activated carbon and other black carbons in sediments. *Chemosphere*.

https://doi.org/10.1016/j.chemosphere.2008.12.054

Gschwend, P. M., Macfarlane, J. K., Reible, D. D., Lu, X., Hawthorne, S. B., Nakles, D. V., & Thompson, T. (2011). Comparison of polymeric samplers for accurately assessing PCBs in pore waters. *Environmental Toxicology and Chemistry*. https://doi.org/10.1002/etc.510

Hawthorne, S. B., Jonker, M. T. O., Van Der Heijden, S. A., Grabanski, C. B., Azzolina, N. A., & Miller, D. J. (2011). Measuring picogram per liter concentrations of freely dissolved parent and alkyl PAHs (PAH-34), using passive sampling with polyoxymethylene. *Analytical Chemistry*, *83*(17), 6754–6761. https://doi.org/10.1021/ac201411v

Hawthorne, S. B., Miller, D. J., & Grabanski, C. B. (2009). Measuring low picogram per liter concentrations of freely dissolved polychlorinated biphenyls in sediment pore water using passive sampling with polyoxymethylene. *Analytical Chemistry*, *81*(22), 9472–9480. https://doi.org/10.1021/ac9019413

Khairy, M. A., & Lohmann, R. (2020). Assessing Benthic Bioaccumulation of Polychlorinated Dioxins/Furans and Polychlorinated Biphenyls in the Lower Passaic River (NJ, USA) Based on In Situ Passive Sampling. *Environmental Toxicology and Chemistry*, *39*(6), 1174–1185. https://doi.org/10.1002/ETC.4716

Kupryianchyk, D., Noori, A., Rakowska, M. I., Grotenhuis, J. T. C., & Koelmans, A. A. (2013). Bioturbation and dissolved organic matter enhance contaminant fluxes from sediment treated with powdered and granular activated carbon. *Environmental Science and Technology*, *47*(10), 5092–5100. https://doi.org/10.1021/ES3040297/SUPPL_FILE/ES3040297_SI_001.PDF

Lampert, D. J., Thomas, C., & Reible, D. D. (2015). Internal and external transport significance for predicting contaminant uptake rates in passive samplers. *Chemosphere*, *119*, 910–916. https://doi.org/10.1016/j.chemosphere.2014.08.063

Lampert, David J., Lu, X., & Reible, D. D. (2013). Long-term PAH monitoring results from the Anacostia River active capping demonstration using polydimethylsiloxane (PDMS) fibers. *Environmental Sciences: Processes and Impacts*. https://doi.org/10.1039/c3em30826j

Lampert, David J., Sarchet, W. V., & Reible, D. D. (2011). Assessing the effectiveness of thin-layer sand caps for contaminated sediment management through passive sampling. *Environmental Science and Technology*. https://doi.org/10.1021/es200406a

Lee, D. R., & Cherry, J. A. (1979). A Field Exercise on Groundwater Flow Using Seepage Meters and Mini-piezometers. *Journal of Geological Education*. https://doi.org/10.5408/0022-1368-27.1.6

Li, L., Barry, D. A., Stagnitti, F., & Parlange, J. Y. (1999). Submarine groundwater discharge and associated chemical input to a coastal sea. *Water Resources Research*, *35*(11), 3253–3259. https://doi.org/10.1029/1999WR900189

Lin, D., Cho, Y. M., Werner, D., & Luthy, R. G. (2014). Bioturbation delays attenuation of DDT by clean sediment cap but promotes sequestration by thin-layered activated carbon. *Environmental Science and Technology*, *48*(2), 1175–1183. https://doi.org/10.1021/ES404108H/SUPPL_FILE/ES404108H_SI_001.PDF

Luthy, R. G., Aiken, G. R., Brusseau, M. L., Cunningham, S. D., Gschwend, P. M., Pignatello, J. J., Reinhard, M., Traina, S. J., Weber, W. J., & Westall, J. C. (1997). Sequestration of hydrophobic organic contaminants by geosorbents. In *Environmental Science and Technology*. https://doi.org/10.1021/es970512m

Lydy, M. J., Landrum, P. F., Oen, A. M., Allinson, M., Smedes, F., Harwood, A. D., Li, H., Maruya, K. A., & Liu, J. (2014). Passive sampling methods for contaminated sediments: state of the science for organic contaminants. In *Integrated environmental assessment and management*. https://doi.org/10.1002/ieam.1503

Mayer, P., Parkerton, T. F., Adams, R. G., Cargill, J. G., Gan, J., Gouin, T., Gschwend, P. M., Hawthorne, S. B., Helm, P., Witt, G., You, J., & Escher, B. I. (2014). Passive sampling methods for contaminated sediments: scientific rationale supporting use of freely dissolved concentrations. In *Integrated environmental assessment and management*. https://doi.org/10.1002/ieam.1508

McDonough, K. M., Murphy, P., Olsta, J., Zhu, Y., Reible, D., & Lowry, G. V. (2007). Development and placement of a sorbent-amended thin layer sediment cap in the Anacostia River. *Soil and Sediment Contamination*, *16*(3), 313–322. https://doi.org/10.1080/15320380701285725

Michalsen, M., Kennedy, A., Lotufo, G., Kerns, K., Suess, A., Mingta, L., Mills, M., Lambert, M., Reible, D., Rakowska, M., Odetayo, A., Ghosh, U., Bokare, M., Yan, S., & Gschwend, P. (2021). *Standardizing Polymeric Sampling Method for Measuring Freely-Dissolved Organic Contaminants in Sediment Porewater,* ESTCP Project ER-201735.

Millington, R. J., & Quirk, J. P. (1961). Permeability of porous solids. *Transactions of the Faraday Society*. https://doi.org/10.1039/TF9615701200

Murphy, P., Marquette, A., Reible, D., & Lowry, G. V. (2006). Predicting the Performance of Activated Carbon-, Coke-, and Soil-Amended Thin Layer Sediment Caps. *Journal of Environmental Engineering*. https://doi.org/10.1061/(ASCE)0733-9372(2006)132:7(787)

National Academies. (2003). Bioavailability of contaminants in soils and sediments: Processes, tools, and applications. In *The National Academies Press, Washington*. https://doi.org/10.17226/661

Nielsen, P. (1990). Tidal dynamics of the water table in beaches. *Water Resources Research*, *26*(9), 2127–2134. https://doi.org/10.1029/WR026I009P02127

O Jonker, M. T., van der Heijden, S. A., Adelman, D., Apell, J. N., Burgess, R. M., Choi, Y., Fernandez, L. A., Flavetta, G. M., Ghosh, U., Gschwend, P. M., Hale, S. E., Jalalizadeh, M., Khairy, M., Lampi, M. A., Lao, W., Lohmann, R., Lydy, M. J.,

Maruya, K. A., Nutile, S. A., … Wu, Y. (2018). Advancing the Use of Passive Sampling in Risk Assessment and Management of Sediments Contaminated with Hydrophobic Organic Chemicals: Results of an International Ex Situ Passive Sampling Interlaboratory Comparison. *Cite This: Environ. Sci. Technol*, *52*, 3582. https://doi.org/10.1021/acs.est.7b05752

Oen, A. M. P., Janssen, E. M. L., Cornelissen, G., Breedveld, G. D., Eek, E., & Luthy, R. G. (2011). In situ measurement of PCB pore water concentration profiles in activated carbon-amended sediment using passive samplers. *Environmental Science and Technology*, *45*(9), 4053–4059. https://doi.org/10.1021/ES200174V/SUPPL_FILE/ES200174V_SI_001.PDF

Parkerton, T. F., & Maruya, K. A. (2014). Passive sampling in contaminated sediment assessment: Building consensus to improve decision making. *Integrated Environmental Assessment and Management*, *10*(2), 163–166. https://doi.org/10.1002/IEAM.1488

Patmont, C. R., Ghosh, U., LaRosa, P., Menzie, C. A., Luthy, R. G., Greenberg, M. S., Cornelissen, G., Eek, E., Collins, J., Hull, J., Hjartland, T., Glaza, E., Bleiler, J., & Quadrini, J. (2015). In situ sediment treatment using activated carbon: A demonstrated sediment cleanup technology. *Integrated Environmental Assessment and Management*, *11*(2), 195–207. https://doi.org/10.1002/IEAM.1589

Pernyeszi, T., Kasteel, R., Witthuhn, B., Klahre, P., Vereecken, H., & Klumpp, E. (2006). Organoclays for soil remediation: Adsorption of 2,4-dichlorophenol on organoclay/aquifer material mixtures studied under static and flow conditions. *Applied Clay Science*, *32*(3–4), 179–189. https://doi.org/10.1016/J.CLAY.2006.01.004

Phillips, T. D., Sarr, A. B., & Grant, P. G. (1995). Selective chemisorption and detoxification of aflatoxins by phyllosilicate clay. *Natural Toxins*, *3*(4), 204–213. https://doi.org/10.1002/NT.2620030407

Rakowska, M. I., Kupryianchyk, D., Harmsen, J., Grotenhuis, T., & Koelmans, A. A. (2012). In situ remediation of contaminated sediments using carbonaceous materials. In *Environmental Toxicology and Chemistry*. https://doi.org/10.1002/etc.1763

Rakowska, Magdalena Iwona. (2014). *Ex Situ Treatment of Sediments With Grandular Activated Carbon: A Novel Remediation Technology* [Wageningen University & Research]. https://doi.org/9798708793478

Reible, D. D. (2005). *Organoclay Laboratory Study*.

Reible, D. D. (2014). Contaminant Processes in Sediments. In *Processes, Assessment and Remediation of Contaminated Sediments*. https://doi.org/10.1007/978-1-4614-6726-7

Reible, D., David, W., Roberts, K., & Zhu, Y. (2004). Active capping demonstration project in anacostia DC. *Remediation of Contaminated Sediments - 2003: Proceedings of the Second International Conference on Remediation of*

Contaminated Sediments.

Reible, D., Lampert, D., Constant, D., Mutch, R. D., & Zhu, Y. (2006). Active capping demonstration in the Anacostia river, Washington, D.C. *Remediation*. https://doi.org/10.1002/rem.20111

Schaanning, M. T., Beylich, B., Gunnarsson, J. S., & Eek, E. (2021). Long-term effects of thin layer capping in the Grenland fjords, Norway: Reduced uptake of dioxins in passive samplers and sediment-dwelling organisms. *Chemosphere*, *264*, 128544. https://doi.org/10.1016/J.CHEMOSPHERE.2020.128544

Schwarzenbach, R. P., Gschwend, P. M., & Imboden, D. M. (2002). Environmental Organic Chemistry. In *Environmental Organic Chemistry*. https://doi.org/10.1002/0471649643

Sharma, B., Gardner, K. H., Melton, J., Hawkins, A., & Tracey, G. (2009). Evaluation of Activated Carbon as a Reactive Cap Sorbent for Sequestration of Polychlorinated Biphenyls in the Presence of Humic Acid. *Https://Home.Liebertpub.Com/Ees*, *26*(9), 1371–1379. https://doi.org/10.1089/EES.2008.0231

Shen, X., Lampert, D., Ogle, S., & Reible, D. (2018). A software tool for simulating contaminant transport and remedial effectiveness in sediment environments. *Environmental Modelling and Software*. https://doi.org/10.1016/j.envsoft.2018.08.014

Shen, X., & Reible, D. (2019). An analytical model for the fate and transport of performance reference compounds and target compounds around cylindrical passive samplers. *Chemosphere*. https://doi.org/10.1016/j.chemosphere.2019.05.198

Sorell, T., & Mcevoy, K. (2013). Incorporating Bioavailability Considerations Into the Evaluation of Contaminated Sediment Sites. *Remediation Journal*, *23*(1), 63–72. https://doi.org/10.1002/REM.21338

Steevens, J. A., Besser, J. M., Dorman, R. A., & Sparks, D. W. (2020). Influence of remediation on sediment toxicity within the Grand Calumet River, Indiana, USA. *Chemosphere*. https://doi.org/10.1016/j.chemosphere.2020.126056

Tcaciuc, A. P., Apell, J. N., & Gschwend, P. M. (2015). Modeling the transport of organic chemicals between polyethylene passive samplers and water in finite and infinite bath conditions. *Environmental Toxicology and Chemistry*, *34*(12), 2739–2749. https://doi.org/10.1002/etc.3128

Thomas, C., Lampert, D., & Reible, D. (2014). Remedy performance monitoring at contaminated sediment sites using profiling solid phase microextraction (SPME) polydimethylsiloxane (PDMS) fibers. *Environmental Sciences: Processes and Impacts*. https://doi.org/10.1039/c3em00695f

Thompson, J. M., Hsieh, C.-H., & Luthy, R. G. (2015). *Modeling Uptake of Hydrophobic Organic Contaminants into Polyethylene Passive Samplers*. https://doi.org/10.1021/es504442s

Thoms, S., Matisoff, G., McCall, P., & Wang, X. (1995). *Models for Alteration of Sediments by Benthic Organisms*. Water Environment Federation.

U.S. Army Corps of Engineers. (1979). Sediment Capping of Subaqueous Dredged Material Disposal Mounds: An Overview of the New England Experience. *Special Technical Report*.

United States Environmental Protection Agency. (2012). *Equilibrium partitioning sediment benchmarks (ESBs) for the protection of benthic organisms: procedures for the determination of the freely dissolved interstitial water concentrations of nonionic organics. EPA-600-R-02-012*. *December*, 65. http://www.epa.gov/nheerl/download_files/publications/RB ESB 2012final_2.pdf

USEPA. (2012). *Guidelines for using passive samplers to monitor organic contaminants at superfund sediment sites*. 32. http://www.epa.gov/superfund/health/conmedia/sediment/pdfs/Passive_Sampler_SAMS_Final_Camera_Ready_-_Jan_2013.pdf

Van Der Heijden, S. A., & Jonker, M. T. O. (2009). PAH bioavailability in field sediments: Comparing different methods for predicting in situ bioaccumulation. *Environmental Science and Technology*, *43*(10), 3757–3763. https://doi.org/10.1021/ES803329P/SUPPL_FILE/ES803329P_SI_001.PDF

Van Genuchten, M. T. (1981). Analytical solutions for chemical transport with simultaneous adsorption, zero-order production and first-order decay. *Journal of Hydrology*. https://doi.org/10.1016/0022-1694(81)90214-6

Walters, R. W., & Luthy, R. G. (1984). Equilibrium Adsorption of Polycyclic Aromatic Hydrocarbons from Water onto Activated Carbon. *Environmental Science and Technology*. https://doi.org/10.1021/es00124a002

Wang, S., Lao, W., Li, H., & You, J. (2020). Measuring bioconcentration factors of sediment-associated fipronil in Lumbriculus variegatus using passive sampling techniques. *Journal of Hazardous Materials*, *393*, 122420. https://doi.org/10.1016/J.JHAZMAT.2020.122420

Wilson, D. J., Clarke, J. H., Reible, D. D., & Mutch, R. D. (2018). Contaminant Transport and Behavior in the Subsurface. In *Hazardous Waste Site Soil Remediation* (pp. 1–49). CRC Press. https://doi.org/10.1201/9780203752258-1

Yan, S., Rakowska, M., Shen, X., Himmer, T., Irvine, C., Zajac-Fay, R., Eby, J., Janda, D., Ohannessian, S., & Reible, D. D. (2020). Bioavailability assessment in activated carbon treated coastal sediment with in situ and ex situ porewater measurements. *Water Research*. https://doi.org/10.1016/j.watres.2020.116259

CHAPTER 3

PARTIAL LOADING OF PERFORMANCE REFERENCE COMPOUNDS IN PASSIVE SAMPLERS AND ITS EFFECT ON THE FRACTIONAL APPROACH TO STEADY STATE[1]

3.1. ABSTRACT

Passive sampling for hydrophobic organics in soils and sediments is typically accomplished by measuring the equilibrium accumulation of the target compounds onto a sorbing polymer. Because the samplers do not often achieve equilibrium in the environment, the release of performance reference compounds (PRCs) pre-loaded on the sampler is used to estimate the extent of equilibrium uptake of a similar target compound. In this work, we evaluate the effect of non-equilibrium loading of PRCs on the estimated equilibration of target compounds. A numerical transport model considering both internal and external mass transfer resistances to the polymer during loading from a finite reservoir was constructed to predict PRC distribution polymer sheets. An analytical internal diffusion, external mass transfer limited model is then employed to simulate the release of the PRCs and predict both the apparent and actual approach to equilibration for the uptake of target compounds. Partial equilibration during loading of PRCs does not lead to inaccuracies in target compound equilibration except when internal resistances control both PRC release and target compound uptake, under which conditions the PRCs overestimate the extent of equilibration of target compounds. This is likely to occur

---

[1]That article was published on June 14, 2022.
Smith, A. V., Garza-Rubalcava, U., Shen, X., & Reible, D. (2022). Partial loading of performance reference compounds in passive samplers and its effect on the fractional approach to steady state. *Journal of Environmental Chemical Engineering*, *10*(3), 108044. https://doi.org/10.1016/J.JECE.2022.108044

during short PRC loading times (e.g., <1 month) and thick polymer sheets (e.g., >100 µm in thickness). If external mass transfer resistances control PRC release and target compound uptake, even partially loaded PRCs can accurately indicate the extent of equilibration of target compounds as long as the initial PRC loading is adequately characterized.

3.2. INTRODUCTION

The freely dissolved concentration determined from polymeric passive samplers is increasingly used to assess the availability of HOCs in sediments, water, and air. The equilibrium uptake onto the polymer can be used to estimate the time-averaged freely available concentration, C_{free}, to which the polymer was exposed (Mayer et al., 2014). At equilibrium, the concentration in the polymer (C_p) is related to the polymer-water partition coefficient and the external water concentration (C_w) (3.1) :

$$C_w = \frac{C_p}{K_{pw}} \tag{3.1}$$

Where C_p and C_w both have units of mass of contaminant per volume of solution. Due to the strongly sorbing nature of HOCs, the equilibration time is often lengthy and is the result of internal and external mass transfer resistances. For example, Cornelissen et al. (2008) observed in a particular application that chrysene ($\log(K_{ow}) = 5.8$) had reached 50±4% equilibrium between the polymer concentration using 100 µm thick low density polyethylene (LDPE) and the total dissolved concentration in water after 63 days of exposure in harbor sediments. When equilibrium cannot be achieved, performance reference compounds (PRCs) are typically used to determine the extent of equilibrium with shorter exposure times. PRCs are typically ^{13}C or ^{2}H labeled compounds loaded into

the polymer prior to exposure to target compounds in the environment. The release and extent of equilibration of the PRCs is calculated by the fractional approach to steady state (f_{ss}^{PRC}, (3.2)). The f_{ss}^{PRC} is used to indicate the uptake and extent of equilibration of unlabeled target compounds assuming that the release and uptake are reversible.

$$f_{ss}^{PRC} = 1 - \frac{C_{t,PRC}}{C_{0,PRC}} \tag{3.2}$$

Here, $C_{t,PRC}$, represents the average concentration of PRCs in the polymer upon retrieval and $C_{0,PRC}$ is the average concentration of PRCs measured at time zero. The average concentration is measured by total extraction of the mass of PRC in the polymer divided by its volume.

A model is often used to interpret the PRC release to estimate equilibration of homologous compounds (Fernandez et al., 2009; Lampert et al., 2015; Shen & Reible, 2019). Fernandez et al. (2009) offers a one-dimensional sorption-diffusion model in an infinite sediment bed to predict the fate and transport of PRCs and target compounds. Tcaciuc et al. (2015) modeled the transfer of chemicals from a well-mixed infinitely large water body through a water boundary layer, while Lampert et al. (2015) explored the internal and external resistances on uptake into the polymer. These models are limited to rectangular sheets of LDPE, PDMS and POM. These models also can be used for PDMS coated cylindrical fibers if the external diffusion lengths are small, and the fibers can be assumed locally flat. Shen & Reible (2019) examined the problem of PRC release and target compound uptake external to the cylindrical geometry typical of PDMS fiber samplers.

Typical analyses when loading PRCs into the passive sampler assume the compounds have reached equilibrium and a uniform concentration across the thickness of the polymer after loading. The loading time should be longer than L^2/D_p where L is the half-thickness of the polymer being loaded and D_p is the diffusivity of the PRC in the polymer to insure uniform loading. It may be necessary to load PRCs over times less than L^2/D_p particularly for thick polymer layers which can lead to non-uniform partial loading of PRCs. The time to full equilibrium with the loading solution can also be much longer than L^2/D_p if controlled by external mass transfer resistances. Mixing and miscible solvents (e.g., methanol/water) are used to reduce external resistances. A wide range of polymer thicknesses and types have been employed and they may exhibit significantly different rates of PRC loading (Table 3-1). It would be expected that thick polymer layers, slow diffusion in polymers (such as observed in LDPE or POM), or changes in external mass transfer resistances during PRC loading and target compound uptake, may all influence the achievement of equilibrium conditions during PRC loading.

In a recent study we loaded approximately 198 LDPE (10 cm x 10 cm x 25.4 µm) sheets with ^{13}C-PCB PRCs from a methanol-water (20:80) mixture. The LDPE was placed with weights at the sediment-water interface to try and identify potential source areas in a study location (Figure 4-1, next chapter). Although the sheets would ideally be loaded individually, they were loaded in groups of 9 individual sheets in 22 different jars due to the logistical challenges of loading 198 sheets separately. The sheets were covered with a stainless-steel mesh both to separate the individual sheets during PRC loading and to protect the LDPE after placement in the environment. Despite these efforts and a

loading time of 30 days ($\sim 500\ L^2/D_p$), equilibrium was not achieved. It was estimated that average equilibration of PRCs ranged from 65-135% of the target loading with individual LDPE sheets showing greater variations. Greater than 100% of target loading is the result of exposure to much higher concentrations initially in sheets that were most exposed to the loading solution. Full equilibration would occur when the initially high concentrations in the most exposed sheets would diffuse back to the loading solution and be taken up by the lower concentration LDPE sheets. The combination of loading and back diffusion provides the potential for non-uniform loading both within a specific polymer sheet as well as difference between the sheets.

Table 3-1 Summary of polymer and thicknesses used in selected polymeric sampler investigations

Polymer	Thickness (μm)	Source
Low Density Polyethylene (LDPE)	100	(Belles et al., 2016; Cornelissen et al., 2008)
	70	(Adams et al., 2007; Booij et al., 2003; Smedes et al., 2009)
	66	(Rusina et al., 2007)
	51	(Adams et al., 2007; Sarah E. Hale et al., 2010)
Polyoxymethylene (POM)	2,000	(Ahn et al., 2005)
	580	(Hong & Luthy, 2008)
	500	(Belles et al., 2016; Cornelissen et al., 2008; Jonker & Koelmans, 2001; Rusina et al., 2007)

Table 3-1, Continued

Polymer	Thickness (μm)	Source
	76	(Arp et al., 2015; Sarah E. Hale et al., 2010; Hawthorne et al., 2011)
Polydimethylsiloxane (PDMS)	3,000*	(Martin et al., 2018)
	1,000	(Fuchte et al., 2020)
	500	(Monteyne et al., 2013)
	400	(Rusina et al., 2007)

* - Cylindrical rods were used in Martin et al. (2018) and the annulus radius of the polymer is given.

In this work we seek to evaluate those conditions where non-equilibrium PRC loading interfere with the assessment of the equilibration of target compounds. Our goal was to identify conditions where this lack of initial equilibrium could influence the estimation of the fractional approach to steady state in the subsequent field exposure of the polymer. A numerical transport model considering both internal and external mass transfer resistances to the polymer during loading from a finite reservoir was constructed to predict PRC distribution in one-dimensional polymer sheets. The calculated nonuniform concentration distribution (in non-equilibrium cases) was then used to predict PRC release during field exposures using an analytical 1-dimensional model of diffusion subject to external mass transfer limitations. The apparent fractional equilibration was then compared to the equilibration of target compounds being adsorbed. Conditions under which the initial disequilibrium of the PRCs would lead to both accurate and inaccurate estimates of equilibration of target compound uptake were identified.

3.3. METHODS

3.3.1 LOADING SCENARIO MASS BALANCE – FINITE DOMAIN

By assuming one-dimensional transport into a polymer of half-thickness, L, and volume $V_p = 2(h\ x\ w\ x\ L)$, where the height and width of the polymer is much greater than the half-thickness ($h, w \gg L$), and applying Fick's second law of diffusion to the polymer, a mass balance around the polymer yields the following governing equation (3.3).

$$\frac{\partial C_p}{\partial t} = D_p \frac{\partial^2 C_p}{\partial x^2} \qquad \text{for} \quad -L < x < L \tag{3.3}$$

With initial and boundary conditions:

$$C_p = 0 \qquad t = 0 \tag{3.4}$$

$$\frac{\partial C_p}{\partial x} = 0 \qquad x = 0 \tag{3.5}$$

$$\mp D_p \frac{\partial C_p}{\partial x} = k_l \left(\frac{C_p}{K_{pw}} - C_w(t) \right) \qquad x = \pm L \tag{3.6}$$

Where L is the half-thickness of the polymer; D_p is the polymer diffusivity (m^2/d) and $C_p$is the concentration within the polymer at time, t, (days). In (3.6), the mass transfer coefficient in the loading solution, k_l (m/d), is external to the polymer and K_{pw} is the ratio of equilibrium concentration between the polymer and the liquid phase. We will assume the loading solution is essentially water but may also be an aqueous solution (e.g., methanol and water). (3.6) indicates the balance between internal diffusion (left hand side) and external mass transfer (right hand side). The zero starting concentration within the polymer means the external mass transfer initially controls uptake (Liu et al.,

2022; Seidensticker et al., 2017) but subsequently the ratio between internal and external mass transfer resistances is controlled by the ratio of the key parameters in (3.6), the Biot number, $Bi = \frac{k_i L}{K_{pw} D_p}$. A similar mass balance is performed on the assumed well-mixed loading solution of volume, V_w, accounting for the uptake on both sides of the polymer, and subject to $C_w = C_{w,0}$ when $t = 0$ (3.7).

$$V_w \frac{dC_w}{dt} = 2hwk_l \left(\frac{C_p(L,t)}{K_{pw}} - C_w(t) \right) \tag{3.7}$$

Solutions to (3.6) and (3.7) for $C_p = C_p(x,t)$ and $C_w = C_w(t)$ can be obtained with the geometry of the system, values of the mass transfer coefficient, diffusivity data in the polymer (Rusina et al., 2010), and the assumption of local equilibrium between the polymer and loading solution. The problem was solved numerically with finite differences in order to allow consideration of both time dependent concentration in the loading solution as well as the full range of internal and external mass transfer resistances. The Matlab® code for this problem is included in Appendix 9.2. The code was evaluated by comparison to analytical solutions that are available for the $Bi \gg 1$ and $Bi \ll 1$ (Appendix 9).

3.3.2 Release Scenario Mass Balance – Infinite Domain

After loading of PRCs, the polymer is exposed to target contaminants either in the laboratory (ex-situ) or in the field (in-situ) to conduct passive sampling. The extent of equilibrium uptake of target compounds can be estimated from the mass of PRCs remaining within the polymer after that exposure. The initial PRC concentration in the polymer, C_p, will reflect the distribution of PRCs at the end of the loading process

(identified as $f(x)$ in (3.8) assuming immediate placement into the release medium after PRC loading. The initial and boundary conditions for the PRC release process are shown below.

$$C_p = f(x) \qquad t = 0 \tag{3.8}$$

$$\frac{\partial C_p}{\partial x} = 0 \qquad x = 0 \tag{3.9}$$

$$\mp D_p \frac{\partial C_p}{\partial x} = k_r \left(\frac{C_p}{K_{pr}} - C_w \right) \qquad x = \pm L \tag{3.10}$$

Where the compound specific mass transfer coefficient for the PRC release and target uptake process is denoted by the subscript, r. In the mass transfer model (3.10), the release of PRCs from the polymer to the aqueous phase or interstitial water phase of sediments is expressed in terms of an overall mass transfer coefficient and driving force (Hong & Luthy, 2008; Tcaciuc et al., 2015). The mass transfer coefficient is assumed constant which is likely to be valid in water or sediment slurry but may also apply to stagnant sediments if there is effectively infinite capacity for the finite amount of PRC in the surrounding media and if the sorption of the target compound does not deplete the contaminant in the sediments. In the general case where depletion may be significant, the mass transfer coefficient could be viewed as an average value over the time of exposure.

The solution for $C_p = C_p(x, t)$, as adapted from Carslaw & Jaeger (1959), assuming an essentially infinite volume around the polymer can be written (3.11).

$$C_p = \sum_{n=1}^{\infty} e^{-D_p \alpha_n^2 t} \frac{c_n \cos(\alpha_n x) + d_n \sin(\alpha_n x)}{(\alpha_n^2 + h^2)L + h} \int_{-L}^{L} (c_n \cos(\alpha_n x) + d_n \sin(a_n x)) f(x) dx \tag{3.11}$$

Where:

$$h = \frac{k_r}{K_{pw} D_p} \tag{3.12}$$

$$c_n = h \sin(a_n L) + a_n \cos(a_n L) \tag{3.13}$$

$$d_n = h \cos(a_n L) - a_n \sin(a_n L) \tag{3.14}$$

Where the eigenvalues, a_n, are the positive roots of $\tan(2a_n L) = \frac{2a_n h}{a_n^2 - h^2}$. The model herein assumes release of PRC into an effectively infinite medium at zero concentration, with a time-independent external mass transfer coefficient, k_r.

3.3.3 Kinetics of Performance Reference Compounds

We can non-dimensionalize Equations (3.11 – (3.14 to form the following key parameters.

$$\theta = \frac{C_p - K_{pw} C_w}{C_{p,0} - K_{pw} C_w} \tag{3.15}$$

$$\tau = \frac{t D_p}{L^2} \tag{3.16}$$

$$\lambda = \frac{x}{L} \tag{3.17}$$

$$Bi = \frac{k_i L}{K_{pw} D_p} \tag{3.18}$$

The solution can then be written

$$\theta = \sum_{n=1}^{\infty} e^{-\beta_n^2 \tau \frac{c_n \cos(\beta_n \lambda) + d_n \sin(\beta_n \lambda)}{\beta_n^2 + Bi^2 + Bi}} \int_{-1}^{1} (c_n \cos(\beta_n \lambda') + d_n \sin(\beta_n \lambda')) \theta_0(\lambda') d\lambda' \tag{3.19}$$

$$c_n = Bi \sin(\beta_n) + a_n \cos(\beta_n) \tag{3.20}$$

$$d_n = Bi\cos(\beta_n) - a_n\sin(\beta_n) \tag{3.21}$$

$$\theta_0(\lambda) = \frac{f(\lambda L) - K_{pw}C_w}{C_{p,0} - K_{pw}C_w} \tag{3.22}$$

$$C_{p,0} = \frac{f(x)}{\int_{-L}^{L} f(x)\,dx} \tag{3.23}$$

Where θ, τ, and λ represent non-dimensional concentration, time, and length, respectively. β_n is the n-th positive root of $\tan(2\beta_n) = \frac{2\beta_n Bi}{\beta_n^2 - Bi^2}$, and k_i refers to the compound specific mass transfer coefficient during either the PRC loading (k_l) or the target compound uptake and PRC release (k_r) process. By using these non-dimensional variables, we can characterize the behavior of the model and the implications for PRC loading and estimation of the extent of equilibration using a minimum set of parameters. The model utilizes the Biot number (Bi) to evaluate whether the uptake and release of PRCs from the polymer are internally or externally controlled. A key parameter in Bi is the polymer water partition coefficient, K_{pw}, which is of the order of 10^5 to 10^7 for typical hydrophobic organics on the polymers normally used for passive sampling (Apell & Gschwend, 2014; Difilippo & Eganhouse, 2010). The polymer thickness can vary from approximately 10 µm to 500 µm or more in thick polymer sheets (Arp et al., 2015; Cornelissen et al., 2008; Hong & Luthy, 2008) and the diffusivity in the polymer can vary from 10^{-6} m^2/d (~ 10^{-11} m^2/s) for PDMS to 10^{-9} m^2/d (~ 10^{-14} m^2/s) for highly hydrophobic compounds in LDPE (Rusina et al., 2010) to 10^{-11} m^2/d (~ 10^{-16} m^2/s) in POM (Belles et al., 2016). The external mass transfer resistances can vary over a wide range depending upon mixing in the water and the rate and magnitude of partitioning in sediments. We will evaluate the behavior of PRC loading and release and target

compound uptake using the dimensionless parameterization and then relate that to common polymers and loading and exposure conditions in dimensional terms.

3.4. RESULTS AND DISCUSSION

3.4.1 MODEL VALIDATION

The numerical and analytical diffusion models were compared to the experimental data presented by Belles et al. (2018) to confirm the accuracy of the model. These experiments were conducted in layers of PDMS in which one layer was uniformly contaminated with a target compound and the concentration changes in other layers over time were used to estimate diffusion coefficients. Belles et al. (2018) presented data for diflufenician for which they reported an average diffusion coefficient of $10^{-12.17}$ m^2/s ($5.84x10^{-8}$ m^2/d). Figure 3-1 shows the comparison of the measured data with the numerical model. The analytical model of Belles et al. (2018) and the analytical model employed here also show identical concentration curves that overlap the numerical solution curves. The apparent deviation at short time (18 hours) is likely the result of the difficulty of defining the initial condition experimentally (numerical and analytical solutions assume an initially uniform concentration in the first layer and diffusion starts at precisely time zero).

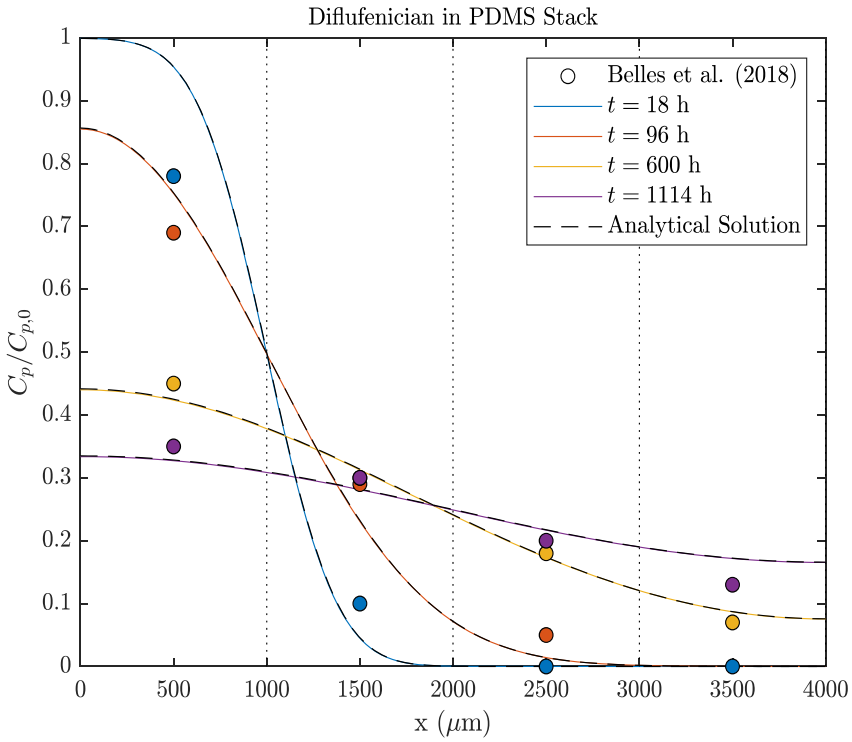

Figure 3-1 Comparison of the numerical model Equations (3.3 – (3.7 to the conditions of Belles et al. (2018). The analytical solution of Belles et al. (2018) and Equations (3.8 – (3.14 coincide with the numerical model. The external mass transfer coefficient is taken as zero (no flux out of the layers of PDMS).

3.4.2 PRC Loading

Externally controlled scenarios for loading PRCs are associated with Biot numbers that are much less than 1 ($Bi \ll 1$). This would be associated with loading of PRCs in thin polymer layers, in systems with high resistance to mass transfer in the liquid phase, or from water (rather than an aqueous solution of an organic solvent) which would maximize K_{pw}. Under these conditions, the diffusional transport across the thickness of the polymer results in a uniform loading even if there is not adequate time to reach equilibrium within the loading vessel (Figure 3-2).

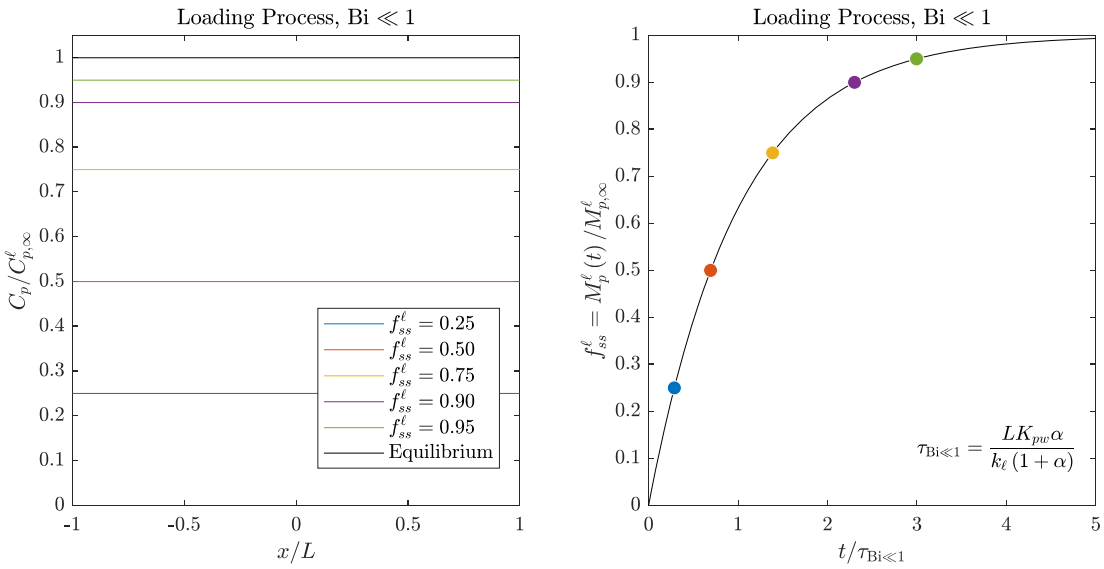

Figure 3-2 (Left) Distribution of the PRC across the thickness of the polymer for externally controlled loading scenarios. (Right) Time required to reach partial mass uptake onto the polymer, which depends on k_l, K_{pw}, and the ratio of mass in the liquid phase to the solid phase at equilibrium, $\alpha = \frac{V_w}{V_p K_{pw}}$. Colors in left plot match the required times to achieve partial f_{ss}^{l} in right plot (colored circles)

The parameter α in Figure 3-2 arises in loading PRCs from a finite solution and is the ratio of the mass of PRC in the loading solution to that in the polymer at equilibrium which can be written as in (3.24.

$$\alpha = \frac{V_w}{V_p * K_{pw}} \tag{3.24}$$

Where V_w is the volume of loading solution and V_p is the volume of the polymer. For large values of α, the concentration in the loading solution is approximately constant. More typically, however, the value of α is small ($\ll 1$) and the external concentration changes greatly during loading. α also influences the kinetics of uptake into the polymer by establishing how fast the external liquid concentration changes. For small values of α,

the PRC is depleted rapidly from the liquid phase and the overall system reaches equilibrium quickly.

A uniform concentration within the polymer is to be expected in an externally controlled system and is typically the case for thin (10 – 30 μm layer) polymer layers with high compound diffusivity (e.g., PDMS). Because the PRC concentration is initially uniform, measurement of the initial and final concentrations of the PRC in the polymer during the subsequent exposure allows accurate estimation of target compound equilibration regardless of the extent of equilibration of the polymer with the loading solution. That is, even if the polymer is not loaded to equilibrium, the measured loading provides an accurate reference for the determination of the extent of equilibrium during the release and target compound uptake.

Conversely, internally controlled systems, when the internal diffusion rate is less than that of the external mass transfer rate, implied Biot number much larger than one ($Bi \gg 1$) during the loading process. This would be applicable to situations where external mixing is rapid but thick polymers with low diffusivity are being loaded with PRCs (e.g., POM/LDPE > 100 μm). When $Bi \gg 1$, the PRC distribution inside the polymer is nonuniform prior to the achievement of equilibrium (Figure 3-3).

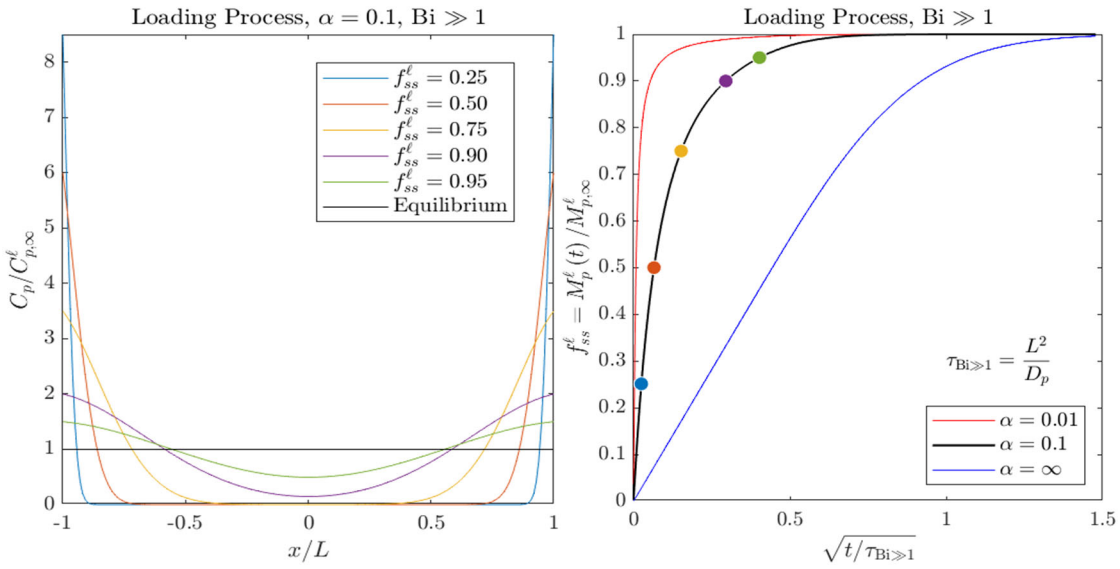

Figure 3-3 (Left) Distribution of the PRC across the thickness of the polymer for internally controlled loading scenarios. (Right) Characteristic time required to reach partial uptake into the polymer, which depends on L, D_p, and the ratio of mass in the liquid phase to the solid phase at equilibrium, $\alpha = V_w/(V_p K_{pw})$. Colors in left plot match the required times to achieve partial f_{ss}^{l} in right plot (colored circles)

3.4.3 PRC LOADING IN MULTIPLE SHEETS WITHIN THE SAME SYSTEM

We can now examine the conditions that might have led to the uneven equilibration of PRCs in the loading of multiple sheets of LDPE simultaneously. We do not have measurements of external mass transfer rates nor measurements of concentration profiles in the thin (25.4 µm) LDPE, but we do have estimates of the range of average concentrations in selected sheets (3 samples per jar for 66 measurements). The relative standard deviation of PRC compounds varied from 65-135% of the expected equilibrium target concentration. We will use the model to examine PRC loading onto the individual sheets over a range of Bi from 0.001 to 10 to reflect differing magnitudes of external mass transfer rates to the multiple LDPE sheets (Figure 3-4). To illustrate the behavior we will focus on a single PRC, ^{13}C-PCB 182 which has a log K_{LDPE-w} of approximately 7.24 (Ghosh et al., 2014) and a log diffusivity in LDPE of about -13.5 m^2/s (Rusina et al.,

2010). The calculated value of α is approximately 10^{-5} which suggests that the loading solution concentration will be depleted nearly completely during the loading process. Based upon the half thickness of the LDPE (12.7 μm), the characteristic time for internal equilibration of the polymer, $\tau = L^2/D_p$ is 1.41 hours or approximately 0.06 days. As noted previously, the high initial concentration and non-uniform exposure on the LDPE sheets can lead to concentrations higher than the final equilibrium in some sheets and far from equilibrium loading in other sheets. As shown in Figure 3-4, this period of equilibration can be exceptionally long. With the assumed range of Bi, the variation across the polymer sheets ranged from 40% to 110% of final equilibrium after $500\tau = 29.5\ days$. The average of 0.75±40% loading extent exhibits a similar variability as was observed in the actual experiment after the loading time of 30 days.

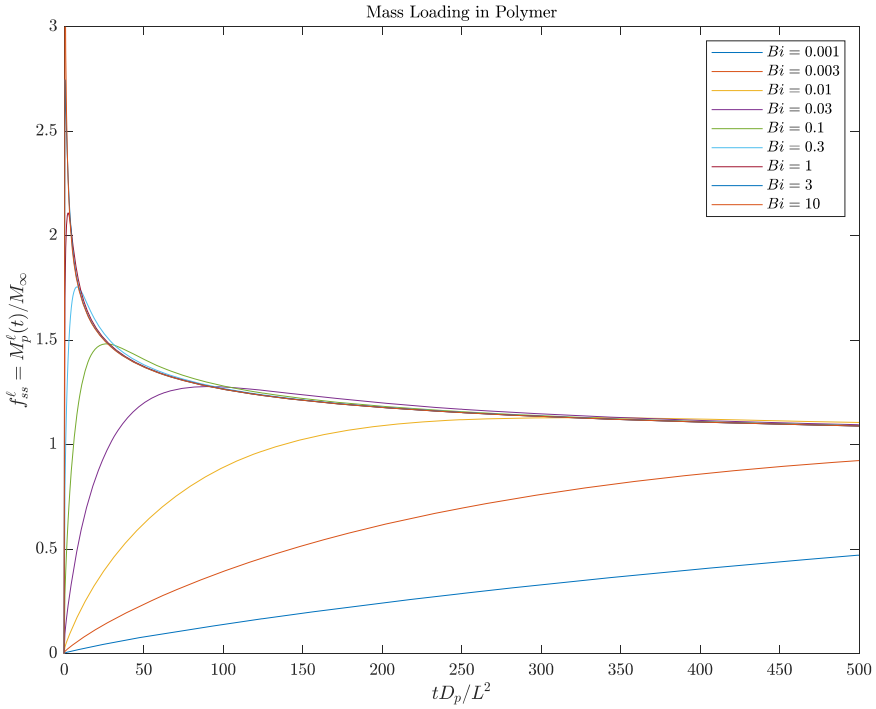

Figure 3-4 Simultaneous loading of multiple LDPE sheets with ^{13}C-PCB 182 PRC over time assuming different levels of exposure (or Bi) for each sheet within the same system. $tL^2/D_p = 500$ is ~30 days.

The modeling suggests that the failure to achieve the equilibrium in the experimental system even at times $\gg L^2/D_p$ is likely due to a significant variation in external mass transfer coefficient on the various LDPE sheets. The very low apparent Bi numbers on some sheets are likely aided by the stainless-steel mesh which limited mixing external to the sheets. The fact that the biggest deviations from equilibrium are associated with the low Bi conditions suggest that the concentration profile within the LDPE sheets are likely uniform (case in Figure 3-2) even when far from equilibrium. This suggest that this situation does not compromise the ability to measure the extent of equilibration of target compound uptake based upon PRC release as long as the initial PRC concentration in the individual LDPE sheets is known.

3.4.4 PRC Release and Target Compound Uptake

The influence of the PRC loading profile as illustrated in Figure 3-2 and Figure 3-3 on estimated target compound equilibration is also simulated. Once the polymer has completed the PRC loading process, it is assumed to be immediately placed into an infinite medium for PRC release and target compound uptake. If significant time separated loading and exposure, internal diffusion within the polymer would continue prior to deployment and could reach uniformity across the thickness of the polymer depending on the elapsed time. Here, however, additional time for equilibration is not assumed.

We will again examine the two limits during PRC release, ($Bi \ll 1$ or $Bi \gg 1$). For PRC release under condition of $Bi \ll 1$, partial loading and non-uniformity of loading does not affect the ability of the PRCs to predict extent of equilibration. That is, if the external mass transfer resistance controls the PRC release and target compound uptake, the fraction approach to steady state is governed by the single curve shown in Figure 3-5 (left), even if the initial PRC concentration profile is non-uniform and regardless of the Bi during PRC loading.

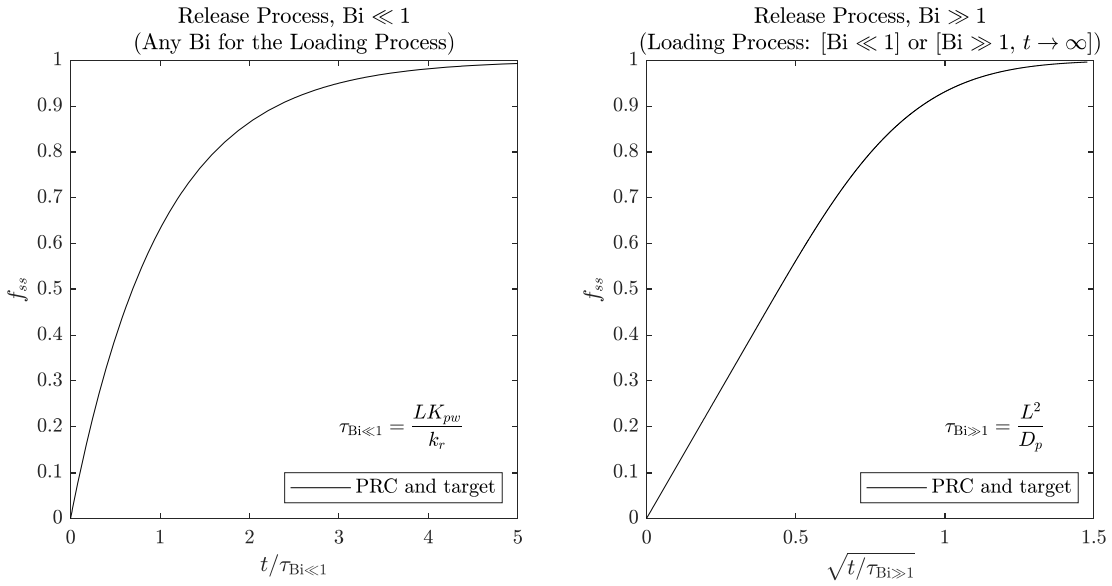

Figure 3-5 The fractional approach to steady state (f_{ss}) of the release of PRC and uptake of target compounds for the externally controlled scenario (left) and the internally controlled scenario (right) after loading in $Bi \ll 1$ (external control) or loading to equilibrium. In both instances the f_{ss} for PRC release and target compound uptake are identical and there are no errors associated with partial loading.

If internal mass transfer resistance controls the PRC release and target compound uptake, however, (i.e., $Bi \gg 1$), the initial PRC concentration profile must be uniform for the PRCs to reflect target compound uptake equilibration (e.g., either $Bi \ll 1$ during loading or the PRC were loaded to equilibrium, $t \to \infty$). Under these conditions the fractional approach to steady state of the PRC release or target compound uptake is described by Figure 3-5 (right).

In all cases with loading under $Bi \ll 1$ and for target compound uptake with $Bi \ll 1$, there is no errors in assessing equilibration with PRCs that were not initially equilibrated with the polymer. Thus, polymer sheets of LDPE exposed to $Bi \ll 1$ (see Figure 3-4) may deviate significantly from equilibrium PRC loading, but this would not

lead to errors in estimating the extent of equilibration of the target compound during passive sampling as long as the initial PRC concentration is known.

3.4.5 Partial PRC Loading and Release Both Controlled by Internal Mass Transfer

When $Bi \gg 1$ during both partial PRC loading and subsequent release, however, the PRC behavior during release differs from the target compound uptake. As a result of a non-uniform concentration of PRC during partial loading, the high concentration of PRC near the surface will lead to a rapid release from the surface of the polymer to the sampled medium during target compound sampling as well as continued diffusion into the polymer. Figure 3-6 shows the apparent fractional approach to steady state from measured PRC concentrations and (3.2) compared to the actual extent of equilibration of target compound uptake. Significant non-equilibrium loading of PRCs can lead to substantial over-estimation of the equilibration of target compounds as shown in Figure 3-5 (left). If loading had only achieved 25% equilibration under conditions of $Bi \gg 1$, for example, an apparent PRC equilibration of ~90% corresponds to an actual equilibration of target compounds of only ~10%. The overestimation of equilibration means that predicted passive sampling water concentrations would be underestimated.

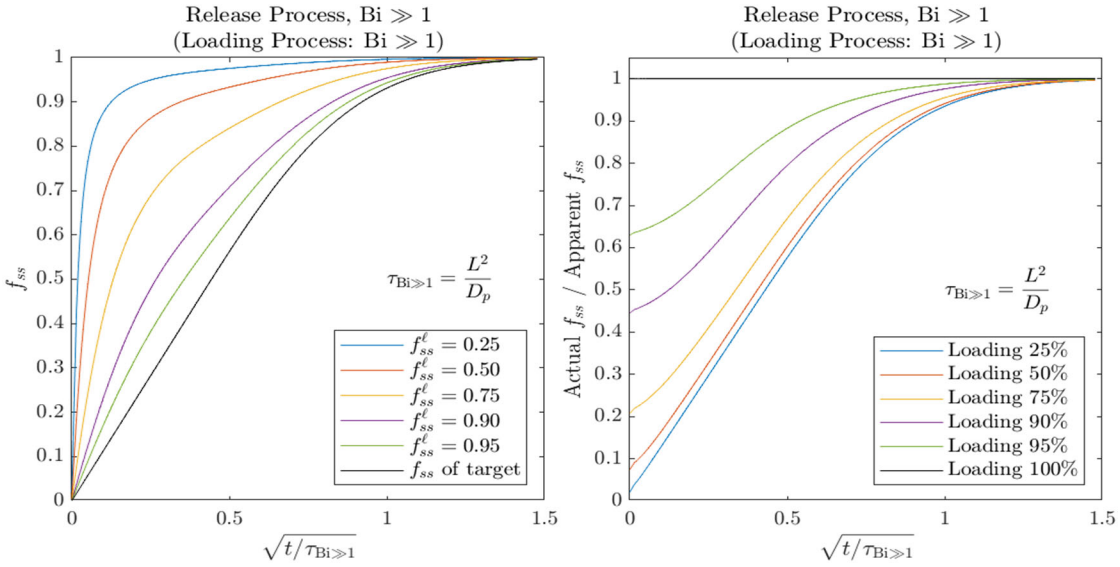

Figure 3-6 (Left) The fractional approach to steady state (f_{ss}) of PRCs for different non-equilibrium loading amounts compared to the actual f_{ss}. (Right) The relative uncertainty of the actual f_{ss} of target compounds to the apparent f_{ss} due to partial loading

In Figure 3-6, the effect of non-equilibrium loading of the PRC is small if the time of loading or release is $\gg L^2/D_p$. At $t = L^2/D_p$, the error is less than 10%. If the PRC diffusivity is low and the polymer layer is thick it may not be possible or convenient to load for time of L^2/D_p or longer. For a POM sheet of 500 µm (half thickness of 250 µm) adsorbing or releasing hydrophobic compounds, e.g., $L^2/D_p = 0.67$ yr for benzo[a]pyrene which has a diffusion coefficient of $10^{-14.53}$ m^2/s (Belles et al., 2016). $L^2/D_p = 38$ days for a 500 µm LDPE sheet ($D_p = 10^{-13.72}$ m^2/s) and L^2/D_p is ~1 hour for PDMS ($D_p = 10^{-10.77}$ m^2/s), diffusivities are from Rusina et al. (2010). The time to equilibrium can be much longer than these times depending upon the significance of external mass transfer resistances, but errors due to partial loading would only be significant for loading conducted at shorter times. Because PRC loading is typically undertaken over several weeks to a month, and often using a thinner layer of polymer, equilibration should not normally be of concern, particularly for LDPE and PDMS,

except when attempting to load multiple sheets simultaneously as discussed previously. Moreover, if external resistances dominate during target compound uptake, non-uniform loading of PRCs is not a concern as long as the initial concentration of the PRC is known. As indicated previously, poor estimation of the fractional approach to equilibration of target compounds would occur only when internal resistances control PRC release and target compound uptake and PRC loading was not conducted to equilibrium.

3.5. CONCLUSION

The use of performance reference compounds to measure the extent of equilibrium for target compounds relies on the polymer to be uniformly loaded with PRCs prior to deployment. Initially, PRC loading and target compound uptake is limited by external resistances when fresh polymer is exposed to the surrounding media. Uniformity is expected when the external mass transfer continues to control uptake after this initial phase.

Three scenarios were considered to illustrate the relationship between PRC release and the kinetics of target compound uptake. In the first scenario, PRC loading is taken to equilibrium and PRC release during passive sampling directly reflects target compound uptake. In a second scenario, equilibrium is not achieved but if $Bi \ll 1$ (i.e., external resistance controls uptake of the PRCs), the polymer is uniformly loaded even during its approach to equilibrium and the PRC release again reflects target compound uptake during passive sampling as long as equilibration is referenced to the actual (measured) uptake of the PRC on the polymer. This is most likely for thin polymer layers of LDPE and POM (<100 μm) and PDMS. In the third scenario, $Bi \gg 1$ (i.e., internal

resistance controls PRC loading) and the PRC concentration profile inside the polymer during loading is non-uniform until equilibrium is achieved. If loading is stopped before complete equilibration, the PRC release will only indicate target compound uptake for the case of externally controlled uptake conditions. If target compound uptake also is controlled by internal mass transfer resistances, the PRC release will overestimate the degree of equilibration of target compounds. This condition can occur when highly hydrophobic compounds with low diffusivity are being monitored via passive sampling with a thick (>100 μm) POM or LDPE polymer using short (≪ 1 month) PRC loading times or target compound exposure times.

Inaccurate and variable estimates of the fractional approach to steady state can still occur if the initial PRC loading measurements do not effectively characterize any variations, for example uneven loading of multiple polymer sheets simultaneously.

3.6. REFERENCES

Adams, R. G., Lohmann, R., Fernandez, L. A., Macfarlane, J. K., & Gschwend, P. M. (2007). Polyethylene Devices: Passive Samplers for Measuring Dissolved Hydrophobic Organic Compounds in Aquatic Environments. *Environmental Science & Technology*, 1317–1323. https://doi.org/10.1021/es0621593

Ahn, S., Werner, D., Karapanagioti, H. K., McGlothlin, D. R., Zare, R. N., & Luthy, R. G. (2005). Phenanthrene and pyrene sorption and intraparticle diffusion in polyoxymethylene, coke, and activated carbon. *Environmental Science and Technology*, *39*(17), 6516–6526. https://doi.org/10.1021/ES050113O/SUPPL_FILE/ES050113OSI20050616_053400.PDF

Apell, J. N., & Gschwend, P. M. (2014). Validating the use of performance reference compounds in passive samplers to assess porewater concentrations in sediment beds. *Environmental Science and Technology*, *48*(17). https://doi.org/10.1021/es502694g

Arp, H. P. H., Hale, S. E., Elmquist Krus??, M., Cornelissen, G., Grabanski, C. B., Miller, D. J., & Hawthorne, S. B. (2015). Review of polyoxymethylene passive sampling methods for quantifying freely dissolved porewater concentrations of hydrophobic organic contaminants. In *Environmental Toxicology and Chemistry* (Vol. 34, Issue 4, pp. 710–720). https://doi.org/10.1002/etc.2864

Belles, A., Alary, C., & Mamindy-Pajany, Y. (2016). Thickness and material selection of polymeric passive samplers for polycyclic aromatic hydrocarbons in water: Which more strongly affects sampler properties? *Environmental Toxicology and Chemistry*, *35*(7), 1708–1717. https://doi.org/10.1002/ETC.3326

Belles, A., Franke, C., Alary, C., Aminot, Y., & Readman, J. W. (2018). Understanding and predicting the diffusivity of organic compounds in polydimethylsiloxane material for passive sampler applications using a simple quantitative structure–property relationship model. *Environmental Toxicology and Chemistry*, *37*(5), 1291–1300. https://doi.org/10.1002/ETC.4101

Booij, K., Hofmans, H. E., Fischer, C. V., & Van Weerlee, E. M. (2003). Temperature-dependent uptake rates of nonpolar organic compounds by semipermeable membrane devices and low-density polyethylene membranes. *Environmental Science and Technology*, *37*(2), 361–366. https://doi.org/10.1021/es025739i

Carslaw, H. S., & Jaeger, J. C. (1959). *Conduction of Heat in Solids* (2nd Editio). Oxford University Press.

Cornelissen, G., Pettersen, A., Broman, D., Mayer, P., & Breedveld, G. D. (2008). Field testing of equilibrium passive samplers to determine freely dissolved native polycyclic aromatic hydrocarbon concentrations. *Environmental Toxicology and Chemistry*, *27*(3), 499–508. https://doi.org/10.1897/07-253.1

Difilippo, E. L., & Eganhouse, R. P. (2010). Assessment of PDMS-water partition coefficients: Implications for passive environmental sampling of hydrophobic

organic compounds. In *Environmental Science and Technology* (Vol. 44, Issue 18, pp. 6917–6925). https://doi.org/10.1021/es101103x

Fernandez, L. A., Harvey, C. F., & Gschwend, P. M. (2009). Using performance reference compounds in polyethylene passive samplers to deduce sediment porewater concentrations for numerous target chemicals. *Environmental Science and Technology*. https://doi.org/10.1021/es901877a

Fuchte, H. E., Schäffer, A., Booij, K., & Smith, K. E. C. (2020). Kinetic Passive Sampling: In Situ Calibration Using the Contaminant Mass Measured in Parallel Samplers with Different Thicknesses. *Environmental Science and Technology*, *54*(24), 15759–15767. https://doi.org/10.1021/ACS.EST.0C04437/SUPPL_FILE/ES0C04437_SI_001.PDF

Ghosh, U., Kane Driscoll, S., Burgess, R. M., Jonker, M. T. O., Reible, D., Gobas, F., Choi, Y., Apitz, S. E., Maruya, K. A., Gala, W. R., Mortimer, M., & Beegan, C. (2014). Passive sampling methods for contaminated sediments: practical guidance for selection, calibration, and implementation. *Integrated Environmental Assessment and Management*, *10*(2), 210–223. https://doi.org/10.1002/ieam.1507

Hale, S. E., Martin, T. J., Goss, K. U., Arp, H. P. H., & Werner, D. (2010). Partitioning of organochlorine pesticides from water to polyethylene passive samplers. *Environmental Pollution*, *158*(7), 2511–2517. https://doi.org/10.1016/J.ENVPOL.2010.03.010

Hawthorne, S. B., Jonker, M. T. O., Van Der Heijden, S. A., Grabanski, C. B., Azzolina, N. A., & Miller, D. J. (2011). Measuring picogram per liter concentrations of freely dissolved parent and alkyl PAHs (PAH-34), using passive sampling with polyoxymethylene. *Analytical Chemistry*, *83*(17), 6754–6761. https://doi.org/10.1021/ac201411v

Hong, L., & Luthy, R. G. (2008). Uptake of PAHs into polyoxymethylene and application to oil-soot (lampblack)-impacted soil samples. *Chemosphere*, *72*(2), 272–281. https://doi.org/10.1016/J.CHEMOSPHERE.2008.01.028

Jonker, M. T. O., & Koelmans, A. A. (2001). Polyoxymethylene solid phase extraction as a partitioning method for hydrophobic organic chemicals in sediment and soot. *Environmental Science and Technology*, *35*(18), 3742–3748. https://doi.org/10.1021/es0100470

Lampert, D. J., Thomas, C., & Reible, D. D. (2015). Internal and external transport significance for predicting contaminant uptake rates in passive samplers. *Chemosphere*, *119*, 910–916. https://doi.org/10.1016/j.chemosphere.2014.08.063

Liu, B., Finkel, M., & Grathwohl, P. (2022). First order approximation for coupled film and intraparticle pore diffusion to model sorption/desorption batch experiments. *Journal of Hazardous Materials*, *429*, 128314. https://doi.org/10.1016/J.JHAZMAT.2022.128314

Martin, A., Margoum, C., Jolivet, A., Assoumani, A., El Moujahid, B., Randon, J., &

Coquery, M. (2018). Calibration of silicone rubber rods as passive samplers for pesticides at two different flow velocities: Modeling of sampling rates under water boundary layer and polymer control. *Environmental Toxicology and Chemistry*, *37*(4), 1208–1218. https://doi.org/10.1002/ETC.4050

Mayer, P., Parkerton, T. F., Adams, R. G., Cargill, J. G., Gan, J., Gouin, T., Gschwend, P. M., Hawthorne, S. B., Helm, P., Witt, G., You, J., & Escher, B. I. (2014). Passive sampling methods for contaminated sediments: scientific rationale supporting use of freely dissolved concentrations. In *Integrated environmental assessment and management*. https://doi.org/10.1002/ieam.1508

Monteyne, E., Roose, P., & Janssen, C. R. (2013). Application of a silicone rubber passive sampling technique for monitoring PAHs and PCBs at three Belgian coastal harbours. *Chemosphere*, *91*(3), 390–398. https://doi.org/10.1016/J.CHEMOSPHERE.2012.11.074

Rusina, T. P., Smedes, F., & Klanova, J. (2010). Diffusion coefficients of polychlorinated biphenyls and polycyclic aromatic hydrocarbons in polydimethylsiloxane and low-density polyethylene polymers. *Journal of Applied Polymer Science*, *116*(3), 1803–1810. https://doi.org/10.1002/APP.31704

Rusina, T. P., Smedes, F., Klanova, J., Booij, K., & Holoubek, I. (2007). Polymer selection for passive sampling: A comparison of critical properties. *Chemosphere*, *68*(7), 1344–1351. https://doi.org/10.1016/J.CHEMOSPHERE.2007.01.025

Seidensticker, S., Zarfl, C., Cirpka, O. A., Fellenberg, G., & Grathwohl, P. (2017). Shift in Mass Transfer of Wastewater Contaminants from Microplastics in the Presence of Dissolved Substances. *Environmental Science and Technology*, *51*(21), 12254–12263. https://doi.org/10.1021/ACS.EST.7B02664/SUPPL_FILE/ES7B02664_SI_004.PDF

Shen, X., & Reible, D. (2019). An analytical model for the fate and transport of performance reference compounds and target compounds around cylindrical passive samplers. *Chemosphere*. https://doi.org/10.1016/j.chemosphere.2019.05.198

Smedes, F., Geertsma, R. W., Van Der Zande, T., & Booij, K. (2009). Polymer-water partition coefficients of hydrophobic compounds for passive sampling: Application of cosolvent models for validation. *Environmental Science and Technology*, *43*(18), 7047–7054. https://doi.org/10.1021/ES9009376/SUPPL_FILE/ES9009376_SI_001.PDF

Tcaciuc, A. P., Apell, J. N., & Gschwend, P. M. (2015). Modeling the transport of organic chemicals between polyethylene passive samplers and water in finite and infinite bath conditions. *Environmental Toxicology and Chemistry*, *34*(12), 2739–2749. https://doi.org/10.1002/etc.3128

Thompson, J. M., Hsieh, C.-H., & Luthy, R. G. (2015). *Modeling Uptake of Hydrophobic Organic Contaminants into Polyethylene Passive Samplers*. https://doi.org/10.1021/es504442s

CHAPTER 4

SOURCE AREA IDENTIFICATION BY IN-SITU PASSIVE SAMPLING AT BRADFORD ISLAND, CASCADE LOCKS, OREGON

4.1. ABSTRACT

Bradford Island forms the southern end of the Bonneville Dam, located on the Oregon shore of the Columbia River. Transformers containing polychlorinated biphenyls (PCBs) were found along the northern shore of Bradford Island as part of an investigation of the upland portions of the site. Following removal of the transformers and associated surficial sediments, elevated PCB concentrations continued to be observed in area sediments and resident fish tissues. Past surveys, however, have not identified any remaining source areas that might explain the continued elevated fish tissue concentrations and a novel alternative approach using a high density of low-density polyethylene (LDPE) sheets was attempted to try to identify source areas. A total of 163 LDPE passive samplers were attached to weighted bags and placed on the sediment surface to measure porewater concentrations at the interface. Because the goal was to identify significantly contaminated areas, the initial analysis focused on a subset of congeners consistent with historical Aroclor 1254 contamination and limited concentration of the samples. Slightly elevated PCB porewater concentrations were found at the eastern tip of the island. For confirmation, a subset of the 163 samples were sent off to a commercial laboratory for the full 209 congener analysis and with further sample concentration to detect low level contamination. The results of the full congener analysis were consistent with the initial analyses in terms of identification of elevated concentration areas and in the identification of the key congeners. This novel application

of a high density of passive samplers shows their capability to be a mapping tool for contaminated sediment source areas.

4.2. INTRODUCTION

The United States Army Corps of Engineers (USACE) have conducted multiple investigations to evaluate environmental conditions in the upland operable unit (OU) of Bradford Island, located just upstream of the Bonneville Dam in Cascade Locks, Oregon. During initial studies, four areas of particular concern (AOPC) were identified during the upland OU where past disposal practiced impacted soil and groundwater within the island. In 2002, electrical equipment believed to contain Aroclor 1254, a polychlorinated biphenyl (PCB) mixture, was removed from the river bottom along the shoreline, and in 2007 USACE dredged approximately one acre of river bottom to remove PCB contamination from the environment (USACE, 2016).

PCBs are a class of chemical compounds in which 1 – 10 chlorine atoms are attached to the biphenyl molecule and are entirely of anthropogenic origin. Industrial PCBs were complex mixtures composed of up to 50 or 60 congeners where the production favors specific congeners within a given industrial mixture (Frame et al., 1996). Each Aroclor code number (e.g. Aroclor 1254) generally has the last two numbers refer to the percent by weight of chlorine in a mixture (National Academy Press, 2001). PCBs accumulate in the environment and do not readily degrade classifying them as persistent organic pollutants that can build up in the body fat of animals, including fish that eat contaminated food over many years (D. D. Reible, 2014).

The two primary goals of this study were to assist in the identification of specific locations or areas along the northern and eastern tip of Bradford Island that are potential source areas. This objective was supported using low-density polyethylene (LDPE) passive samplers as a line of evidence to eliminate source areas along the northern and eastern tip. By incorporating a high density of passive samplers across these locations any ongoing source areas present or localized areas that are acting as a source of PCBs to the sediment and biota of Bradford Island could be identified. By using passive sampling, water concentrations at the sediment water interface could be inferred to identify areas where high concentration of PCBs might be released into the overlying water. A total of 163 LDPE passive samplers were deployed over the study area of approximately 3.7 acres (1.5 hectares).

4.3. MATERIALS AND METHODS

4.3.1 LDPE SAMPLING APPARATUS

Low-density polyethylene sheets (10 cm x 10 cm x 25.4 μm) as a polymer sorbent for PCBs were encased in a Type 316 stainless steel mesh with a 4.5 μm diameter wire and fastened to weighted pouches to keep passive samplers in direct contact with surficial sediment during the deployment time. The weighted pouch construction includes wire mesh with openings, at minimum of 1.3 cm, and included 4.5 kg of 4- and 5-cm diameter steel ball bearings (Figure 4-1).

Figure 4-1 LDPE sampling apparatus for Bradford Island. The LDPE samplers (10 cm x 10 cm coupon) is placed underneath the steel balls in a stainless-steel wired mesh and lowered down to the sediment water-interface

Prior to deployment the LDPE sheets are cleaned by consecutive solvent rinses of dichloromethane, hexane, methanol, and ultrapure water to remove impurities from the polymer. Once cleaned the polymers are weighed and impregnated, in a water-methanol (80:20, v/v) solution, with C^{13}-labeled performance reference compounds (PRCs). The sheets were left on a 1-D shaker table for approximately 35 days before being removed and enclosed in the previously mentioned stainless steel mesh and taken to the field.

Research grade C^{13}-labeled PCB compounds (Cambridge Isotope Labs) were used as performance reference compounds for low sensitivity analysis and three alternative C^{13}-labeled PCB compounds were used as recovery standards during the extraction process. Analysis was performed for individual PCB congeners by gas chromatography paired with a triple quadrupole mass spectrometer (GC-TQMS, Agilent 7890B) using SIM/SIM mode following EPA Method 1668c using internal standards as reference compounds (USEPA, 2010). This methodology has been highly cited and documented among other scientists and engineers familiar with passive sampling practices in contaminated sediments (Apell & Gschwend, 2016; Ghosh et al., 2014; Thomas et al., 2014; USEPA, 2012).

The freely dissolved porewater concentrations (C_{pw}) can be calculated from the accumulated uptake in the polymer (C_{pe}) and the polymer-water partition coefficient (K_{pe-w}, derived from Ghosh et al., 2014) as shown in the following (4.1).

$$C_{pw} = \frac{C_{pe}}{K_{pe-w}} = \frac{C_{extract} * V_{solvent}}{M_{pe} * K_{pe-w} * f_{ss}} \quad (4.1)$$

Where $C_{extract}$ and $V_{solvent}$ are the contaminant concentration extracted from the individual sheet of polymer and the volume of solvent analyzed, respectively. While M_{pe} and f_{ss} are the mass of polymer sheet extracted and the compound specific fractional approach to steady state, respectively. The compound specific f_{ss} is assumed to facilitate linear partitioning to the polymer, scale with hydrophobicity, and be reversible (Ghosh et al., 2014; Mayer et al., 2014).

4.3.1.1 PARTIAL PRC LOADING IN LDPE

To prepare for the field event a total of 198 LDPE coupons (10 cm x 10 cm) were impregnated with ^{13}C-PCB PRCs. Although the sheets would ideally be loaded individually, they were loaded in groups of 9 individual sheets in 22 different jars due to the logistical challenges of loading 198 sheets separately. The sheets were covered with a stainless-steel mesh both to separate the individual sheets during PRC loading and to protect the LDPE after placement in the environment. Despite these efforts and a loading time of 30 days ($\sim 500\ L^2/D_p$, Figure 3-4), equilibrium was not achieved. It was estimated that average equilibration of PRCs ranged from 65-135% of the target loading with individual LDPE sheets showing greater variations, as shown in Figure 4-2. Greater than 100% of target loading is the result of exposure to much higher concentrations initially in sheets that were most exposed to the loading solution and was the motivation of developing the model in Chapter 3.

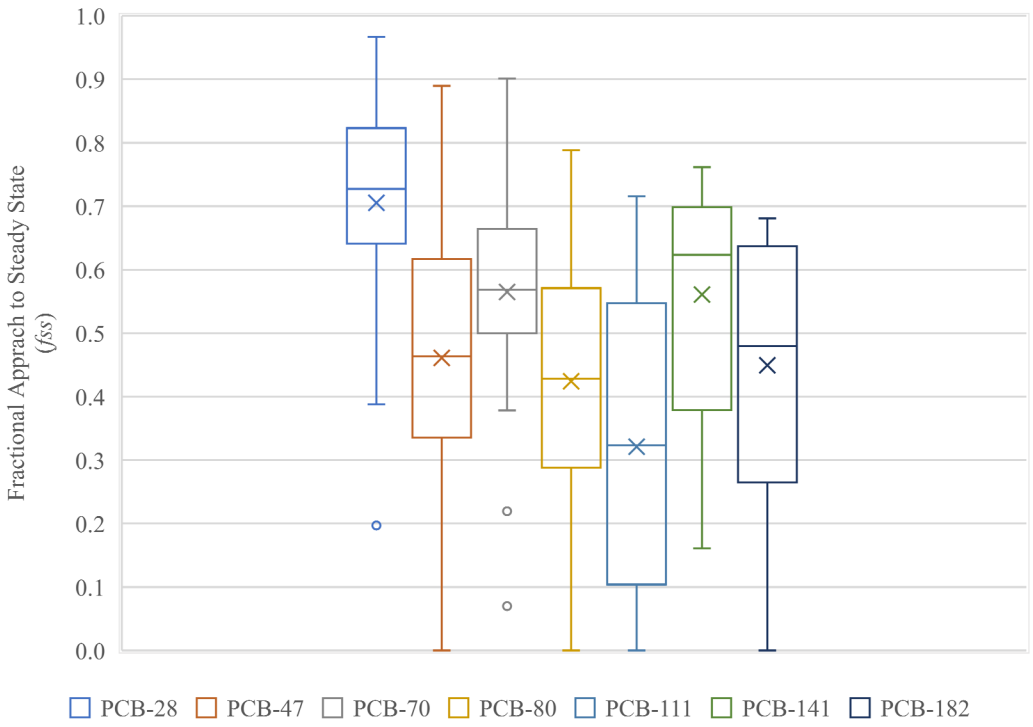

Figure 4-2 Distribution of f_{ss} for individual ^{13}C-PCB PRCs from 22 LDPE C0's

As discussed in Section 3.4.3 the modeling suggests that the failure to achieve the equilibrium in the experimental system even at times $\gg L^2/D_p$ is likely due to a significant variation in external mass transfer coefficient on the various LDPE sheets. The very low apparent Bi numbers on some sheets are likely aided by the stainless-steel mesh which limited mixing external to the sheets. The fact that the biggest deviations from equilibrium are associated with the low Bi conditions suggest that the concentration profile within the LDPE sheets are likely uniform (case in Figure 3-2) even when far from equilibrium. The previous model indicates that measurements of individual ^{13}C-PCB PRCs are not incorrect, and likely would not be a problem if individual measurements of C0 were possible, but due to this fact the averaged measurement of C/C0 for the ^{13}C-PCB PRCs to determine f_{ss} was used.

4.3.2 Passive Sampler Placement

The stainless-steel enclosed LDPE passive samplers were fastened to the weighted pouch, global positioning system (GPS) coordinates were used on board to navigate to the 163 predetermined locations, and the samplers were lowered to the sediment-water interface. The pulley system was camera guided to ensure the passive sampler was not placed on large debris, and a buoy was attached to the line to spot during the retrieval event.

Figure 4-3 LDPE sampling stations along the Bradford Island shoreline. A total of 163 LDPE samplers were deployed

Upon retrieval, after 35 days of exposure at the sediment-water interface, any adhering material was removed from the polymer with a lint-free damp tissue before segmented into halves (5 cm x 10 cm x 25.4 µm) for replicates at each of the sample stations. The polymers are then placed in amber vials with 20 mL of hexane and extracted for 24 hours three times, for a total of 60 mL of solvent extract. The vial is then placed under a gentle stream of nitrogen until the desired extract volume was achieved prior to

analysis. Because the locations of highly elevated concentrations were the target of the study, samples were concentrated to 1 mL (60 times concentration) for analysis.

4.3.3 APPROACH TO SUMMARIZING SAMPLING RESULTS

Because the primary objective was identification of source areas, results were reported primarily as a sums of PCB congener concentrations in porewater . Table 4-1 includes various ∑PCB congener concentrations calculated. The full method by TTU quantifies concentration in 141 congeners which was evaluated on a subset of 30 samples. For this study, it was proposed to evaluate the ∑PCB of 46 congeners that were of special interest to the project sponsor based upon the frequency at which they are observed, their presence in Aroclor 1254, based on the work done by Frame et al., (1996), or their relevance to ecological risk assessment. Final specific congener indicators of Aroclor 1254 or of specific ecological concern were summed as shown in Table 4-1.

Table 4-1 List of PCB Congeners for Analysis. Note certain PCB congeners co-elute with the GC-TQMS method and are reported as the sum of multiple congeners.

PCB Congener for TTU Analysis $\sum PCB_{141}$	**Common in Bradford Island Media $\sum PCB_{46}$**	**Component of Aroclor 1254 (Frame, 1996)**	**Congener of Ecological Concern**
1			
2			
3			
4			
10			
9+7			
6	*		
8	*	*	*
5			
19	*		

Table 4-1, Continued

30			
11	*		
18	*	*	*
17			
15			
27			
24			
32			
34			
16	*	*	
29			
26			
25			
31+50			
28			
20+33+21+53			
51			
22			
45			
46			
69			
52	*	*	*
49		*	
47		*	*
48			
65			*
44		*	*
42			
37			
71			
41			
64			
103			
40			
67			
100	*		
74	*	*	
61	*		
70	*	*	
76	*	*	

Table 4-1, Continued

102+98	*	*	
66			
93+95	*	*	
92			
60			
56			
84			
101	*	*	*
90	*	*	
113	*		
99	*	*	
119	*	*	
83	*	*	
97	*	*	
86+125	*	*	
87	*	*	
81			
115	*	*	
136			
110	*	*	
77			
82			
151			
144+135			
147	*	*	
107			
108	*		
123			
149	*	*	
118	*	*	*
134			
114			
131			
146			
153	*	*	*
132			
168	*		
105	*	*	*
141			
179			

Table 4-1, Continued

163	*	*	
138	*	*	*
158		*	
160	*	*	
178			
129	*	*	
126			
187	*	*	*
183			
128+167			
174			
177			
171			
156			
157			
172			
173			
197			
180	*	*	*
193	*	*	
191			
169			
170			
190			
198			
196			
203			
189			
208			
195			
207			
194			
205			
206			
209			

Because initial concentrations were observed to be low (equivalently sub ng/L), due to the small number of congeners measured or detectable in most samples at the

limited initial dilution, and limited congener analysis, a separate set of 35 duplicate samples were concentrated to 100 µL (600 times concentration compared to the original extract) and analyzed at Eurofins Test America in Knoxville, TN for a full PCB 209 congener analysis. These sums were also compared to congener sums identified in Table 4-1. See Appendix 9.3 for full analysis and ranked summary.

4.4. RESULTS AND DISCUSSION

4.4.1 POREWATER CONCENTRATION HEAT MAP

Given the polymer is placed at the sediment-water interface, and not inserted into the sediment the PCB concentration can be viewed as either the surficial sediment porewater concentration or water upwelling from the sediment. Although concentrations would be expected to be lower than if passive sampler were inserted directly into sediments, any highly concentrated source areas would be expected to be easily identifiable. Highly concentrated samples were not observed, although certain areas were identified that exhibited higher concentrations than other sampling locations. An area of a previously observed debris piles on the eastern tip of the island exhibited concentrations about an order of magnitude higher than typical locations around Bradford Island (Figure 4-4). Two samples were the highest observed freely dissolved concentration at 0.14 and 0.08 ng/L ($\sum_{n=46} PCB$), respectively.

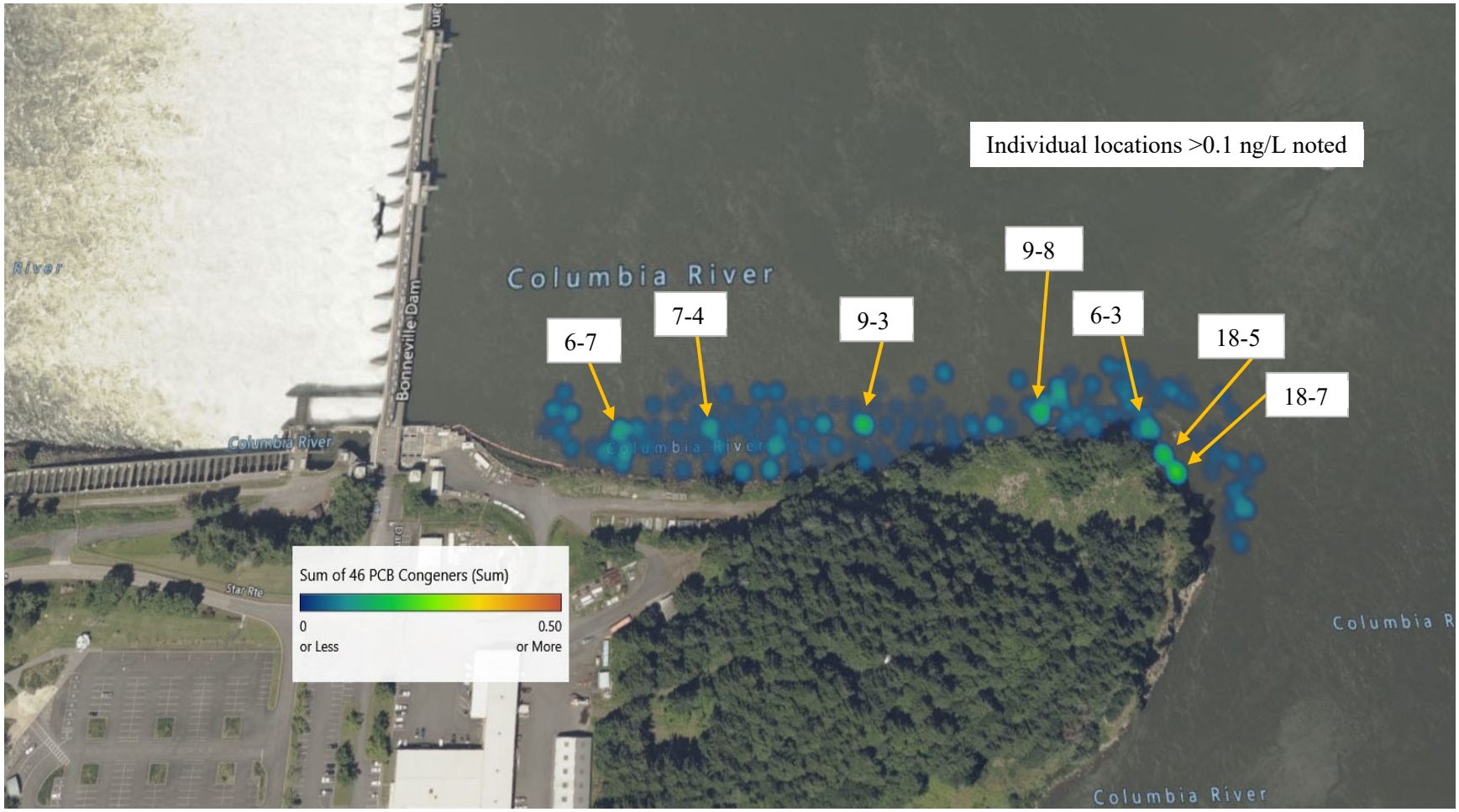

Figure 4-4 Porewater concentration heat map of retrieved LDPE samplers. Specific stations are called out that were found to have a total PCB ($\sum PCB_{46}$) concentration above 0.1 ng/L

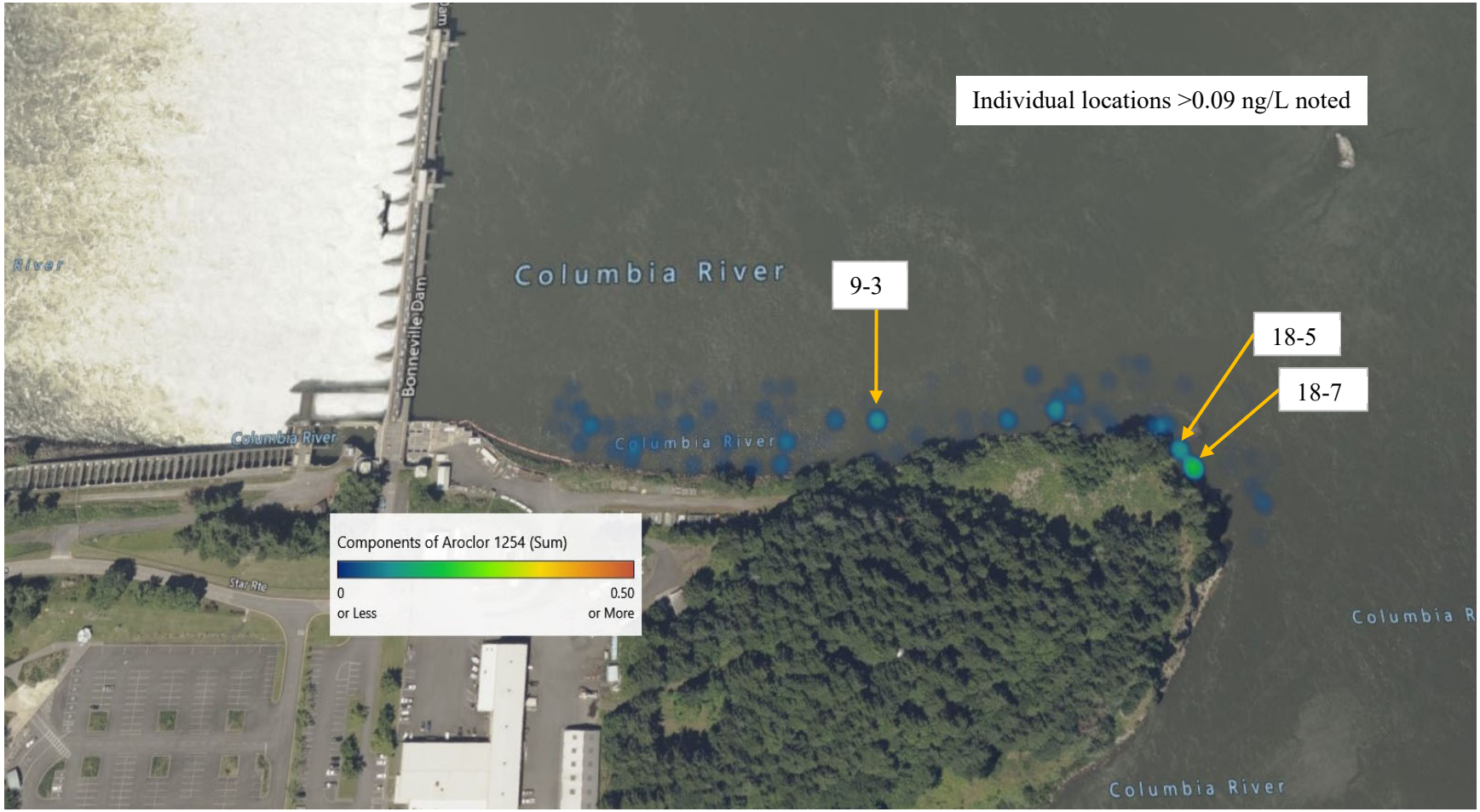

Figure 4-5 Porewater concentration heat map of retrieved LDPE samplers. Individual stations are called out that exhibited >0.09 ng/L of PCB congeners found in Aroclor 1254 as cited in Frame et al. (1996)

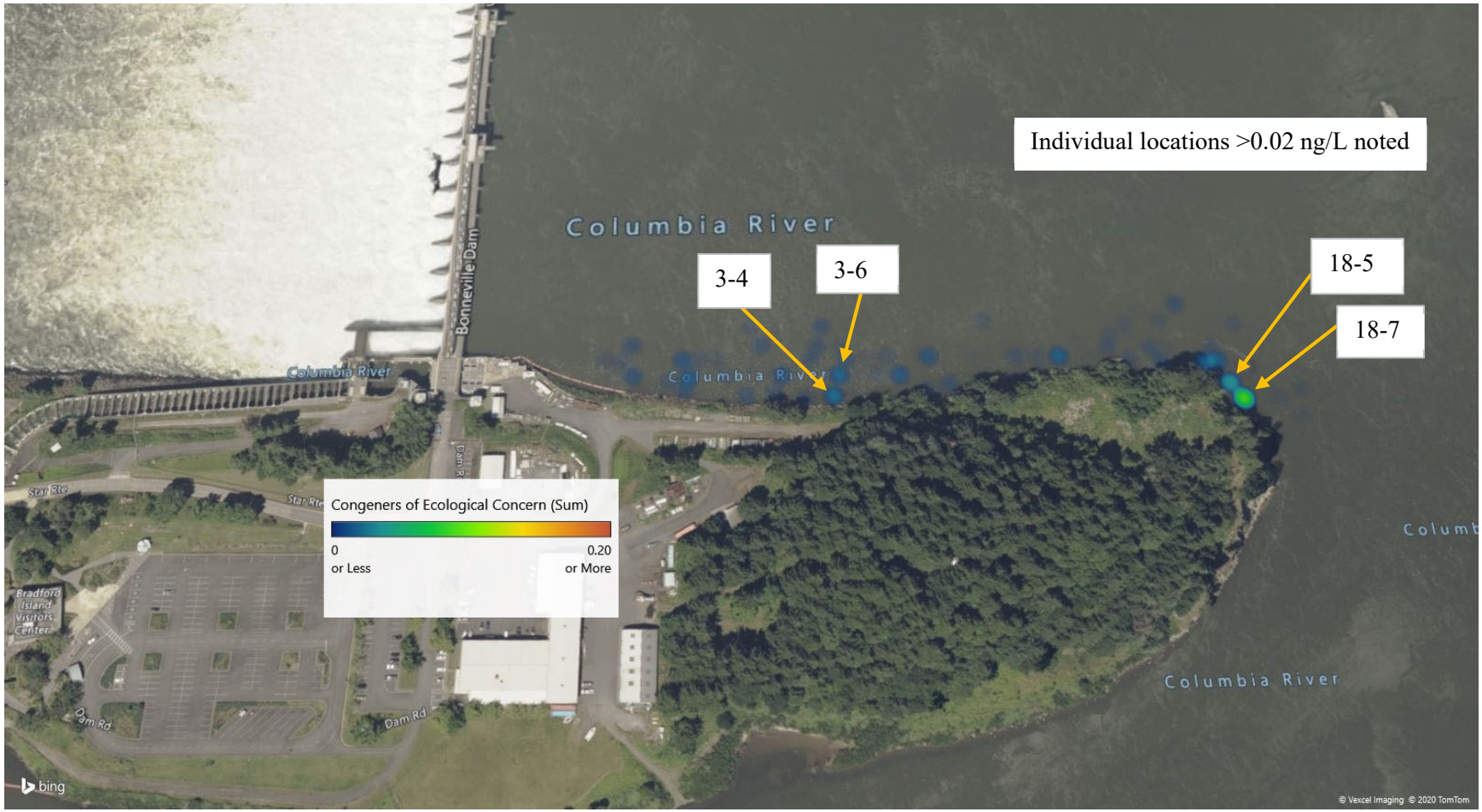

Figure 4-6 Porewater concentration heat map of retrieved LDPE samplers. Individual stations are called out that exhibited >0.02 ng/L of PCB congeners of ecological concern.

There was a second area of elevated concentration halfway along the northern shore of the island (Figure 4-4). This area previously contained a historical debris pile likely from the accumulation of PCB mixture containing structures. Most concentrations (sum of 46 congeners) on the surface of the sediments were roughly 0.05 ng/L and roughly half of the observed congeners were composed of Aroclor 1254 congeners.

4.4.2 Freely Dissolved Porewater Concentration Compared to Observed Fish Tissue

Historical documents indicate significant impacts to sediment and the fractured bedrock river-bottom in the vicinity of Bradford Island has occurred and resident fish such as smallmouth bass caught near Bradford Island contain elevated PCB tissue concentrations (USACE, 2016). In areas previously known to contain elevated measurements of PCBs (measured individual congeners and summed as Aroclor 1254) in smallmouth bass LDPE passive samplers were suspended within the water column to report a freely dissolved water concentration (Figure 4-7).

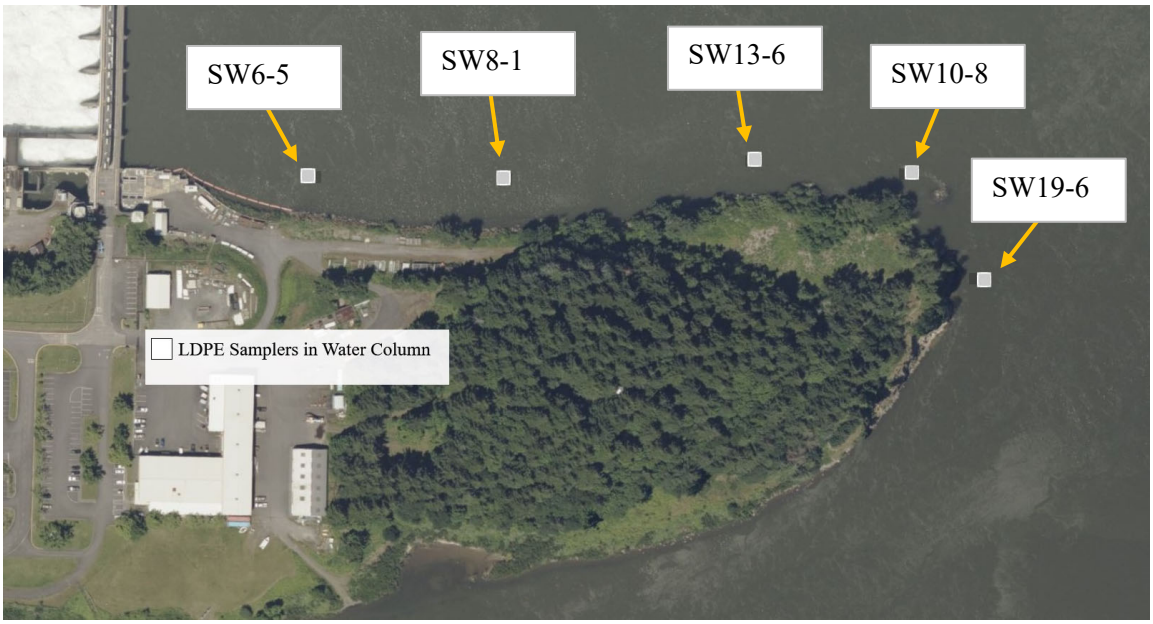

Figure 4-7 Surface water LDPE Passive Sampler stations that coincide with previously captured smallmouth bass

The elevated fish tissue concentrations continues to be a driving force for regulatory guidance on the island and on September 8, 2021 the U.S. Environmental Protection Agency announced it would propose adding Bradford Island to the National Priorities List (Wirtis, 2021). Given the overlap in sampling stations a bioconcentration factor (BCF) is used to compare the freely dissolved porewater concentrations to the tissue concentrations found by URS (2013) and URS (2012). Note, however, that although the URS (2012) report was submitted in 2012 the analysis of smallmouth bass was conducted in 2006 (Table 4-2).

Bioconcentration factor (BCF) is usually estimated as chemical concentration in an organism (C_b) divided by water concentration at equilibrium to screen for bioaccumulation potential (S. Wang et al., 2020; W.-X. Wang, 2016), shown in (4.2).

$$BCF = \frac{C_b}{C_w} \tag{4.2}$$

Where C_b is the contaminant concentrations in the organism (µg/kg) under equilibrium conditions and C_w is the contaminant concentration in the water (µg/L).

Table 4-2 Freely dissolved water concentrations of Aroclor 1254 from LDPE passive samplers (C_w^{LDPE}) suspended in the water column compared to measured smallmouth bass tissue concentrations from previous sampling events and calculated bioaccumulation factors $\log(BCF)$.

Sample ID	∑PCB Aroclor 1254 (µg/L)	∑PCB Aroclor 1254 Tissue concentration in smallmouth bass (µg/kg, wet)		Bioconcentration Factor (BCF)	
	C_w^{LDPE} (2020)	URS (2013)	URS (2012)**	Log(BCF) 2013	Log(BCF)2012
SW6-5	6.02E-05	65,000	1,193	9.0	7.3
SW8-1	8.38E-05	13,000	-	8.2	-
SW13-6	7.91E-05	29,000	-	8.6	-
SW10-8	3.40E-05	-	26,500	-	8.9
SW19-6	7.04E-05	-	2,482	-	7.5

** - URS, (2012) report submission was in 2012, however the sampling of small mouth bass was conducted in 2006.

The above values were compared to peer reviewed literature for confidence in reporting. Mackay et al. (1992) reported Aroclor 1254 as a surrogate for other Aroclor mixtures and lists a BCF value of 164,000 ($\log BCF = 5.21$) for fish while the Office of Environmental Health Hazard Assessment (2000) is recommending the arithmetic mean of fish, oyster and shrimp values reported by Mackay et al. (1992) of 99,667 ($\log BCF = 4.99$) as representative of PCBs. Arnot & Gobas (2006) published a review of acceptable bioconcentration factor (BCF) lab data in fish as a function of the octanol-water partitioning coefficient for 2,527 distinct types of fish across 770 chemicals and found a median $\log BCF$ values of 2.45 – 4.65. The range includes HOCs with $\log Kow$ ranging

from 3.72 – 6.91 as chemical mixtures (e.g., Aroclor) were not included in this study. This is similar to the values found in Gobas et al. (1989) for PCBs accumulated in guppy (*Poecilia reticulata*).

Although Oregon Department of Environmental Quality (ODEQ) reports a smallmouth bass tissue concentrations as high as 183,140 parts per billion (ODEQ, 2010), these values were not found in URS (2013) or URS (2012). However, no "free phase" total PCB concentrations were identified, and the relatively low concentrations suggest that the high concentrations observed in some fish is likely not be due to the elevated areas identified (Table 4-2).

4.4.3 Full 209 PCB Congener Analysis

Due to the concern of the low $\sum PCB_{46}$ and $\sum PCB_{141}$ porewater concentrations (TTU analysis) concerns arose of the potential of an incomplete analysis and relative dilution of the samples. This led to 35 duplicate (solvent extracted from adjacent 5 cm x 10 cm coupon) samples being concentrated to 100 µL and submitted for full PCB congener analysis. At Eurofins Test America, the samples were concentration to 100 µL and analyzed for all PCB congeners. Note the TTU analysis was performed at 1 mL solvent extract, and by concentrating to 100 µL, congener concentrations would increase by a factor of 10. Therefore, the total PCB concentrations analyzed by Eurofins Test America are expected to be higher than those reported by TTU due both to the summation of 209 congeners instead of 46, and the inclusion of congeners that were below reportable limits in the more dilute samples analyzed at TTU. See Appendix 9.3 for entire analysis and ranking.

Figure 4-8 shows the location of all 35 samples sent to Eurofins Test America and specifically identifies the six highest concentration locations. While Figure 4-9 shows the magnitude of $\sum PCB_{209}$ porewater concentrations that will be compared to the $\sum PCB_{46}$ porewater concentrations at the same locations found in Figure 4-10.

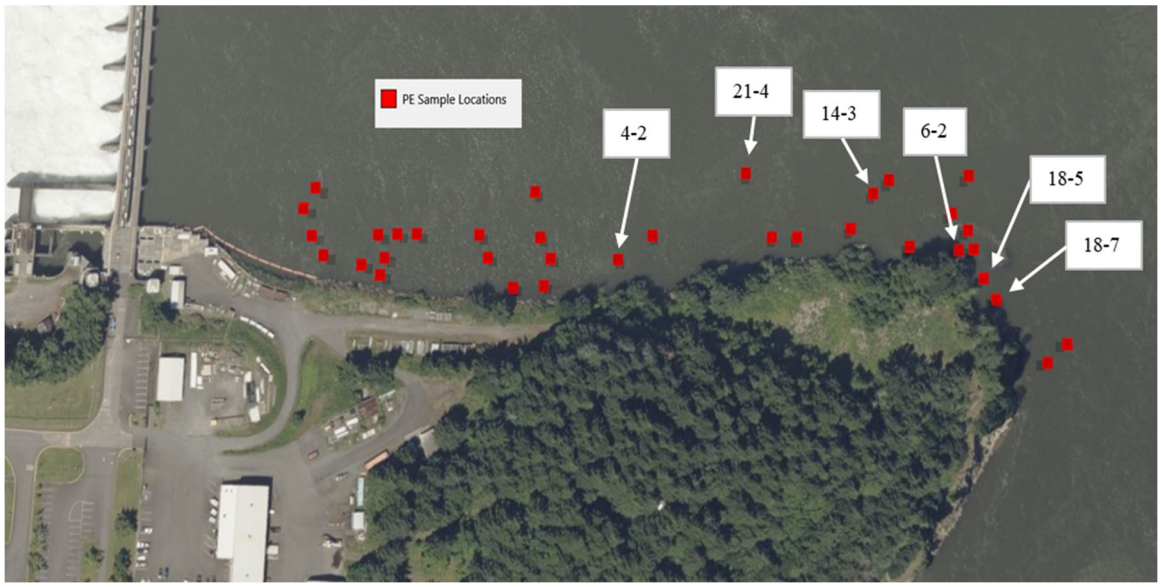

Figure 4-8 Locations of LDPE samples sent for full congener analysis by Eurofins Test America. The labeled locations represent the locations with the highest $\sum PCB_{209}$ porewater concentrations

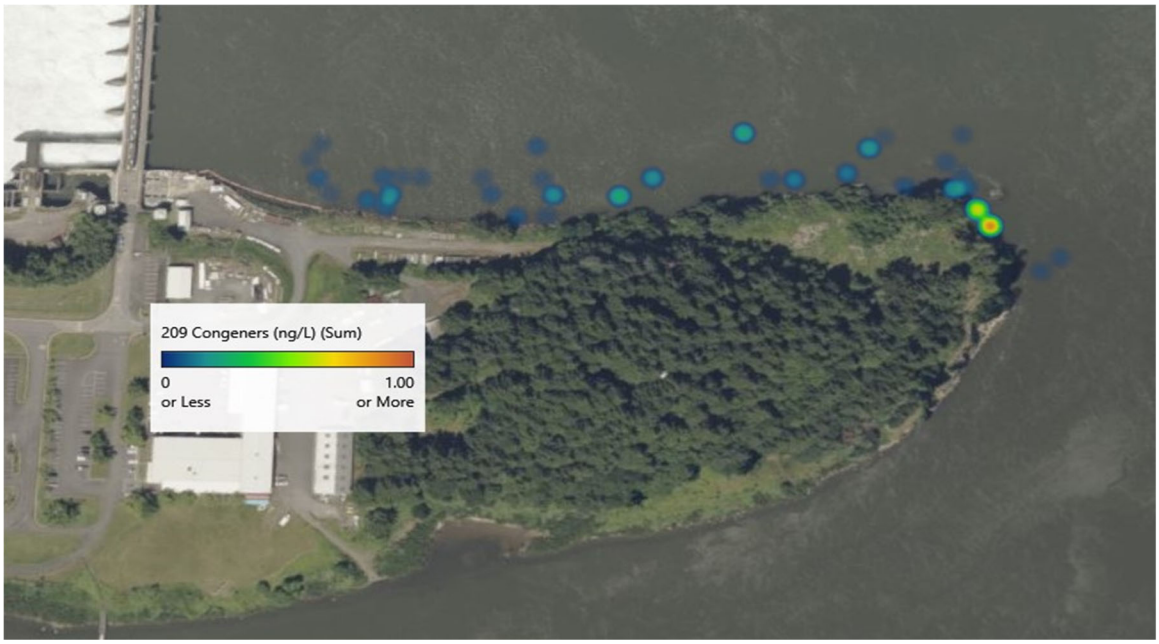

Figure 4-9 Magnitude of $\sum PCB_{209}$ porewater concentrations estimated for all locations sent for analysis by Eurofins Test America.

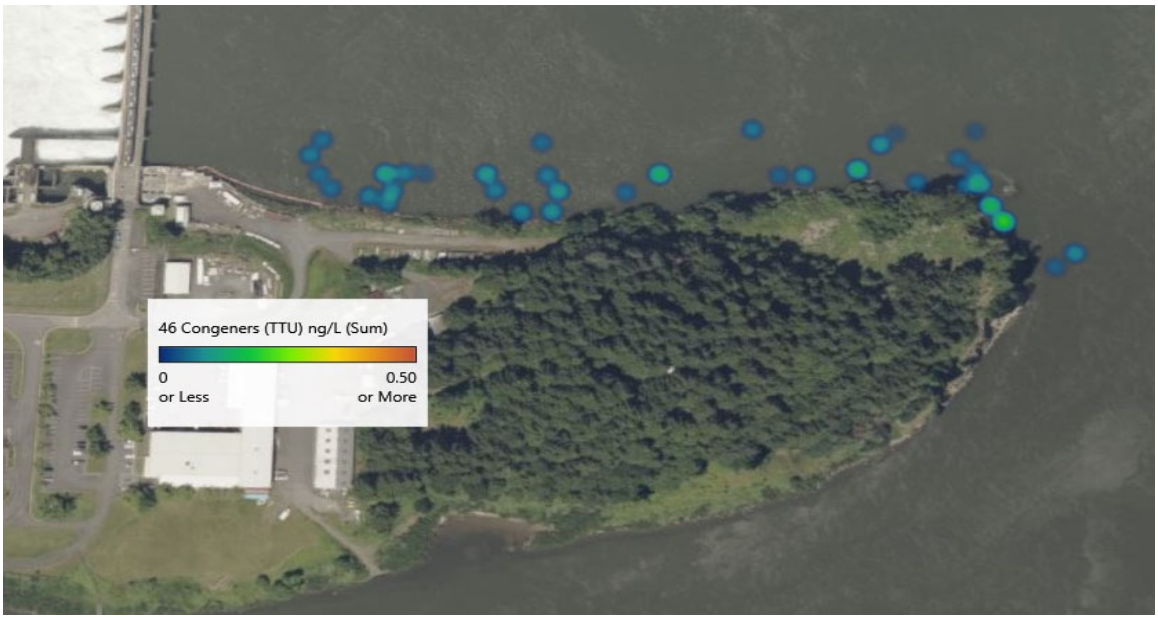

Figure 4-10 Magnitude of $\sum PCB_{46}$ porewater concentrations from Texas Tech University analysis for the locations shown in Figure 4-8 and Figure 4-9.

Figure 4-11 shows a comparison of the 10 highest concentration samples from the $\sum_{46}$ porewater congeners (TTU analysis) and the $\sum_{209}$ porewater congeners (Eurofins Test America analysis). The correlation is quite good although the absolute concentrations in

the TTU analysis are much lower due to the sum over a smaller number of congeners and the increased dilution and inability to see low concentration congeners in the TTU analysis. Thus the $\sum_{46}$ porewater congeners (TTU analysis) are expected to provide a good indication of the locations most elevated in concentration compared to the full 209 congener analysis. The TTU and Eurofins Test America analysis is expected to show greater differences at lower concentration locations as a result of the smaller number of congeners summed and the more limited number of congeners that can be quantified due to detection limits in the more dilute samples. The $\sum_{46}$ porewater congeners (TTU analysis) can only characterize locations that involve congener distributions that are well represented by the 46 congeners. In particular, the $\sum_{46}$ porewater congener analysis is not expected to be able to identify locations unless they are impacted by sources from mid-range Aroclor mixtures like 1242, 1248 and 1254.

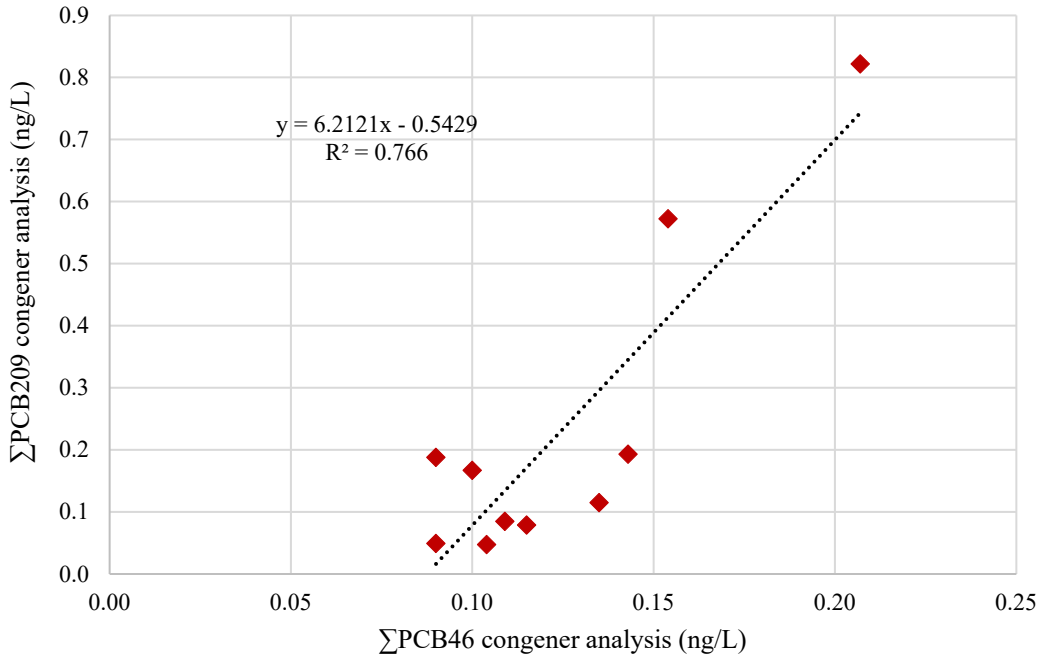

Figure 4-11 Correlation of 10 highest porewater concentrations by the TTU analysis compared to the Eurofins Test America concentrations full congener analysis at the same locations

The 209-congener analysis identified several locations with relatively high porewater concentrations but with a congener distribution that did not reflect impacts of mid-range Aroclor mixtures. Figure 4-12 shows the porewater congener distribution in Location 18-7, the highest concentration location at the eastern tip of Bradford Island. This is compared to the anomalous congener distribution in sample 4-2 in Figure 4-13. Similar anomalous congener distributions that were biased toward low molecular weight congeners was observed at 21-4 and 14-3. The relative proportion of the higher molecular weight congeners in these samples were much less than at the significantly elevated concentrations of 18-7 and 18-5. This would suggest that the PCB distribution at these locations is from a different source or subject to a separate set of fate processes than at locations 18-7 and 18-5.

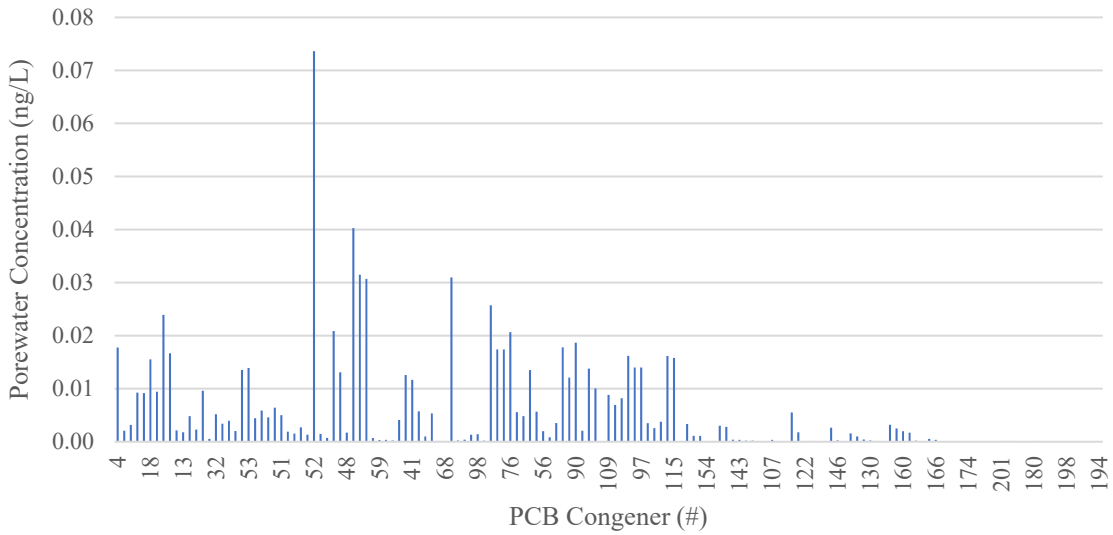

Figure 4-12 Full 209 PCB congener distribution porewater concentration of Sample 18-7. The summation of all detected PCB congeners equates to a 0.84 ng/L porewater concentration.

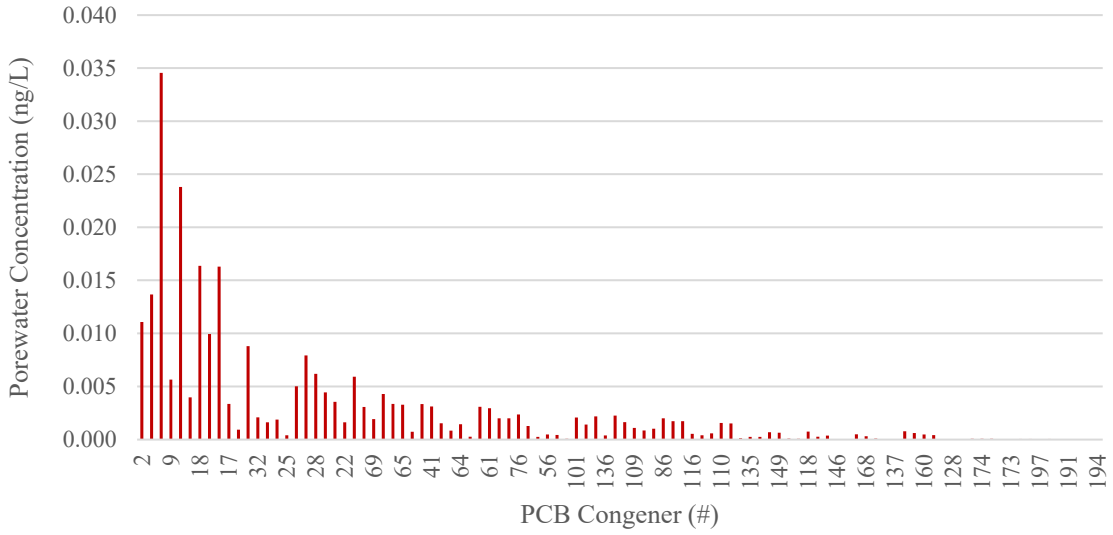

Figure 4-13 Full 209 PCB congener distribution porewater concentration of Sample 4-2. The summation of all detected PCB congeners equates to a 0.26 ng/L porewater concentration.

The occurrence of congener PCB-11 constituted approximately 6 – 20% of the total PCB congener burden to samples with lower total PCB concentrations. This is consistent with the results where other regional studies have noted airborne PCBs in the

Willamette airshed have contributed to the ubiquitous occurrence of PCBs in sediments and that PCB-11 is one of the indicator PCB congeners for evidence of airborne deposition (Hope, 2008). Part of the reason it is so ubiquitous may be that it is not derived by Aroclor mixtures but is instead found in unregulated paints, pigments, and in other source matrixes such as incineration (Anderson, 1991; Fraser, 2010; Hu & Hornbuckle, 2010; Rodenburg et al., 2010).

4.5. CONCLUSION

Both the full congener analysis and the previous partial congener analysis by TTU showed that highest concentrations detected were along the eastern tip of Bradford Island. The porewater concentrations measured there were 3-4 times concentrations detected elsewhere in the full congener analysis. The TTU analysis was successful at meeting the objectives of the initial study which was to identify locations with elevated concentrations. Neither the TTU or Eurofins Test America analysis found any locations that might be associated with separate phase or highly contaminated regions. The partial congener analysis by TTU can be used to evaluate the highest concentration locations impacted by mid-range Aroclor mixtures but due to the more dilute samples and the sum over a smaller number of congeners, it does not provide a good relative ranking of locations that are low in concentration nor those that are impacted by low molecular weight congeners that are not included in the 46 congeners selected for evaluation.

The full congener analysis suggests that the concentrations along the north side of Bradford Island are significantly lower than at the eastern tip. The locations of highest concentration along the north side of the island were dominated by low molecular weight PCB congeners and the congener distribution was inconsistent with a mid-range Aroclor

signature. Surface water samples were also dominated by low molecular weight congeners. All samples showed a relatively uniform concentration of PCB 11 which does not have a clear genesis in commercial Aroclor mixtures, and this congener was a significant component of low concentration samples.

Additionally, bioconcentration factors (BCF) were determined for the six greatest $\sum PCB_{209}$ porewater concentrations, called out in Figure 4-8, and ranged from 7.5 – 8.2 ($\log BCF$). Although smallmouth bass was not directly captured from these stations the chemical concentration in the organism (C_b) most near the station was used. These values continue to vary greatly from observed $\log BCF$ literature values. Concluding either the smallmouth bass are concentrating the PCBs to a greater extent that other sites, we potentially missed the significant source areas despite the large number of samples, or the elevated tissue concentrations are coming from other source areas upstream rather than Bradford Island.

4.6. REFERENCES

Anderson, J. W. (1991). Determination of congeners of polychlorinated biphenyls in reference materials. *Journal of High Resolution Chromatography*, *14*(6), 369–372. https://doi.org/10.1002/JHRC.1240140603

Apell, J. N., & Gschwend, P. M. (2016). In situ passive sampling of sediments in the Lower Duwamish Waterway Superfund site: Replicability, comparison with ex situ measurements, and use of data. *Environmental Pollution*. https://doi.org/10.1016/j.envpol.2016.08.023

Arnot, J. A., & Gobas, F. A. P. C. (2006). A review of bioconcentration factor (BCF) and bioaccumulation factor (BAF) assessments for organic chemicals in aquatic organisms. In *Environmental Reviews* (14th ed., pp. 257–297). Canadian Science Publishing.

Frame, G. M., Cochran, J. W., & Bøwadt, S. S. (1996). Complete PCB Congener Distributions for 17 Aroclor Mixtures Determined by 3 HRGC Systems Optimized for Comprehensive, Quantitative, Congener-Specific Analysis. *HRC Journal of High Resolution Chromatography*. https://doi.org/10.1002/jhrc.1240191202

Fraser, B. (2010). Researchers find little-known PCB "pretty much everywhere." *Environmental Science and Technology*, *44*(8), 2753–2754. https://doi.org/10.1021/ES100692H

Ghosh, U., Kane Driscoll, S., Burgess, R. M., Jonker, M. T. O., Reible, D., Gobas, F., Choi, Y., Apitz, S. E., Maruya, K. A., Gala, W. R., Mortimer, M., & Beegan, C. (2014). Passive sampling methods for contaminated sediments: practical guidance for selection, calibration, and implementation. *Integrated Environmental Assessment and Management*, *10*(2), 210–223. https://doi.org/10.1002/ieam.1507

Gobas, F. A. P. C., Clark, K. E., Shiu, W. Y., & Mackay, D. (1989). Bioconcentration of polybrominated benzenes and biphenyls and related superhydrophobic chemicals in fish: Role of bioavailability and elimination into the feces. *Environmental Toxicology and Chemistry*, *8*(3), 231–245. https://doi.org/10.1002/ETC.5620080306

Gross, M. (2013). *Analytical Results for Sediment, Clams, and Bass collected from Forebay September/October 2011 and Bass collected from Reference Area August 2011, Bradford Island Pre-Feasibility Study*.

Hope, B. K. (2008). A model for the presence of polychlorinated biphenyls (PCBs) in the Willamette River basin (Oregon). *Environmental Science and Technology*, *42*(16), 5998–6006. https://doi.org/10.1021/ES8000213/SUPPL_FILE/ES8000213-FILE002.PDF

Hu, D., & Hornbuckle, K. C. (2010). Inadvertent polychlorinated biphenyls in commercial paint pigments. *Environmental Science and Technology*, *44*(8), 2822–2827. https://doi.org/10.1021/ES902413K/SUPPL_FILE/ES902413K_SI_001.PDF

Mackay, D., Shiu, W. Y., & Ma, K. C. (1992). *Illustrated Handbook of Physical-*

Chemical Properties and Environmental Fate for Organic Chemicals: Polynuclear Aromatic Hydrocarbons, Polychlorinated Dioxins and Debenzofurans. Lewis Publishers.

Mayer, P., Parkerton, T. F., Adams, R. G., Cargill, J. G., Gan, J., Gouin, T., Gschwend, P. M., Hawthorne, S. B., Helm, P., Witt, G., You, J., & Escher, B. I. (2014). Passive sampling methods for contaminated sediments: scientific rationale supporting use of freely dissolved concentrations. In *Integrated environmental assessment and management*. https://doi.org/10.1002/ieam.1508

National Academy Press. (2001). A Risk Management Strategy for PCB-Contaminated Sediments. *A Risk Management Strategy for PCB-Contaminated Sediments*. https://doi.org/10.17226/10041

ODEQ. (2010). *State of Oregon: Cleanup Sites - Bradford Island at Bonneville Dam*. https://www.oregon.gov/deq/Hazards-and-Cleanup/CleanupSites/Pages/Bradford-Island.aspx

Office of Environmental Health Hazard Assessment. (2000). *Appendix H - Fish Bioconcentration Factors; Appendix H - Fish Bioconcentration Factors*.

Reible, D. D. (2014). Contaminant Processes in Sediments. In *Processes, Assessment and Remediation of Contaminated Sediments*. https://doi.org/10.1007/978-1-4614-6726-7

Rodenburg, L. A., Guo, J., Du, S., & Cavallo, G. J. (2010). Evidence for unique and ubiquitous environmental sources of 3,3′-dichlorobiphenyl (PCB 11). *Environmental Science and Technology*, *44*(8), 2816–2821. https://doi.org/10.1021/ES901155H/SUPPL_FILE/ES901155H_SI_001.PDF

Thomas, C., Lampert, D., & Reible, D. (2014). Remedy performance monitoring at contaminated sediment sites using profiling solid phase microextraction (SPME) polydimethylsiloxane (PDMS) fibers. *Environmental Sciences: Processes and Impacts*. https://doi.org/10.1039/c3em00695f

URS. (2012). *Upland and River Operable Units Remedial Investigation Report for Bradford Island, Cascade Locks, Oregon*.

USACE. (2016). *Final feasibility study: Bradford Island Upland Operable Unit, Cascade Locks, Oregon - Project Management Reports - USACE Digital Library*. https://usace.contentdm.oclc.org/digital/collection/p16021coll7/id/4742

USEPA. (2010). *Method 1668C: Chlorinated Biphenyl Congeners in Water, Soil, Sediment, Biosolids, and Tissue by HRGC/HRMS*. www.epa.gov/waterscience/methods.

USEPA. (2012). *Guidelines for using passive samplers to monitor organic contaminants at superfund sediment sites*. 32. http://www.epa.gov/superfund/health/conmedia/sediment/pdfs/Passive_Sampler_SAMS_Final_Camera_Ready_-_Jan_2013.pdf

Wang, S., Lao, W., Li, H., & You, J. (2020). Measuring bioconcentration factors of sediment-associated fipronil in Lumbriculus variegatus using passive sampling techniques. *Journal of Hazardous Materials*, *393*, 122420. https://doi.org/10.1016/J.JHAZMAT.2020.122420

Wang, W.-X. (2016). Bioaccumulation and Biomonitoring. *Marine Ecotoxicology*, 99–119. https://doi.org/10.1016/B978-0-12-803371-5.00004-7

Wirtis, L. (2021). *Department of Environmental Quality : Bradford Island at Bonneville Dam : Cleanup Sites : State of Oregon*. Oregon Department of Environmental Quality. https://www.oregon.gov/deq/Hazards-and-Cleanup/CleanupSites/Pages/Bradford-Island.aspx

CHAPTER 5

IN-SITU PASSIVE SAMPLING TO MONITOR LONG-TERM CAP EFFECTIVENESS AT A TIDALLY INFLUENCED SHORELINE[2]

5.1. ABSTRACT

Polydimethylsiloxane solid phase microextraction passive samplers were used to evaluate long-term performance of a sand/gravel cap placed on 2005 in a tidally influenced shoreline in Puget Sound, west Seattle, Washington, to reduce polycyclic aromatic hydrocarbon (PAH) transport into overlying surface water. Sampling in both 2010 and 2018 measured porewater concentrations of <1 ng/L total PAHs in the cap layer. d-PAH performance reference compounds were used to evaluate the extent of equilibration of the contaminants onto the samplers and to estimate net upwelling velocities through a mass-transfer model. The upwelling velocities were used to predict long-term migration of selected PAHs through the cap, showing that the cap is expected to continue being effective at limiting exposure of contaminants at the cap-water interface.

5.2. INTRODUCTION

Contaminated sediment caps physically isolate environmental contamination and delay or eliminate significant release of hydrophobic organic compounds (HOCs). In the absence of advection, transport below surface layers is driven by sorption retarded

---

[2] This article was published on 23 February 2022.
Smith AV, Shen X, Garza-Rubalcava U, Gardiner W, Reible D. In Situ Passive Sampling to Monitor Long Term Cap Effectiveness at a Tidally Influenced Shoreline. *Toxics*. 2022;10(3):106. doi:10.3390/toxics10030106

diffusion and long-term effectiveness is typically observed (Eek et al., 2008; D. D. Reible, 2014). Sediment caps are challenged, however, in environments where advective transport such as groundwater upwelling or tidal pumping of groundwater is important. Evaluating the effect of these processes is a critical component of long-term monitoring of cap effectiveness.

Freely dissolved concentrations of HOCs can be measured via passive sampling, for example, by solid phase microextraction (SPME) utilizing polydimethylsiloxane (PDMS) as a sorbent (Mayer et al., 2014). Freely dissolved concentrations provide an indication of the contaminant that is mobile and available in a stable sediment cap. Previous studies have demonstrated the use of passive sampling to estimate concentrations influencing the benthic community in surficial sediments (David J. Lampert et al., 2011; M. I. Rakowska et al., 2012), and calculating the diffusive flux at the sediment-water interface (Fernandez et al., 2014; Thompson et al., 2015).

A 1-2 meter sand and gravel cap was placed in 2005 in the area offshore of a former creosote processing facility (Puget Sound Resources) to contain polycyclic aromatic hydrocarbons (PAHs). The site is subject to both groundwater upwelling and tidal variations that would be expected to lead to tidal pumping of groundwater. Passive sampling measurements in 2010 (D. Reible & Lu, 2012) showed that 5 years after placement, porewater concentrations over the upper 90 cm of the cap layer were not significantly different from concentrations in the overlying water. In a few locations, near-surface concentrations (<10 cm) were slightly above surface water concentrations either due to the deposition of sediments containing PAHs or intermixing of

contaminated sediments during placement. There was no evidence at that time of significant PAH contamination relative to concentration levels of concern or evidence of migration of PAHs through the cap.

In this study, PDMS SPME fibers were used to evaluate long term performance of a sediment cap by measuring porewater concentration profiles in 2018, 13 years after cap placement. Performance reference compounds were used to both estimate extent of equilibration and upwelling velocities through application of a porous media mass transfer model based upon the theory of Kimura (1988). The upwelling velocities and measured site porewater/sediment partitioning were used to predict long term migration of PAHs in the sediment cap using CapSim (Shen et al., 2018), a model of near-surface contaminant transport in sediments. The study provides evidence of the long-term performance of a sand and gravel sediment cap in an environment subject to groundwater upwelling and tidal pumping and demonstrates the use of performance reference compounds to both estimate equilibrium for passive sampling evaluation of cap performance and estimate the magnitude of the net groundwater upwelling.

5.3. MATERIALS AND METHODS

5.3.1 PDMS SPME FIBERS, SAMPLING DEVICES, AND PRCS

The PDMS SPME fibers were fabricated by Polymicro Technologies (Phoenix, AZ, USA). The fibers are composed of a 562 µm outer diameter of PDMS coating on a 485 µm glass core for a volume of 0.64 µL/cm of PDMS. Prior to deployment, the PDMS fibers were cut into 90 cm segments, washed twice with hexane, acetonitrile, and methylene chloride sequentially for 30 minutes each, rinsed with ultrapure distilled

deionized water (DDI), and dried with lint free tissue. Only high purity solvents were used in the preparation process of these PDMS fibers.

This study utilized the use of PRCs to evaluate fiber uptake kinetics, and deuterated PAHs spanning the range of hydrophobicity of the target compounds were selected. The polymers were impregnated with four deuterated PAHs, d10-fluoranthene, d12-chrysene, d12-benzo[b]fluoranthene, and d14-dibenzo[a,h]anthracene, purchased from Cambridge Isotope Labs (Tewksbury, MA, USA). Once the fibers were chemically cleaned, they were inserted into a methanol/water mix (20:80 v/v) that was spiked with the four d-PAH PRCs and left to equilibrate for a minimum of 28 days.

For ease of insertion and protection from sand and gravel in the sediments, the fibers were secured in stainless-steel modified Henry PushPoint samplers (M.H.E. Products, East Tawas, MI, USA) with a ¼" (6.5 mm) outer tube and smaller-diameter inner rod. The sampler was modified by perforating the outer (shield) tube along its length with 4 mm-diameter holes and cutting a slit along the length of the inner rod to which the fibers were secured by using waterproof silicone (caulk) at the two ends of the fiber. Prior to use, the stainless-steel samplers were washed with hot water and detergent, soaked sequentially in hexane, acetonitrile, and methylene chloride (Thermo Fisher Scientific, Waltham, MA, USA), flushed with deionized water, and dried at 105°C overnight.

The approaches to passive sampling in 2010 and 2018 were essentially identical, except that both thicker and thinner PDMS fibers were employed in 2010 to allow

estimation of equilibration, while PRCs were employed for the same purpose in 2018 (Lampert et al., 2011; Reible & Lu, 2012).

5.3.2 Site and Sampling Design

The subtidal sediments at the former Pacific Sound Resources site in West Seattle along the southern shore of Puget Sound were capped with sand and gravel borrow materials in 2005 (Figure 5-1). These sediments had been impacted by creosote-containing PAHs migrating through the subsurface. A slurry wall was also placed at the shoreline to control any further migration from upland areas.

Figure 5-1 Location of Puget Sound Resources in West Seattle, Washington. The ellipse shows the location of the site.

The cap material contained approximately 0.3% organic carbon and was placed to a thickness of 1 m (offshore) to 2 m (nearshore). The site is subject to a typical tidal range of 2-3 m. In-situ SPME passive samplers were placed at 24 individual monitoring locations along 7 transects extending out from the coastline in 2010 and again in 2018.

Sample locations 1 – 12 are in the northwestern (NW) part of the site along three transects (1-3) while 13 – 24 are in the eastern along an additional three transects (4-6) as shown in Figure 5-2. Samplers were deployed at these locations on 13-14 March 2018, and 22 of the 24 locations were retrieved on 28-29 March 2018. A sampler could not be deployed at locations 9, and the sampler at location 8 was found on the sediment surface upon retrieval. A sampler was also placed at a new location in 2018. Locations 8, 9, and the new location were all located on the western edge of the sampling array. No data could be retrieved from samplers at locations 8 and 9, but a nearby location showed low PAH concentration in porewater (∑PAH = 138 ng/L) consistent with other locations in the NE sampling area. Three samplers were suspended in the surface water: two in the water above the site and one in a reference location well away from the site. Figure 5-3 shows the SPME sampler used at the site.

As noted previously, the measurements collected in 2010 showed no evidence of migration of PAHs within the upper 90 cm of the cap layer, and porewater concentrations measured at that time were essentially uniform and approximately equal to that measured in the overlying water, except for slightly higher (2-3 times surface water concentrations) in the near surface (upper 10 cm) of 10-20% of the sampling locations. Because of the lack of significant contamination observed during the 2010 sampling, the analysis herein will focus on the 2018 sampling program, although the results will be compared to the 2010 data.

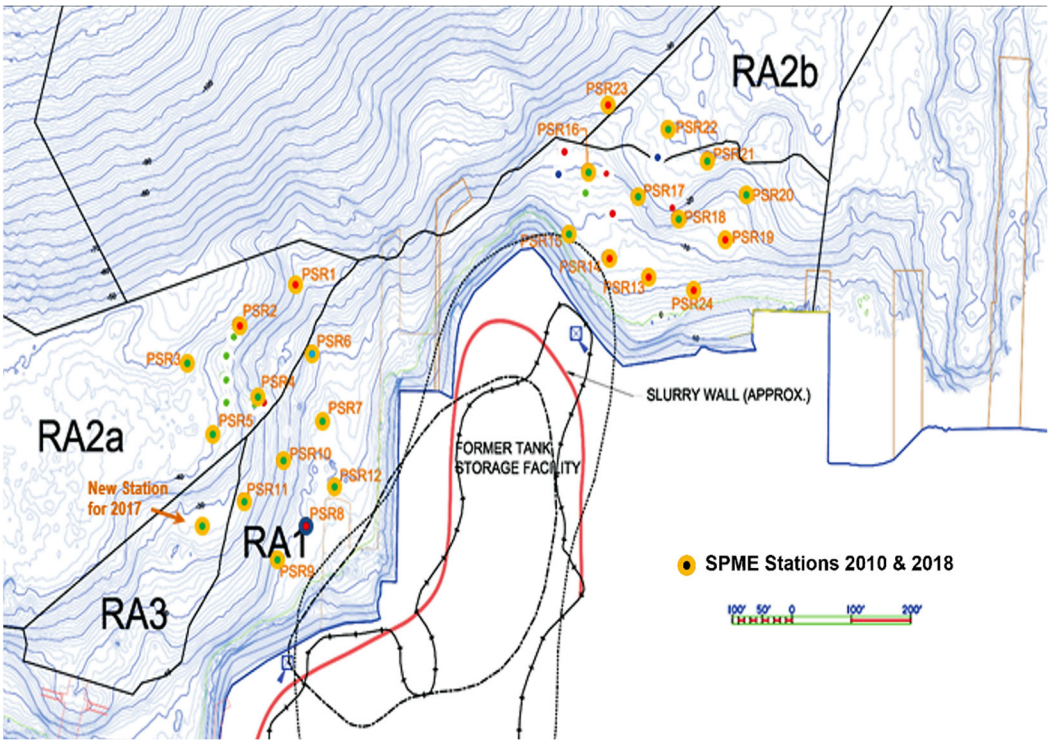

Figure 5-2 SPME Sampling locations for the 2010 and 2018 sampling event at the Puget Sound Resources Superfund Site. SPME sampling locations that had an increase in porewater concentration in 3018 compared to 2010 are marked red; those that did not increase are black.

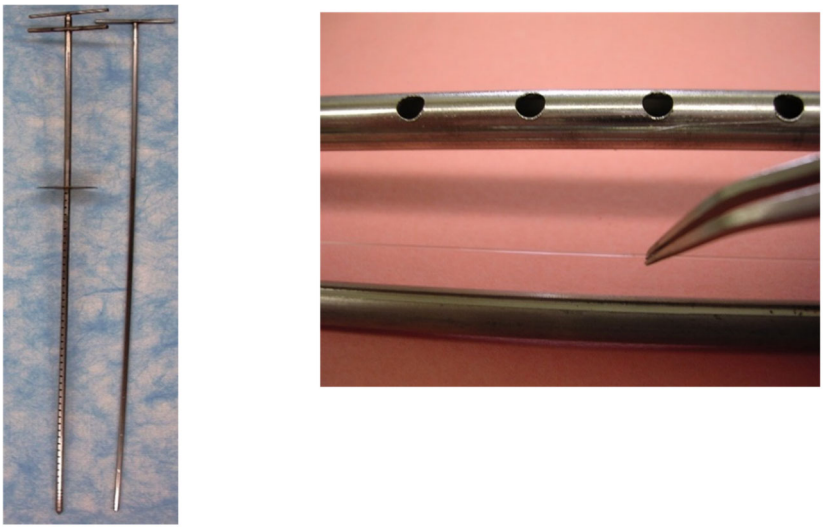

Figure 5-3 SPME sampler with a 90 cm working section showing perforated outer shield tube and inner rod (left). Close-up of the perforated shield tube; the inner rod with slit and the PDMS are also shown (right). The fiber has 0.59 µL/cm of PDMS around a 497 µm-diameter glass core.

5.3.3 CHEMICAL ANALYSIS

Upon retrieval, the stainless-steel PushPoint samplers were dismantled, the PDMS fibers removed from the stainless-steel housing, and wiped clean with DDI water to remove any residual sediment from the fiber. Once all visible organic matter was removed, the SPME fibers were sectioned into adjacent 2-cm segments for every target depth in between the 90 cm exposure section. All fibers were placed in autosampler vials pre-filled with 200 μL of acetonitrile immediately after segmentation from the main fiber length and shipped back to Texas Tech University (Lubbock, TX, USA) for processing. Previous studies had shown that extraction of contaminants from the fibers is essentially complete within 24 hours.

Once received, the PDMS-solvent extracts were analyzed using High Performance Liquid Chromatography (HPLC, Agilent 1260, Agilent Technologies, Santa Clara, CA, USA) in accordance with EPA method 8310, SW-846 3rd edition (United States Environmental Protection Agency, 1986), with fluorescence detection (FLD). The target compounds included the deuterated PAHs serving as PRCs, the 16 priority pollutant PAHs (Reible & Lu, 2012), 2-methylnaphthalene (2-MNP), and dibenzofuran (DBF). Of the 16 priority PAHs acenaphthylene is not detectable by FLD and benzo[g,h,i]perylene and indeno[1,2,3-cd]pyrene coelute and are reported as a sum of both compounds. The sum of the 13 measured PAHs, the combined coeluting compounds, plus 2-MNP and DBF are referred to here as ∑PAH. Chromatographic separation was conducted using a 1.0 mL/min isocratic flow composed of 3:7 (v:v) water:acetonitrile at 40° C, and retention times for the target compounds are shown in Table 5-1.

Table 5-1 Priority pollutant PAHs + 2-MNP and DBF retention times using HPLC with fluorescence detection (FLD)

Priority Pollutant PAHs (PAH_{16}) + 2MNP +DBF	Retention Time (minutes)
Naphthalene	7.789
2-Methylnaphthalene	9.821
Fluorene	10.743
Dibenzofuran	11.021
Acenaphthene	11.127
Phenanthrene	11.692
Anthracene	12.450
Fluoranthene	14.543
Pyrene	15.674
Chrysene	19.254
Benz[a]anthracene	19.949
Benzo[b]fluoranthene	25.658
Benzo[k]fluoranthene	26.616
Benzo[a]pyrene	27.732
Dibenzo[a,h]anthracene	33.892
Benzo[g,h,i]perylene+Ideno[1,2,3-cd]pyrene	36.795

Note: acenaphthylene is not detectable by FLD and benzo[g,h,i]perylene and indeno[1,2,3-cd]pyrene co-elute.

Calibration standards were prepared from stock solutions (Cambridge Isotope Labs) ranging from 0.5 µg/L to 100 µg/L. Calibrations were linear with r^2 >0.999 and a relative standard deviation (RSD) of <20% at all concentrations. For every 10 field samples analyzed, a 5 µg/L or 10 µg/L calibration quality check (QC) standard confirmed stability of the calibration. Equipment blanks (EBs), containing only acetonitrile, were ran periodically throughout the sequence to ensure no background interferences were present.

5.3.4 Determination of the Freely Dissolved Concentration

The estimation of the freely dissolved porewater concentration (C_{pw}) using SPME PDMS passive samplers involves the quantification of the concentration sorbed to the polymer (C_{PDMS}, Equation (5.1)) and the polymer-water partitioning coefficient (K_{pw}, (5.2)) that assumes linear and reversible uptake to the target compounds and correlates with hydrophobicity as measured by the octanol-water partitioning coefficient (K_{ow}) (Ghosh et al., 2014). The mass on the polymer is calculated based on the specific geometry of the sampler and amount of solvent used to extract the contaminates of concern.

$$C_{PDMS} = \frac{A * RSF_{HOC} * V_s}{L_f * V_f} \tag{5.1}$$

Where A represents the integration area from a specific compound from the HPLC, RSF_{HOC} is the response factor from a standard calibration curve unique to each chemical class of HOCs, V_s is the volume of solvent used, and V_f is the volume of PDMS per unit length (0.585 µL/cm), and L_f, or length of fiber. The freely dissolved porewater concentration, C_{pw}, is given by (5.2).

$$C_{pw} = \frac{C_{PDMS}}{K_{pw} * f_{ss}} \tag{5.2}$$

Where K_{pw} represents the polymer-water partitioning coefficient for PAHs found in Ghosh et al. (2014). The f_{ss} calculation uses the observed release of PRCs and assumes reversible desorption, which effectively recognizes that half of the PRC initially loaded onto the fiber would be released during the time that an equivalent target compound has achieved 50% equilibration during uptake. The extrapolation to other PAH

compounds follows the methodology described in Shen and Reible (2019) that takes into account the cylindrical geometry of the fiber.

Both PRC release and target-compound uptake are expected to be controlled by external mass-transfer processes and sediment-water partitioning (Lampert et al., 2015), and thus the PRC release data could also be used to estimate mass transfer in the sediment surrounding the sampler (discussed below).

5.3.5 CapSim Modeling

A software-modeling tool, CapSim (Shen et al., 2018), was used to predict contamination migration in the future based on the measured concentrations and estimated upwelling velocities. The model accounts for multiple layers of varying properties and allows the user to input specific properties of the material or use typical values from a database of characteristics for different sediment and capping materials. The model incorporates traditional porous media transport processes including advection, diffusion, dispersion, reaction, and sorption, but also includes the capability to simulate processes specific to the near-surface sediment including deposition, consolidation, bioturbation, and exchange with the overlying water (Shen et al., 2018). For the purposes of the current simulation, the measured porewater concentrations in 2018 were used as initial conditions. Default parameters were used in the model, except for two site-specific parameters: groundwater upwelling rates, and partition coefficients in the cap materials and near-surface sediments. Groundwater upwelling rates were estimated from the PRC data (described below) while paired sediment and porewater samples were collected in the near surface (0-10 cm) of a nearby Puget Sound site that was also capped with sand and gravel at the same time as this site. This data was used to estimate partitioning and

organic carbon content in near-surface sediments (Thomas et al., 2012). Partitioning in the lower portion of the cap (>10 cm depth) was estimated from contaminant organic carbon-based partition coefficients and the original organic carbon content (0.3%) of the placed cap material. Changes were note expected to sorption or organic carbon content in the deeper parts of the cap. Only the surface layer of the cap would be affected by sediment deposition and near-surface mixing processes such as bioturbation. Other model parameters which would have a minor impact on contaminant migration over most of the cap either employed model defaults or were directly estimable from the site characteristics (Reible, 2014).

5.4. RESULTS

5.4.1 REMEDY EFFECTIVENESS

As stated previously the sampling event was split into the N.E. and N.W. shoreline with the tip of the isthmus being the divider. Samplers 1 – 12 were within the NW sampling region while samplers 13-24 were located in the NE sampling region, as shown in Figure 5-2. Note that all locations exhibited averaged porewater concentrations ∑PAH < 1 μg/L, and 50% or more of the porewater concentrations were often associated with DBF and 2-MNP in 2010. Three-ring and larger PAHs totaled less than 50 ng/L in 2010. The PAHs observed in the northwestern zone in 2010 were associated with sediment intermixed into the cap during placement in 2005 or as a result of equilibration with overlying water. No distinct profiles, such as higher concentrations at depth due to the higher concentrations in the contaminated sediment below the cap, were noted.

Samplers in the NW region exhibited porewater concentrations in 2018 that were similar or lower than those observed during the baseline 2010 sampling event. There was

an average 45% decrease in ∑PAH in sediment porewater in the NW region with a 23% decrease in the higher-molecular-weight PAHs (three rings or greater).

Porewater concentrations in the NE section, however, were generally higher in 2018 than in 2010. This is shown by the different colored locations in Figure 5-2. Eleven out of the 12 individual sampling locations showed increased porewater concentrations between 2010 and 2018, with the highest increases near the shore and in the eastern and central portions of the NE area (notably locations 17, 18, 20, 21, 22, 24 which all showed increases in concentration more than a factor of 2 over 2010). In 2018, the three-ring and larger PAHs ranged from 134 to 408 ng/L at the NE locations of 16, 17, 18, 20, and 24, while all other locations in the NE area showed under 100 ng/L for three-ring and larger PAHs. Unlike 2010, the porewater concentrations were also highest at the bottom of the profiles, i.e., near the bottom of the cap layer and extending into the underlying contaminated sediment.

Table 5-2 shows the differences in ∑PAH between 2010 and 2018 at each location. Such a comparison does not reflect any variations in depth in the cap, nor does it recognize the typically higher mobility and higher porewater concentrations of low-molecular-weight compounds compared to the lower porewater concentrations and much lower mobility of the higher-molecular-weight PAHs. The comparison does provide a crude picture of the magnitude of changes between 2010 and 2018 and indicates that the bulk of the increased observed concentrations were in the NE region.

Table 5-2 Sum of porewater PAHs averaged over depth in 2010 and 2018

Sample Location		∑PAH (2010) ng/L	∑PAH (2018) ng/L
Northwest	1	70	121
	2	170	92
	3	34	125
	4	97	85
	5	490	124
	6	71	27
	7	104	21
	8	170	-
	9	89	-
	10	66	66
	11	315	111
	12	67	12
Northeast	13	89	384
	14	66	186
	15	75	324
	16	58	809
	17	74	690
	18	68	567
	19	170	33
	20	83	876
	21	99	413
	22	47	439
	23	56	378
	24	86	576

The conclusion from the 2018 observations were that although porewater PAH concentrations in the cap, and particularly near the cap–water interface remained relatively low, higher concentrations were detected in the lower portions of the porewater sampler potentially as a result of migration into the bottom of the cap from below or as a result of the samplers being inserted into the underlying contaminated sediments. Table 5-3 summarizes the measured porewater concentrations in 2018, including ∑PAH

averaged over depth and the concentrations for three selected PAHs in the top 10 cm and bottom 10 cm at each location. The individually identified PAHs in Table 5-2, phenanthrene ($LogK_{ow}$ = 4.74), fluoranthene ($LogK_{ow}$ = 5.29), and chrysene ($LogK_{ow}$ = 5.9) represent compounds detected at most locations and cover a wide range of hydrophobicity which is related to sorption and contaminant migration rates.

Table 5-3 Summary of $\sum_{16}$PAH averaged over depth and the concentrations for three selected PAHs in the top 10 cm and the bottom 10 cm at each location sampled in 2018. Estimated velocity at each location is also included (discussed later).

Station ID	$\sum PAH_{16}$ ng/L	Top 10-cm Depth (0-10 cm)				Bottom 10-cm Depth (80 - 90 cm)			
		U_z (cm/d)	Porewater Concentration (ng/L)			U_z (cm/d)	Porewater Concentration (ng/L)		
			PHE	FLUOR	CHRY		PHE	FLUOR	CHRY
Northwest									
1	121	1.4	2.5	<1.0	<0.1	0.02	11.6	9.8	0.8
2	92	2.4	5.7	21.6	2.3	0.08	1.3	7.8	2.5
3	125	8.3	<1.0	10.1	<0.1	0.10	0.1	<1.0	<0.1
4	85	1.7	15.7	20.3	<0.1	0.01	12.3	8.1	<0.1
5	124	5.7	0.8	9.9	1.1	0.02	48.6	12.4	1.2
6	27	10.1	2.1	7.9	<0.1	0.02	12.1	9.1	<0.1
7	21	6.5	1.3	14.1	2.5	0.00	<1.0	<1.0	<0.1
10	66	3.4	15.7	20.5	<0.1	0.02	<1.0	8.1	<0.1
11	111	2.7	1.2	0.1	<0.1	0.02	61.2	12.4	1.2
12	12	10.4	1.3	14.1	1.8	0.01	<1.0	<1.0	0.8
Northeast									
13	384	6.7	15.5	9.3	<0.1	0.02	8.3	16.5	1.1
14	186	<0.1	<1.0	<1.0	<0.1	0.10	10.9	<1.0	<0.1
15	324	4.6	8.6	6.4	<0.1	0.12	1.0	<1.0	<0.1
16	809	2.8	28.3	49.6	1.7	0.01	44.9	38.2	1.0
17	690	6.6	147.7	162.5	2.1	0.08	28.8	13.9	1.6
18	567	1.1	18.3	32.9	0.7	0.02	461.4	132.2	<0.1
19	33	2.2	2.2	18.7	<0.1	0.06	6.6	27.3	<0.1
20	876	1.3	26.3	24.6	3.1	0.26	350.5	78.3	46.8

Table 5-3, Continued

Station ID	∑PAH16 ng/L	Top 10-cm Depth (0-10 cm)				Bottom 10-cm Depth (80 - 90 cm)			
		U_z (cm/d)	Porewater Concentration (ng/L)			U_z (cm/d)	Porewater Concentration (ng/L)		
			PHE	FLUOR	CHRY		PHE	FLUOR	CHRY
21	412	2.7	39.6	39.3	<0.1	0.05	24.6	12.3	<0.1
22	439	0.7	21.9	25.5	0.9	0.02	38.3	17.2	0.8
23	378	1.0	50.8	21.2	<0.1	0.03	17.2	11.6	<0.1
24	576	14.9	26.2	54.6	1.7	0.32	84.1	159.3	14.4

5.4.2 Estimating Groundwater Upwelling Velocity from Performance Reference Compounds

The higher concentrations at the bottom of the porewater concentration profiles in 2018 suggested that an evaluation of future migration would assist in evaluating the long-term performance of the cap layer. PRCs were employed to estimate the degree of equilibration of target compounds using the methods of Shen and Reible (2019). As indicated in Lampert et al. (2015), however, PRC release from thin PDMS fibers is normally controlled by external mass-transfer resistances. Thus, the PRC release can also be used to estimate the magnitude of those external mass-transfer resistances and—indirectly—the groundwater upwelling rates.

Kimura (1988) examined the advective/diffusive transport of contaminants from a cylindrical source in a porous media subjected to a uniform velocity profile. With z being the vertical direction (along the axis of the cylindrical PDMS fiber holder, with z=0 being at the bottom of the PDMS fiber holder), the theory estimates the effective mass-transfer coefficient at the surface of the PDMS fiber (k) subject to the velocity along the fiber (U_z) and the diffusion (D_{eff}) in the surrounding porous medium. In this analysis, the dimensionless Peclet number (ratio of advective to diffusive transport) and Sherwood number (dimensionless mass flux) are defined as

$$Pe_z = \frac{U_z z}{D_{eff}} \qquad Sh = \frac{kz}{D_{eff}} = \frac{Flux}{C_0 - C_\infty}\frac{z}{D_{eff}} \tag{5.3}$$

The resulting model (Appendix 9.2) suggests that the mass-transfer coefficient is dependent upon the ratio of the vertical distance to the local curvature of the fiber (or in this case the fiber holder). The key parameter is ξ which is related to the chemical concentration boundary layer thickness relative to the radius of the cylinder holding the PDMS fiber, shown in Equation (5.4).

$$\xi = \frac{z}{r_0 R_f \sqrt{Pe}} \tag{5.4}$$

Here, r_0 is the radius of the fiber holder and $R_f = \varepsilon + \rho_b K_d$ is the ratio of the total concentration in the medium r to that in the porewater (or retardation factor), where ε is the void fraction t, ρ_b is the bulk density of the cap media, and K_d is the partition coefficient between the cap media and porewater (estimated by $K_{oc} f_{oc}$, the product of the organic carbon based partition coefficient and the fraction organic carbon in the cap media). The thickness of the concentration boundary layer is reduced by sediment sorption effects and leads to the boundary layer being effectively "flat" on the surface of the PDMS holder, that is, $\xi \ll 1$, and the limit of forced convection on a flat surface in a porous medium applies to the release of the PRCs from the fiber (or the uptake of the target compounds). Using typical values of all parameters the value of ξ is less than 0.1 over the entire 1 m sampler length for the PAHs of interest (see Appendix 9.2). Thus, under locally flat conditions, the mass transfer from the fiber to the porous medium is described by (Bejan & Poulikakos, 1984). See also Appendix 9.2.

$$Sh = \frac{1}{\sqrt{\pi}} Pe_z^{\frac{1}{2}} \tag{5.5}$$

The local mass-transfer coefficient, k, in Sh can be obtained from the release of PRCs from the passive sampler upon retrieval (Equation (5.6).

$$V \frac{dC_{PRC,fiber}}{dt} = kS(C_{PRC}|_\infty - C_{PRC}|_0) \tag{5.6}$$

where V is the volume of the SPME fiber layer, S is the surface area of the PDMS, and the gradient of concentration is the difference between the total concentration in the surrounding medium (i.e., mass of PRC in the solid and the liquid phases) and the media at the surface of the PDMS. Note that $C_{PRC}|_\infty = 0$ since the PRCs are not naturally present.

To obtain the total concentration in the porous media (C_{PRC}), consider that the PRC released from the polymer equilibrates with the adjacent sediment, where the total concentration includes both a dissolved and sorbed component (Equation (5.7).

$$C_{PRC} = \varepsilon \frac{C_{PRC,fiber}}{K_{fiber}} + \rho_b K_d \frac{C_{PRC,fiber}}{K_{fiber}} \tag{5.7}$$

where ε is the porosity and ρ_b is the bulk density of the capping material, K_{fiber} is the fiber-water partitioning coefficient (Ghosh et al., 2014), and K_d is the sediment–water partitioning coefficient derived from Thomas et al. (2014). Here, we estimate K_d using the linear $K_{oc}f_{oc}$ relationship in the cap material in which the PDMS is inserted. From Equation (5.5) above, integrating assuming a constant mass-transfer coefficient, k, yields (Equation (5.8):

$$k = -\ln\left(\frac{C_{PRC,t}}{C_{PRC,0}}\right)\frac{V}{St}\frac{K_{fiber}}{\varepsilon + \rho_b K_d} = -\ln(1 - f_{ss})\frac{V}{St}\frac{K_{fiber}}{\varepsilon + \rho_b K_{oc} f_{oc}} \quad (5.8)$$

where $C_{PRC,t}$ is the PRC mass remaining on the polymer layer after an exposure time, t; and $C_{PRC,0}$ is the initial concentration of PRC concentration. At steady state, $C_{PRC,\infty} = 0$, but none of the PRCs achieved complete equilibration with the surrounding media due to the relatively short (14-day) exposure time. The fractional approach to steady state, f_{ss}, varied between approximately 0.75 for the lightest PRC, d10-fluoranthene; to as low as 0.2 for the heaviest, d14-dibenzo[a,h]anthracene. For the purposes of the estimation of a mass-transfer coefficient and upwelling velocity, it is important that the PRCs do not approach equilibrium, at which point velocity estimation is no longer possible.

The local mass-transfer coefficient used to calculate the upwelling velocity was obtained from the PRC losses at each point of the sampler and at each sampling location. Figure 5-4 shows the calculated mass-transfer coefficient, k, for a representative location, 20, in the NE portion of the site. Location 20 was chosen because it is representative of the locations that exhibit both elevated concentrations in the bottom of the profile but also upwelling velocities typical of the NE area. The relative uncertainty in mass-transfer coefficient in Figure 5-4 reflects the uncertainty in PRC quantified from the PDMS passive samplers.

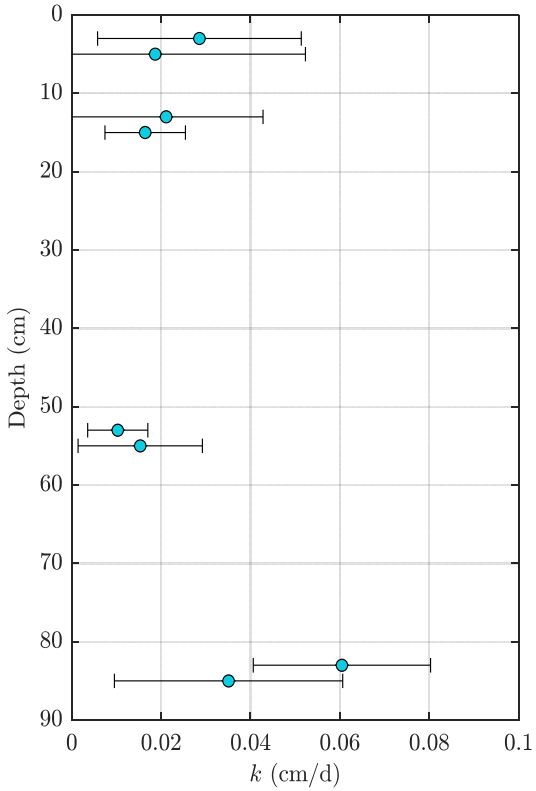

Figure 5-4 Local mass-transfer coefficient (k, cm/d) at depth of d-PAH performance reference compounds at sample locations 20 (S20) within the NE sampling locations. That standard deviation in mass transfer reflects the uncertainty in PRC quantified from the PDMS passive samplers.

By solving for the advective transport, U_z, from Pe (Equation (5.3) and relating Sh to the localized mass-transfer coefficient, the upwelling velocity can be determined by Equation (5.9). See also Appendix 9.2.

$$U_z = k^2\pi\left(\frac{z}{D_{eff}}\right) \tag{5.9}$$

The upwelling velocity from the contaminated sediment beneath the cap was taken to be defined by that estimated at the bottom of the sampler that was likely not significantly influenced by near-surface tidal and wave fluctuations. The average

groundwater velocity in the NW portion of the site was estimated to be about 0.09 cm/day (32 cm/yr) while the average in the NE portion of the site was about 0.03 cm/day (13 cm/yr). The top 10 cm in both areas exhibited an average of 4–5 cm/day, reflecting the greater movement due to tidal and wave action. Figure 5-5 shows a heat map of the estimated upwelling groundwater flow determined from Equation (5.9) averaged across the bottom 10 cm of the SPME passive sampler.

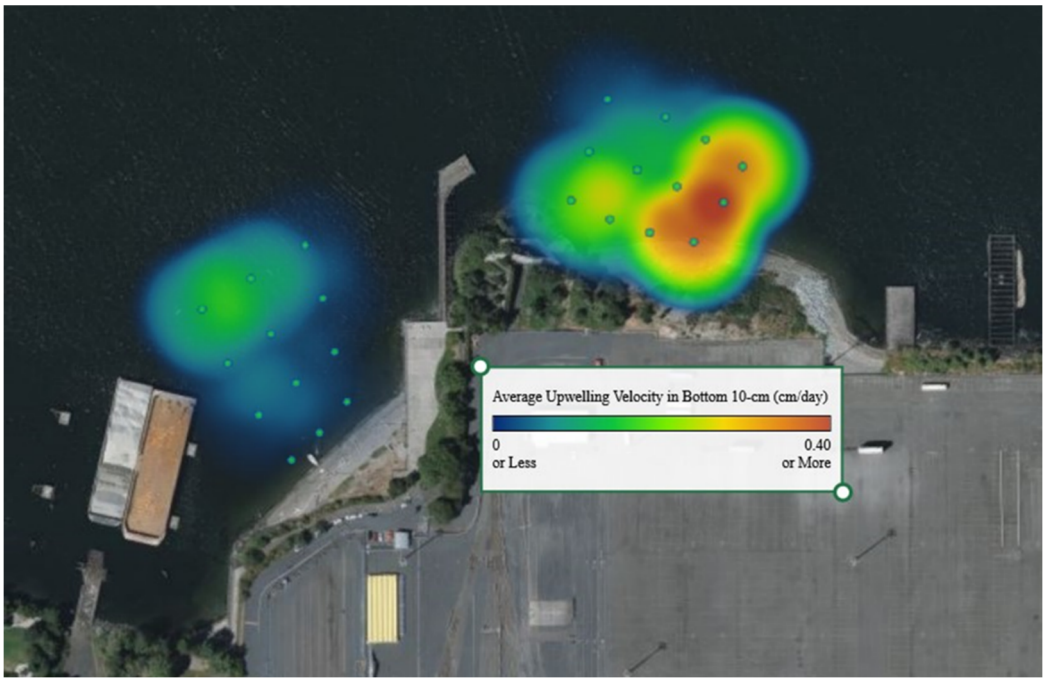

Figure 5-5 A heat map of the estimated distribution of upwelling groundwater flow (cm/day) averaged across the bottom 10 cm of the SPME sampler within the NW and NE sampling locations. The dots indicate the 24 SPME sampling stations.

The upwelling velocity is the highest along the shoreline where hydraulic gradients are expected to be the greatest, and in those areas where the greatest increases in porewater concentration were observed. This provides support for the use of the model to estimate upwelling velocities. The upwelling velocity along the length of the sampler at location 20 is shown in Figure 5-6.

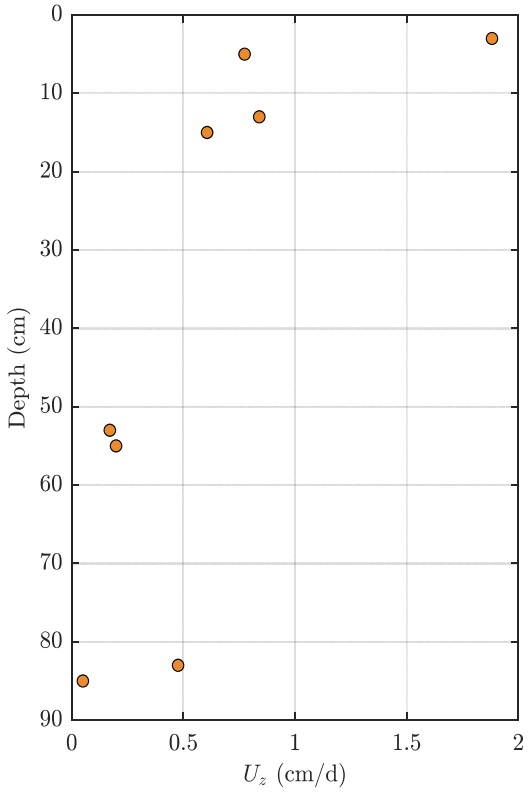

Figure 5-6 Upwelling velocity (U_z) in the vertical direction at sample location 20 (S20) within the NE sampling region.

5.4.3 Modelled Cap Breakthrough

The observed porewater concentrations at the bottom of the profiles in the NE portion of the site in 2018 combined with groundwater upwelling suggest that there is likely to be contaminant migration over time, and the one-dimensional fate and transport software, CapSim (Shen et al., 2018), was used to estimate that migration. The modeling was focused on location 20 as a representative location showing both elevated concentrations at the bottom of the profile and substantial groundwater upwelling. Key CapSim parameters used in the simulation are included in Table 5-4.

Table 5-4 Key model parameters for simulations shown in Figure 5-7

Layer	**Depth (cm)**	f_{oc}	**U_z (cm/day)**	**Boundary Condition**	**Comments**
Sediment	10	0.01	0.21	Mass transfer	Bioturbation in top 5 cm at 2 cm^2/y
Sand/Gravel	90	0.003	0.21	Constant Concentration	No depletion in bottom concentration

Contaminant	**K_{oc}**	**Initial Concentrations**
Phenanthrene	3.93	2018 porewater concentrations as shown in Figure 5-7 Local equilibrium with adjacent solids assumed
Fluoranthene	4.51	
Chrysene	5.09	

Figure 5-7 shows the porewater depth profiles for phenanthrene, fluoranthene, and chrysene at individual depth intervals and modeled depth profiles based on the upwelling velocity, U_z, calculated over the bottom half of the sampler as shown in Figure 5-6 (0.21 cm/day), and the initial porewater concentration defined by 2018 measurements.

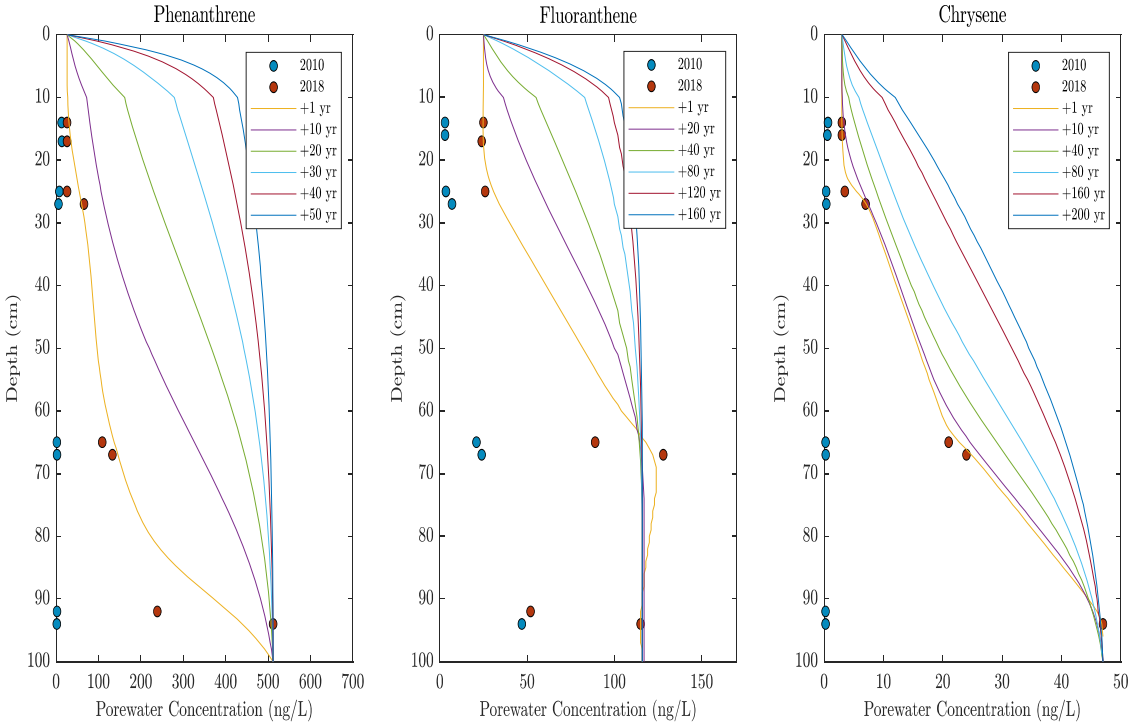

(a) (b) (c)

Figure 5-7 Depth-profile porewater concentrations from 2010 (blue circles) and 2018 (red circles) of (**a**) phenanthrene, (**b**) fluoranthene, and (**c**) chrysene at sampling location 20. Each graph has modeled contaminant transport through the cap based on the calculated mass-transfer coefficient, k, and upwelling velocity, U_z, of the d-PAH performance reference compounds.

Based on the modelled results, phenanthrene (Figure 5-7a) is expected to migrate relatively rapidly through the cap, and porewater concentrations over most of the cap should be similar to the concentrations at the bottom within 50 years if no degradation is assumed. Phenanthrene is a PAH that is subject to biological degradation under aerobic conditions, however, and this will likely lead to significant reductions in phenanthrene concentrations in the near-surface sediments. Significantly less migration of the more hydrophobic and more sorbing fluoranthene and chrysene is expected with porewater concentrations of fluoranthene becoming approximately uniform—except for the surface

layer—within 200 years, while an even longer period would be expected to be required for chrysene and other high-molecular-weight PAHs. Note that these simulations assume that there is no degradation and that the source concentrations of PAHs at the bottom of the cap is not depleted over time.

5.5. DISCUSSION

Passive samplers were deployed at the Pacific Sound Resources (PSR) Superfund Site (the site) in Puget Sound, west Seattle, WA to measure near-surface contaminant porewater concentrations using solid-phase microextraction (SPME) by sorption onto polydimethylsiloxane (PDMS). PRCs of d-PAH compounds were used to assess the degree of equilibration of the target compounds. The objective of the study was to evaluate whether contaminated interstitial and groundwaters could be negatively impacting surficial sediment cap or surface water quality. The passive samplers were deployed in areas where potentially contaminated groundwater may discharge to surface waters through the sediment cap. By measuring profiles of porewater concentration, the contaminant in the mobile phase (water) can be directly assessed and migration from underlying source areas into the bottom layers of a cap can be directly measured without waiting for breakthrough of contamination at the surface.

The release of the d-PAH PRCs also provided a means of estimating upwelling velocities in the cap. The local Sherwood number can be estimated via passive sampling and used to estimate effective Peclet number or velocity, and this was used to predict long-term migration of contaminants of concern in the cap layer. One important assumption of the method to estimate groundwater upwelling velocity is that the cylindrical holder is locally “flat.” This is valid as a result of the sorption onto the

surrounding sediment/cap material which keeps the PRC concentration boundary layer around the sampler "thin" compared to the diameter of the sampler. The method developed provides an estimate of groundwater upwelling velocity; however, there are no independent estimates to evaluate the validity of the results. The method does, however, suggest that the maximum upwelling occurs in the locations where the highest porewater concentrations were measured in 2018 relative to 2010. These locations also tended to be located in the shallowest water near the shore, where the effects of groundwater gradients and tidal variations in water depth and hydraulic head are expected to be the greatest. The correspondence between the locations with the greatest upwelling velocities and the largest increases in porewater concentrations and the greatest expected influence of hydraulic gradients suggests that the method at least provides an indication of the relative transport or mixing rates at the various locations.

The method also cannot indicate flow direction; that is, it does not differentiate between upwelling or downwelling. The observed groundwater gradients are generally from the upland area to Puget Sound, however, so the net movement is expected to be toward the Sound. The tidal fluctuations up and down in the near-surface sediment/cap, however, likely suggest that the observed estimated velocity in the near-surface environment represents a magnitude that includes water being both retained and lost from Puget Sound.

The estimated groundwater migration rates were used to predict future cap performance using CapSim. A key parameter for the future performance predictions, in addition to the groundwater migration rates, is the partition coefficient in the sediment

and/or capping material, which can be directly measured through samples collected via cores or estimated by compound properties and the fraction organic carbon in the capping layer.

5.6. CONCLUSIONS

This work shows the ability to determine the groundwater upwelling velocity and contaminant flux using the rate of equilibration of performance refence compounds. The approach to estimation of the groundwater upwelling velocity is a novel use of the PRCs that can be employed at other locations.

The work also illustrates the capability of using measured porewater concentration profiles to not only indicate current cap performance but also to provide a basis for prediction in the future. In this case, the estimated upwelling velocities allowed estimation of the migration of currently observed porewater concentrations through the cap over time using CapSim. The time predictions are improved by profile monitoring over long time periods so that contaminant migration into the cap layer from source areas below can be assessed, as well as ultimately provide data that could be used to evaluate or calibrate models. In this case, the lack of significant porewater concentrations in the cap in 2010 means that only the 2018 data could be used to predict long-term performance. Subsequent sampling, however, could continue to be used to update and refine the model predictions.

5.7. REFERENCES

Bejan, A., & Poulikakos, D. (1984). The nondarcy regime for vertical boundary layer natural convection in a porous medium. *International Journal of Heat and Mass Transfer*. https://doi.org/10.1016/0017-9310(84)90141-8

Eek, E., Cornelissen, G., Kibsgaard, A., & Breedveld, G. D. (2008). Diffusion of PAH and PCB from contaminated sediments with and without mineral capping; measurement and modelling. *Chemosphere*. https://doi.org/10.1016/j.chemosphere.2008.01.051

Epa. (1986). Method 8310: Polynuclear aromatic hydrocarbons. *Chemistry & …*.

Fernandez, L. A., Lao, W., Maruya, K. A., & Burgess, R. M. (2014). Calculating the diffusive flux of persistent organic pollutants between sediments and the water column on the palos verdes shelf superfund site using polymeric passive samplers. *Environmental Science and Technology*. https://doi.org/10.1021/es404475c

Ghosh, U., Kane Driscoll, S., Burgess, R. M., Jonker, M. T. O., Reible, D., Gobas, F., Choi, Y., Apitz, S. E., Maruya, K. A., Gala, W. R., Mortimer, M., & Beegan, C. (2014). Passive sampling methods for contaminated sediments: practical guidance for selection, calibration, and implementation. *Integrated Environmental Assessment and Management*, *10*(2), 210–223. https://doi.org/10.1002/ieam.1507

Kimura, S. (1988). Forced convection heat transfer about a cylinder placed in porous media with longitudinal flows. *International Journal of Heat and Fluid Flow*, *9*(1), 83–86. https://doi.org/10.1016/0142-727X(88)90035-5

Lampert, D. J., Thomas, C., & Reible, D. D. (2015). Internal and external transport significance for predicting contaminant uptake rates in passive samplers. *Chemosphere*, *119*, 910–916. https://doi.org/10.1016/j.chemosphere.2014.08.063

Lampert, David J., Sarchet, W. V., & Reible, D. D. (2011). Assessing the effectiveness of thin-layer sand caps for contaminated sediment management through passive sampling. *Environmental Science and Technology*. https://doi.org/10.1021/es200406a

Mayer, P., Parkerton, T. F., Adams, R. G., Cargill, J. G., Gan, J., Gouin, T., Gschwend, P. M., Hawthorne, S. B., Helm, P., Witt, G., You, J., & Escher, B. I. (2014). Passive sampling methods for contaminated sediments: scientific rationale supporting use of freely dissolved concentrations. In *Integrated environmental assessment and management*. https://doi.org/10.1002/ieam.1508

Rakowska, M. I., Kupryianchyk, D., Harmsen, J., Grotenhuis, T., & Koelmans, A. A. (2012). In situ remediation of contaminated sediments using carbonaceous materials. In *Environmental Toxicology and Chemistry*. https://doi.org/10.1002/etc.1763

Reible, D. D. (2014). Contaminant Processes in Sediments. In *Processes, Assessment and Remediation of Contaminated Sediments*. https://doi.org/10.1007/978-1-4614-6726-7

Reible, D., & Lu, X. (2012). *Solid-Phase Microextraction Field Deployment and Analysis Pacific Sound Resources*.

Shen, X., Lampert, D., Ogle, S., & Reible, D. (2018). A software tool for simulating contaminant transport and remedial effectiveness in sediment environments. *Environmental Modelling and Software*. https://doi.org/10.1016/j.envsoft.2018.08.014

Shen, X., & Reible, D. (2019). An analytical model for the fate and transport of performance reference compounds and target compounds around cylindrical passive samplers. *Chemosphere*. https://doi.org/10.1016/j.chemosphere.2019.05.198

Thomas, C. (2014). *Passive Sampling to Evaluate Performance of in-situ sediment remediation*. University of Texas.

Thomas, C., Lu, X., & Reible, D. (2012). *Solid-Phase Microextraction Field Deployment and Analysis Wyckoff/Eagle Harbor*.

Thompson, J. M., Hsieh, C.-H., & Luthy, R. G. (2015). *Modeling Uptake of Hydrophobic Organic Contaminants into Polyethylene Passive Samplers*. https://doi.org/10.1021/es504442s

CHAPTER 6

LONG-TERM MONITORING OF PAHS USING IN-SITU PASSIVE SAMPLERS IN A CAPPED RIVERBED

6.1. ABSTRACT

The U.S. Environmental Protection Agency Great Lakes National Program Office oversaw the remediation of the West Branch of the Grand Calumet River (WBGCR) in Hammond, Indiana as part of the Roxana Marsh Great Lakes Legacy Act Project. Phase II of the remediation involved the placement of a sediment cap in May 2012. The cap consisted of 6 inches of organoclay intermixed with sand and covered by an additional 12 inches of sand, and the cap covers approximately 345,000 cubic yards of contaminated sediment. The performance of the cap was monitored by passive sampling utilizing solid phase microextraction (SPME) with polydimethylsiloxane (PDMS) coated glass fibers at 21 subsurface locations after cap placement in 2012 and again in 2013 and 2014. The passive sampling sediment porewater monitoring technology provides depth profiles of the freely dissolved contaminant concentrations in the sediment porewater and overlying water column. The initial sampling efforts showed a variety of behaviors around the site including a thick, clean capping layer in some areas from sediment deposition and caps that were re-contaminated at the surface due to site activities after cap placement.

In 2019, the in-situ passive sampling was repeated at the same 21 locations providing a unique opportunity to examine the performance of the capping layer 7 years after placement. This work will summarize the changes observed in the cap and the containment of PAH compounds. Statistical methods to analysis the variance (one-way ANOVA) is incorporated to quantify the changes in porewater concentrations from year

to year at the varying depths by looking at benzo(a)pyrene equivalent porewater concentrations. Depth profiles were evaluated to determine an average thickness of the effective cap as well as trends for migration into the cap and sediment deposition at the surface. To further identify areas of potential concern, concentrations are also compared to surface water quality criteria as a screening criterion.

6.2. INTRODUCTION

The sampling was conducted in a segment of the West Branch of the Grand Calumet River, which is listed in the Great Lakes Areas of Concern and is in the cities of East Chicago and Hammond, IN (USA). Remediation of the studied section of the river started in 2011 and was completed in April 2012. It consisted of the dredging of approximately 585,000 cubic yards of contaminated sediments and the placement of ~15 cm of organophilic clay (Organoclay® PM-199, CETCO, Hoffman Estates, IL) and ~30 cm of sand (Ingersoll et al., 2001; Steevens et al., 2020).

The long-term performance of the cap was evaluated utilizing solid phase microextraction (SPME) using polydimethylsiloxane (PDMS) coated glass fibers. This monitoring approach provides depth profiles of the freely dissolved PAH contaminant concentrations in the sediment porewater. The 14 long-term monitoring (LTM) stations included in this study are shown in Figure 6-1 (red boxes) and are part of a larger network of 21 stations. Depth profiling using PDMS SPME at the 21 long term monitoring locations was undertaken immediately after cap placement to define baseline cap conditions in 2012, and again in 2013 and 2014. Sampling was also conducted along transects in the western section of the site and near the eastern end of the site. The transect sampling was undertaken as part of a separate effort led by U.S. Environmental

Protection Agency and the primary focus of this work is on the 21 long term monitoring locations. In 2019 another round of sampling with SPME using PDMS was used to evaluate the long term (7 years) performance of the cap.

Figure 6-1 SPME PDMS long-term monitoring stations within the West Branch of the Grand Calumet River. Area 1 is in reference to the east sampling section and Area 2 represents the west sampling stations

This work compares the results of the 2019 sampling event to explore long-term (7 years) performance of the cap compared to the same long-term monitoring locations as in the 2012-2014 events at Roxana Marsh (Thomas, 2014). The objectives of this study were to evaluate cap performance through SPME using PDMS porewater data, investigate the long-term trends in porewater concentration from cap placement at the surface, and interpret target compound concentration profiles from sampler transects to predict future cap performance. Priority pollutant PAH_{16} compounds will be discussed, however, a focus on benzo(a)pyrene equivalents due to their carcinogenetic effects will be the focus of this work.

To address these objectives the compound distribution from the previous years within the west branch of the Grand Calumet River were evaluated through a one-way ANOVA statistical method to verify changes in mobility of carcinogenic PAHs, by looking at the benzo(a)pyrene equivalent concentrations (BaP equivalents, shown in Table 6-1), at discrete depth intervals, compared to previous years. BaP equivalents were chosen to compare processes in this particular work because the risks of PAHs are largely controlled by these high molecular weight PAHs. Vertical profiles of porewater concentration were used to assess contaminate transport mechanisms and rates of the BaP equivalent contamination.

Table 6-1 Toxicity equivalency factors (TEFs) for the minimum required carcinogenic polycyclic aromatic hydrocarbons as adapted from Nisbet & LaGoy (1992)

CAS Number	Polyaromatic Hydrocarbon (PAH)	TEF (Unitless)
50-32-8	Benzo(a)pyrene	1
56-55-3	Benzo(a)anthracene	0.1
205-99-2	Benzo(b)fluoranthene	0.1
207-08-9	Benzo(k)fluoranthene	0.01
218-01-9	Chrysene	0.001
53-70-3	Dibenz(a,h)anthracene	1
191-24-2	Benzo(g,h,i)perylene	0.1
193-39-5	Indeno(1,2,3-cd)pyrene	0.1

Other studies were also undertaken to examine lower molecular weight PAHs and evaluate the fate and behavior of these less refractory contaminants but that is not the

subject of the current analysis. See also Garza-Rubalcava, 2022 (in revision). Additional to the pore water sampling, cores were extracted in 2013 and 2019 in the vicinity of each LTM station to measure bulk concentrations of PAHs and to evaluate changes in the cap thickness.

6.3. MATERIALS AND METHODS

6.3.1 PREPARATION OF SPME PDMS FIBERS

The SPME PDMS fibers were fabricated by Polymicro Technologies (Phoenix, AZ). The fibers are composed of a 562 μm outer diameter of PDMS coating on a 485 μm glass core for a volume of 0.64 μL/cm of PDMS. Prior to deployment, the PDMS fibers were cut into 90 cm segments, washed twice with hexane, acetonitrile, and methylene chloride sequentially for 30 minutes each, rinsed with ultrapure distilled deionized water (DDI), and dried with Kimwipes™. Only high purity solvents were used in the preparation process of these PDMS fibers.

Once the polymers have been chemically cleaned the PDMS fibers were impregnated with four deuterated PAHs (d10-fluoranthene, d12-chrysene, d12-benzo[b]fluoranthene, and d14-dibenzo[a,h]anthracene) as performance reference compounds (PRCs) to assess the extent of equilibrium achieved by the target compound during their deployment. The initial PRC concentration on the fibers (post-loading) was analyzed through solvent extraction and analysis by high-performance liquid chromatography (HPLC). The fractional approach to equilibration of the PRCs (f_{ss}) is estimated by the ratio of the residual PRC concentration after environmental exposure,$C_{PRC}(t)$, to the initial PRC concentration, $C_{PRC}(0)$, shown in (6.1).

$$f_{ss} = 1 - \frac{C_{PRC}(t)}{C_{PRC}(0)} \quad (6.1)$$

The fractional approach to steady state after environmental exposure of the PRCs was then used to estimate f_{ss} for other compounds using the methods of Shen and Reible (2019). Prior to deployment the fibers were housed in a stainless-steel modified PushPoint sampler (M.H.E. Products) with a 90 cm inner "trench" to hold the PDMS fiber and an outer stainless-steel shield component (Figure 6-2). The outer shield is slotted to allow the exchange of interstitial water to the PDMS fiber and provides an ease of insertion into fine grain sediments.

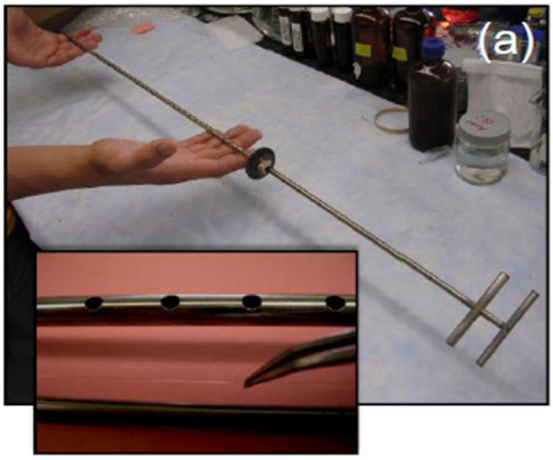

Figure 6-2 A shielded holder for the 90-cm working section for PDMS coated SPME fibers with inserts showing the SPME fiber for in-situ deployments

6.3.2 Sampling Design

6.3.2.1 Sediment Cores

Sediment cores for this study were retrieved in the 2013 and 2019 sampling events. At each LTM station, the boat was anchored, and sediment cores were collected using a push corer or piston corer. Corers were driven until refusal, with an initial target at each station of 3 feet deep. Once all sampling was completed, sediment cores were

returned to the mobile field staging area for preparing for shipment. The samples were shipped to the U.S. Army Engineer Research and Development Center (ERDC) in Vicksburg, MS for core characterization and sub-sampling. Once the cores were fully characterized, they were segmented into intervals based on stratification of sediment types throughout the core. Sediment material from the middle of the core (i.e., not touching the sides of the core) was collected and placed into a stainless-steel bowl for compositing and subsampling for chemical analysis. Each interval was submitted for PAH analysis to Battelle (Columbus, OH).

Sediment samples were extracted for PAHs following Battelle SOP 5-192, *Soil/Sediment Extraction Using an Orbital Shaker Table Method for Trace Level Semi-Volatile Organic Contaminant Analysis* (a modification of EPA SW846 Method 3540C). Approximately 20 g of wet sediment were mixed with Na_2SO_4 (a drying agent), fortified with a set of surrogates, and extracted three times with methylene chloride using shaker table techniques. The combined extracts were dried over anhydrous Na_2SO_4 and cleaned using alumina column (Battelle SOP 5-329), activated copper (Battelle SOP 5-328) and size exclusion GPC (Battelle SOP 5-191). The post-GPC extract was solvent-exchanged to *n*-hexane, concentrated to approximately 1 mL, and fortified with a set of internal standard compounds prior to analysis. Battelle analyzed sample extracts for the target PAHs by GC/MS operating in the SIM mode, following procedures defined in Battelle SOP 5-157, *Identification and Quantification of Semi-Volatile Organic Compounds by Gas Chromatograph/Mass Spectrometry* (based on EPA Method 8270D). Finally, concentrations in the extract were converted to solid concentrations (W) based on the mass of dried sediment used for extraction.

6.3.2.2 SPME USING PDMS PASSIVE SAMPLING AT LONG TERM MONITORING LOCATIONS

Once prepared, 32 samplers were deployed on September 4-5, 2019, at sub-surface and/or surface water locations within the capped region in the West Branch of the Grand Calumet River (Figure 6-1). The samplers were deployed at the 21 long term monitoring locations, previously sampled in 2012, 2013, and 2014 (Thomas, 2014), as well as at 9 locations on the west and east transects. Retrieval of the SPME-PDMS passive samplers occurred on October 2, 2019, to end a 28-day exposure of the PDMS to the sediment porewater.

The processing of the samplers involved dismantling the samplers, removing the fibers from the stainless-steel housing using a thin metal blade and wiping the fibers with a Kimpwipe™ tissue damped in deionized water to remove any particulate matter that would be stuck to the fiber. Once all visible organic matter was removed, the SPME fibers were sectioned into adjacent 2-cm segments from each target depth: 3-5 cm, 5-7 cm, 13-15 cm, 15-17 cm, 23-25 cm, 25-27 cm, 33-35 cm, 35-37 cm, 43-45 cm, 45-47 cm, 53-55 cm, 55-57 cm, 63-65 cm, 65-67 cm, 73-75 cm, 75-77 cm, 85-87 cm, 87-89 cm. The fiber deployed in the water column was sectioned into 2-cm fiber segments from the following target depth: 2-4 cm, 12-14 cm, and 24-26 cm.

6.3.3 CHEMICAL ANALYSIS OF SPME PASSIVE SAMPLERS

Upon retrieval the stainless-steel PushPoint samplers were dismantled, the PDMS fibers removed from the stainless-steel housing, and wiped clean with DDI water to remove any residual sediment from the fiber. Once all visible organic matter was removed, the SPME fibers were sectioned into adjacent 2-cm segments from each target

depth in between the 90 cm exposure section. All fibers were placed in autosampler vials pre-filled with 200 µL of acetonitrile immediately after segmentation from the main fiber length and shipped back to Texas Tech University for processing.

Once received, the PDMS-solvent extracts were analyzed using an Agilent 1260 HPLC in accordance with EPA method 8310, SW-846 3rd edition, (United States Environmental Protection Agency, 1986) with fluorescence detection (FLD). The target compounds were priority pollutant PAHs (PAH_{16}) although acenaphthylene is not detectable by FLD and benzo(g,h,i)perylene and indeno(1,2,3-cd)pyrene coelute and are reported as a sum of the two compounds. Chromatographic separation was conducted using a 1.0 mL/min isocratic flow composed of 3:7 (v:v) water:acetonitrile at 40° C.

Calibration standards were prepared from stock solutions (Cambridge Isotope Labs) ranging from 0.5 µg/L to 100 µg/L. Calibrations were linear with R^2 >0.999 and a relative standard deviation (RSD) of <20% at all concentrations. For every 10 field samples analyzed, a 5 µg/L or 10 µg/L calibration quality check (QC) standard confirmed stability of the calibration. Equipment blanks (EBs), containing only acetonitrile, were ran periodically throughout the sequence to ensure no background interferences were present. Some compounds did not meet a calibration acceptance criterion of 20% RSD for the lowest concentration (0.5 µg/L) and 1 µg/L in extract was set as a practical quantification limit (PQL). This suggests that the HPLC analyses were somewhat less sensitive at low concentrations than in the previous studies where a practical quantification limit of 0.5 µg/L in extract with < 20% RSD was obtained.

6.3.4 Determination of the Porewater Concentration

The estimation of the freely dissolved porewater concentration (C_{pw}) using PDMS SPME passive samplers involves the quantification of the concentration sorbed to the polymer (C_{PDMS}, (6.2) and the polymer-water partitioning coefficient (K_{pw}, (6.2)

$$C_{pw} = \frac{C_{PDMS}}{K_{pw} * f_{ss}} \tag{6.2}$$

Where K_{pw} represents the polymer-water partitioning coefficient for PDMS to target PAHs found in Ghosh et al. (2014), and a the f_{ss} was based on the release of the pre-loaded PRC compounds. The distribution of f_{ss} in target compounds and the d-PAH PRCs is shown in Figure 6-3.

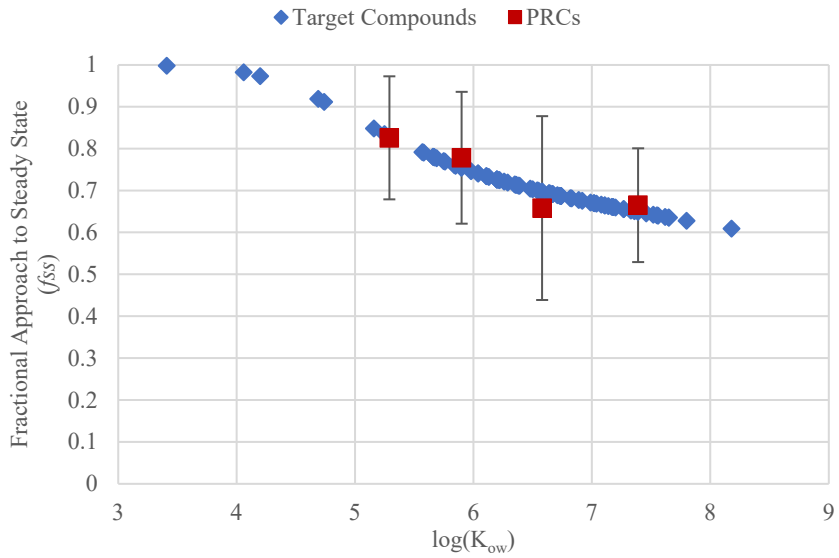

Figure 6-3 Fractional approach to steady state (f_{ss}) for target PAH_{16} compounds based on the distribution of C0s at the 21 LTM stations. Error bars represent the standard deviation of C_{PRC}^{fss}

When characterizing all 21 LTM stations the f_{ss} of C0's did not vary significantly across the site or with depth. The biggest variation was 0.20 was observed in d12-benzo(b)fluoranthene and was consistently the greatest variation in all four PRCs when

examined across the site and with depth. Ranging from 0.23 when examining only the cap across the LTM stations to 0.11 within the native sediment in west sampling area. The d-PAH PRCs seem to be more equilibrated within the sediment, although not surprising, and more variable in the cap. The greatest overall variation of C_{PRC}^{fss} was observed in the cap within the east sampling locations. PRC f_{ss} ranged from 0.83 for d12-chrysene to 0.42 for d12-benzo(b)fluoranthene. The complete list of C_{PRC}^{fss} values across the site in varying depth intervals is shown in Appendix 9.5. Calculations of the f_{ss} follow the methodology described in (Shen & Reible, 2019). This process was repeated for all samples collected and all sampling events during the WBGCR sampling events.

For each PAH at each long-term monitoring (LTM) station and year, the discrete porewater concentration data was smoothed using piecewise cubic Hermite interpolating polynomials (PCHIP in Matlab®). Then, an average porewater concentration (C_{av}) was calculated in the cap and in the underlying sediment at each LTM station to evaluate the total mass according to Equation (6.3.

$$C_{av} = \frac{1}{b-a}\int_a^b Cw(z)dz \tag{6.3}$$

Where the interval $[a, b]$ is bound to each layer. Here, the thickness of each layer was estimated by the substrate changes in cores retrieved from each station in both 2013 and 2019. Additionally, the averaged concentration in the solid phase from the cores (W_{av})

completed the material balance and allowed estimation of site-specific sediment-water partition coefficients ($K_d = W_{av}/C_{av}$).

6.4. RESULTS AND DISCUSSION

6.4.1 CAP THICKNESS AND BULK SEDIMENT CONCENTRATIONS OF PAHS

Cores were retrieved from the 21 LTM stations in 2013 and again in 2019. These observations indicated that the cap thickness was 33±2 cm in 2013 and 40±3 cm in 2019 (Mills, 2015). Change in cap thickness averaged 7.5-cm between the 21 LTM stations from the initial 2013 sampling event and increased by as much as 32-cm at station 16. Based on the retrieved cores (2013 and 2019), the averaged bulk concentration of PAHs in the native sediments were of the order of 10^4 µg/kg for select PAHs, while in the cap layer were 50-250 µg/kg (Garza-Rubalcava et al., 2022 in revision). This consistent order of magnitude difference demonstrates the effectiveness of the engineered cap to isolate native contaminated sediments from the aquatic ecosystem (Lampert et al., 2011; Reible, 2014).

Overall, between the baseline sampling years, a trend of increased cap thickness was found ($p<0.1$) likely due to newly deposited sediments (Garza-Rubalcava et al., 2022, in revision). However, the changes in cap thickness indicate that deposition occurs only in certain LTM stations.

6.4.2 CHANGES IN FREELY DISSOLVED PAHS

The application of benzo(a)pyrene-toxic equivalent factor to PAH concentrations can provide a more accurate risk assessment from environmental exposure to PAH (Nisbet & LaGoy, 1992). The use of the benzo(a)pyrene equivalents evaluated over

sampling years can be a strong indicator of cap effectiveness of carcinogenic PAHs where further analysis can lead to contaminant transport across the sediment-cap interface (Barth et al., 2008; Lampert et al., 2013; Garza-Rubalcava et al., 2022 in revision). Equation (0.4) shows the calculation of benzo(a)pyrene equivalents (BaP_{eqv}) based on the TEF's adapted Nisbet & LaGoy (1992) shown in Table 6-1.

$$BaP_{eqv} = 0.001CHRY + 0.01BkF + 0.1\left(BbF + BaA + \frac{BghiP}{IP}\right) + BaP + DBA \quad (0.4)$$

Where $CHRY, BkF, BbF, BaA, BghiP, IP, BaP, and\ DBA$, represent the chrysene, benzo(k)fluoranthene, benzo(b)fluoranthene, benzo(a)anthracene, benzo(g,h,i)perylene, indeno(1,2,3-cd)pyrene, benzo(a)pyrene, and dibenz(a,h)anthracene porewater concentrations determined from the passive samplers deployed.

The use of a one-way ANOVA statistical method could evaluate the distribution of benzo(a)pyrene equivalents in the previous sampling years (2012, 2013, and 2014) to evaluate the difference in average concentration within the cap and the underlying sediment. There was no statistical difference in benzo(a)pyrene equivalent concentration results from the first three years across the site and the hypothesis that the year-to-year data was different was rejected ($p = 0.8554$) in the cap and the underlying sediments ($p = 0.3143$). Indicating the sampling years have a similar mean and can be treated as a single population. This is similar to the results found by Garza-Rubalcava et al. (2022) for individual PAH compounds. The one-way ANOVA was performed on specific depth intervals and found comparable results in the cap ($p = 0.8021$) and the underlying sediment ($p = 0.2978$) for the west, however within the east sampling area the porewater measurements to be significant ($p < 0.05$). The east sampling area shows significant

local variations in groundwater-surface water exchange as evidenced by variations in measured upwelling velocity and chloride profiles in the near surface (Garza-Rubalcava et al., 2022 in revision). These facts make it difficult to make conclusions about long-term contaminant migration in that area, although a comparison of cap and underlying sediment concentrations still suggested an effective sediment cap to-date.

Based on the distribution of average porewater concentrations, C_{av}, in sediments and the cap, the measured C_{pw} values from 2012-2014 were geometrically averaged at each depth and LTM station to provide a representation of the baseline conditions after the cap placement and will hereafter be referred to as "BL". The geometric means of BaP_{eqv} for the BL and 2019 sampling events can be found in Appendix 9.5.

When comparing benzo(a)pyrene equivalents in the averaged BL population to the averaged 2019 sampling equivalents a t-test statistical analysis was used. For assessing the statistical significance of the difference between two samples (one-way ANOVA requires a minimum of three arguments), the construction of confidence intervals for the difference between two populations means, and in linear regression analyses. No difference was found in the population means between the underlying sediment ($p = 0.3461$) or the cap ($p = 0.6013$) between the BL conditions and 2019. Figure 6-4 shows the distribution of the benzo(a)pyrene equivalents in the cap and the underlying sediments during the BL and the 2019 sampling conditions previously described.

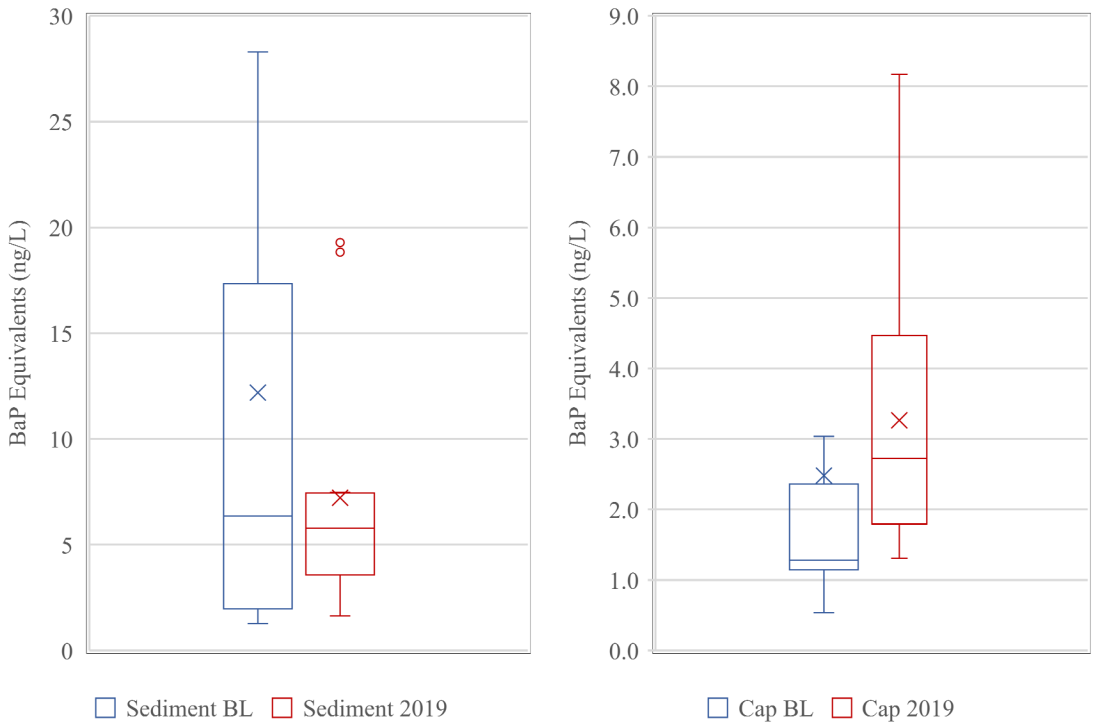

Figure 6-4 Benzo(a)pyrene equivalent depth-averaged porewater distribution at the long-term monitoring stations 1-14 in the sediment (left) and the cap (right).

Concluding that unless there was significant migration of the higher molecular weight PAHs out of the cap or into the sediment the distribution should be similar specifically when examining vertically averaged samples. Providing evidence of effective performance of the cap placement. Although spatial movements within the cap is likely due to deposition (Table 9-1 in Appendix 9.5) and is examined more closely in the following section.

6.4.3 SPME Depth Profiles

Given no significance across the 2012-2014 sampling events BaP_{eqv} were geometrically averaged to form BL conditions at all depth intervals to look at key processes occurring across the site. Long-term change in porewater concentrations can be used to determine stability of the cap and identify potential areas of concern, however by

focusing on heavier molecular weight PAHs (i.e., BaP_{eqv}) compound degradation or even significant migration is not to be expected (Chang et al., 2003; Mihelcic & Luthy, 1988).

Figure 6-5 examines the depth SPME depth profiles for benzo(a)pyrene at stations 2 (S2) and 11 (S11), respectively. There appears to be ~20 cm (~2.86 cm/yr) of newly deposited material between the two sampling periods. The deposition of new, clean material is simply moving the PAH contamination to a deeper depth interval. An example can be viewed for benzo(a)pyrene at station 2, Figure 6-5 (left), at depth interval 24 cm for the BL sampling event is likely correlated with discrete depth interval 44 cm for the 2019 sampling event. The increase in porewater concentration within the deeper sediment found in 2012 is likely not noticed by the 2019 sampling event due to this displacement. Sample station 11 was of particular interest being located adjacent to an outfall of a wastewater treatment plant. The discharge here is expected to be greater than surrounding areas and a likely candidate for newly deposited materials. Like station 2 deposition can be noticed in the porewater depth profile for benzo(a)pyrene at station 11, (right), at the 44 cm (BL) depth interval compared to the 64 cm (2019) depth interval.

The use of SPME using PDMS passive samplers shows the accurate characterization of porewater across multiple sampling years. Given relatively no migration of benzo(a)pyrene can be attributed to the increased hydrophobicity ($\log K_{ow} = 6.04$), the calculated geometrically average sediment partitioning coefficient throughout the cap at station 2 ($\log K_d = 3.42 \pm 0.6$) indicates strong sorption of heavier molecular weight compounds. The sediment partitioning coefficient is within the range determined by Garza-Rubalcava et al. (2022 in revision) and concluded similarly that high molecular

weight PAHs within the cap would not be affected by diffusional transport, but deposition of new material can be observed at multiple locations.

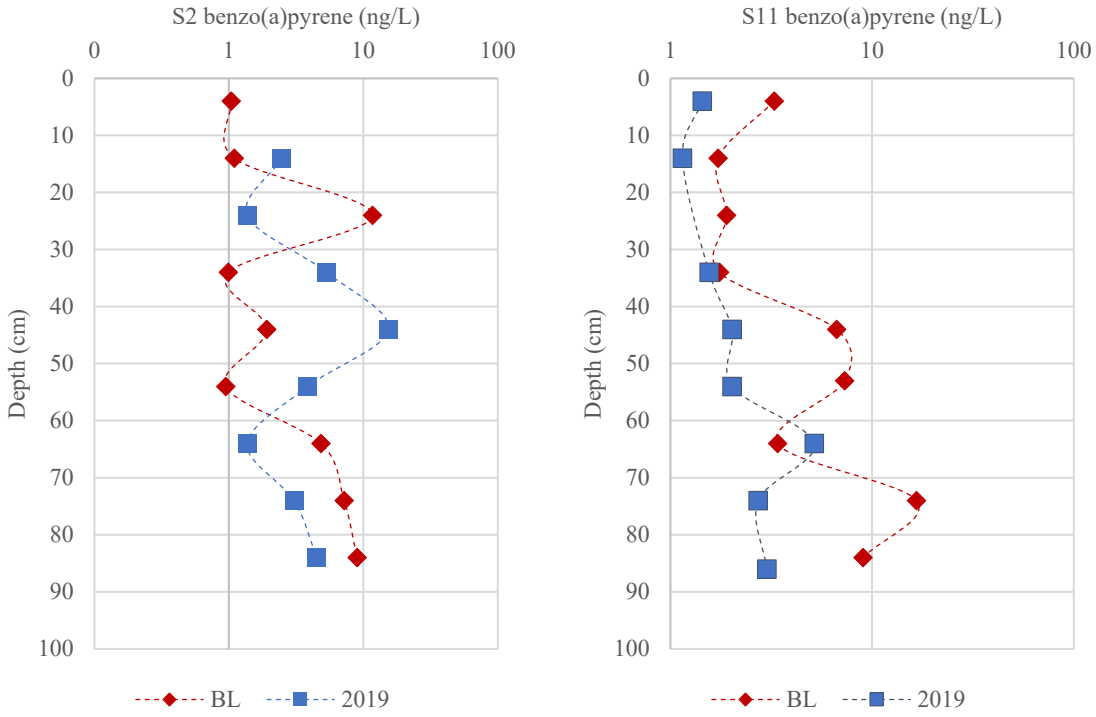

Figure 6-5 Log-scale porewater concentration depth profiles of benzo(a)pyrene. The baseline (BL) and 2019 sampling events for station 2 (left) and station 11 (right) are shown. The discrete depth intervals are connected by a dashed line to help follow the different sampling event intervals.

Containment of high molecular weight PAHs indicate the cap is functioning properly while the depth profiles indicate deposition of new cleaner material is shifting the porewater concentrations down, at ~2.86 cm/year, as depicted in the SPME depth profiles (Figure 6-5). Conservative estimates determined benzo(a)pyrene is expected to migrate throughout the lower 25 cm of the capping layer over approximately 100 years (Garza-Rubalcava et al., 2022 in revision). Further analysis is performed in the next section to explore changes in surficial sediment across the LTM stations.

6.4.4 Remedy Effectiveness

To better understand the variation between these LTM stations, an additional analysis consisted in finding the relative change in porewater concentration within the cap and underlying sediment from the 2019 sampling event (Table 6-1). The BaP_{eqv} porewater concentrations measured across the WBGCR were geometrically averaged over the upper 40 cm (Mills (2015) reported cap layer thickness on average) and the sediments below 40 cm (Table 6-2). This ratio can change significantly over the depth of the porewater profile, so the logarithm of the ratio is reported. Positive log ratios shown in red indicate the surface layer is more contaminated, on average, than the underlying sediments while negative log ratios imply the surface layer is cleaner than the underlying layer. A log ratio near zero implies that there is little difference between the average near-surface porewater concentration and the porewater concentrations at depth. A good example of this is at station 18 where no cap was placed and a log-ratio of -0.01 is reported indicating uniform porewater concentrations over the sampled depth interval. A similar table for all priority pollutant PAHs across the 21 LTM stations can be found in Appendix 9.5.

Table 6-2 The log-ratio of the average measured BaP_{eqv} porewater concentration for depths of less than 40-cm (cap thickness on average) and greater than 40-cm. Log ratios shown in red represent profiles in which the near surface concentration is greater than concentration at depth.

Location	BaP_{eqv}
01A	-0.03
02	-0.30
03	-0.31
04	-1.34
05	0.13

Table 6-2, Continued

Location	BaP_{eqv}
25	-0.24
06	-1.18
07	0.04
08	-0.52
10	0.07
11	-0.45
12A	0.06
13	-0.54
14	0.11
15	0.19
16	-0.01
17	0.14
18	-0.01
19	-0.38
20A	0.22
21	0.00

These differences in freely dissolved concentrations between the layers demonstrate the effectiveness of the cap to decrease fluxes of contaminants into the surface water (Reible, 2014). However, differences in BaP_{eqv} in the layers were not as pronounced as in bulk values. A possible explanation for this discrepancy comes from the fact that portions of the PAHs are associated with strongly sorbing phases (i.e., black carbon) and are not readily available to dissolve and be mobilized in porewater (Khairy et al., 2019; Rakowska et al., 2012).

The largest difference in surficial to underlying porewater concentrations was observed at station 4 where the log ratio is -1.34. That is the near-surface average porewater concentration of 0.0026 µg/L is more than twenty times smaller than the underlying average porewater concentration of 0.056 µg/L. The log ratio between the surface concentrations and the underlying sediment concentrations is typically the most negative

for the low molecular PAHs for both the East and West sampling locations (Appendix 9.5). Indicating the presence of the cap and its effectiveness.

Station 20A showed the greatest increase in BaP_{eqv} concentrations within the surficial sediment (log ratio of 0.22). Although low, average of 0.008 µg/L in surficial sediments, the depth profile of the 2019 event compared to the BL conditions shows an instance where newly deposited sediment paired with the reworking of surficial sediments from bioturbation could be in effect. Denoted by the uniform profiles in the 2019 sampling events increasing the presence of high molecular weight PAHs from deeper sediment. A similar instance was observed in station 15 which had the second greatest increase in BaP_{eqv}, average of 0.002 µg/L, within surficial sediments (Figure 6-6, right).

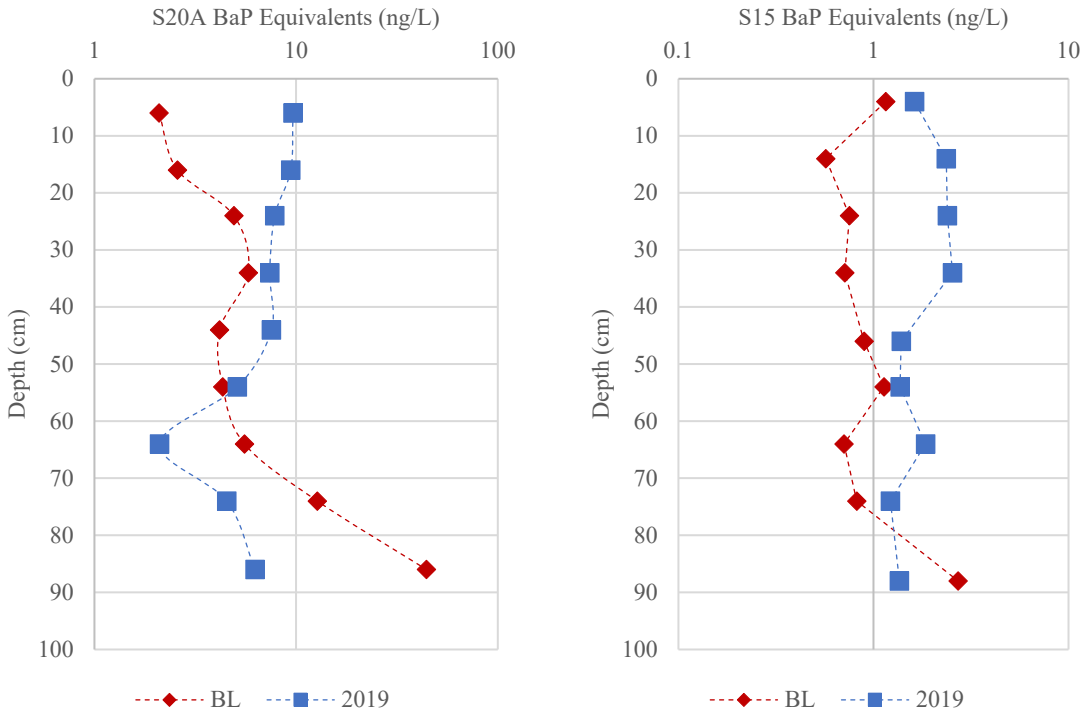

Figure 6-6 Porewater depth profiles of BaP_{eqv} during the baseline (BL) and 2019 sampling events at station 20 (S20A, left) and station 15 (S15, right). The discrete depth concentrations are connected to show continuity within sampling events.

On average the low molecular weight PAHs in the upper 40 cm were less than half of the concentration in the lower layer. This may reflect greater flushing of low molecular weight PAHs from the surficial cap material or their tendency to degrade over time (Garza-Rubalcava et al., 2022 in revision). High molecular weight carcinogenic PAHs, however, tend to show relatively uniform concentrations from the underlying sediment to the surficial cap layer at many locations with the concentrations in the upper layer approximately 80% of the concentrations in the lower layer in both sampling areas. These compounds may not be flushed as readily from the surficial sediments and are not subject to significant degradation.

6.4.5 Porewater Concentration Compared to National Recommended Water Quality Criteria

The measured concentrations were also compared to National Recommended Water Quality Criteria (NRWQC) (EPA, 2018). The NRWQC is a conservative comparison since the surface water concentrations are not directly applicable to porewater and considerable dilution would occur between the porewater and surface water at the site. The NRWQC for the high molecular weight PAHs are also very low including 0.12 ng/L for benzo(a)pyrene which is approximately an order of magnitude below the PQL for these analyses. Thus, all detectable concentrations of benzo(a)pyrene exceeded the NRWQC. It is possible to achieve lower quantification limits using additional PDMS fiber or concentrating samples, but the methodology employed herein was maintained to be consistent with previous analyses. To provide a more useful and realistic comparison criteria for the porewater concentrations, the Washington Department of Ecology 2015 Sediment Cleanup Objectives (WDE SCO), sited in McGrath et al. (2019), were converted to an equivalent porewater concentration for the high molecular weight PAHs used in estimating equivalent benzo(a)pyrene concentrations. The porewater concentration expected in the sediment associated with the cleanup objectives was estimated by assuming a typical value of 1% fraction organic carbon in the sediments and equilibrium partitioning as calculated by Equation (6.5).

$$C_{pw,SCO} = \frac{W_{SCO}}{K_{oc} f_{oc}} \tag{6.5}$$

Where $C_{pw,SCO}$ is the SCO equivalent porewater concentration, W_{SCO} represents the sediment cleanup objective (in µg/kg), $K_{oc}f_{oc}$ represents the organic carbon-based partitioning coefficient for the PAH and the fraction organic carbon of the sediment (1%).

In general, only surficial samples that exceed this screening criteria may be of concern in that only these samples are exposed to surface water and the benthic community (Mayer et al., 2014). The locations flagged as of potential concern were those where either the average in the near surface or the BaP_{eqv} concentrations exceeded the higher of the screening values (NWRQC or SCO Equivalent).

Table 6-3 compares the highest measured surficial average concentration of the PAHs at any of the sites to the two criteria identified above. The surficial average concentrations were all well below the NRWQC criteria for the low molecular weight PAHs and pyrene and fluoranthene. The high molecular weight carcinogenic PAHs were all above the NWRQC criteria but below the WDE SCO equivalent porewater concentration comparisons calculated except at location 18 where no cap has been placed. The highest surficial average concentrations observed were measured at locations 10 and 18 as noted in the Table.

Table 6-3 Human Health Ambient Water Quality Criteria, Water+Organism for primary pollutant PAHs presented with the highest depth-averaged porewater concentration found in surficial sediments (0 - 40 cm) within log-term monitoring (LTM) stations at WBGCR

Compound	**Human Health NRWQC Water+Organism[1] (µg/L)**	**Equivalent Porewater Concentration to WDE SCO[2] (µg/L)**	**Highest Average Near Surface Concentration and LTM Location (µg/L)**
Naphthalene	-		0.371 (10)
Acenaphthene	70		2.86 (18)
Fluorene	50		2.15 (18)
Anthracene	300		0.56 (18)
Phenanthrene	-		9.56 (10)
Pyrene	20		1.15 (18)
Fluoranthene	20		0.39 (18)

Table 6-3, Continued

Compound	Human Health NRWQC Water+Organism[1] (µg/L)	Equivalent Porewater Concentration to WDE SCO[2] (µg/L)	Highest Average Near Surface Concentration and LTM Location (µg/L)
Benzo[b]fluoranthene	0.0012	0.051	0.023 (18)
Benzo[a]anthracene	0.0012	0.045	0.063 (18)
Chrysene	0.12	0.041	0.064 (18)
Benzo[k]fluoranthene	0.012	0.034	0.006 (10)
Benzo[a]pyrene	0.00012	0.028	0.016 (10)
Benzo(g,h,i)perylene + Indeno(1,2,3-cd)pyrene	0.0012	0.007	0.0014 (18)
Dibenzo(a,h)anthracene	0.00012	0.001	0.0009 (21)

[1] NRWQC concentrations can be found at (EPA, 2018)
[2] Washington Department of Ecology Sediment Cleanup Objective assuming 1% organic carbon and equilibrium partitioning as cited in McGrath et al. (2019)

6.5. CONCLUSION

The use of PDMS SPME for passive sampling at Roxana Marsh and the West Branch of the Grand Calumet River were successful in measuring profiles of PAHs in the cap and underlying sediment. High underlying sediment porewater concentrations were noted at depth greater than 40 cm below the cap-water interface and relatively low porewater concentrations were observed in the surficial 40 cm. The cap layer continues to function to reduce surficial contaminant concentrations in the biologically active zone.

The 2019 profiles also showed trends and magnitudes of porewater concentrations of total PAHs that were very similar to those observed in 2012, however displaced by ~20 cm of new, cleaner material. This is likely due to the disposition of surficial sediment in locations where historical outfalls have been found as the background station 18 showed no evidence of vertical shifts in concentration. There is a general loss of low molecular weight PAHs from the surface capping layer with an overall 48% decrease in

average surficial porewater concentration (0-40 cm) especially in low molecular weight PAHs. There are more uniform concentrations of high molecular weight carcinogenic PAHs in the surficial cap layers and there was a modest increase in B(a)P and B(a)P equivalent porewater concentrations in most locations.

6.6. REFERENCES

Barth, E. F., Reible, D., & Bullard, A. (2008). Evaluation of the physical stability, groundwater seepage control, and faunal changes associated with an AquaBlok® sediment cap. *Remediation*. https://doi.org/10.1002/rem.20183

Chang, B. V., Chang, S. W., & Yuan, S. Y. (2003). Anaerobic degradation of polycyclic aromatic hydrocarbons in sludge. *Advances in Environmental Research*, *7*(3), 623–628. https://doi.org/10.1016/S1093-0191(02)00047-3

Epa. (1986). Method 8310: Polynuclear aromatic hydrocarbons. *Chemistry & …*.

EPA. (2018). National recommended water quality criteria - aquatic life criteria table. *Https://Www.Epa.Gov/Wqc/National-Recommended-Water-Quality-Criteria-Aquatic-Life-Criteria-Table#table.*

Ghosh, U., Kane Driscoll, S., Burgess, R. M., Jonker, M. T. O., Reible, D., Gobas, F., Choi, Y., Apitz, S. E., Maruya, K. A., Gala, W. R., Mortimer, M., & Beegan, C. (2014). Passive sampling methods for contaminated sediments: practical guidance for selection, calibration, and implementation. *Integrated Environmental Assessment and Management*, *10*(2), 210–223. https://doi.org/10.1002/ieam.1507

Ingersoll, C. G., MacDonald, D. D., Brumbaugh, W. G., Johnson, B. T., Kemble, N. E., Kunz, J. L., May, T. W., Wang, N., Smith, J. R., Sparks, D. W., & Ireland, D. S. (2001). Toxicity Assessment of Sediments from the Grand Calumet River and Indiana Harbor Canal in Northwestern Indiana, USA. *Archives of Environmental Contamination and Toxicology 2002 43:2*, *43*(2), 156–167. https://doi.org/10.1007/S00244-001-0051-0

Khairy, M. A., Noonan, G. O., & Lohmann, R. (2019). Uptake of hydrophobic organic compounds, including organochlorine pesticides, polybrominated diphenyl ethers, and perfluoroalkyl acids in fish and blue crabs of the lower Passaic River, New Jersey, USA. *Environmental Toxicology and Chemistry*, *38*(4), 872–882. https://doi.org/10.1002/ETC.4354

Lampert, D. J., Lu, X., & Reible, D. D. (2013). Long-term PAH monitoring results from the Anacostia River active capping demonstration using polydimethylsiloxane (PDMS) fibers. *Environmental Sciences: Processes and Impacts*. https://doi.org/10.1039/c3em30826j

Lampert, D. J., Sarchet, W. V., & Reible, D. D. (2011). Assessing the effectiveness of thin-layer sand caps for contaminated sediment management through passive sampling. *Environmental Science and Technology*. https://doi.org/10.1021/es200406a

Mayer, P., Parkerton, T. F., Adams, R. G., Cargill, J. G., Gan, J., Gouin, T., Gschwend, P. M., Hawthorne, S. B., Helm, P., Witt, G., You, J., & Escher, B. I. (2014). Passive sampling methods for contaminated sediments: scientific rationale supporting use of freely dissolved concentrations. In *Integrated environmental assessment and management*. https://doi.org/10.1002/ieam.1508

McGrath, J. A., Joshua, N., Bess, A. S., & Parkerton, T. F. (2019). Review of Polycyclic Aromatic Hydrocarbons (PAHs) Sediment Quality Guidelines for the Protection of Benthic Life. In *Integrated Environmental Assessment and Management*. https://doi.org/10.1002/ieam.4142

Mihelcic, J. R., & Luthy, R. G. (1988). Degradation of polycyclic aromatic hydrocarbon compounds under various redox conditions in soil-water systems. *Applied and Environmental Microbiology*, *54*(5), 1182–1187. https://doi.org/10.1128/AEM.54.5.1182-1187.1988

Mills, M. (2015). *Cap Performance Monitoring Using Forensic Chemistry Methods*.

Nisbet, I. C. T., & LaGoy, P. K. (1992). Toxic equivalency factors (TEFs) for polycyclic aromatic hydrocarbons (PAHs). *Regulatory Toxicology and Pharmacology : RTP*, *16*(3), 290–300. https://doi.org/10.1016/0273-2300(92)90009-X

Rakowska, M. I., Kupryianchyk, D., Harmsen, J., Grotenhuis, T., & Koelmans, A. A. (2012). In situ remediation of contaminated sediments using carbonaceous materials. In *Environmental Toxicology and Chemistry*. https://doi.org/10.1002/etc.1763

Reible, D. D. (2014). Contaminant Processes in Sediments. In *Processes, Assessment and Remediation of Contaminated Sediments*. https://doi.org/10.1007/978-1-4614-6726-7

Shen, X., & Reible, D. (2019). An analytical model for the fate and transport of performance reference compounds and target compounds around cylindrical passive samplers. *Chemosphere*. https://doi.org/10.1016/j.chemosphere.2019.05.198

Steevens, J. A., Besser, J. M., Dorman, R. A., & Sparks, D. W. (2020). Influence of remediation on sediment toxicity within the Grand Calumet River, Indiana, USA. *Chemosphere*. https://doi.org/10.1016/j.chemosphere.2020.126056

Thomas, C. (2014). *Passive Sampling to Evaluate Performance of in-situ sediment remediation*. University of Texas.

CHAPTER 7

IN-SITU PASSIVE SAMPLING FOR THE EVALUATION OF CARBON AMENDMENT PERFORMANCE

7.1. ABSTRACT

In 2006, the Portland District of the U.S. Army Corps of Engineers collected sediment samples from varying depths near a portion of the Lower Columbia Slough at the Pacific Meats cleanup site. Sediment samples contained polychlorinated biphenyl (PCB) concentrations up to 2,450 µg/kg. The PCB concentrations were found to be higher in the Lower Slough than in other reaches and were detected more consistently within the more industrial and commercial development of this area.

In 2015, Texas Tech University performed a baseline study by evaluating in-situ and ex-situ porewater sample analyses at 20 locations at two depth intervals (0-13.5 cm and 13.5-29 cm). In-situ sampling was performed by solid-phase microextraction (SPME) passive sampling using polydimethylsiloxane (PDMS) coating on a glass fiber to function as a sorbent for PCBs. In 2016, a thin cap of activated carbon (AC) was placed across two separate plots (East and West). After the placement of AC in two forms, as amendments of Sedimite™ and Aquagate+PAC™, the analysis and comparison of porewater concentrations within the 20 approximately identical cap locations across the two plots was determined. SPME samplers were deployed in triplicate in the sediment for 28 days to achieve equilibrium with the contaminants of concern for both the baseline analysis and the carbon amendment results.

After a 13-month application of AC's the reductions from the baseline porewater concentrations ranged from 58-82% in the surficial sediment layer, and a range of 56-76% reduction in porewater concentrations was determined in the porewater measurements at depth. The activated carbon amendments primarily stayed within their original footprint at the site. A material balance was performed using measured organic carbon and black carbon in captured sediment and noted the difference from the baseline (2015) sampling event. Comparing to the pre-placement average of 3%, this suggests that Aquagate+PAC™ plot contains about 80% of that originally placed with 20% migrating to the deeper (13.5-29 cm) sediment. Approximately 27% of the Sedimite™ was retained within the original placement footprint with greater than 70% of the AC migrating into the deeper depth interval. Areas for improved AC measurements in the future are also discussed.

7.2. INTRODUCTION

Previous investigations within the lower Columbia Slough area in Portland, Oregon have found chemicals associated with industrial uses such as pesticides and polychlorinated biphenyls (PCBs) in surficial sediments above acceptable limits for bioaccumulation in fish (Sutter, 2012). In 2006, the Portland District of the U.S. Army Corps of Engineers (USACE) collected sediment samples from varying depths near a portion of the Lower Columbia Slough at the Pacific Meats cleanup site. Where sediment samples analyzed contained PCB concentrations up to 2,450 µg/kg. The PCB concentrations were found to be higher in the lower slough than in other reaches and were detected more consistently within the more industrial and commercial developments

in the area. This study is located within the middle portion of the lower slough section of the Columbia River just west of the former Pacific Meat property (Figure 7-1).

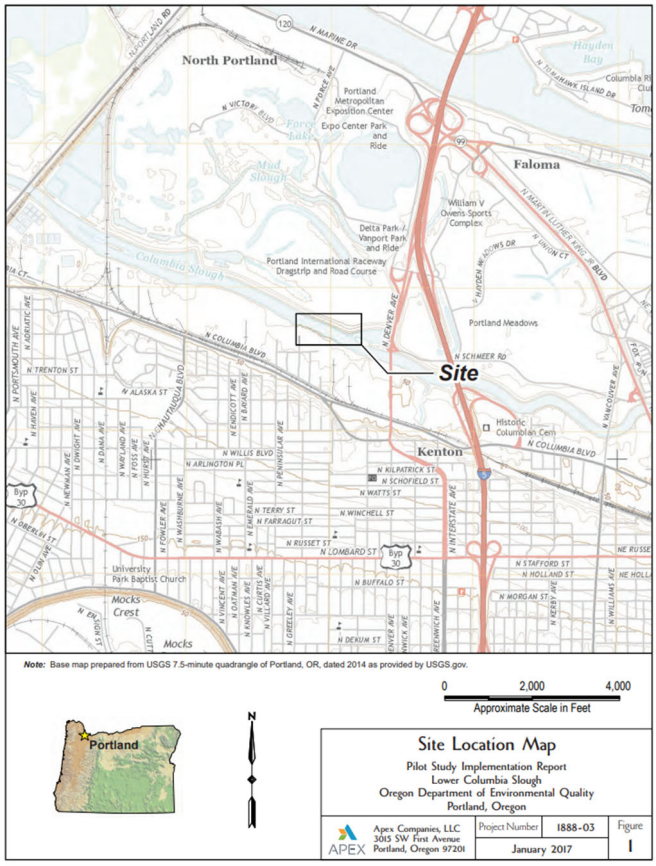

Figure 7-1 Sampling site location of the Lower Columbia Slough in Portland, Oregon

Following the initial baseline investigation, a PCB sediment cleanup pilot study was conducted, in 2015, involving the implementation of solid phase microextraction (SPME) passive samplers using polydimethylsiloxane (PDMS) as a sorbent for PCBs at twenty individual locations (Figure 7-2). The passive samplers were implemented in-situ and in the lab (ex-situ) with captured sediment from adjacent locations. Additional sediment was collected in both the surficial (0 – 13.5 cm) and deeper sediment (13.5 – 29) for bulk sediment chemistry, total organic carbon (TOC), and black carbon (BC) measurements. These analyses will be referred to as the baseline monitoring event

throughout the remainder of the study. After the baseline monitoring event the placement of two diverse types of activated carbon (AC) amendment caps across two 20,000 ft^2 sections of the impacted sediment were installed in September 2016. Activated carbon has proven to be a strong sorbent of HOCs in contaminated sediments (Luthy et al., 1997; Murphy et al., 2006; Danny Reible et al., 2006). Of the two types of AC capping materials used, Sedimite™ from Sediment Solutions (Elliot City, Maryland) and Aquagate+PAC™ from AquaBlok Ltd. (Swanton, Ohio) were selected as the AC products for this site. Sedimite™ was applied to the east plot and Aquagate+PAC™ to the west (Figure 7-2). The target thickness was 0.6 inches for Sedimite™ and 1.7 inches for Aquagate+PAC™. The goal of this placement was to raise the percentage of black carbon in the upper 15 centimeters of sediment to 3 percent throughout the application area.

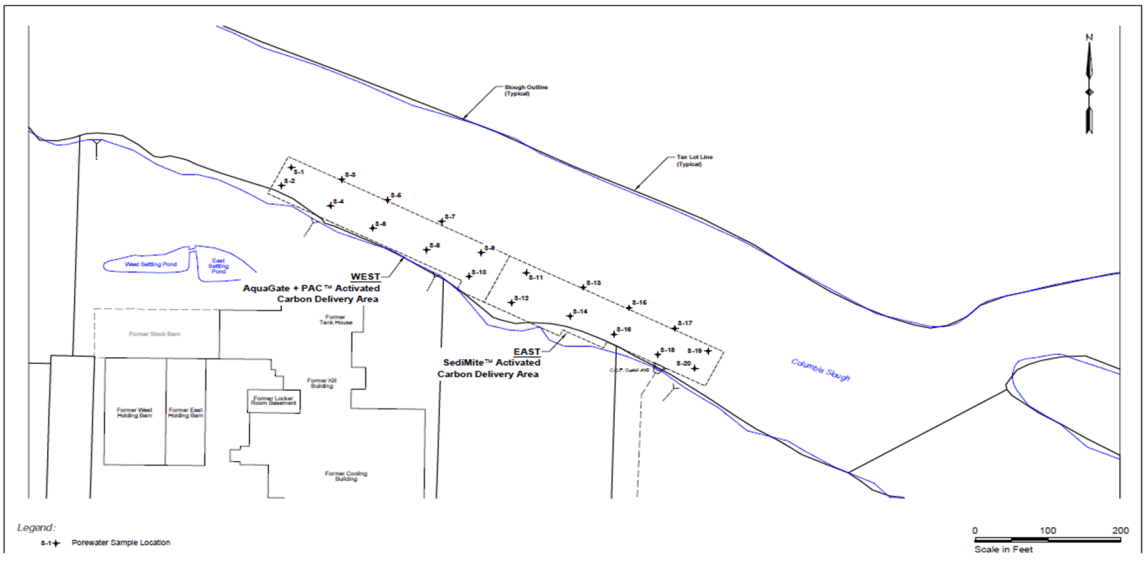

Figure 7-2 Porewater sampling locations S1 - S20. S1-S10 are within the Aquagate+PAC™ amended area while S11-S20 are within the Sedimite™ amended area

In this study, bulk solid and freely dissolved porewater concentrations (C_{pw}) of PCBs in sediments samples are reported prior to AC placement in September 2015 to determine baseline characteristics of the sediment and porewater concentrations, and again in October 2017 after the placement of two forms of AC in September 2016. SPME PDMS passive samplers were used to evaluate performance and implantability of two forms of AC to reduce bioavailable fractions of elevated PCBs in sediment. The effectiveness is determined by the reduction in porewater concentration over time. From the captured sediment a calculated mass of AC remaining within the original footprint application is determined. The sediment was captured from two depth intervals and from the mass of AC present vertical mixing of AC over time is estimated and correlated to the SPME PCB porewater concentration depth profiles.

7.3. MATERIALS AND METHODS

7.3.1 SAMPLING LOCATIONS

Individual sampling locations for the twenty in-situ samples (S1-S20) are shown in Figure 7-2. The locations of the west and east sampling areas and the areas of the carbon amendment placement are shown in Figure 7-3.

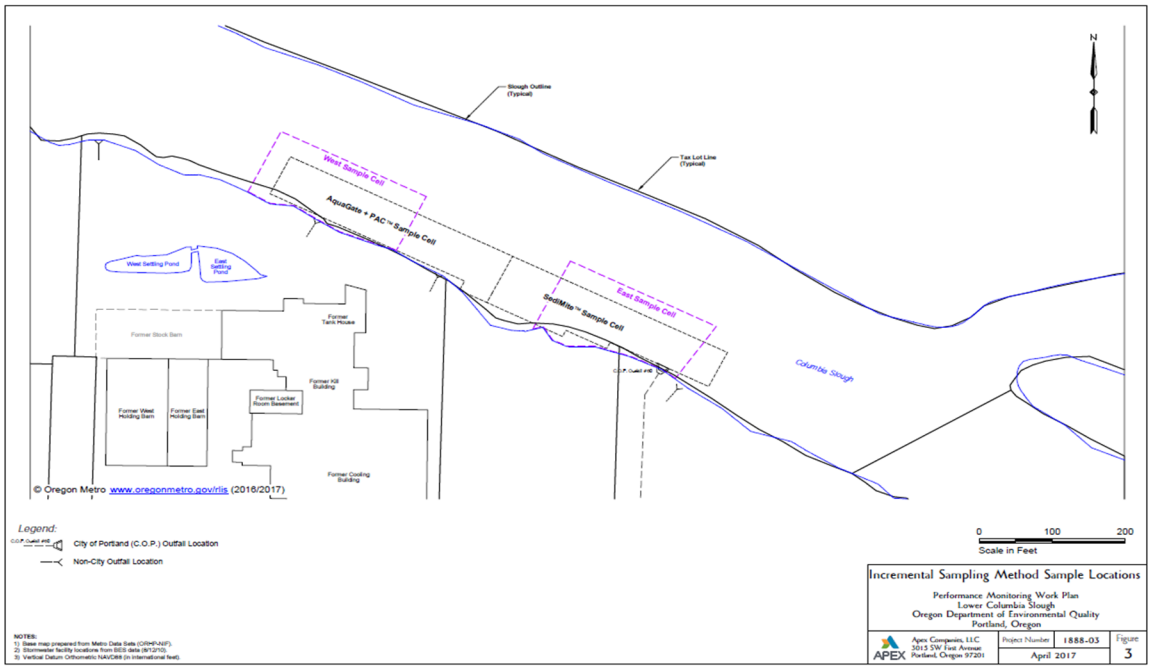

Figure 7-3 Lower Columbia Slough bulk sediment collection areas (red dotted line) and Aquagate+PAC™ and Sedimite™ application areas (black dotted line)

Composite sediment samples that were collected from multiple points within the west and east sampling cells were homogenized and sent to Texas Tech University for processing. These bulk sediment samples were distributed into five replicates per plot.

7.3.2 Total Organic Carbon and Black Carbon

Total organic carbon (TOC) and black carbon (BC) were determined in duplicate using chemothermal oxidation (Gustafsson et al., 2001). Sediment samples are dried in the over at 105°C overnight, stored in a desiccator to cool down and homogenized. Inorganic carbon is removed by adding 1 N hydrochloric acid (HCl) into the sample. Treated samples are allowed to dry in the oven for 1 hour (at 105°C). Following this procedure, the samples are weighed palletized and analyzed for TOC using a Vario TOC Select (Elementar). For BC analysis, the samples are heated in a muffle furnace at 375°C for 24 hours before proceeding with the acidification step and subsequent analysis. The

organic carbon content that excludes the BC fraction can be obtained by the difference between TOC and BC. Note that during baseline sampling, black carbon is primarily anthropogenic carbon from combustion processes (soot carbon) and can include AC after AC placement. Unfortunately, the black carbon cannot be used as an indicator of the amount of AC because a portion of the AC is volatized at temperatures below that used to measure black carbon (375°C), that is, AC also contributes to the organic carbon other than BC. Instead, the amount of AC in a placement plot was estimated by difference between the baseline and final TOC. A series of black and QC standards (Standard Reference Material – SRM1941b) was used to determine the analytical integrity of the method.

7.3.3 Determination of PCB Concentrations in Bulk Sediment Samples

Prior to extraction, wet sediment subsamples were weighed and dried in an oven at 35°C until the moisture content of the sediment was 20%. Samples were further mixed with diatomaceous earth, spiked with a surrogate standard containing C^{13} labeled PCs: 25/52/101/153/138/180/209 (Cambridge Isotope Laboratories) and extracted using accelerated solvent extraction (ASE 350, Dionex, USA) with a mixture of Hexane/Acetone (3:1 v/v) at 100°C. Two extraction cycles of 5 min each with 40% final rinse were used in the procedure. Sediment extracts were further cleaned up by eluting the samples with hexane through a column packed with sodium sulfate and florisil. Extracts were desulphurized in the presence of copper powder in an ultrasonic bath and concentrated to 1 mL.

Sediment extracts were also analyzed for individual PCB congeners by gas chromatography with a triple quadrupole mass selective detector (GCTQMS, Agilent 7980B) using a SIM/SIM mode (USEPA, 2010). Internal standards containing C^{13} labeled PCBs 9/118/188 are added to the extracts prior to analysis. Recoveries of seven C^{13} surrogate spikes in sediment extracts were also monitored using the GC-MS method. A series of black and QC standards (SRM-1941b) were used to determine the recoveries of certified PCB values and thus analytical integrity of the method.

7.3.4 Determination of PCB Freely Dissolved Concentrations

7.3.4.1 Preparation of PDMS Fibers

PCB concentrations in sediment porewater for analyzing ex-situ and in-situ were determined using SPME fibers (Polymicro Technologies, Phoenix, AZ) containing 25 µm layer of PDMS coating on a glass core with a diameter of 497 µm. Prior to use, the fibers were cut into 6 cm (ex-situ) and 30 cm (in-situ) length pieces washed twice with hexane, acetonitrile, and methylene chloride sequentially for 30 minutes each, rinsed with MiliQ water and dried with Kimwipes™. Only high purity solvents were used in the preparation process. PDMS fibers were impregnated with PRCs to assess the fraction of steady state achieved during the deployment. A mix containing C^{13} labeled PCBs 25/52/101/153/138/180/209 were used as PRCs. Fibers were preloaded with the PRCs by exposure to a spiked methanol:water solution (20:80 v/v) for three weeks on a shaking table. Because AC can lead to inaccurate estimation of steady state releases, the baseline conditions in September 2015 were assumed to predict the degree of equilibration for both the 2015 and 2017 conditions. In short, the degree of release of the PRCs indicates the degree of equilibration of the equivalent unlabeled target compounds. Other

congeners are estimated by fitting the degree of equilibration of the known compounds to standard models (Ghosh et al., 2014; Shen & Reible, 2019).

7.3.4.2 Ex-situ Passive Porewater Sampling

Composite sediment samples collected from the west and east sampling cells were subjected to ex-situ porewater analysis. Ex-situ analysis was also performed on the porewater sampling locations S1-S20 (Figure 7-2) at two depth intervals (0-13.5 cm and 13.5-29 cm). Prior to exposure, ex-situ sediment samples from each sampled location were dosed with Sodium Azide (NaN_3) at a concentration of 100 mg/L to prevent biological activity, and homogenized. Approximately 30 – 32 grams of wet sediment were subsampled from individual containers and placed into 20 mL amber vials for measurement of the freely dissolved concentration. The cleaned and PRC loaded SPME fibers were introduced to the individual vials containing sediment subsamples (i.e., one 6-cm fiber per one sediment sample and closed). Ex-situ stations were made to be comparable to a full length (30 cm) SPME sampler. SPME fiber Samples were allowed to equilibrate for 30 days with gentle shaking on a shaking table at 20°C.

Once finished, the 6-cm fibers were withdrawn one-by-one and processed into autosampler vials with 100 µL of Hexane. The samples were stored at -20°C overnight, vortexed for 1 minute the following day to allow target analytes to desorb from the PDMS. Following the procedure, SPME extracts were transferred to clean autosampler vials with inserts for analysis on the GCTQMS.

7.3.4.3 In-Situ Passive Porewater Sampling

In-situ porewater monitoring at 20 sample stations (Figure 7-2) was conducted using triplicate SPME samplers deployed from a tripod (Figure 7-4). The tripods were

able to house three passive samplers each, with each sampler containing two 30-cm SPME fibers for a total of 60 samplers deployed. The samplers were embedded vertically at each location to a depth of 30 centimeters. Following sample deployment, a weighted line was attached to the sampler and anchored to an inconspicuous point on the shore for retrieval.

Figure 7-4 Tripod sample holder for in-situ passive sampling. Each SPME sampler contains two 30-cm PDMS fibers. The yellow and black deployment rod is fastened onto the top of the tripod for ease of deployment in deeper surface waters and is easily removed

Passive samplers were deployed for 30 days to allow the PDMS fibers to reach equilibrium with the sediment porewater. At the end of the 30-day duration, the tripod sample holder is removed from the sediment, and each of the three passive samplers are gently removed from the tripod. Once removed, each individual sampler is tagged with a number, and wrapped in aluminum foil. Once this step is complete all three replicates from a specific sample site are bound together with aluminum foil. Once all 20 sampling

locations were retrieved, labeled, and bound, ice packs were placed in the cooler to maintain integrity and shipped back to TTU for analysis.

7.3.4.4 CHEMICAL ANALYSIS OF PCBS

SPME extracts in hexane were directly analyzed for 66 individual PCB congeners by GCTQMS (Agilent 7890B) using SIM/SIM mode (USEPA, 2010). Internal standards containing ^{13}C labeled PCBs 9/118/188 were added to the SPME extracts prior to analysis. Calibration standards ranging from 0.08 µg/L to 50 µg/L in hexane were prepared from a 10,000 µg/L PCB stock solution (AccuStandards). An eleven-point calibration led to a linear calibration with an r^2>0.999 for all compounds.

The freely dissolved porewater concentrations were calculated from the accumulated uptake in the fiber and the fiber-water partitioning coefficients (7.1).

$$C_{pw} = \frac{C_{PDMS}}{K_{pw} * f_{ss}} \tag{7.1}$$

Where C_{PDMS} is the equilibrium concentration measured in PDMS (µg/L), K_{pw} is the dimensionless polymer-water partitioning coefficient found in Ghosh et al., (2014) and f_{ss} is the fraction steady state achieved. Two separate calculations of the f_{ss} were utilized within the surficial sediment 0-13.5 cm and the deeper depth interval (13.5-29 cm) of the SPME fiber. Figure 7-5 shows the distribution of ^{13}C-PCB PRCs utilized and Appendix 9.6 contains the full list of f_{ss} for the PCB target compounds.

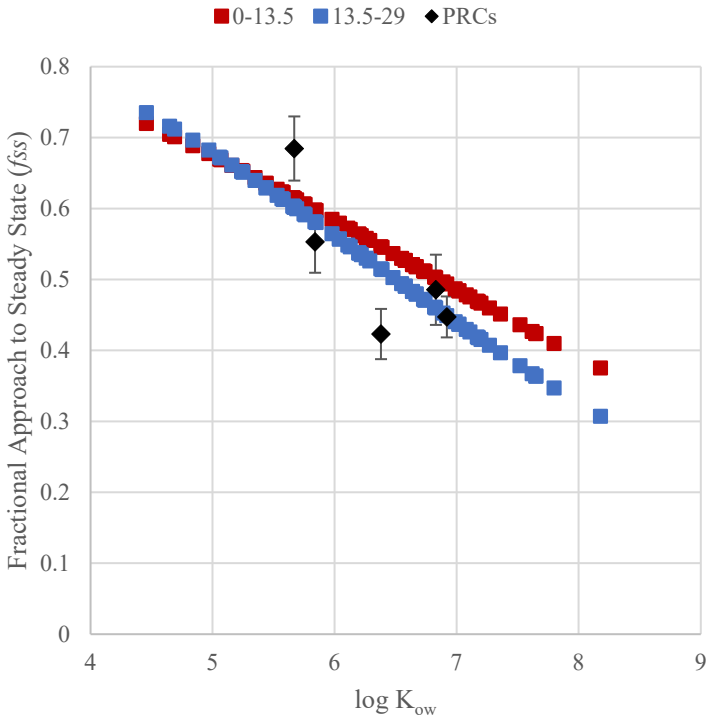

Figure 7-5 The fractional approach to steady state (f_{ss}) for the surficial sediment (0-13.5 cm) and the deeper depth interval (13.5-29 cm) determined by the distribution of ^{13}C-PCB PRCs. The error bars show the variance in PRCs across both depth intervals.

7.4. Results and Discussion

7.4.1 TOC Analysis and Correlation with AC Mass

The average thicknesses of the Aquagate+PAC™ and Sedimite™ layers were found to be 4.96±2.3 cm and 2.95±1.9 cm, respectively with the goal of raising the black carbon (BC) content within the surficial sediments to 3%. The total organic carbon (TOC) in the post-amendment sediments compared to the TOC during pre-treatment sampling was used to estimate the amount of AC in the sediment. In the pre-treatment sampling event, the sediment samples collected within the east, west, and central plots had an average TOC of 3.43±0.3%, 2.91±0.2%, and 2.93±0.2% respectively. Black carbon was also measured and remained consistent across the site at 0.14±0.01%. The averaged TOC content within the surficial sediment 13-months after placement of AC

treatment, Sedimite™ in the east and Aquagate+PAC™ in the west, increased to 5.78±0.5% and 5.52±0.4% in the east and west cells, respectively, while the BC increased significantly to 3.42±0.2% and 3.20±0.1% for the same sampling cells, respectively. The fraction of organic carbon found during the pre-treated sampling event in 2015 was found to be 3% averaged across the entire site. While this was the average of the composite samples, there were individual areas with different concentrations. The west area where Aquagate+PAC™ was placed had a slightly lower average of 2.91% and the east area where Sedimite™ was place had an average of 3.4%. There were inadequate data to support these variations, however, the global average of 3% pre-treatment was used to estimate the AC post placement from the change in TOC. Note that while much of AC is BC, some of the AC is also volatile carbon so change in BC cannot be used to estimate AC (Brändli et al., 2009; Grossman & Ghosh, 2009).

A summary of organic carbon (OC), total organic carbon (TOC), and black carbon (BC) for the 2017 and 2015 sampling events was determined from measured values of TOC and BC and the difference between them (Equation (7.2).

$$OC(\%) = TOC(\%) - BC(\%) \tag{7.2}$$

Organic carbon measurements for the various sampling cells and at the 20 passive sampling locations at two depth intervals can be found in Appendix 9.6

7.4.1.1 Material Balance on Aquagate+PAC™ and Sedimite™ Post Amendment

Given the varying physical properties of Aquagate+PAC™ and Sedimite™ (Table 7-1) a material balance was conducted to examine if the AC remained within the original footprint.

Table 7-1 Comparison of physical characteristics of Aquagate+PAC™ and Sedimite™

Activated Carbon	AC by Dry Weight	Dry Bulk Density (lbs./ft^3)	Moisture Content
Aquagate+PAC™	10%	85-90	-
Sedimite™	50%	45	5-10%

Based on the AC characteristics provided from the manufacturer (APEX, 2017) and the corresponding TOC data in Table 9-5 (Appendix 9.6) a material balance can be performed on a dry basis to determine the presence of activated carbon within each of the plots. The overall material balance is presented below in (7.3 with an explanation of each term that follows.

$$AC_{mass} = \rho_b * \left(TOC_{post} - TOC_{baseline}\right) * V_{cell} \quad (7.3)$$

Where AC_{mass} is the total mass of AC within each of the AC amended areas over a certain depth profile and will be calculated in kilograms. The ρ_b denotes the dry bulk density of the activated carbon within the specific site and is determined by Equation (7.4.

$$\rho_b = \rho_s * (1 - \varphi) \quad (7.4)$$

Where ρ_s corresponds to the grain density of the soil and is assumed to be 2.5 g/cm^3 across the entire site. The φ variable corresponds to the moisture content of the soil within each individual AC plot and depth interval. The averaged moisture content was found to be 39.5% and 39.6% for the top and bottom depth interval within

Aquagate+PAC™, and 47.3% and 48.9% within the two depth intervals within Sedimite™ cell.

For the geospatial data provided for the material balance, the site surface encompassed roughly 40,000 ft^2. This is broken down to a 20,000 ft^2 surface area per AC amended area, or roughly 1,868 m^2. The estimated dry mass of AC placed and accounted for in this manner is summarized Table 7-2.

Table 7-2 Calculated mass of Aquagate+PAC™ and Sedimite™ contained in the original footprint after 13-month placement within the surficial sediment layer (0-13.5 cm) and deeper sediment (13.5-29 cm)

Activated Carbon	Depth Interval (cm)	Mass AC Applied (kg)	Mass AC Remaining (kg)	∑AC Remaining (kg)
Aquagate+PAC™	0-13.5	11,500	4,300	5,400 (47%)
	13.5-29		1,100	
Sedimite™	0-13.5	10,100	1,200	4,500 (45%)
	13.5-29		3,300	

Comparing to the pre-placement average of 3%, this suggests the Aquagate+PAC™ plot contains about 47% of that originally placed with 20% migrating to the deeper (13.5-29 cm) sediment. About 45% of the Sedimite™ was retained within the original placement footprint with greater than 70% of it in the deeper depth interval. The movement of Sedimite™ both deeper and outside of the placement footprint is consistent with the much lower density shown in Table 7-1. However, the Aquagate+PAC™ placement plot is downstream of the Sedimite™ area and some of the

Sedimite™ may have migrated into the downstream plot. This variation could also account for the differing application methods. Sedimite™ was applied through a hose on shore while Aquagate+PAC™ utilized a crane to deposit the AC at the surface (APEX, 2017). Figure 7-6 provides a visual illustration of the calculated AC_{mass} within the individual sampling stations. Note if AC_{mass} was determined to be negative the station is left at zero. This is likely due to the variation in TOC from the initial measurement if less than 3% (TOC during 2015 sampling event). The full calculation can be found in Appendix 9.6.

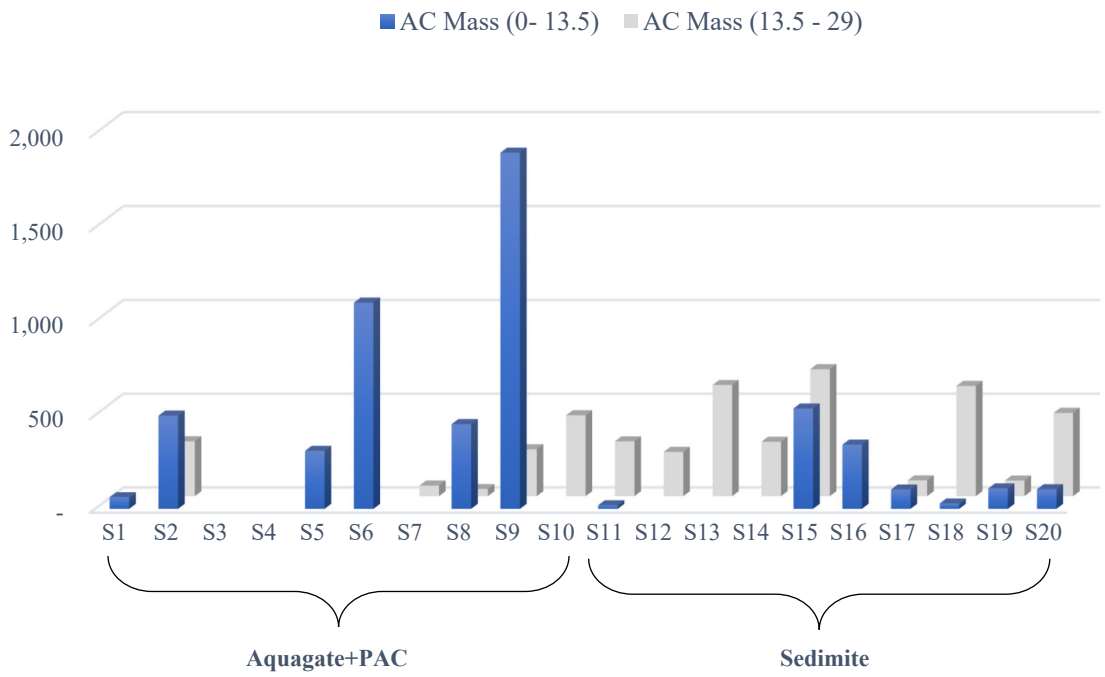

Figure 7-6 Calculated AC mass (kg) at individual sampling stations (S1-S20) within Aquagate+PAC™ and Sedimite™ amended areas. The blue bars correspond to the surficial sediment (0-13.5 cm) and the orange bars correspond to the deeper depth interval (13.5-29 cm)

Due to the potential errors in the calculation including TOC level variability and the TOC levels in the deeper layer, the total AC retained is estimated to be within the range of 25-75% of that originally placed in both plots. AC losses from the placement footprint could be due to reworking of surficial sediments by bioturbation moving AC deeper into the sediment and high flows during storm events leading to movement of AC outside of the original placement. The losses may reflect the relatively small size of the placement plots and a larger placement area may minimize relative losses.

7.4.2 In-Situ PCB Porewater Measurements

The in-situ porewater concentrations of target PCBs during baseline monitoring were measured in June 2015. In total 66 PCB congeners were detected and the ∑PCB porewater concentrations averaged 1.1 ng/L and 0.94 ng/L for the 0-13.5 cm depth intervals in the Aquagate+PAC™ and Sedimite™ areas, respectively (Figure 7-7, left).

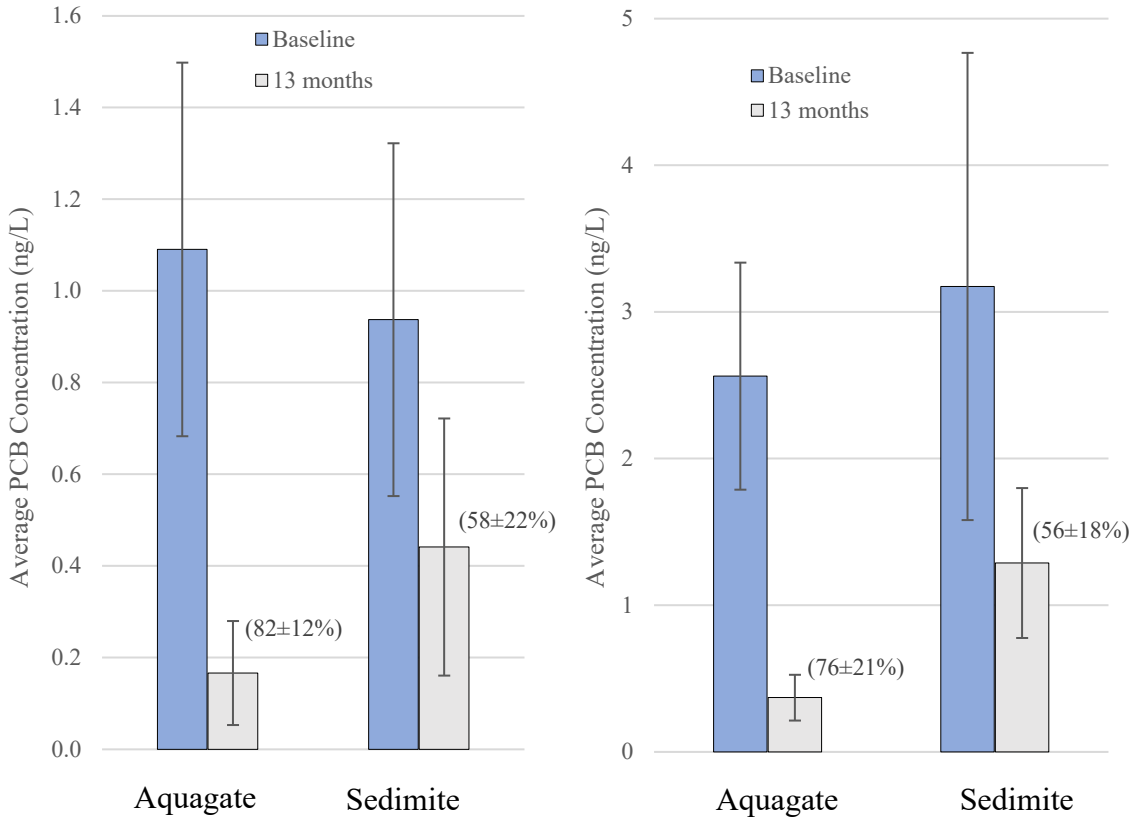

Figure 7-7 Measured in-situ porewater concentrations of $\sum PCB_{66}$ across the two different AC treatment plots. The colored bars represent the baseline (2015) and 13-month (2017) post AC amendment within the 0-13.5 cm depth (left) and 13.5-29 cm depth (right) sampling intervals. The error bars represent one standard deviation (SD) and the numbers in brackets show the percent reduction in porewater concentration ±SD from the baseline data.

For the 13-month post AC amendment application, the in-situ $\sum PCB_{66}$ porewater concentration was reduced by 82±12% in the AquaGate+PAC treatment plot and 58±22% reduction in the Sedimite amended area. These are consistent reductions for AquaGate+PAC (Kirtay et al., 2018; Yan et al., 2020), but Sedimite performed slightly below literature values (Beckingham & Ghosh, 2011; Sanders et al., 2018; Yan et al., 2020). This is due in part by the max replicate average porewater concentration of 2.1

ng/L found at station location 20 (S20) resulting from a 14% reduction from the baseline sampling event.

Within the Aquagate+PAC sampling section (S1-S10) the largest concentration reductions were observed in the low molecular weight PCB homologues (mono-, di-, tri-), which is also consistent with literature evaluating PCB reduction with direct application of AC at the surface (Kupryianchyk et al., 2012; Patmont et al., 2015; Rakowska et al., 2012; Yan et al., 2020). As shown in Figure 7-8 the Sedimite application zone (S11-S20) showed good reduction of tri-chlorobiphenyl congeners, ~67% reduction, but the hexachlorobiphenyl congeners showed the greatest reduction at ~87%. The lack of dichlorobiphenyl reduction in Sedimite is due in part, again, to station 20. The replicate average for station 20 increased in porewater concentration from 1.23 ng/L in the pre-amendment sampling to 1.42 ng/L in the 2017 post amendment sampling event. A full comparison of homologue distribution between the pre- and post-amendment sampling can be found in Appendix 9.6.

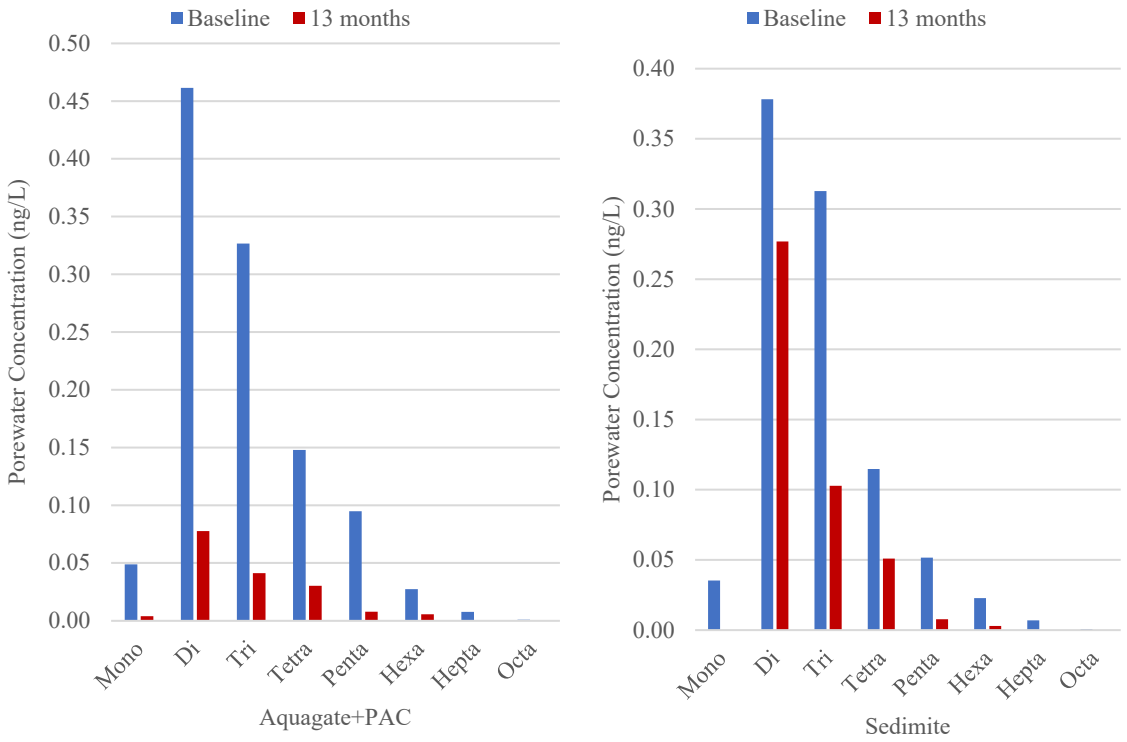

Figure 7-8 PCB homologue concentration comparison in sediment porewater (ng/L) in Aquagate+PAC (left) and Sedimite (right) within the surficial sediment (0-13.5 cm) layer.

Visual representations of congener reductions are shown below that express a comparison of the baseline in-situ porewater sampling to the 2017 porewater sampling event. The reductions shown in Figure 7-9 and Figure 7-10 closely reflect the average reduction across each specific AC amendment area. Note that sample locations S6 and S12 indicate high baseline concentrations for in-situ sampling and are located near the shoreline and downstream of different historical outfalls.

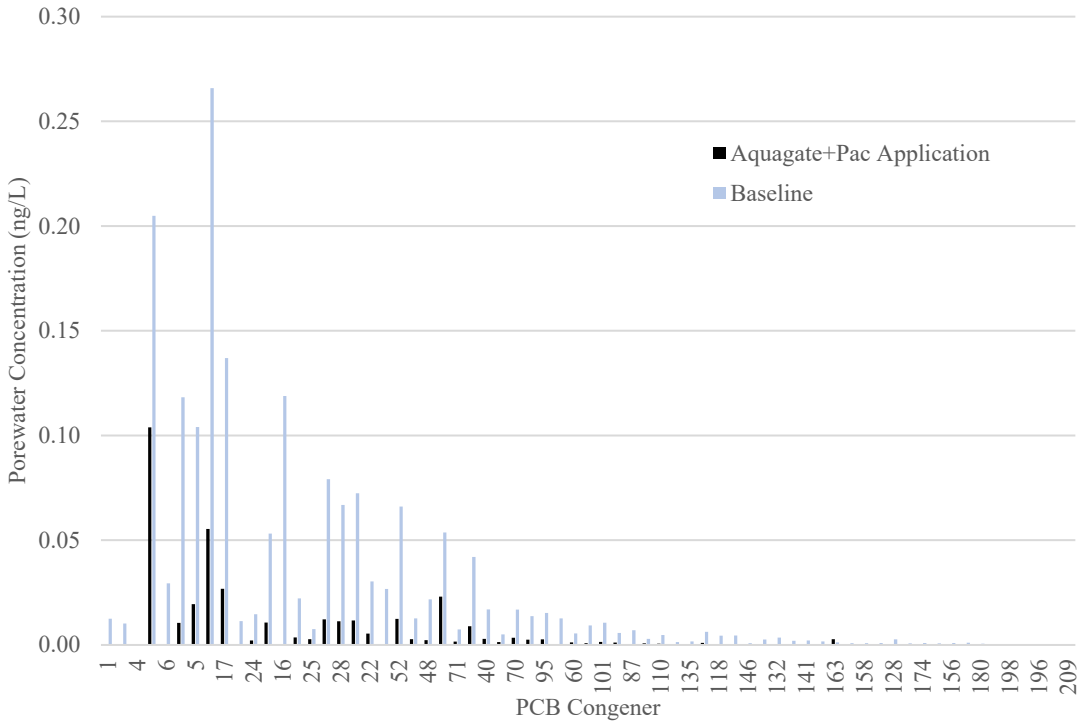

Figure 7-9 Aquagate+PAC™ application congener distribution at sample location S6 from 0-13.5 cm depth showing an 80% reduction in PCB porewater concentration

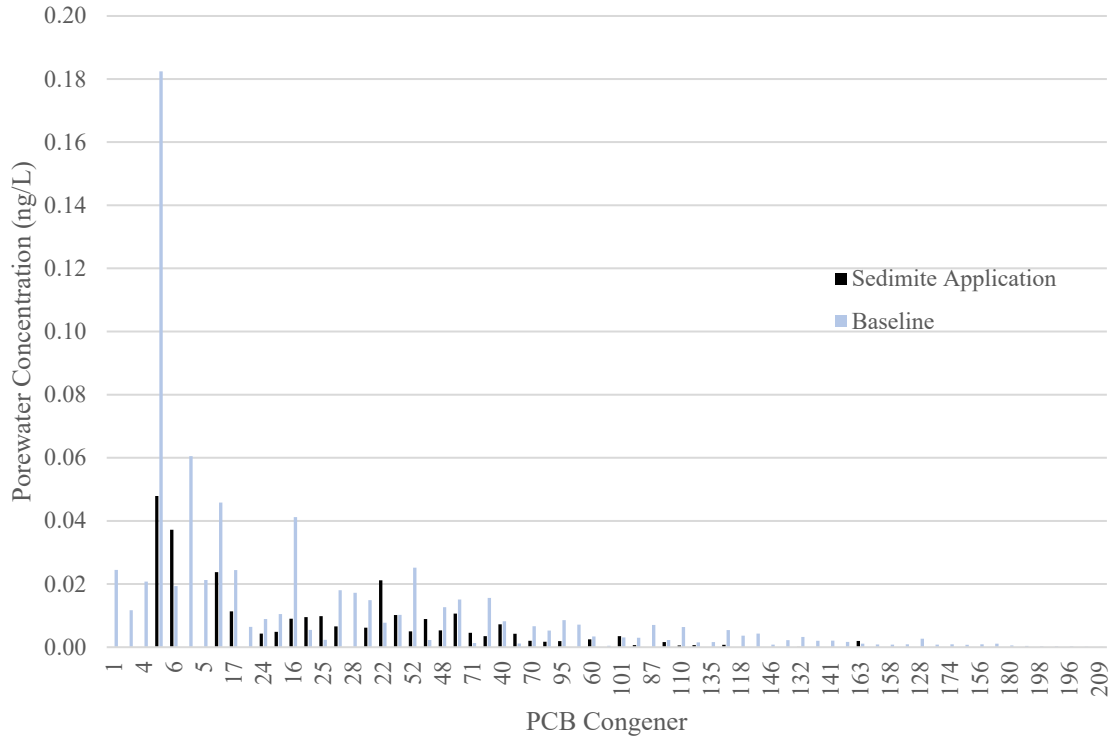

Figure 7-10 Sedimite™ application congener distribution at sample location S12 from 0-13.5 cm depth showing an 63% reduction in PCB porewater concentration

In general, both Aquagate+PAC™ and Sedimite™ AC amendments significantly reduced congener concentrations. The clearest reductions are noted in the low molecular weight congeners. The very low concentrations in the high molecular weight congeners may mean that post-AC placement concentrations may be below detection limits making it difficult to identify the actual reduction.

7.4.3 Ex-Situ Porewater Measurements

From the pre-amendment monitoring event, the in-situ porewater concentration ranged from 0.15-0.22 times lower than compared to ex-situ porewater concentrations within the surficial sediment layer and comparable 0.23-0.6 times lower in the deeper depth interval. The wide range of variability could be due to the lack of station specific

sediment samples during the baseline event. Instead, the sediment was collected throughout the sampling cell and homogenized. Undoubtedly the ex-situ higher porewater concentrations are likely related to the absence of dilution effects as a result of bioirrigation or hyporheic exchange, however, the in-situ station specific porewater measurements are more prone to sediment heterogeneity (Apell & Gschwend, 2016; Kupryianchyk et al., 2012; Jonker et al., 2018).

Comparable results were observed in the post-amendment sampling event where the in-situ porewater concentrations are approximately 0.53 times lower than the in-situ porewater concentration within the Aquagate+PAC sampling cell. This was comparable to both near shore (0.72) and offshore (0.34) sampled locations. Sedimite had greater variability with an average of approximately 0.16 times lower porewater concentration from the in-situ analysis in the near shore, but due to the replicate average increased porewater concentration at station 20 a 1.84 factor increase in the in-situ porewater concentration compared to the ex-situ analysis. These facts make the inclusion of S20 difficult to measure the remedial effectiveness of Sedimite in the east sampling plot.

The ratio of in-situ to ex-situ indicates the relatively low in-situ porewater concentration was caused by rapid exchange with the sediment layer above and the surface water (Gidley et al., 2012). The ex-situ analysis, absent of upwelling from groundwater or other hyporheic exchange processes, is used to determine the underestimation of such exposure compared to the in-situ analysis. The ratio difference found in Aquagate+PAC™ compared to Sedimite™ is similar but the overall driver of this underestimation is believed to be from the rapid exchange between the sediment and

the groundwater. The in-situ samples show some flushing of the surface layers that reflects exchange with the overlying water while ex-situ samples would represent the equilibrium pore water concentrations which would occur without flushing. The in-situ, slightly diluted, represents the actual concentration in porewater that defines flux to overlying water and water exposure in the surficial sediments.

7.4.4 SORPTION OF PCBS ONTO AC

Here we explore to what extent the PCBs binding to AC may be generalized for the two varying AC types (Sedimite and Aquagate+PAC) to the native sediments. However, bulk sediment chemistry from the baseline sampling event within the west sampling is not included due to the lack of congener specific data and partitioning coefficients for Aquagate+PAC can be found in Appendix 9.6. Figure 7-11 shows sediment-SPME and AC-SPME partitioning coefficients ($\log K_d$). These coefficients measured in sediment porewater along the east sampling section which contained Sedimite in the 2017 sampling event. Logarithmic K_d values averaged 4.79 and 6.06 for the pre- and post-Sedimite application, respectively. Logarithmic K_d values ranged from 5.11 (PCB-26) to 6.80 (PCB-93) for the tri-, tetra-, and penta-chlorinated PCBs demonstrating a strong adsorption of these compounds to Sedimite (Apell & Gschwend, 2016; Hale et al., 2010; McDonough et al., 2008).

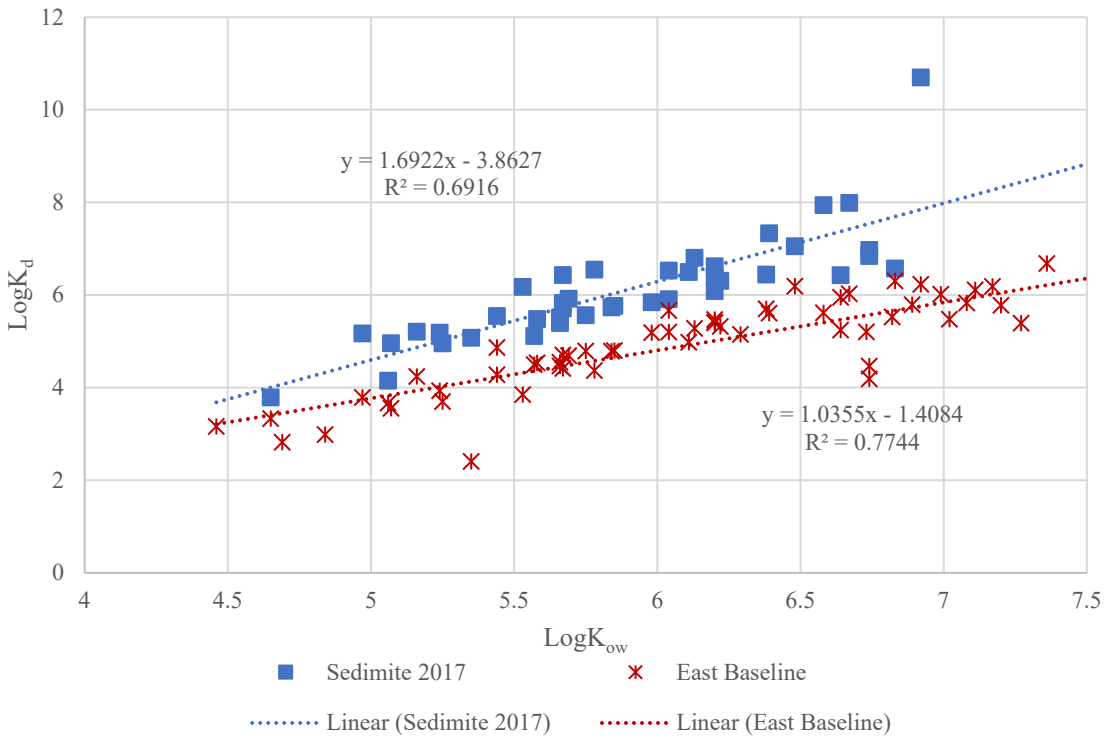

Figure 7-11 Calculated sediment partitioning coefficients ($\log K_d$) for the pre- (orange stars) and post-Sedimite (blue squares) application. Linear best fit correlations respective to each sampling event is included.

7.5. CONCLUSIONS

There is a strong agreement between the surficial sediment layer (0-13.5 cm) and the deeper interval (13.5-29 cm) with respect to overall PCB reduction for the Aquagate+PAC™ amended area likely due to particle mixing. Sediment cores retrieved 12 months after AC application indicated particle mixing by as much as 20 cm (8”) below the interface (Nelson, 2019). In addition, this could be due to active flushing by groundwater, tides, and other hyporheic exchange processes that keep the porewater relatively well mixed between the surficial sediment layer and the layer immediately below (Reible, 2014).

The ratio of in-situ to ex-situ porewater concentration in the 2017 samples are more variable than those observed in 2015 (baseline) and appear to show that the surface layer is less influenced by surface water -porewater exchange. This anomalous result is possibly the result of the influence of the activated carbon and may represent substantial variability/heterogeneity in the small ex-situ sediment samples compared to the in-situ samples. It may also be due to the kinetics of sorption onto the activated carbon that causes greater sorption in the unflushed ex-situ samples.

In summary, Aquagate+PAC™ showed a total PCB reduction in porewater concentrations of 82% and 76% in the upper and lower sediment layers, respectively, with much of the AC (80%) remaining in the top sediment layer (Figure 7-6). Sedimite™ reduced total PCB porewater concentrations by 56-58%, with 73% of the overall AC mass penetrating into the deeper sediment interval. Overall AC has shown to be a successful remedial tool for reducing PCB sediment porewater concentrations and would be an effective means of mitigating the effects of PCB contamination in sediments.

7.6. REFERENCES

Apell, J. N., & Gschwend, P. M. (2016). In situ passive sampling of sediments in the Lower Duwamish Waterway Superfund site: Replicability, comparison with ex situ measurements, and use of data. *Environmental Pollution*. https://doi.org/10.1016/j.envpol.2016.08.023

APEX. (2017). *Performance Monitoring Work Plan Lower Columbia Slough - Pacific Meats Cleanup Site Portland, Oregon*.

Beckingham, B., & Ghosh, U. (2011). Field-scale reduction of PCB bioavailability with activated carbon amendment to river sediments. *Environmental Science and Technology*, *45*(24), 10567–10574. https://doi.org/10.1021/ES202218P/SUPPL_FILE/ES202218P_SI_001.PDF

Brändli, R. C., Bergsli, A., Ghosh, U., Hartnik, T., Breedveld, G. D., & Cornelissen, G. (2009). Quantification of activated carbon contents in soils and sediments using chemothermal and wet oxidation methods. *Environmental Pollution*, *157*(12), 3465–3470. https://doi.org/10.1016/J.ENVPOL.2009.06.015

Ghosh, U., Kane Driscoll, S., Burgess, R. M., Jonker, M. T. O., Reible, D., Gobas, F., Choi, Y., Apitz, S. E., Maruya, K. A., Gala, W. R., Mortimer, M., & Beegan, C. (2014). Passive sampling methods for contaminated sediments: practical guidance for selection, calibration, and implementation. *Integrated Environmental Assessment and Management*, *10*(2), 210–223. https://doi.org/10.1002/ieam.1507

Gidley, P. T., Kwon, S., Yakirevich, A., Magar, V. S., & Ghosh, U. (2012). Advection dominated transport of polycyclic aromatic hydrocarbons in amended sediment caps. *Environmental Science and Technology*, *46*(9), 5032–5039. https://doi.org/10.1021/ES202910C/SUPPL_FILE/ES202910C_SI_001.PDF

Grossman, A., & Ghosh, U. (2009). Measurement of activated carbon and other black carbons in sediments. *Chemosphere*. https://doi.org/10.1016/j.chemosphere.2008.12.054

Gustafsson, Ö., Bucheli, T. D., Kukulska, Z., Andersson, M., Largeau, C., Rouzaud, J. N., Reddy, C. M., & Eglinton, T. I. (2001). Evaluation of a protocol for the quantification of black carbon in sediments. *Global Biogeochemical Cycles*. https://doi.org/10.1029/2000GB001380

Hale, S. E., Kwon, S., Ghosh, U., & Werner, D. (2010). POLYCHLORINATED BIPHENYL SORPTION TO ACTIVATED CARBON AND THE ATTENUATION CAUSED BY SEDIMENT. *Global NEST Journal*, *12*(3), 318–326.

Kirtay, V., Conder, J., Rosen, G., Magar, V., Grover, M., Arblaster, J., Fetters, K., & Chadwick, B. (2018). Performance of an in situ activated carbon treatment to reduce PCB availability in an active harbor. *Environmental Toxicology and Chemistry*, *37*(6), 1767–1777. https://doi.org/10.1002/ETC.4121

Kupryianchyk, D., Rakowska, M. I., Grotenhuis, J. T. C., & Koelmans, A. A. (2012). In situ sorption of hydrophobic organic compounds to sediment amended with activated carbon. *Environmental Pollution*, *161*, 23–29. https://doi.org/10.1016/J.ENVPOL.2011.09.043

Luthy, R. G., Aiken, G. R., Brusseau, M. L., Cunningham, S. D., Gschwend, P. M., Pignatello, J. J., Reinhard, M., Traina, S. J., Weber, W. J., & Westall, J. C. (1997). Sequestration of hydrophobic organic contaminants by geosorbents. In *Environmental Science and Technology*. https://doi.org/10.1021/es970512m

McDonough, K. M., Fairey, J. L., & Lowry, G. V. (2008). Adsorption of polychlorinated biphenyls to activated carbon: Equilibrium isotherms and a preliminary assessment of the effect of dissolved organic matter and biofilm loadings. *Water Research*, *42*(3), 575–584. https://doi.org/10.1016/J.WATRES.2007.07.053

Murphy, P., Marquette, A., Reible, D., & Lowry, G. V. (2006). Predicting the Performance of Activated Carbon-, Coke-, and Soil-Amended Thin Layer Sediment Caps. *Journal of Environmental Engineering*. https://doi.org/10.1061/(ASCE)0733-9372(2006)132:7(787)

Nelson, H. (2019). Pacific Meat Sediment Remedy Leads to Evaluation of Columbia Slough Cleanup by Presumptive Remedy. *International Conference on the Remediation and Management of Contaminated Sediments*.

O Jonker, M. T., van der Heijden, S. A., Adelman, D., Apell, J. N., Burgess, R. M., Choi, Y., Fernandez, L. A., Flavetta, G. M., Ghosh, U., Gschwend, P. M., Hale, S. E., Jalalizadeh, M., Khairy, M., Lampi, M. A., Lao, W., Lohmann, R., Lydy, M. J., Maruya, K. A., Nutile, S. A., … Wu, Y. (2018). Advancing the Use of Passive Sampling in Risk Assessment and Management of Sediments Contaminated with Hydrophobic Organic Chemicals: Results of an International Ex Situ Passive Sampling Interlaboratory Comparison. *Cite This: Environ. Sci. Technol*, *52*, 3582. https://doi.org/10.1021/acs.est.7b05752

Patmont, C. R., Ghosh, U., LaRosa, P., Menzie, C. A., Luthy, R. G., Greenberg, M. S., Cornelissen, G., Eek, E., Collins, J., Hull, J., Hjartland, T., Glaza, E., Bleiler, J., & Quadrini, J. (2015). In situ sediment treatment using activated carbon: A demonstrated sediment cleanup technology. *Integrated Environmental Assessment and Management*, *11*(2), 195–207. https://doi.org/10.1002/IEAM.1589

Rakowska, M. I., Kupryianchyk, D., Harmsen, J., Grotenhuis, T., & Koelmans, A. A. (2012). In situ remediation of contaminated sediments using carbonaceous materials. In *Environmental Toxicology and Chemistry*. https://doi.org/10.1002/etc.1763

Reible, D. D. (2014). Contaminant Processes in Sediments. In *Processes, Assessment and Remediation of Contaminated Sediments*. https://doi.org/10.1007/978-1-4614-6726-7

Reible, D., Lampert, D., Constant, D., Mutch, R. D., & Zhu, Y. (2006). Active capping demonstration in the Anacostia river, Washington, D.C. *Remediation*.

https://doi.org/10.1002/rem.20111

Sanders, J. P., Andrade, N. A., Menzie, C. A., Amos, C. B., Gilmour, C. C., Henry, E. A., Brown, S. S., & Ghosh, U. (2018). Persistent reductions in the bioavailability of PCBs at a tidally inundated Phragmites australis marsh amended with activated carbon. *Environmental Toxicology and Chemistry*, *37*(9), 2496–2505. https://doi.org/10.1002/ETC.4186

Shen, X., & Reible, D. (2019). An analytical model for the fate and transport of performance reference compounds and target compounds around cylindrical passive samplers. *Chemosphere*. https://doi.org/10.1016/j.chemosphere.2019.05.198

Sutter, J. (2012). *Land Quality Division Environmental Cleanup Program Northwest Region 2020 SW 4 th Ave Suite #400*. 1–3. www.oregon.gov/DEQ

USEPA. (2010). *Method 1668C: Chlorinated Biphenyl Congeners in Water, Soil, Sediment, Biosolids, and Tissue by HRGC/HRMS*. www.epa.gov/waterscience/methods.

Yan, S., Rakowska, M., Shen, X., Himmer, T., Irvine, C., Zajac-Fay, R., Eby, J., Janda, D., Ohannessian, S., & Reible, D. D. (2020). Bioavailability assessment in activated carbon treated coastal sediment with in situ and ex situ porewater measurements. *Water Research*. https://doi.org/10.1016/j.watres.2020.116259

CHAPTER 8

SUMMARY AND CONCLUSIONS

8.1. RESEARCH OBJECTIVES

The research described herein this dissertation demonstrated the ability of passive sampling techniques to obtain truly dissolved hydrophobic organic compounds in aquatic environments and expanded applications of passive sampling methods to evaluate long-term performance of remedial efforts and the management of these HOC contaminated sediments.

This dissertation had the following:

i. the development of a mathematical modeling approach to evaluate the effect of non-equilibrium loading of performance reference compounds on the estimated equilibrium of target compounds in passive samplers
ii. the novel application of a high density of LDPE passive samplers placed at the sediment-water interface as a mapping tool to identify likely source areas at historical disposal locations for contaminated sediments
iii. the application SPME PDMS sampling devices to estimate groundwater upwelling from the release of performance reference compounds to infer long-term remedial effectiveness at a tidally influenced shoreline
iv. a discussion of the results from the field study within the West Branch of the Grand Calumet River (Hammond, Indiana) with a focus on the statistical significance of long-term contaminant profile changes from the sampled years and modelled remedy performance of the organophilic clay cap liner

v. the application of in-situ passive samplers for evaluating a pilot test on the use of varying activated carbon amendments for long-term remedy performance

The objectives were investigated through bench scale experiments performed in the laboratory at Texas Tech University and with field demonstrations at contaminated sediment sites in Bradford Island (Hood River, OR), Puget Sound Superfund Site (Seattle, WA), The West Branch of the Grand Calumet River (Hammond, IN), and the Lower Columbia Slough (Portland, OR).

8.2. RESEARCH CONCLUSIONS

The use of performance reference compounds to measure the extent of equilibrium for target compounds relies on the polymer to be uniformly loaded with PRCs prior to deployment and was explored in with the mathematical model from Carslaw and Jaeger (1959). Uniformity is expected when the external mass transfer is the controlling mechanism, which is typically the case for the loading thin layers of SPME, LDPE, and POM polymeric passive samplers. Inaccurate and variable estimates of the fractional approach to steady state of target compound uptake can still occur if the PRC is loaded nonuniformly (either on portions of a single sheet or across multiple sheets due to variations in external mass transfer coefficients) and samples evaluated for initial PRC concentration are not representative. This is the most likely cause of poor or highly variable estimates of extent of equilibration in typical polymers and conditions.

It became evident that the eastern tip of Bradford Island would likely be the area of concern due to the elevated PCB concentrations relative to the other samples locations.

This study illustrates the versatile application of passive samplers not only as a porewater sampling tool, but as a preliminary screening tool to reduce areas of concern when remedial investigations are underway.

The primary goal of the PDMS sampling events at the Puget Sound Superfund Site and the West Branch of the Grand Calumet River (WBGCR) were to evaluate the performance of the cap based on porewater concentration depth profiles and to evaluate whether contaminated groundwaters are negatively impacting surficial cap layers. The release of the d-PAH performance reference compounds provided a means of estimating net upwelling velocities in the cap, and these were used to predict long-term migration of contaminants of concern in the cap layer at Puget Sound. This is a novel use of PRCs that may be applicable at other locations and allowed estimation of the migration of currently observed porewater concentrations through the cap over time using CapSim. The WBGCR utilized statistical modeling, the Friedman Test, to rank the performance of the cap over the sampling years providing evidence of movement above the organophilic cap layer. This resulting in misleading depth profiles that indicated the presence of newly deposited sediments that shifted the porewater depth profile down ~20 cm over the 7 years.

The AC amendments were highly successful in reducing sediment porewater concentrations of total PCBs in the lower Columbia Slough and would likely be an effective means of mitigating the effects of PCB contamination of the sediments. The Aquagate+PAC™ has the advantage of a higher density making it easy to place through deposition and likely more easily retained at the surface during high flow events while

the Sedimite™ allows more AC to be placed per unit mass of amendment and appears to be worked more rapidly deeper into the sediments, aiding its long-term retention.

APPENDIX

9.1. LOADING AND RELEASE OF PRCS DERIVATION

Dimensions of the polymer sheet: $h\ x\ w\ x\ 2L = V_p$, where $h, w \gg L$. Volume of water:V_w

i. Loading Process

Mass balance for transported species in the polymer is

$$\frac{\partial C_p}{\partial t} = D_p \frac{\partial^2 C_p}{\partial x^2} \qquad t > 0, -L < x < L$$

with initial and boundary conditions

$$\begin{aligned} C_p &= 0 && t = 0 \\ \frac{\partial C_p}{\partial x} &= 0 && x = 0 \\ \mp D_p \frac{\partial C_p}{\partial x} &= k_l \left(\frac{C_p}{K_{pw}} - C_w(t) \right) && x = \pm L \end{aligned}$$

Where D_p is the diffusivity in water, determined from Rusina et al. (2010), K_{pw} is the polymer-water partitioning coefficient, k_l is the compound specific mass transfer coefficient during the loading phase, denoted by the l, and C_w is the PRC concentration in the water, which is expected to be zero at $t = 0$.

Mass balance for the transported species in the loading solution is

$$V_w \frac{dC_w}{dt} = 2hwk_l \left(\frac{C_p(L,t)}{K_{pw}} - C_w(t) \right)$$

ii. Extreme case: internally controlled mass-transfer ($Bi \gg 1$)

In this case, the boundary and initial conditions are

$$\begin{aligned} C_p &= 0 && t = 0 \\ \frac{\partial C_p}{\partial x} &= 0 && x = 0 \\ -2D_p hw \frac{\partial C_p}{\partial x} &= \frac{V_w}{K_{pw}} \frac{\partial C_p}{\partial t} && x = L \end{aligned}$$

The solution to the problem is provided by Crank (1979):

$$\frac{C_p(x,t)}{C_{p,\infty}} = 1 + \sum_{n=1}^{\infty} \frac{2(1+\alpha)\exp\left(-D_p q_n^2 t/L^2\right)}{1+\alpha+\alpha^2 q_n^2} \frac{\cos(q_n x/L)}{\cos q_n}$$

where $C_{p,\infty}$ is the equilibrium concentration of solute in the polymer:

$$C_{p,\infty} = \frac{V_w C_{w,0} K_{pw}}{V_w + V_p K_{pw}}$$

and

$$\alpha = \frac{V_w}{K_{pw} V_p}$$

The eigenvalues are the positive non-zero roots of

$$\tan q_n = -\alpha q_n$$

The fraction of mass in the polymer respect to the equilibrium uptake is given by

$$\frac{M_p(t)}{M_{p,\infty}} = 1 - \sum_{n=1}^{\infty} \frac{2\alpha(1+\alpha)}{1+\alpha+\alpha^2 q_n^2} \exp\left(-D_p q_n^2 t/L^2\right)$$

Where $M_p(t)$ is the mass of solute in the polymer at any given time during the loading process and $M_{p,\infty} = V_p C_{p,\infty}$.

The characteristic time is given by

$$\tau = \frac{L^2}{D_p}$$

Thus:

$$f_{ss} = 1 - \sum_{n=1}^{\infty} \frac{2\alpha(1+\alpha)}{1+\alpha+\alpha^2 q_n^2} \exp(-t/\tau)$$

iii. Extreme case: externally controlled mass-transfer ($Bi \ll 1$)

In this case, transport inside the polymer is fast enough that concentration in the polymer is uniform. The mass-balance for transported species in both phases is given by

$$V_P \frac{dC_P}{dt} = 2hwk_l \left(C_w - \frac{C_p}{K_{pw}} \right)$$

$$V_w \frac{dC_w}{dt} = 2hwk_l \left(\frac{C_p}{K_{pw}} - C_w \right)$$

The mass balance can be transformed into a single equation

$$V_P \frac{dC_P}{dt} = 2hwk_l \left(\frac{V_w C_{w,0} - V_p C_p}{V_w} - \frac{C_p}{K_{pw}} \right)$$

Where $C_{w,0}$ is the concentration in the loading solution at $t = 0$.

The solution is given by

$$C_p(t) = \frac{V_w C_{w,0} K_{pw}}{V_w + V_p K_{pw}} \left(1 - \exp\left\{ -\frac{2hwk_l}{V_p} \left(\frac{V_p}{V_w} + \frac{1}{K_{pw}} \right) t \right\} \right)$$

The characteristic time is

$$\tau = \left[\frac{2hwk_l}{V_p} \left(\frac{V_p}{V_w} + \frac{1}{K_{pw}} \right) \right]^{-1}$$

That is simplified to

$$\tau = \frac{LK_{pw}\alpha}{k_l(1+\alpha)}$$

Where

$$\alpha = \frac{V_w}{K_{pw}V_p}$$

Thus

$$f_{ss} = 1 - \exp\left\{-\frac{t}{\tau}\right\}$$

iv. Release Process

Mass balance for transported species in the polymer is

$$\frac{\partial C_p}{\partial t} = D_p \frac{\partial^2 C_p}{\partial x^2} \qquad t > 0, -L < x < L,$$

with initial and boundary conditions

$$\begin{aligned} C_p &= f(x) && t = 0 \\ \frac{\partial C_p}{\partial x} &= 0 && x = 0 \\ -D_p \frac{\partial C_p}{\partial x} &= k_r \frac{C_p}{K_{pw}} && x = L \end{aligned}$$

Note that $f(x)$ is the profile of concentration in the polymer after loading.

The solution to the problem is analytical Carslaw and Jaeger (1959):

$$C_p = \sum_{n=1}^{\infty} e^{-D_p \alpha_n^2 t} \frac{c_n \cos\alpha_n x + d_n \sin\alpha_n x}{(\alpha_n^2 + h^2)L + h} \int_{-L}^{L} (c_n \cos\alpha_n \xi + d_n \sin\alpha_n \xi) f(\xi) d\xi$$

where

$$h = \frac{k_r}{K_{pw}D_p}$$

$$c_n = h \sin \alpha_n L + \alpha_n \cos \alpha_n L$$

$$d_n = h \cos \alpha_n L - \alpha_n \sin \alpha_n L$$

and the eigenvalues are the positive roots of

$$\tan 2\,\alpha_n L = \frac{2\alpha_n h}{\alpha_n^2 - h^2}$$

v. Extreme case: internally controlled process ($Bi \gg 1$)

Mass balance for transported species in the polymer is

$$\frac{\partial C_p}{\partial t} = D_p \frac{\partial^2 C_p}{\partial x^2} \qquad t > 0, -L < x < L,$$

with initial and boundary conditions

$$\begin{aligned} C_p &= f(x) \quad t = 0 \\ \frac{\partial C_p}{\partial x} &= 0 \quad x = 0 \\ C_p &= 0 \quad x = L \end{aligned}$$

The solution to the problem is presented by Carslaw and Jaeger (1959):

$$C_p = \frac{2}{L} \sum_{n=0}^{\infty} \exp\left(\frac{-D_p (2n+1)^2 \pi^2 t}{4L^2}\right) \cos \frac{(2n+1)\pi x}{2L} \int_0^L f(\xi) \cos \frac{(2n+1)\pi \xi}{2L} d\xi$$

The characteristic time is given by

$$\tau = \frac{L^2}{D_p}$$

vi. Extreme case: externally controlled process ($Bi \ll 1$)

In this case, the mass balance for the polymer is given by

$$V_P \frac{dC_P}{dt} = -2hwk_r \frac{C_p}{K_{pw}}$$

The solution is given by

$$C_p = C_{p0} \exp\left\{-\frac{2hwk_r}{V_p K_{pw}} t\right\}$$

Characteristic time is given by

$$\tau = \frac{LK_{pw}}{k_r}$$

Thus

$$f_{ss} = 1 - \exp\left\{-\frac{t}{\tau}\right\}$$

9.2. MATLAB CODE FOR PARTIAL LOADING AND RELEASE OF PRCS

```
clc

close all
clear variables

%%%%%%%%%%%%%%%%%%%%%%%%%%%%%%%%%%%%%%%%%%%%%%%%%%%%%%%%%%%%%%%%%%%%%%%%%%%%%%%
%Input parameters
Cw0 = 1;                          %Initial concentration in H20:MeOH (ng/mL)
Kpw = 10^6.27;                        %Partition, Kpw = Cp/Cw(dimensionless)
W = 25.4;                          %Total thickness of sheet (um)
Vp = 10*10*W*1e-4;                 %Total volume of polymer (mL)
Vw = 1000;                         %Total volume of water (mL)
Dp = 10^-13.5;                     %Diffusion coefficient (m^2/s)
t_l = 5;                           %Loading time(day)
t_r = 10;                           %Release time (day)


% Mass transfer coefficients (in terms of gradients in liquid phase)
k_load_liq  = .94;                    %Mass-transfer coefficient for the loading
process (cm/day)
```

```
k_rel_liq = 100;                    %Mass-transfer coefficient for the release
process (cm/day)

n  = 200;                          %Intended terms for eigenvalues
tt_l = 30;                          %Maximum time in fss plot for loading
tt_r = 30;                          %Maximum time in fss plot for release
Resol = 10;                         %Resolution (time points) for fss plot of
loading
                                   %The higher the number of Resol, the higher
                                   %the simulation time for loading (recommended
20 to
                                   %100)
%%%%%%%%%%%%%%%%%%%%%%%%%%%%%%%%%%%%%%%%%%%%%%%%%%%%%%%%%%%%%%%%%%%%%%%%%%%%%%%
% Parameters

L = W*1e-4/2;                  %Characteristic length (half of the sheet) (cm)
a = Vw/Vp/Kpw;                 %Ratio of capacities between phases
fw = Vw/(Vw+Vp*Kpw);           %Fraction of total mass in water at equilibrium
M_inf = Vw*Cw0*(1-fw);         %Mass in polymer at equilibrium (ng)
C_inf = M_inf/Vp;              %Concentration in polymer at equilibrium (ng/mL)
Dp = Dp*3600*24*100^2;         %Diffusion coefficient (cm^2/d)
M  = Cw0*Vw;                   %Total mass(ng)
Bi_load = k_load_liq*L/Dp/Kpw;       %Biot number for loading
Bi_rel = k_rel_liq*L/Dp/Kpw;         %Biot number for release

tim_l = linspace(tt_l*1e-4,tt_l,Resol);
tim_r = linspace(0,tt_r,1000);

%% Loading Process k < \infty, Numerical Solution
numx = 1000;                   % number of grids
numt = 1000;                   % number of time steps
```

```
tic
delx = L / numx;              % size of grids
delt = t_l / numt;            % size of time steps

Cp  = zeros(numx+2, numt+1);     % polymer concentration
Cw  = zeros(1,      numt+1);     % water concentration
Mp  = zeros(1,      numt+1);     % polymer mass
x   = linspace(0,L, numx+1);      % polymer concentration
t   = linspace(0,t_l,numt+1);    % polymer concentration

Cp(numx+2, 1) = M / Vw;

A = zeros(numx+2, numx+2);
B = zeros(numx+2, numx+2);

% Governing equations
A(2       :numx+3:(numx-1)*(numx+2)) = -Dp /delx^2;
A(numx+4  :numx+3:(numx)  *(numx+2)) = 2*Dp /delx^2 + 1/delt;
A(numx*2+6:numx+3:(numx+1)*(numx+2)) = -Dp /delx^2;

B(numx+4  :numx+3:(numx)  *(numx+2)) = 1/delt;

% Internal BC
A(1, 1) = -1;
A(1, 2) = 1;

% polymer-water BC
A(numx+1, numx) = Dp /delx;
A(numx+1, numx+1) = -Dp /delx- k_load_liq / Kpw;
A(numx+1, numx+2) = + k_load_liq;

% Conservation in water phase
```

```
A(numx+2, numx+1) = -k_load_liq*Vp/L/Kpw;

A(numx+2, numx+2) = Vw/delt+k_load_liq*Vp/L;

B(numx+2, numx+2) = Vw/delt;


for i = 1: numt

    Cp(:,i+1) = A\(B * Cp(:,i));

end


Cp_l_num = transpose(Cp(1:numx+1,numt+1));

Cp_av_l = trapz(x,Cp_l_num)/L;

Mp_l = Cp_av_l*Vp;


ti_load = toc;

figure(1)

plot([fliplr(-x),x]*1e4, [fliplr(Cp_l_num),Cp_l_num])

xlabel('x ($$\mu$$m)','Interpreter','latex','FontSize',10)

ylabel('$$C_{p}$$ (ng/mL)','Interpreter','latex','FontSize',10)

set(gca,'TickLabelInterpreter','latex','FontSize',10)

title({['Profile of Concentration After Loading for ',num2str(t_l),' day']},...

    'Interpreter','latex','FontSize',10)

xlim([-Inf,Inf])

box on

hold on


figure(2)

hold on

plot([fliplr(-x),x]*1e4, [fliplr(Cp_l_num),Cp_l_num])

xlabel('x ($$\mu$$m)','Interpreter','latex','FontSize',10)

ylabel('$$C_{p}$$ (ng/mL)','Interpreter','latex','FontSize',10)

set(gca,'TickLabelInterpreter','latex','FontSize',10)

title({'Profiles of Concentration in Polymer'},...

    'Interpreter','latex','FontSize',10)
```

```
xlim([-Inf,Inf])
box on


%% Loading, Crank Solution (Bi = \infty)
% Find eigenvalues with fixed-point method
f1 = @(qn) -a*qn;
qn2 = @(f) atan(f);
qn = NaN*ones(1,n);
for i = 1:n
    xfp1_UJ = 0;
    xfp2_GR = i*pi;
    flag = 0;
    while abs(xfp1_UJ-xfp2_GR) > 1e-12
        xfp1_UJ = xfp2_GR;
        xfp2_GR = qn2(f1(xfp1_UJ))+i*pi;
        flag = flag+1;
        if flag == 50
            error('Too many iterations to find eigenvalues')
        end
    end
    qn(i) = xfp2_GR;
end
n = length(qn);          %Terms in expansion

%Solution of equation 4.45 of Crank starts here
f = 1;
for j = 1:n
    f = f+2*(1+a)*exp(-
Dp*qn(j)^2*t_l/L^2)/(1+a+a^2*qn(j)^2)*cos(qn(j)*x/L)/cos(qn(j));
end
```

```
Cp_Crank = C_inf*f;

%Total mass in polymer
f = 1;
for i = 1:n
    f = f-2*a*(1+a)/(1+a+a^2*qn(i)^2)*exp(-
Dp*qn(i)^2*linspace(0,tt_l,1e3)/L^2);
end
Mtt_l_Crank = M_inf*f;

figure(1)
plot([fliplr(-x),x]*1e4,[fliplr(Cp_Crank),Cp_Crank])
plot([-L,L]*1e4,[C_inf,C_inf],'--k')
plot(0,0,':k')

legend({['Bi = ',num2str(Bi_load,3)],...
    'Bi $$\rightarrow \infty$$','Equilibrium $$(t=\infty)$$'},...
    'Interpreter','latex','FontSize',10,'Location','Best')

%% Release Process (Numerical Integration of I.C. with eigenfunction)
tic

%Calculate eigenvalues
h = k_rel_liq/Dp/Kpw;

f1 = @(an) h/an;
an2 = @(f2) atan(f2)/L;
f2 = @(an) tan(an*L);
an_f1 = NaN*ones(1,round(n/2));

for i = 1:round(n/2)
    xfp1_UJ = 0;
```

```
    xfp2_GR = (i-.9999999)*pi/L;
    flag = 0;
    while abs(xfp1_UJ-xfp2_GR) > 1e-12/L/h
        %disp(abs(xfp1-xfp2))
        %plot(xfp1,f1(xfp1),'*r')
        xfp1_UJ = xfp2_GR;
        xfp2_GR = an2(f1(xfp1_UJ))+ pi*(i-1)/L;
        %plot(xfp2,f2(xfp2),'*r')
        flag = flag+1;
        if flag == 1e11
            error('Too many iterations to find eigenvalues, f1')
        end
        %pause
    end
    if flag == 0
        error('Method could not find eigenvalue')
    end
    %disp(flag)
    %plot(xfp2,f1(xfp2),'*r')
    an_f1(i) = xfp2_GR;
end

f3 = @(an) -h/an;
an4 = @(f2) acot(f2)/L;
f4 = @(an) cot(an*L);
an_f2 = NaN*ones(1,round(n/2));
for i = 1:round(n/2)
    xfp1_UJ = 0;
    xfp2_GR = (i-.4999999)*pi/L;
    flag = 0;
    while abs(xfp1_UJ-xfp2_GR) > 1e-12/L/h
```

```
        %disp(abs(xfp1-xfp2))
        %plot(xfp1,f3(xfp1),'*r')
        xfp1_UJ = xfp2_GR;
        xfp2_GR = an4(f3(xfp1_UJ))+ pi*i/L;
        %plot(xfp2,f4(xfp2),'*r')
        flag = flag+1;
        if flag == 1e11
            error('Too many iteractions to find eigenvalues, f2')
        end
        %pause
    end
    if flag == 0
        error('Method could not find eigenvalue')
    end
    %disp(flag)
    %plot(xfp2,f3(xfp2),'*r')
    an_f2(i) = xfp2_GR;
end

an = [an_f1,an_f2];
an = sort(an);
cn = h*sin(an*L)+an.*cos(an*L);
dn = h*cos(an*L)-an.*sin(an*L);

Cp_r = 0;
for i = 1:n
   Cp_r = Cp_r + exp(-
Dp*an(i)^2*t_r)*(cn(i)*cos(an(i)*x)+dn(i)*sin(an(i)*x))/...
       ((an(i)^2+h^2)*L+h)*trapz([fliplr(-x),x],...
       [fliplr(Cp_l_num),Cp_l_num].*(cn(i)*cos(an(i)*[fliplr(-x),x])+...
       dn(i)*sin(an(i)*[fliplr(-x),x])));
```

```
end

Cp_av_r = trapz(x,Cp_r)/L;
Mp_r = Cp_av_r*Vp;
ti_rel = toc;

figure(2)
plot([fliplr(-x),x]*1e4,[fliplr(Cp_r),Cp_r])
plot([fliplr(-x),x]*1e4,0,'k')
legend({['Loading after ',num2str(t_l),' d (Biot =
',num2str(Bi_load,3),')'],...
    ['Release after ',num2str(t_r),' d (Biot = ',num2str(Bi_rel,3),')']},...
    'Interpreter','latex','FontSize',10,'Location','best')

%% Kinetics of loading process
choice = menu(['Do you want to simulate kinetics of loading? It may take up to
',...
    num2str(round(1.1*ti_load/60*length(tim_l),1)),' minutes'],'Yes','No');
if choice == 1
    tic
    Mtt_l = NaN*ones(size(tim_l));
    for i=1:length(tim_l)
        delt = tim_l(i) / numt;           % size of time steps
        Cp(numx+2, 1) = M / Vw;

        A = zeros(numx+2, numx+2);
        B = zeros(numx+2, numx+2);

        % Governing equations
        A(2       :numx+3:(numx-1)*(numx+2)) = -Dp /delx^2;
        A(numx+4  :numx+3:(numx)  *(numx+2)) = 2*Dp /delx^2 + 1/delt;
        A(numx*2+6:numx+3:(numx+1)*(numx+2)) = -Dp /delx^2;
```

```
    B(numx+4  :numx+3:(numx)  *(numx+2)) = 1/delt;

    % Internal BC
    A(1, 1) = -1;
    A(1, 2) = 1;

    % polymer-water BC
    A(numx+1, numx) = Dp /delx;
    A(numx+1, numx+1) = -Dp /delx- k_load_liq / Kpw;
    A(numx+1, numx+2) = + k_load_liq;

    % Conservation in water phase
    A(numx+2, numx+1) = -k_load_liq*Vp/L/Kpw;
    A(numx+2, numx+2) = Vw/delt+k_load_liq*Vp/L;
    B(numx+2, numx+2) = Vw/delt;

    for j = 1: numt
        Cp(:,j+1) = A\(B * Cp(:,j));
    end

    Cp_l_num_mul = transpose(Cp(1:numx+1,numt+1));
    Cp_av_l = trapz(x,Cp_l_num_mul)/L;
    Mtt_l(i) = Cp_av_l*Vp;
end
toc

% Loading with Biot = 0
%T_Bi0 = 1/(k_load_liq/L*(Vp/Vw+1/Kpw));
T_Bi0 = L*Kpw*a/k_load_liq/(1+a);
fss_Bi0_load = 1-exp(-linspace(0,tt_l,1e3)/T_Bi0);
```

```
    fss_real_load = Mtt_l/M_inf;
    fss_BiInf_load = Mtt_l_Crank/M_inf;



    figure(3)
    hold on
    plot(tim_l,fss_real_load)
    plot(linspace(0,tt_l,1e3),fss_BiInf_load)
    plot(linspace(0,tt_l,1e3),fss_Bi0_load);
    title('Loading Kinetics','Interpreter','latex')
    plot(t_l,Mp_l/M_inf,'*r')
    xlabel('$$t$$ (day)','Interpreter','latex','FontSize',10)

ylabel('$$f^{\ell}_{ss}=M^{\ell}_p(t)/M_{\infty}$$','Interpreter','latex','Font
Size',10)
    set(gca,'TickLabelInterpreter','latex','FontSize',10)
    ylim([0,1.05])
    grid on
    grid minor
    box on
    legend({['Loading Biot = ',num2str(Bi_load,3)],...
        'Loading Biot $$\rightarrow \infty$$'...
        ['Biot $$\rightarrow$$ 0 ($$k=$$ ',num2str(round(k_load_liq,2)),'
cm/d)']...
        },'Interpreter','latex','FontSize',10,'Location','best')
else
    fss_real_load = NaN*ones(size(tim_l));
    fss_BiInf_load = fss_real_load;
end

%% Kinetics of release
```

```
Mtt_r_id = NaN*ones(size(tim_r));
Mtt_r_real = NaN*ones(size(tim_r));

for j = 1:length(tim_r)
    %Ideal (i.e., target fss)
    Cp_r = 0;
    for i = 1:n
        Cp_r = Cp_r + exp(-
Dp*an(i)^2*tim_r(j))*(cn(i)*cos(an(i)*x)+dn(i)*sin(an(i)*x))/...
            ((an(i)^2+h^2)*L+h)*trapz([fliplr(-x),x],...
            Cp_av_l*ones(size([fliplr(-x),x])).*(cn(i)*cos(an(i)*[fliplr(-
x),x])+...
            dn(i)*sin(an(i)*[fliplr(-x),x])));
    end
    Mtt_r_id(j) = trapz(x,Cp_r)/L*Vp;

    %Real
    Cp_r = 0;
    for i = 1:n
        Cp_r = Cp_r + exp(-
Dp*an(i)^2*tim_r(j))*(cn(i)*cos(an(i)*x)+dn(i)*sin(an(i)*x))/...
            ((an(i)^2+h^2)*L+h)*trapz([fliplr(-x),x],...
            [fliplr(Cp_l_num),Cp_l_num].*(cn(i)*cos(an(i)*[fliplr(-x),x])+...
            dn(i)*sin(an(i)*[fliplr(-x),x])));
    end
    Mtt_r_real(j) = trapz(x,Cp_r)/L*Vp;
end
fss_id_rel = 1-Mtt_r_id/Mtt_r_id(1);            %i.e, fss of target
fss_real_rel = 1-Mtt_r_real/Mtt_r_real(1);

tau_rel_Bi0 = L*Kpw/k_rel_liq;
```

```
fss_release_Bi0 = 1-exp(-tim_r/tau_rel_Bi0);


figure(4)
hold on
plot(tim_r,fss_real_rel)
plot(tim_r,fss_id_rel)
plot(tim_r,fss_release_Bi0)
title(['Release Kinetics, Biot = ',num2str(Bi_rel,3)],'Interpreter','latex')
plot(t_r,1-Mp_r/Mp_l,'*r')
xlabel('$$t$$ (day)','Interpreter','latex','FontSize',10)
ylabel('$$f_{ss}^r=1-
M_{p}^{r}\left(t\right)/M_{p}^{\ell}\left(f_{ss}^{\ell},k\right)$$',...
    'Interpreter','latex','FontSize',10)
ylim([0,1.05])
set(gca,'TickLabelInterpreter','latex','FontSize',10)
grid on
grid minor
box on
legend({'$$f_{ss}$$ of PRC',...
    '$$f_{ss}$$ of Target','$$f_{ss}$$ if release Bi$$\rightarrow 0$$'},...
    'Interpreter','latex','FontSize',10,'location','SouthEast')


prompt = 'Enter Upper Limit for Y-axis of Figures 1 and 2';
dlgtitle = 'Y-axis';
dims = [1 35];
definput = {'300'};
yax2 = inputdlg(prompt,dlgtitle,dims,definput);
figure(1)
ylim([0,str2double(cell2mat(yax2))])
figure(2)
ylim([0,str2double(cell2mat(yax2))])
```

```
ExcelVar = NaN*ones(1000,8);
ExcelVar(1:Resol,1) = tim_l;
ExcelVar(1:Resol,2) = fss_real_load;
if choice == 1
    ExcelVar(:,3) = linspace(0,tt_l,1e3);
    ExcelVar(:,4) = fss_BiInf_load;
else
    ExcelVar(1:Resol,3) = linspace(0,tt_l,Resol);
    ExcelVar(1:Resol,4) = fss_BiInf_load;
end
ExcelVar(:,5) = tim_r;
ExcelVar(:,6) = fss_real_rel;
ExcelVar(:,7) = fss_id_rel;
ExcelVar(1,8) = Cw0;        %Initial concentration in H20:MeOH (ng/mL)
ExcelVar(2,8) = Kpw;        %Partition, Kpw = Cp/Cw(dimensionless)
ExcelVar(3,8) = W;          %Total thickness of sheet (um)
ExcelVar(4,8) = Vp;         %Total volume of polymer (mL)
ExcelVar(5,8) = Vw;         %Total volume of water (mL)
ExcelVar(6,8) = Dp;         %Diffusion coefficient (cm^2/d)
ExcelVar(7,8) = k_load_liq; %Mass-transfer coefficient for the loading process
(cm/day)
ExcelVar(8,8) = k_rel_liq;  %Mass-transfer coefficient for the release process
(cm/day)
ExcelVar(9,8) = Bi_load;    %Biot number for loading
ExcelVar(10,8) = Bi_rel;    %%Biot number for release
ExcelVar(11,8) = t_l;
ExcelVar(12,8) = Mp_l/M_inf;
ExcelVar(13,8) = t_r;
ExcelVar(14,8) = 1-Mp_r/Mp_l;
```

9.3. RANKED SUMMARY OF ANALYSES OF THE 35 SAMPLES SUBMITTED TO EUROFINS TEST AMERICA FOR FULL PCB CONGENER ANALYSIS.

USACE #	Sample #	Latitude	Longitude	209 Congeners (ng/L)	46 Congeners (TTU) ng/L	46 congeners+N estimates (TTU) ng/L	209 Congeners in polymer ug/kg	TTU Cpolymer ug/kg	TTU Cpolymer + N estimate ug/kg
Number of top 11 locations ranked in top 11 by analysis				**11**	**7**	**7**	**8**	**5**	**4**
119	18-7	45.64256386	-121.93496	0.822	0.207	0.271	414.3	58.0	111.2
117	18-5	45.64264883	-121.9350406	0.572	0.154	0.208	160.4	45.2	78.9
207	21-4	45.64307147	-121.9366328	0.262	0.067	0.092	25.8	3.4	6.9
57	4-2	45.64272431	-121.9374914	0.243	0.055	0.090	61.7	11.5	34.6
109	6-2	45.64276167	-121.9352036	0.193	0.060	0.070	125.4	34.0	39.7
60	9-3	45.64282189	-121.9372613	0.193	0.143	0.202	51.7	17.6	28.5
86	14-3	45.64298889	-121.9357723	0.188	0.090	0.120	28.0	37.7	40.9
42	1-8	45.64273222	-121.9390585	0.168	0.080	0.090	57.3	35.6	41.4
88	3-6	45.64273019	-121.9379434	0.167	0.100	0.164	80.9	11.9	23.1
79	5-3	45.64281278	-121.936292	0.128	0.085	0.129	76.8	25.1	55.9
88	9-8	45.64284786	-121.9359293	0.115	0.135	0.187	36.5	15.3	26.4
14	1-2	45.64270439	-121.9392136	0.092	0.070	0.070	42.1	51.8	53.9
116	6-3	45.64276767	-121.9351043	0.085	0.109	0.125	46.1	15.7	41.3
34	3-2	45.64261317	-121.9381916	0.083	0.080	0.100	36.3	38.5	46.3
2	11-5	45.64282175	-121.9395525	0.081	0.060	0.080	44.4	10.4	38.2
12	6-7	45.64282536	-121.9391059	0.079	0.115	0.166	44.5	12.9	25.3
90	1-3	45.64266344	-121.9390866	0.078	0.070	0.080	38.3	55.4	57.7
102	6-1	45.64277778	-121.935532	0.072	0.060	0.070	35.6	25.4	31.1
77	9-7	45.64281444	-121.9364581	0.069	0.050	0.070	38.9	17.7	28.9
57	2-8	45.64273325	-121.9383645	0.069	0.070	0.090	33.5	25.4	36.8
188	22-7	45.64299747	-121.9380556	0.065	0.057	0.084	30.8	6.2	12.5
107	14-7	45.64290903	-121.9352458	0.058	0.056	0.088	22.8	3.0	6.0
156SW	SW19-6	45.64231486	-121.9346288	0.056	0.050	0.070	20.0	24.2	30.6
40SW	SW8-1	45.64281481	-121.9380168	0.055	0.070	0.080	15.8	30.7	38.3

USACE #	Sample #	Latitude	Longitude	209 Congeners (ng/L)	46 Congeners (TTU) ng/L	46 congeners+N estimates (TTU) ng/L	209 Congeners in polymer ug/kg	TTU Cpolymer ug/kg	TTU Cpolymer + N estimate ug/kg
155	19-7	45.64238875	-121.9344941	0.052	0.080	0.090	18.3	35.4	41.9
19	7-5	45.64282753	-121.938845	0.051	0.040	0.060	24.4	22.4	31.7
43	3-4	45.64261856	-121.9379869	0.049	0.090	0.010	43.9	35.0	43.2
110	10-7	45.64284258	-121.9351381	0.049	0.055	0.076	19.2	3.5	7.5
30	7-4	45.64282281	-121.9384272	0.047	0.104	0.116	14.2	10.8	27.8
6	1-7	45.642742	-121.93947	0.046	0.060	0.080	14.6	21.7	31.3
168	17-2	45.64301311	-121.9395379	0.044	0.060	0.080	23.1	26.9	34.1
243	18-4	45.64306228	-121.935126	0.043	0.034	0.054	16.6	1.4	4.8
165	17-1	45.64292953	-121.9396146	0.040	0.070	0.090	22.8	56.1	59.5
16	6-8	45.64282722	-121.9389785	0.039	0.071	0.090	13.9	29.1	30.0
231	17-7	45.64304486	-121.9356652	0.035	0.032	0.038	12.3	2.6	7.6

Yellow highlighting in full congener analysis porewater column represents 11 samples with $\sum_{209}$ porewater concentration >0.1 ng/L and likely to be dominated by local contamination (more than 2 x surface water concentrations). Yellow highlighting in other columns identifies those same samples and their ranking by the analysis in that column.

9.4. UPWELLING VELOCITY DERIVED FROM PECLET-SHERWOOD RELATIONS

i. Diffusive – Advective Transport in Porous Media

Advective and diffusional transport in a porous media at quasi steady state is given by

$$U\frac{\partial C_p}{\partial t} = D_z\frac{\partial^2 C_p}{\partial z^2} \qquad t > 0, -L < z < L,$$

If we assume the concentration and the upwelling groundwater water flow rate are uniform on the y-axis. Then the equation above can be expressed as;

$$U\frac{dC}{dz} = D_{eff}\left(\frac{d^2C}{dx^2} + \frac{d^2C}{dy^2} + \frac{d^2C}{dz^2}\right)$$

Transport in the direction perpendicular to the fiber is assumed to occur only by diffusion. Advection is assumed to dominate the transport in the z-axis which reduces the above equation.

$$U_z\frac{dC}{dz} = D_{eff}\frac{d^2C}{dx^2}$$

We can non-dimensionalize concentration (C) by

$$\theta = \frac{C_* - C_0}{C_\infty - C_0}$$

ii. Peclet – Sherwood Relationship

The relative magnitude of advective to diffusive mass transfer processes is expressed by the Peclet number (Pe).

$$Pe_z = \frac{U_z z}{D_{eff}}$$

Introducing a similarity variable suggested by the scaling law:

$$\eta = \frac{x}{z} Pe_z^{1/2}$$

Then the equation becomes;

$$\theta'' + \frac{1}{2}\eta\theta' = 0$$

With boundary conditions

$$\theta(0) = 0$$

$$\theta(\infty) = 1$$

Incorporating the initial conditions to the previous equation, separation of variables can be used to generate the following expression.

$$\left(\frac{d\theta}{d\eta}\right)_{\eta=0} = \pi^{-\frac{1}{2}} = 0.564$$

The local Sherwood number (Sh), which represents the ratio of the convective mass transfer to the rate of diffusive mass transport can be estimated by the Pe.

$$Sh = \frac{kz_*}{D_{eff}} = \frac{flux}{C_0 - C_\infty}\frac{z}{D_{eff}} = \left(\frac{d\theta}{d\eta}\right)_{\eta=0} Pe_z^{1/2} = 0.564 Pe_z^{1/2}$$

This analytical relationship between the Sherwood number and Peclet number was developed by Bejan & Poulikakos (1984), and Ping (1977) found the same result by numerical methods.

iii. Determining the mass transfer coefficient, k, and upwelling velocity, U_z

The mass transfer coefficient, k, can be obtained from the fraction of performance reference compounds, f_{PRC}, lost from the passive sampling fiber layer.

$$f_{PRC} = V\frac{dC_{PRC}}{dt} = kA\left(\overline{C_{PRC}}\,\middle|_{z\to\infty} - \overline{C_{PRC}}\,\middle|_{z=0}\right)$$

Where V is the volume of PDMS fiber, A is the surface area of PDMS fiber, C_{PRC} is the concentration in fiber, and $\overline{C_{PRC}}$ is the overall concentration in sediment, K_{PDMS} is the water-PDMS partition coefficient.

At $z = 0$ the PRC release from the polymer equilibrates with the adjacent sediment of porosity ε and bulk density ρ_b and the concentration includes both a term for porewater and for sediment partition coefficient K_d.

$$\overline{C_{PRC}} = \frac{\varepsilon + \rho_b K_d}{K_{PDMS}} C_{PRC}$$

Solving for the mass transfer coefficient from the fraction of PRC we get;

$$k = -\ln\left(\frac{C_{PRC}(t)}{C_{PRC}(t=0)}\right)\frac{V}{At}\frac{K_{PDMS}}{\varepsilon + \rho_b K_d}$$

Based on the definition of the Peclet number, Sherwood number, and their relationship. The groundwater upwelling velocity (U_z) can be expressed as a function of effective diffusivity:

$$U_z = \frac{z}{D_{eff}}\left(\frac{k}{0.564}\right)^2$$

9.5. SUPPLEMENTAL INFORMATION FOR LONG TERM MONITORING OF PAHS USING IN-SITU PASSIVE SAMPLING AT A CAPPED RIVERBED

Table 9-1 Cap thickness and depth-averaged porewater concentrations for select LTM stations for phenanthrene, pyrene, and benzo(a)pyrene adapted from (Garza-Rubalcava et al., 2022 in revision).

Depth to native sediment (cm)			**Change (cm)**
LTM	**2013**	**2019**	
08	39	46	7
09	33	46	13
10	33	46	13
11	31	34	3
12A	39	49	10
13	31	18	-13
14	20	30	10
15	42	30	-12
16	12	44	32
17	44	52	8
18	0	0	0
19	28	30	2

Depth to native sediment (cm)			Change (cm)
LTM	**2013**	**2019**	
20A	40	52	12
21	36	49	13

Table 9-2 Fractional Approach to Steady State (f_{ss}) of d-PAH PRCs

PRC	d10-FLUOR	SD	d12-CHRY	SD	d12-B(b)F	SD	d14-DBA	SD
LTM Stations	0.83	0.13	0.75	0.17	0.68	0.20	0.67	0.14
Cap	0.85	0.11	0.77	0.14	0.64	0.23	0.62	0.14
Cap East	0.81	0.09	0.83	0.11	0.42	0.25	0.59	0.15
Cap West	0.88	0.09	0.77	0.12	0.74	0.15	0.66	0.15
Sediment	0.82	0.14	0.73	0.20	0.72	0.17	0.71	0.12
Sediment East	0.79	0.18	0.85	0.13	0.58	0.23	0.73	0.13
Sediment West	0.82	0.09	0.71	0.14	0.79	0.11	0.74	0.12

LTM – includes the 21 LTM stations across the entire 90-cm working section of the fiber.
Cap – includes all 21 LTM stations within the upper 40-cm of the PDMS fiber
Sediment – includes all 21 LTM stations at >40-cm depths of the PDMS fiber
East – includes stations 1-7
West – includes stations 8-14

Table 9-3 Geometric mean of BaP_{eqv} within the cap and underlying sediment for the BL (2012-2014) and 2019 sampling event in the east (S1-S7) and west (S8-S14) sampling areas

Station ID	Cap BL	Cap 2019	Sediment BL	Sediment 2019
S1	1.11	4.68	1.27	5.32
S2	1.16	1.88	1.74	6.08
S3	1.24	3.37	9.04	7.43
S4	1.19	1.71	21.53	19.28
S5	1.48	1.99	1.70	2.89
S6	1.29	4.25	3.16	18.83
S7	0.54	8.17	2.05	7.48
S8	3.04	1.63	7.57	5.33
S9	1.10	-	15.94	-

S10	1.40	4.97	5.12	5.78
S11	1.28	1.31	9.22	4.28
S12	2.16	2.73	4.09	2.32
S13	14.78	2.33	59.94	7.16
S14	2.95	3.43	28.29	1.65

All BaP_{eqv} concentrations are in ng/L.
Sample station S9 was not retrieved during the 2019 sampling event.

Table 9-4 The log ratio of the average measured porewater concentration for depths of less than 40-cm and greater than 40-cm for priority pollutant PAHs (PAH_{16}) at LTM stations in the WBGCR. Log ratios shown in red represent profiles in which the near surface concentration is greater than the concentration at depth.

Location	NAP	FL	ACE	PHE	ANT	FLUOR	PYR	CHRY	B(a)A	B(b)F	B(k)F	B(a)P	DBA	B(g,h,i)P + IP
01A	0.25	0.32	-	-0.53	-0.55	-0.13	-0.13	0.09	0.00	0.02	0.08	-0.05	-	-0.11
02	-	0.29	-	0.40	-	0.02	0.01	0.04	0.04	0.11	0.07	0.04	-	0.06
03	-	-0.66	-0.83	-0.76	-0.63	-0.30	-0.44	-0.21	-0.23	-0.12	-	-0.13	-	-0.18
04	-	-1.19	-	-2.79	-	-1.70	-2.02	-1.46	-1.51	-1.10	-1.15	-1.33	-	-1.14
05	-	0.31	-	0.08	-	0.10	0.10	0.20	0.19	0.35	-	0.28	-	-
25	-	0.22	-	-0.08	-	-0.28	-0.25	-0.33	-0.25	-0.30	-	-0.26	-	-
06	-	-0.99	-	-2.40	-	-1.32	-1.71	-1.36	-1.35	-1.14	-	-1.34	-	-
07	-	-0.67	-	-1.41	-0.86	-0.18	-0.39	0.02	-0.06	-0.48	0.74	-0.01	-	-
08	-	-0.29	-0.70	-0.33	-0.19	-0.34	-0.41	-0.46	-0.50	-0.21	-	-0.32	-	-
10	-	-0.06	-0.29	0.33	0.17	0.31	0.25	0.16	0.22	0.16	-	0.22	-	-
11	-	-0.32	-0.48	-0.62	-0.59	-0.49	-0.69	-0.31	-0.41	-0.17	-	-0.32	-	-
12A	-	-	-	-0.66	-	-0.08	-0.31	-0.07	-0.20	0.18	-	0.07	-	-
13	-	-0.20	-	-1.53	-	-0.71	-1.15	-0.89	-0.99	-0.23	-	-0.54	-	-0.26
14	-	-0.29	-0.28	-0.50	0.14	0.41	0.50	0.72	0.70	-	-	0.39	-	-
15	-	0.02	-	-0.31	-	0.06	-0.11	0.24	0.05	0.17	-	-	-	-
16	-	-0.24	-	-	-	-0.08	-0.08	-0.06	0.00	0.05	-	0.03	-	-0.02

Location	NAP	FL	ACE	PHE	ANT	FLUOR	PYR	CHRY	B(a)A	B(b)F	B(k)F	B(a)P	DBA	B(g,h,i)P + IP
17	-	0.08	-	-	-	0.15	0.27	0.17	0.06	0.24	-0.14	0.22	-	-0.06
18	-0.01	0.11	0.23	-0.27	0.09	0.08	0.07	-0.02	-0.02	-0.04	-0.07	-0.08	-	0.05
19	-	-0.22	0.06	-0.46	-0.46	-0.37	-0.43	-0.29	-0.33	-0.15	-0.08	-0.27	-	-0.09
20A	-	0.00	-0.19	-0.40	0.18	0.25	0.14	0.28	0.26	0.16	-	0.27	-	0.13
21	-	-1.01	-	-1.38	-1.28	-0.51	-0.71	-0.10	-0.28	-0.02	0.01	-0.05	-	0.05

9.6. SUPPLEMENTAL INFORMATION FOR IN SITU PASSIVE SAMPLING FOR THE EVALUATION OF CARBON AMENDMENT PERFORMANCE

Table 9-5 Total Organic Carbon and Black Carbon Results from the East, West, Central, Sedimite™, Aquagate+PAC™ Sampling Cells and the 20 Passive Sampling Stations at Two Depth Intervals

Sample Name	TOC (%)	SD	BC (%)	SD	OC %
East-2015	3.43	0.29	0.15	0.01	3.28
West-2015	2.91	0.23	0.14	0.01	2.77
Central-2015	2.93	0.21	0.14	0.01	2.78
East	5.78	0.46	3.42	0.16	2.35
West	5.52	0.41	3.20	0.08	2.32
Sedimite™	3.45	0.32	0.87	0.26	2.58
Aquagate+PAC ™	3.57	0.34	1.02	0.03	2.55
S1 (0-13.5 cm)	3.21	0.15	0.71	0.03	2.50
S1 (13.5-29 cm)	2.56	0.08	0.50	0.02	2.06
S2 (0-13.5 cm)	4.13	0.31	3.48	0.47	0.65
S2 (13.5-29 cm)	3.66	0.17	0.52	0.02	3.14
S3 (0-13.5 cm)	2.62	0.07	0.64	0.03	1.98
S3 (13.5-29 cm)	2.48	0.00	0.51	0.01	1.97
S4 (0-13.5 cm)	1.14	0.17	0.42	0.21	0.72
S4 (13.5-29 cm)	2.56	0.25	0.29	0.04	2.27
S5 (0-13.5 cm)	4.01	0.10	1.82	0.03	2.20
S5 (13.5-29 cm)	2.86	0.01	0.64	0.03	2.22
S6 (0-13.5 cm)	5.90	0.75	1.87	0.14	4.02
S6 (13.5-29 cm)	2.65	0.48	0.60	0.04	2.05
S7 (0-13.5 cm)	2.73	0.07	0.62	0.02	2.10
S7 (13.5-29 cm)	3.18	0.12	0.76	0.08	2.43

Sample Name	TOC (%)	SD	BC (%)	SD	OC %
East-2015	3.43	0.29	0.15	0.01	3.28
West-2015	2.91	0.23	0.14	0.01	2.77
Central-2015	2.93	0.21	0.14	0.01	2.78
S8 (0-13.5 cm)	4.14	0.01	3.52	0.41	0.62
S8 (13.5-29 cm)	3.10	0.09	1.53	0.58	1.57
S9 (0-13.5 cm)	9.36	0.06	8.13	0.87	1.24
S9 (13.5-29 cm)	3.75	0.33	0.85	0.08	2.89
S10 (0-13.5 cm)	2.54	0.21	0.68	0.00	1.85
S10 (13.5-29 cm)	4.34	0.33	1.15	0.06	3.19
S11 (0-13.5 cm)	3.06	0.30	0.91	0.01	2.15
S11 (13.5-29 cm)	3.93	0.21	1.24	0.10	2.69
S12 (0-13.5 cm)	2.82	0.27	1.15	0.04	1.67
S12 (13.5-29 cm)	3.68	0.06	0.98	0.01	2.70
S13 (0-13.5 cm)	2.95	0.25	1.00	0.02	1.95
S13 (13.5-29 cm)	4.90	0.48	1.58	0.06	3.32
S14 (0-13.5 cm)	2.76	0.04	0.86	0.03	1.91
S14 (13.5-29 cm)	3.88	0.21	1.36	0.39	2.52
S15 (0-13.5 cm)	4.72	0.14	1.65	0.20	3.07
S15 (13.5-29 cm)	5.22	0.46	1.83	0.07	3.39
S16 (0-13.5 cm)	3.93	0.64	2.08	0.03	1.85
S16 (13.5-29 cm)	2.77	0.07	1.05	0.03	1.72
S17 (0-13.5 cm)	3.36	0.01	1.15	0.06	2.21
S17 (13.5-29 cm)	3.28	0.30	0.84	0.01	2.44
S18 (0-13.5 cm)	3.08	0.32	1.67	0.04	1.41
S18 (13.5-29 cm)	4.71	0.00	1.43	0.09	3.28

Sample Name	TOC (%)	SD	BC (%)	SD	OC %
East-2015	3.43	0.29	0.15	0.01	3.28
West-2015	2.91	0.23	0.14	0.01	2.77
Central-2015	2.93	0.21	0.14	0.01	2.78
S19 (0-13.5 cm)	3.40	0.01	1.11	0.03	2.30
S19 (13.5-29 cm)	3.29	0.00	0.92	0.01	2.37
S20 (0-13.5 cm)	3.31	0.39	1.19	0.04	2.12
S20 (13.5-29 cm)	4.38	0.32	1.49	0.00	2.89

Table 9-6 Calculated mass of AC within the 20 individual passive sampling stations.

	Sample Location	Depth	Moisture Content %	TOC %	AC%	Bulk Density g/cm3	M(ac) grams	M(ac) kg	Average in Top Layer (kg)	Average in Bottom Layer (kg)
Aquagate+PAC	S1	0 - 13.5	53.8	3.21	0.21	1.16	62,092.66	62.09	720.20	214.14
		13.5 - 29	52.7	2.56	-0.44	1.18	(131,363.74)			
	S2	0 - 13.5	30.2	4.13	1.13	1.75	497,578.21	497.58		
		13.5 - 29	29.5	3.66	0.66	1.76	293,243.11	293.24		
	S3	0 - 13.5	51.4	2.62	-0.38	1.22	(116,513.27)			
		13.5 - 29	51.3	2.48	-0.52	1.22	(159,625.85)			
	S4	0 - 13.5	22.0	1.14	-1.86	1.95	(914,364.84)			
		13.5 - 29	36.4	2.56	-0.44	1.59	(176,419.44)			
	S5	0 - 13.5	51.4	4.01	1.01	1.22	309,758.67	309.76		
		13.5 - 29	49.1	2.86	-0.14	1.27	(44,973.71)			
	S6	0 - 13.5	39.8	5.90	2.90	1.50	1,100,588.77	1,100.59		
		13.5 - 29	31.6	2.65	-0.35	1.71	(151,043.59)			
	S7	0 - 13.5	52.8	2.73	-0.27	1.18	(80,299.72)			
		13.5 - 29	49.8	3.18	0.18	1.25	56,921.40	56.92		
	S8	0 - 13.5	37.1	4.14	1.14	1.57	452,315.74	452.32		
		13.5 - 29	39.4	3.10	0.10	1.52	38,240.45	38.24		
	S9	0 - 13.5	52.7	9.36	6.36	1.18	1,898,871.65	1,898.87		
		13.5 - 29	47.1	3.75	0.75	1.32	250,331.37	250.33		
	S10	0 - 13.5	42.9	2.54	-0.46	1.43	(165,689.54)			
		13.5 - 29	48.9	4.34	1.34	1.28	431,942.07	431.94		
TOTAL MASS OF AQUGATE+PAC APPLIED = 4,608 KG							**SUM**	**5,391.88**		

	Sample Location	Depth	Moisture Content %	TOC %	AC%	Bulk Density g/cm3	M(ac) grams	M(ac) kg	Average in Top Layer (kg)	Average in Bottom Layer (kg)
Sedimite	S11	0 - 13.5	49.1	3.06	0.06	1.27	19,261.28	19.26	177.68	365.96
		13.5 - 29	50.0	3.93	0.93	1.25	292,919.26	292.92		
	S12	0 - 13.5	43.2	2.82	-0.18	1.42	(64,506.42)			
		13.5 - 29	44.8	3.68	0.68	1.38	236,633.27	236.63		
	S13	0 - 13.5	46.6	2.95	-0.05	1.34	(16,849.36)			
		13.5 - 29	50.5	4.90	1.90	1.24	593,615.18	593.62		
	S14	0 - 13.5	41.5	2.76	-0.24	1.46	(88,545.08)			
		13.5 - 29	47.6	3.88	0.88	1.31	290,796.24	290.80		
	S15	0 - 13.5	50.6	4.72	1.72	1.24	535,960.30	535.96		
		13.5 - 29	51.6	5.22	2.22	1.21	678,083.58	678.08		
	S16	0 - 13.5	41.6	3.93	0.93	1.46	342,671.26	342.67		
		13.5 - 29	44.0	2.77	-0.23	1.40	(81,186.64)			
	S17	0 - 13.5	54.5	3.36	0.36	1.14	103,276.10	103.28		
		13.5 - 29	52.2	3.28	0.28	1.20	84,475.64	84.48		
	S18	0 - 13.5	42.8	3.08	0.08	1.43	28,834.82	28.83		
		13.5 - 29	45.4	4.71	1.71	1.36	588,660.76	588.66		
	S19	0 - 13.5	56.8	3.40	0.40	1.08	109,043.65	109.04		
		13.5 - 29	54.2	3.29	0.29	1.14	83,710.98	83.71		
	S20	0 - 13.5	46.4	3.31	0.31	1.34	104,712.59	104.71		
		13.5 - 29	48.9	4.38	1.38	1.28	444,701.33	444.70		
TOTAL MASS OF SEDIMITE APPLIED = 10,104 kg							**SUM**	**4,537.36**		

Table 9-7 Replicate SPME porewater average ($n = 3$) of $\sum PCB_{66}$ homologues from the 2017 sampling event. There were no nonachlorobiphenyls analyzed from the 66 PCB congener method.

SPME Porewater Concentrations for 0-13.5 cm Depth										
Sample Location	**S1**	**S2**	**S3**	**S4**	**S5**	**S6**	**S7**	**S8**	**S9**	**S10**
Mono, ng/L	0.00	0.01	0.00	0.00	0.00	0.00	0.00	0.03	0.00	0.00
Di, ng/L	0.07	0.25	0.07	0.01	0.03	0.13	0.03	0.13	0.00	0.06
Tri, ng/L	0.06	0.01	0.04	0.04	0.01	0.14	0.06	0.02	0.00	0.02
Tetra, ng/L	0.02	0.00	0.04	0.02	0.01	0.06	0.07	0.04	0.00	0.03
Penta, ng/L	0.00	0.00	0.00	0.00	0.01	0.01	0.02	0.02	0.01	0.01
Hexa, ng/L	0.00	0.00	0.01	0.01	0.00	0.01	0.01	0.01	0.00	0.01
Hepta, ng/L	0.00	0.00	0.00	0.00	0.00	0.00	0.00	0.00	0.00	0.00
Octa, ng/L	0.00	0.00	0.00	0.00	0.00	0.00	0.00	0.00	0.00	0.00
Nona, ng/L	-	-	-	-	-	-	-	-	-	-
Deca, ng/L	0.00	0.00	0.00	0.00	0.00	0.00	0.00	0.00	0.00	0.00
Total Sum congeners, ng/L	**0.15**	**0.27**	**0.16**	**0.09**	**0.05**	**0.35**	**0.20**	**0.25**	**0.02**	**0.13**
Sample Average, ng/L	**0.02**	**0.03**	**0.02**	**0.01**	**0.01**	**0.04**	**0.02**	**0.03**	**0.00**	**0.01**

Sample Location	**S11**	**S12**	**S13**	**S14**	**S15**	**S16**	**S17**	**S18**	**S19**	**S20**
Mono, ng/L	0.00	0.00	0.00	0.00	0.00	0.00	0.00	0.00	0.00	0.00
Di, ng/L	0.12	0.09	0.14	0.20	0.10	0.24	0.04	0.38	0.04	1.42
Tri, ng/L	0.08	0.11	0.03	0.12	0.04	0.13	0.05	0.05	0.02	0.41
Tetra, ng/L	0.07	0.07	0.03	0.04	0.02	0.04	0.00	0.01	0.02	0.22
Penta, ng/L	0.01	0.01	0.00	0.00	0.01	0.01	0.02	0.01	0.00	0.01
Hexa, ng/L	0.00	0.01	0.00	0.00	0.00	0.00	0.00	0.01	0.00	0.00
Hepta, ng/L	0.00	0.00	0.00	0.00	0.00	0.00	0.00	0.00	0.00	0.00
Octa, ng/L	0.00	0.00	0.00	0.00	0.00	0.00	0.00	0.00	0.00	0.00
Nona, ng/L	-	-	-	-	-	-	-	-	-	-
Deca, ng/L	0.00	0.00	0.00	0.00	0.00	0.00	0.00	0.00	0.00	0.00
Total Sum Congeners, ng/L	**0.28**	**0.27**	**0.20**	**0.37**	**0.18**	**0.42**	**0.11**	**0.45**	**0.08**	**2.06**
Sample Average, ng/L	**0.03**	**0.03**	**0.02**	**0.04**	**0.02**	**0.05**	**0.01**	**0.05**	**0.01**	**0.23**

	Mono	**Di**	**Tri**	**Tetra**	**Penta**	**Hexa**	**Hepta**	**Octa**	**Nona**	**Deca**
Homologue Average, ng/L	**0.00**	**0.18**	**0.07**	**0.04**	**0.01**	**0.00**	**0.00**	**0.00**	**-**	**0.00**

Table 9-8 Replicate SPME porewater average ($n = 3$) of $\sum PCB_{66}$ homologues from the 2015 baseline sampling event. There were no nonachlorobiphenyls analyzed from the 66 PCB congener method.

SPME Porewater Concentrations for 0-13.5 cm Depth Baseline Analysis										
Sample Location	**S1**	**S2**	**S3**	**S4**	**S5**	**S6**	**S7**	**S8**	**S9**	**S10**
Mono, ng/L	0.06	0.03	0.04	0.02	0.07	0.02	0.05	0.12	0.03	0.04
Di, ng/L	0.10	0.96	0.25	0.36	0.21	0.46	0.26	1.25	0.14	0.64
Tri, ng/L	0.11	0.29	0.11	0.43	0.18	0.88	0.17	0.74	0.12	0.24
Tetra, ng/L	0.07	0.12	0.07	0.12	0.09	0.29	0.09	0.46	0.07	0.12
Penta, ng/L	0.02	0.04	0.36	0.04	0.04	0.04	0.02	0.19	0.02	0.18
Hexa, ng/L	0.02	0.03	0.02	0.03	0.02	0.03	0.02	0.05	0.02	0.02
Hepta, ng/L	0.01	0.01	0.01	0.01	0.01	0.01	0.01	0.01	0.01	0.01
Octa, ng/L	0.00	0.00	0.00	0.00	0.00	0.00	0.00	0.00	0.00	0.00
Nona, ng/L	-	-	-	-	-	-	-	-	-	-
Deca, ng/L	0.00	0.00	0.00	0.00	0.00	0.00	0.00	0.00	0.00	0.00
Total Sum congeners, ng/L	**0.39**	**1.48**	**0.86**	**1.01**	**0.62**	**1.72**	**0.62**	**2.81**	**0.40**	**1.25**
Sample Average, ng/L	**0.04**	**0.16**	**0.10**	**0.11**	**0.07**	**0.19**	**0.07**	**0.31**	**0.04**	**0.14**

Sample Location	**S11**	**S12**	**S13**	**S14**	**S15**	**S16**	**S17**	**S18**	**S19**	**S20**
Mono, ng/L	0.03	0.04	0.03	0.03	0.02	0.03	0.02	0.03	0.04	0.08
Di, ng/L	0.15	0.30	0.16	0.57	0.19	0.26	0.12	0.60	0.19	1.23
Tri, ng/L	0.12	0.20	0.13	0.77	0.10	0.24	0.13	0.55	0.13	0.76
Tetra, ng/L	0.07	0.11	0.07	0.23	0.06	0.09	0.07	0.17	0.07	0.20
Penta, ng/L	0.02	0.06	0.03	0.06	0.01	0.07	0.02	0.04	0.03	0.18
Hexa, ng/L	0.02	0.03	0.02	0.03	0.02	0.02	0.02	0.02	0.02	0.03
Hepta, ng/L	0.01	0.01	0.01	0.01	0.00	0.01	0.01	0.01	0.01	0.01
Octa, ng/L	0.00	0.00	0.00	0.00	0.00	0.00	0.00	0.00	0.00	0.00
Nona, ng/L	-	-	-	-	-	-	-	-	-	-
Deca, ng/L	0.00	0.00	0.00	0.00	0.00	0.00	0.00	0.00	0.00	0.00
Total Sum Congeners, ng/L	**0.42**	**0.75**	**0.45**	**1.71**	**0.40**	**0.72**	**0.38**	**1.42**	**0.50**	**2.49**
Sample Average, ng/L	**0.05**	**0.08**	**0.05**	**0.19**	**0.04**	**0.08**	**0.04**	**0.16**	**0.06**	**0.28**

	Mono	**Di**	**Tri**	**Tetra**	**Penta**	**Hexa**	**Hepta**	**Octa**	**Nona**	**Deca**
Homologue Average, ng/L	**0.04**	**0.42**	**0.32**	**0.13**	**0.07**	**0.03**	**0.01**	**0.00**	**-**	**0.00**

Table 9-9 The fractional approach of steady state in the surficial sediment (0-13.5 cm) depth interval and the deeper sediment (13.5-29 cm) for target PCB congeners

Congener #	$\log K_{ow}$	$\log K_f$	f_{ss} Top	f_{ss} Bottom
1	4.46	4.21	0.74	0.72
2	4.69	4.42	0.71	0.70
10	4.84	4.57	0.70	0.69
4	4.65	4.39	0.72	0.70
6	5.06	4.77	0.67	0.67
8	5.07	4.78	0.67	0.67
5	4.97	4.69	0.68	0.68
18	5.24	4.95	0.65	0.65
17	5.25	4.95	0.65	0.65
27	5.44	5.13	0.63	0.64
24	5.35	5.05	0.64	0.64
32	5.44	5.13	0.63	0.64
16	5.16	4.87	0.66	0.66
26	5.66	5.34	0.60	0.62
25	5.67	5.35	0.60	0.61
31	5.67	5.35	0.60	0.61
28	5.67	5.35	0.60	0.61
20	5.57	5.26	0.61	0.62
22	5.58	5.27	0.61	0.62
45	5.53	5.22	0.62	0.63
52	5.84	5.51	0.58	0.60
47	5.85	5.52	0.58	0.60
44	5.75	5.43	0.59	0.61
42	5.76	5.44	0.59	0.61
71	5.98	5.65	0.56	0.58
41	5.69	5.37	0.60	0.61
40	5.66	5.34	0.60	0.62
74	6.2	5.85	0.54	0.56
70	6.2	5.85	0.54	0.56
66	6.2	5.85	0.54	0.56
93	6.04	5.70	0.56	0.58
95	6.13	5.79	0.55	0.57
60	6.11	5.77	0.55	0.57
84	6.04	5.70	0.56	0.58
101	6.38	6.02	0.52	0.55
99	6.39	6.03	0.51	0.55
83	6.26	5.91	0.53	0.56
87	6.29	5.94	0.53	0.55

Congener #	$\log K_{ow}$	$\log K_f$	f_{ss} Top	f_{ss} Bottom
136	6.22	5.87	0.53	0.56
110	6.48	6.12	0.50	0.54
151	6.64	6.27	0.48	0.52
135	6.64	6.27	0.48	0.52
144	6.67	6.30	0.48	0.52
118/123	6.74	6.37	0.47	0.51
149	6.67	6.30	0.48	0.52
134	6.55	6.19	0.49	0.53
131	6.58	6.21	0.49	0.53
146	6.89	6.51	0.45	0.50
153	6.92	6.54	0.45	0.49
132	6.58	6.21	0.49	0.53
141	6.82	6.44	0.46	0.50
179	6.73	6.36	0.47	0.51
163	6.99	6.60	0.44	0.49
138	6.83	6.45	0.46	0.50
158	7.02	6.63	0.44	0.48
175	7.17	6.77	0.42	0.47
183	7.2	6.80	0.42	0.47
128	6.74	6.37	0.47	0.51
167	7.27	6.87	0.41	0.46
174	7.11	6.72	0.43	0.48
177	7.08	6.69	0.43	0.48
156	7.18	6.78	0.42	0.47
173	7.02	6.63	0.44	0.48
180	7.36	6.95	0.40	0.45
193	7.52	7.10	0.38	0.44
198	7.62	7.20	0.37	0.43
203	7.65	7.23	0.36	0.42
196	7.65	7.23	0.36	0.42
194	7.8	7.37	0.35	0.41
209	8.18	7.73	0.31	0.38

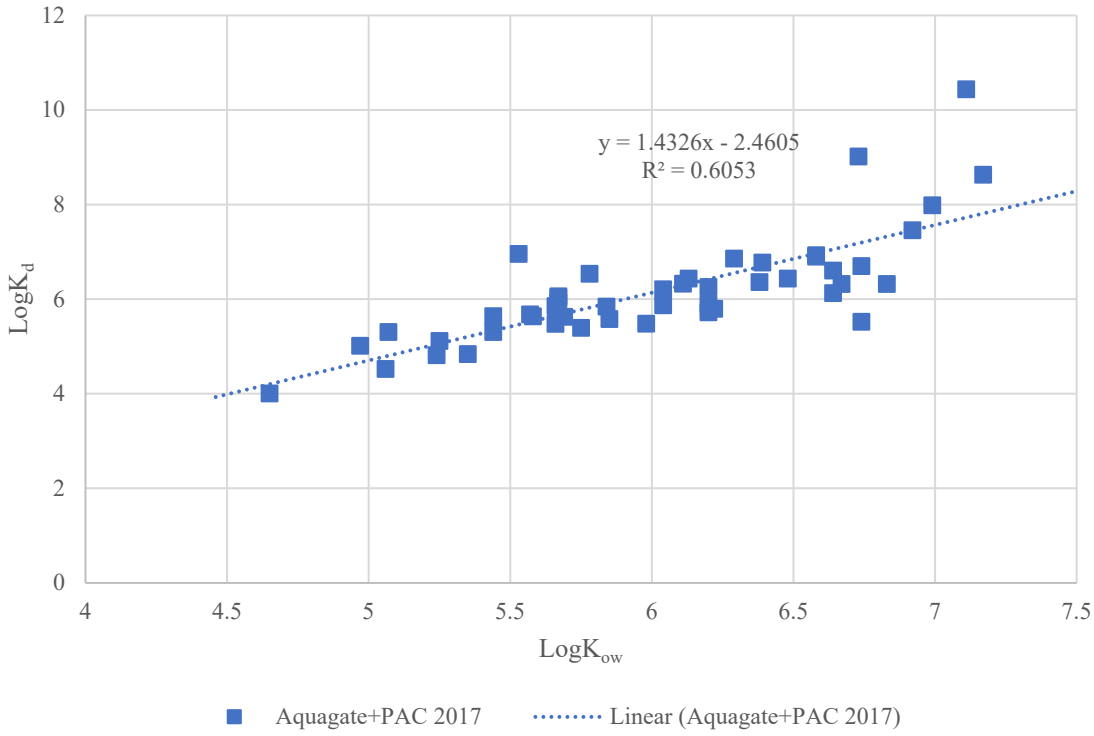

Figure 9-10 Calculated sediment partitioning coefficients ($\log K_d$) for post-Aquagate+PAC (blue squares) application. Linear best fit correlation is included.